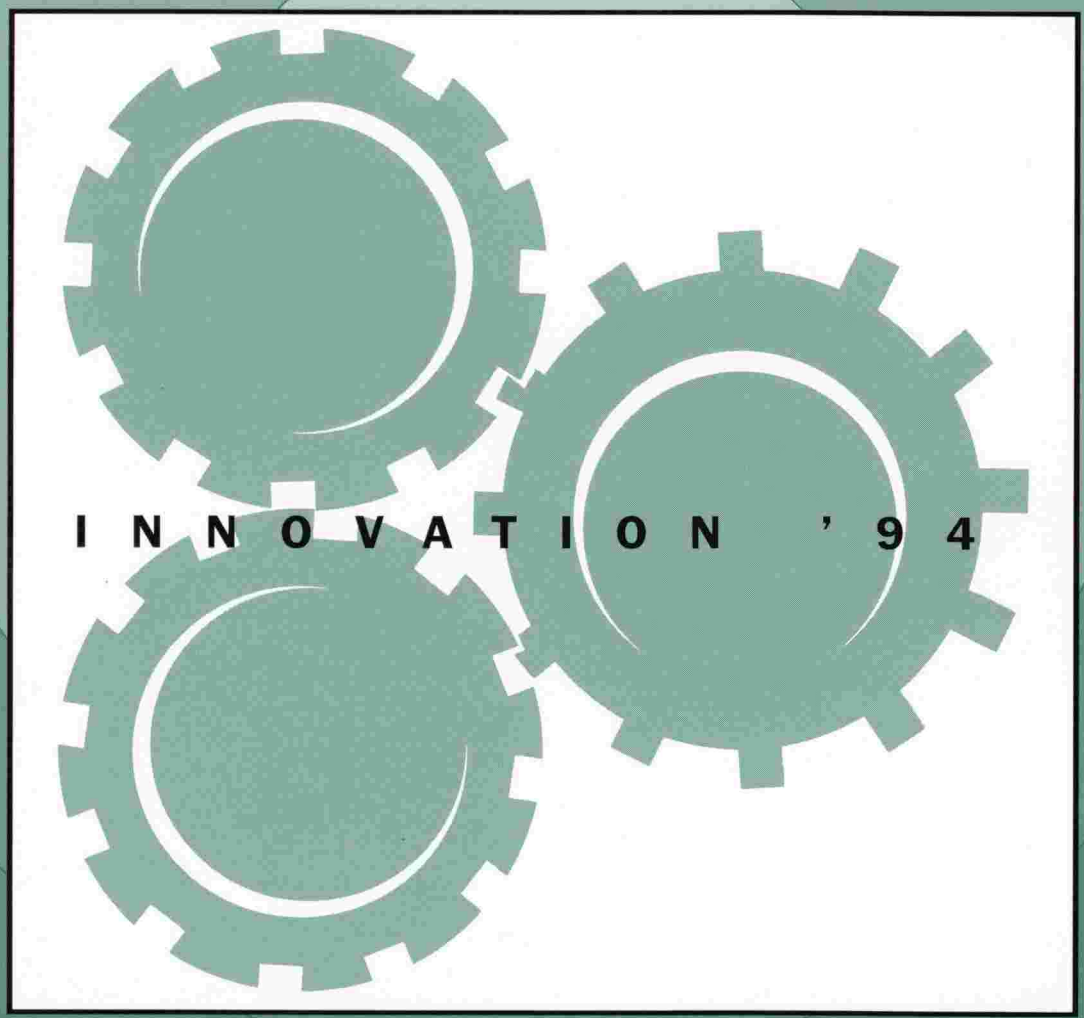

First Meeting of the Society of Magnetic Resonance

Printed Program

Guest Editors
Laurence P Clarke, PhD
Richard L Ehman, MD
Norbert J Pelc, ScD
Jeffrey S Ross, MD

Journal of Magnetic Resonance Imaging
Published by the Society of Magnetic Resonance

A supplement to JMRI January/February 1994 Issue, Volume 4(P)

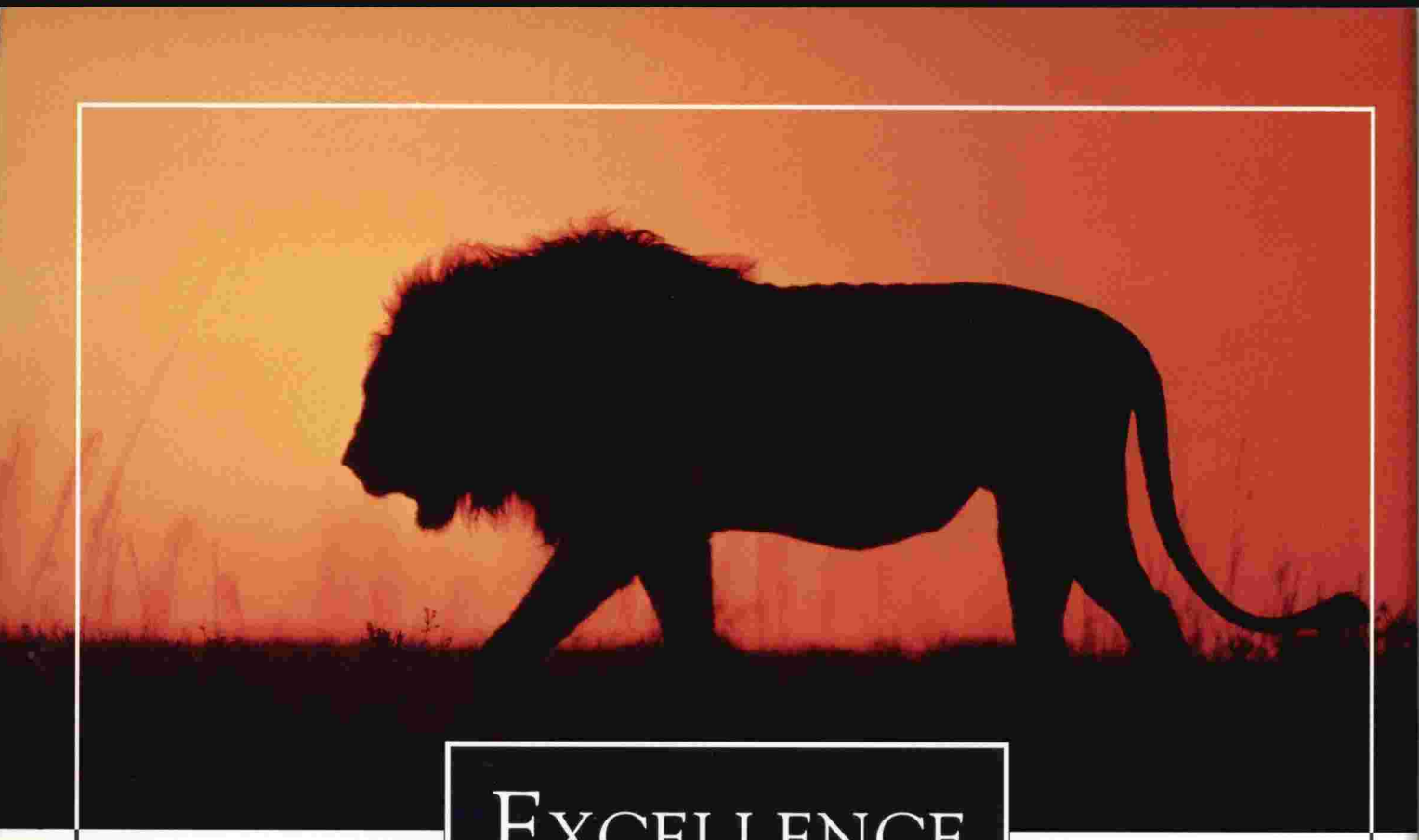

EXCELLENCE

EVOLVES THROUGH COMMITMENT.

For over a century, Shimadzu Corporation has taken pride in leading the medical imaging industry by providing high technology and value oriented imaging systems that have evolved through a commitment to excellence.

Today, this heritage continues with the revolutionary new MAGNEX 100/HP 1.0T MRI system, delivering the most complete high performance imaging package in the industry. Standard features include fast spin echo (RISE), sub-second imaging (SMASH), and MTC-MRA, while a new shielded gradient coil design provides optimal image quality.

MAGNEX 100/HP

The advanced computer and high speed image accelerator enables MRA MIP processing in only four seconds. And MIP processing can be done concurrently with scan acquisition, improving patient throughput and efficiency.

As always, value is also standard with Shimadzu MRI. Product longevity and reliability reduce system life cost, while obsolescence is reduced through hardware and software advancements and upgrades.

Shimadzu's MAGNEX 100/HP, by nature, is leading the evolution of MRI.

SHIMADZU

Solutions Engineered for Life.[SM]

20101 SOUTH VERMONT, TORRANCE, CA 90502

800.228.1429

This system is currently pending FDA 510(K) certification.

JMRI Journal of Magnetic Resonance Imaging

Owned and published by the Society of Magnetic Resonance, and produced with the assistance of the Radiological Society of North America.

Contrast Agent Special Issue Order Form

JMRI,
the critical link
between pharmaceutical
manufacturers and the
clinical user of medicine,
provides yet another
important and helpful
tool...
the Contrast Agent Special Issue.

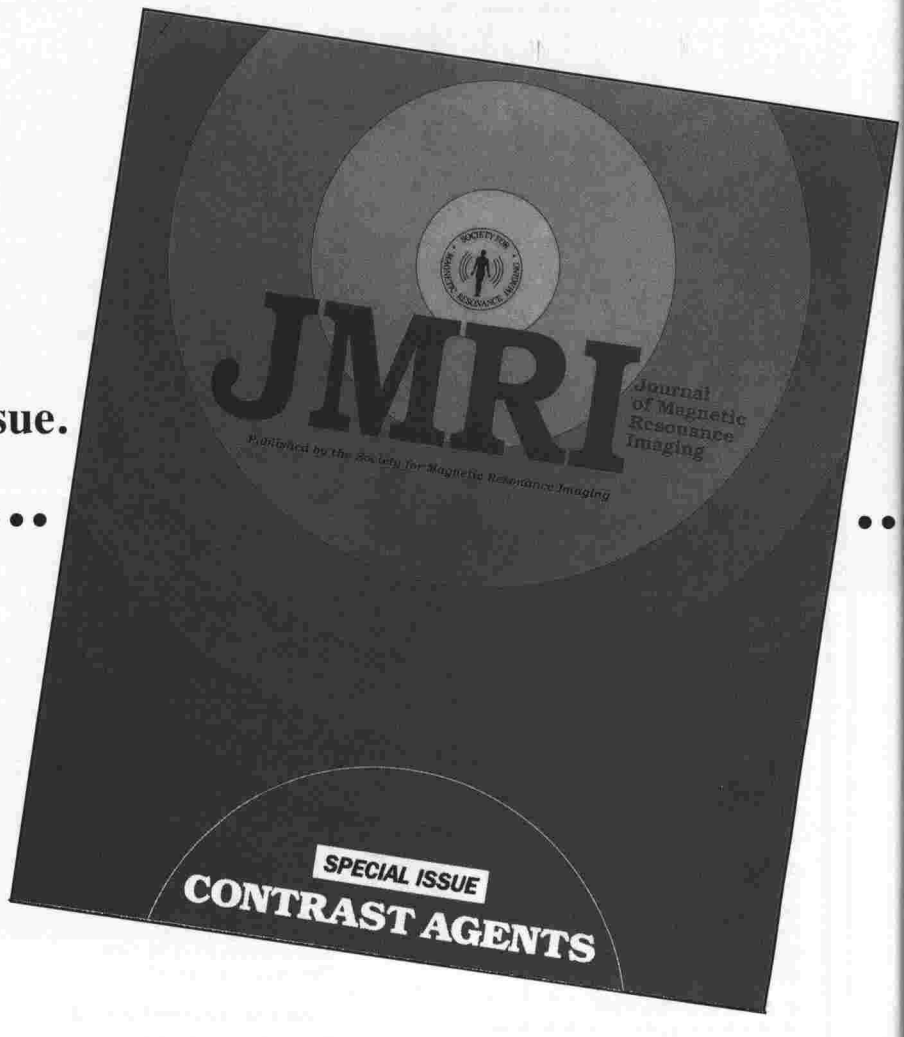

The Contrast Agent Special Issue will be published in the May/June 1994 **JMRI** double issue. Additional copies of the issue will be available and may be ordered by faxing this Order Form to the **SMRI** Central Office at 312/951-6474. If questions, call 312/751-2590.

***Take** control of a critical variable in magnetic resonance...order your Contrast Agent Special Issue today.*

Number of Issues: ☐ 1993 Edition ☐ 1994 Edition

@ $25.00 each $ _____

Payment enclosed (U.S. funds only) ☐

MasterCard/Visa ☐

Name _____

Address _____

City/State/Zip Code _____

Country _____

Phone _____ FAX _____

Name _____

Account #/Exp. date _____

JMRI
Journal of Magnetic Resonance Imaging

213 West Institute Place, Suite 501, Chicago, Illinois 60610, Phone: 312/751-2590 FAX: 312/951-6474

JMRI Journal of Magnetic Resonance Imaging

Continued

POSTER EXHIBIT ABSTRACTS

LETTER FROM THE SMRI PRESIDENT

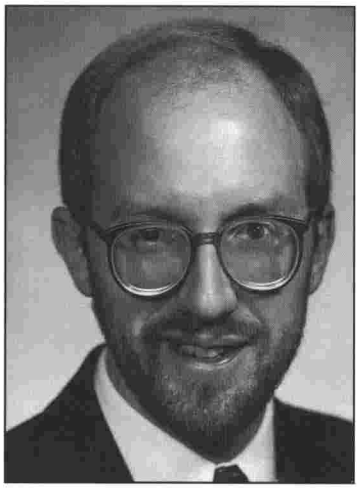

Stephen J. Riederer, PhD
SMRI President 1993

Dear Colleague:

The Society of Magnetic Resonance invites you to its First Meeting! This meeting, to be held in Dallas March 5-9, 1994, was organized by the program committees of the Society for Magnetic Resonance Imaging prior to its merger with the Society of Magnetic Resonance in Medicine on January 1, 1994. In my capacity, at press time, as SMRI president I invite you to join us in Dallas.

This First SMR Meeting will contain several major programs, beginning with the Educational Program on Saturday and Sunday, March 5 - 6. This program will provide a comprehensive review of MRI principles as well as a discussion of neuro and body imaging applications. The Economics Symposium on Monday, March 7, a component of the Educational Program, will address various issues related to the cost and reimbursement of MR procedures.

The Scientific Program, consisting of plenary and proffered paper sessions, will run Sunday through Wednesday. The centerpiece of the Scientific Program will be the Topical Conference on Sunday, March 6 addressing "MRI in a Quality and Cost-Conscious Environment". This will consider MR from many perspectives, including an assessment of current status, consideration of costs and benefits, and predictions of possible improvements as provided by future technology.

As a consequence of its popularity last year, the 1994 Morning Tutorial Program has expanded to three sessions daily, Monday - Wednesday (6:45 AM-7:45 AM). The Scientific Poster Exhibition, a showcase of recent scientific developments, is available throughout the meeting.

In addition, the First SMR Meeting contains several other features...

The Technical Exhibits Area will display state-of-the-art MR commercial equipment and accessories. An exhibit on interactive educational activities is also scheduled.

The Combined Section on Magnetic Resonance Technologists (SMRT) will hold its Annual Meeting on Saturday and Sunday, March 5 - 6.

Registrants to the SMR Meeting will also be able to attend, at no additional charge, the sessions of the North American Society for Cardiac Imaging (NASCI) on Friday and Saturday, March 4-5.

The First SMR Meeting will provide ample opportunity to meet and confer with your colleagues on an informal basis. Special events include the Technical Exhibits Reception (Saturday, 5:00 PM - 7:00 PM), the SMRT Poster Reception (Saturday, 7:00 PM - 9:00 PM), the SMR Scientific Poster Reception (Sunday, 5:30 PM - 7:30 PM) and the Gala Reception (Monday, 7:30 PM - 10:30 PM). Please plan to attend these special social events.

The SMR publishes two official journals, the **Journal of Magnetic Resonance Imaging** and **Magnetic Resonance in Medicine.** Both are proven resources for current developments in the field of magnetic resonance as applied to medicine and biology. You are strongly encouraged to submit manuscripts based on your work to either of these journals.

The SMR is excited about its First Meeting as a merged Society and cordially invites you to participate. We look forward to seeing you in Dallas!

Sincerely,

Stephen J. Riederer

Stephen J. Riederer, PhD
SMRI President, 1993

About The Society

Letter from the President

Greetings! For all merged Society and MR colleagues who are confused by the alphabet soup that you are being asked to digest, please let me take a moment to clarify a few items in this Printed Program, in general, and on these next pages in particular...

The following "About the Society" information provides a cursory glance at the breadth and depth of the SMR's educational and scientific mission. The Society has expanded under the merger and, thus, it is difficult to capture, in such limited space, the rich background that both the SMRM and SMRI bring to the merged entity. The following information is an initial attempt to do so.

The "SMR at Work" page details the leadership involved with the current SMRI and SMR activities. Both are included as it is under their stewardship that the Dallas meeting was organized (SMRI Annual Meeting and Education Coordination Council and SMRI Executive Committee) and the SMR has come into fruition (SMR Interim Officers and Board of Trustees). The SMR Officers and Trustees rosters list those individuals who will govern starting on March 7, 1994. This Board, coupled with those nominees elected by the membership to the Board, will comprise the next SMR Board.

The SMR is indebted to all individuals, past and present, who through their contributions to the SMRI and SMRM have provided the strong foundation on which SMR is based. The SMR hopes these "founding parents" will continue their involvement as SMR leads the entire scientific community into the 21st century.

E. Mark Haacke, PhD
SMR President

History of the Society

The Society of Magnetic Resonance is a non-profit professional association formed in 1993 as a result of a merger between the Society for Magnetic Resonance Imaging and the Society of Magnetic Resonance in Medicine. It became the sole Society encompassing SMRI and SMRM on January 1, 1994. Dallas marks the First Meeting of the merged Society, formerly the Twelfth Annual Meeting of the Society for Magnetic Resonance Imaging, with the Second Meeting, formerly the Thirteenth Annual Scientific Meeting and Exhibition of the Society of Magnetic Resonance in Medicine, to be held August 6-12, 1994 in San Francisco, California. Details regarding the Society's mission and educational/scientific vehicles are listed below.

Mission

The Society of Magnetic Resonance is an international scientific association of over 3600 clinicians, physicists, engineers and other scientists devoted to furthering the development and application of Magnetic Resonance techniques in medicine and biology, to promoting communication and to providing channels for continuing education in the Magnetic Resonance field. This mission is achieved through the Society's educational and scientific methods below.

Membership

Membership in the Society shall be open to all persons who share the stated purposes of the Society. Full, Student and Technologist categories exist (refer to membership forms at the rear of this book). Highlights regarding the Section for MR Technologists (SMRT) and Society Study Groups and Chapters are detailed below.

SMRT

The Section for MR Technologists (SMRT) was formed on December 1, 1991. Designed to provide MR technologists with a separate forum within the Society, the SMRT is governed by a distinct Policy Board and Executive Committee. The SMRT hosts an Annual Meeting, Regional Meetings and educational workshops throughout the year. In addition, it publishes a newsletter, *Signals*, 4 times annually. SMRT is in the process of establishing local chapters, having finalized a relationship with one region to date (4 are pending).

Study Groups

Study Groups may be established to satisfy a scientific community of interest and are to be based on topical and active areas of Magnetic Resonance. The Groups are designed to provide a dialogue with Annual Meeting, Education and Workshop programming committees regarding potential topics for inclusion in Society educational and scientific activities.

Chapters

Chapters may be established on a geographical basis and shall attempt to reflect the multi-disciplinary nature and intellectual balance of the Society.

Annual Meeting

Both the Society for Magnetic Resonance Imaging and the Society of Magnetic Resonance in Medicine have hosted separate Annual Meetings since 1982. Both meetings offered a comprehensive forum for the exchange of scientific, technical and product information related to research techniques, equipment and clinical applications of magnetic resonance.

The First Meeting of the SMR will offer a Scientific Program consisting of more than 30 plenary symposia and 550 peer-reviewed papers, works in progress presentations and scientific posters. Additionally, a three-day Educational Program provides an intro-

SMRI / SMRM PAST

SMRI	**1982** Organizational Meeting - *Houston, TX*	**1983** First Annual Meeting - *Denver, CO*	**1984** Second Annual Meeting - *Orlando, FL*	**1985** Third Annual Meeting - *San Diego, CA*	**1986** Fourth Annual Meeting - *Philadelphia, PA*	**1987** Fifth Annual Meeting - *San Antonio, TX*
SMRM	**1982** First Annual Meeting - Boston, MA	**1983** Second Annual Meeting - San Francisco, CA	**1984** Third Annual Meeting - New York, NY	**1985** Fourth Annual Meeting - London, UK	**1986** Fifth Annual Meeting - Montreal, Quebec, Canada	**1987** Sixth Annual Meeting - New York, NY

About The Society

duction to MRI basics and an in-depth-analysis of MR Economics. Also, the Third Annual Meeting of the SMRT and a Morning Tutorial Workshop are included in the scientific agenda.

An integral component of the Annual Meeting is the technical exhibition of MRI products, accessories and services. Over 40 leading companies from around the world participate in presenting over 12,000 square feet of technical exhibits. The Meeting provides a forum for the discussion and exchange of ideas between clinical and basic scientists, technologists, radiology business managers and administrators, purchasing agents and manufacturers. The SMR Meeting will also offer an Interactive Education Exhibit, framed in a very "hands-on" format, focusing on CD ROM and other interactive technologies and will be located in the Technical Exhibits Area.

Beginning in 1995, the merged Society will host a single Annual Meeting. Additionally, future Annual Meetings will adopt a rotation pattern designed by SMRM wherein each third meeting will be held at a non-North American site. This schedule will be launched with the 1995 Annual Meeting in Nice, France.

Publications

With the merger of the two Societies, the SMR will produce two official journals: Magnetic Resonance in Medicine (MRM) and Journal of Magnetic Resonance Imaging (JMRI).

Magnetic Resonance in Medicine (MRM)

Published monthly in association with Williams and Wilkins, MRM is an international, peer-reviewed journal devoted to the publication of original investigations concerned with all aspects of the development and use of nuclear magnetic resonance and electron paramagnetic resonance techniques for medical

applications. Reports of original investigations in the areas of mathematics, computing, engineering, physics, biophysics, chemistry, biochemistry, and physiology directly relevant to magnetic resonance are published, as well as methodology-oriented clinical studies. MRM publishes 140 pages per month and over 250 papers annually. The Editor-in-Chief is Felix W. Wehrli, PhD, Professor of Radiologic Science, Biochemistry, and Biophysics at the University of Pennsylvania Medical Center, Philadelphia, Pennsylvania.

Journal of Magnetic Resonance Imaging (JMRI)

JMRI, under the direction of Gary D. Fullerton, PhD, Professor and Chief of Radiological Sciences at the University of Texas Health Science Center, San Antonio, presents a balance of technical and clinical articles on MR imaging and spectroscopy research. JMRI, bimonthly, publishes 120 pages of peer-reviewed original research, works in progress, review articles, Society reports and other special features, with more than 100 manuscripts published annually. Owned by the SMR, JMRI is produced in collaboration with the Radiological Society of North America, publisher of Radiology and other radiology-related journals. It addresses major clinical and technical developments in magnetic resonance imaging. JMRI expanded its scope in 1992 to launch production of an MResource Guide, a directory of MR equipment, service and accessory manufacturers, coupled with a compendium of MR definitions, pulse sequences and acronyms. The 1994 edition was expanded to include a reprint of the ACR Glossary of MR Terms. Additionally, JMRI annually publishes special interest issues such as the 1994 May/June issue on Contrast Agents. JMRI is currently in the process of transferring the journal into CD ROM format; this will be completed in early 1994 for consumer availability.

Pulse

1994 introduces the first volume of Pulse, the newsletter of the newly merged Society. Distributed three times annually, the newsletter will provide important Society updates as well as state-of-the-art technical notes and clinical protocols to the membership. Edited by Roxanne Deslauriers, PhD, Head of the Biosystems Group at the Institute of Biodiagnostics, Winnipeg, Manitoba, Canada and Paul T. Weatherall, MD, Director of Clinical MRI, Rogers MR Center of the University of Texas, the newsletter will provide an open communications forum to the membership.

Future Meetings

Upcoming Society Meetings will include:

1994: August 6-12, San Francisco, CA
1995: August 19-25, Nice, France
1996: Spring, New York, NY
1997: April 10-19, Vancouver, BC

Workshops

SMR annually hosts 3-4 scientific workshops. To date, a combined SMRI/SMRM Workshop Committee has hosted 4 workshops. Conceived of and organized by experts in the field, the workshop address focused topics of interest for specialized basic and clinical scientists.

ANNUAL MEETINGS

SMRI	**1988** Sixth Annual Meeting - *Boston, MA*	**1989** Seventh Annual Meeting - *Los Angeles, CA*	**1990** Eighth Annual Meeting - *Washington, DC*	**1991** Ninth Annual Meeting - *Chicago, IL*	**1992** Tenth Annual Meeting - *New York, NY*	**1993** Eleventh Annual Meeting - *San Francisco, CA*
SMRM	**1988** Seventh Annual Meeting - *San Francisco, CA*	**1989** Eighth Annual Meeting - *Amsterdam, The Netherlands*	**1990** Ninth Annual Meeting - *New York, NY*	**1991** Tenth Annual Meeting - *San Francisco, CA*	**1992** Eleventh Annual Meeting - *Berlin, Germany*	**1993** Twelfth Annual Meeting - *New York, NY*

SOCIETIES AT WORK

SMRI

1993 SMRI Officers

Stephen J Riederer, PhD
President

Steven E Harms, MD
Past President

John V Crues III, MD
President-Elect

Michael L Wood, PhD
Treasurer

Stephen R Thomas, PhD
Secretary

1993 SMRI Annual Meeting and Education Coordination Council

Co-Chairmen
Laurence P Clarke, PhD
Jeffrey S Ross, MD
William T C Yuh, MD, MSEE
Steven E Harms, MD (Ex Com Liaison)

Scientific Program Committee
Richard L Ehman, MD
Norbert J Pelc, ScD

Scientific Poster Program Committee
Patrick A Turski, MD
Michael E Moseley, PhD

Education Program Committee
Jeffrey L Duerk, PhD
Donald G Mitchell, MD

Morning Tutorial Program Committee
Dwight G Nishimura, PhD
Charles E Spritzer, MD

MR Economics Symposium
Herbert L Abrams, MD
Stuart W Young, MD

Technical Exhibits Program Committee
Jeffrey C Weinreb, MD

SMR

SMR Interim Officers

E Mark Haacke, PhD
President

Herbert Y Kressel, MD
Past President

Stephen J Riederer, PhD
President-Elect

Robert S Balaban, PhD
Senior Vice President

John V Crues III, MD
First Vice President

Thomas J Brady, MD
Second Vice President

Michael L Wood, PhD
Treasurer

Ian R Young, PhD
Secretary

SMR Interim Board of Trustees

Robert S Balaban, PhD
Thomas J Brady, MD
John V Crues III, MD
E Mark Haacke, PhD
Steven E Harms, MD
Joanne S Ingwall, PhD
Herbert Y Kressel, MD
Robert B Lufkin, MD
Michael T Modic, MD
Stephen J Riederer, PhD
Ian C P Smith, PhD
Stephen R Thomas, PhD
Michael L Wood, PhD
Ian R Young, PhD

1994 SMR Officers

Stephen J. Riederer, PhD
President

Michael T. Modic, MD
Past President

Robert S Balaban, PhD
President Elect

John V Crues, III, MD
Senior Vice President

Thomas J Brady, MD
Vice President

1994 SMR Board of Trustees

Danielle Balberiaux, MD
SMRM Board, 1995

Jacques Bittoun, MD, PhD
SMRM Board, 1996

Johannes Bloem, MD, PhD
SMRM Board, 1994

William R Brody, MD, PhD
SMRM Board, 1995

Mark S Cohen, PhD
SMRI Board, 1996

Patrick J Cozzone, PhD
SMRM Board, 1995

Jeffrey L Duerk, PhD
SMRI Board, 1996

Robert R Edelman, MD
SMRM Board, 1994

Gary D Fullerton, PhD
JMRI Editor, Ex-Officio

Gary H Glover, PhD
SMRI/SMRM Board, 1995

Axel Haase, PhD
SMRM Board, 1996

Steven E Harms, MD
SMRM Board, 1995

R Mark Henkelman, PhD
SMRM Board, 1994

Robert J Herfkens, MD
SMRM Board, 1996

Peter Luyten, PhD
SMRM Board, 1995

Albert Macovski, PhD
SMRM Board, 1994

Andrew A Maudsley, PhD
SMRM Board, 1996

Shirley M McCarthy, MD, PhD
SMRM Board, 1994

Michael E Moseley, PhD
SMRI/SMRM Board, 1996

Carolyn E Mountford, PhD
SMRM Board, 1994

Dwight G Nishimura, PhD,
SMRI Board, 1995

Bruce R Rosen, MD, PhD
SMRI/SMRM Board, 1996

Brian Ross, MD, PhD
SMRM Board, 1995

Jeffrey S Ross, MD
SMRI Board, 1996

David D Stark, MD
SMRI Board, 1995

Felix W Wehrli, PhD
MRM Editor, Ex-Officio

William T C Yuh, MD, MSEE
SMRI Board, 1995

SMRI Honorary Member Award

The Society for Magnetic Resonance Imaging has traditionally announced its awardees in November of each year and recognized the awardees at its Annual Meeting the following spring. In November 1993, the SMRI Awards Committee announced one recipient for Honorary Membership of the SMRI and nine recipients for Fellowship of the SMRI, as de-- tailed on the next several pages.

Because of the merger with the SMRM on January 1, 1994 there technically would have been no official SMRI meeting at which these November awardees could have been honored. However, in order to provide such a forum, the Board of the SMR has extended the invitation to the SMRI Awards Committee, chaired by C. Leon Partain, MD, PhD, to honor these SMRI awardees at this First Meeting of the SMR.

About the Award

Honorary membership in the Society for Magnetic Resonance Imaging is conferred on an individual who has rendered unusual service to the science of Magnetic Resonance. It is the highest honor the Society can bestow upon an individual.

Past Honorary Member Award Recipients

1993: Wiliam G Bradley, Jr. MD, PhD

1992: Graeme Bydder, ChMB

1990: Francis W Smith, MD

1989: Ian R Young, PhD

1988: Paul C Lauterbur, PhD

HONORARY MEMBER

Sir Peter Mansfield, FRS

Sir Peter Mansfield, FRS, knighted in the 1993 New Year's Honours List by Her Majesty, Queen Elizabeth II for his pioneering development of MRI, is currently a Professor of Physics at the Magnetic Resonance Centre in the University of Nottingham, England.

He received his first degree in 1959 and PhD in Physics in 1962 from Queen Mary College, University of London and then spent two years as a post doctoral Research Associate in Charlie Slichter's laboratory in Urbana, Illinois. Dr. Mansfield returned to England as a lecturer in Physics at Nottingham in 1964.

In addition to his early work in MRI, including the conception of imaging and the use of k-space, the basis for the description of MR imaging methods, he has made numerous contributions to the further development of MRI. These include the introduction of the principles of selective excitation, ultra high-speed (echo-planar) imaging and active magnetic screening of gradient coils.

His work has been widely acknowledged in Britain and internationally by the award of numerous medals, prizes and honorary fellowships and memberships of other Societies. His book, co-authored by P.G. Morris, "NMR Imaging in the Biomedicine" published in 1982, was widely acclaimed as the first comprehensive text on the detailed theory of MRI.

Sir Peter lives in Bramcote, Nottingham with his wife, Jean. He has two daughters, Sarah and Gillian, both of whom have recently married.

SMRI Fellows of the Society Awards

About the Award...

Fellow of the Society awards are conferred on those individuals who have made both a significant contribution to the science of MRI and rendered outstanding service to the Society.

Past Award Recipients

1993: Jeffrey L Duerk, PhD
Steven E Harms, MD

1992: E Mark Haacke, PhD
Kenneth R Maravilla, MD
Jeffrey C Weinreb, MD
Michael L Wood, PhD

1991: Graeme Bydder, MD
R Mark Henkelman, PhD
Robert B Lufkin, MD
Felix W Wehrli, PhD

1990: C Leon Partain, MD, PhD
Val M Runge, MD
David D Stark, MD

1989: Sharad R Amtey, PhD
Paul A Bottomley, PhD
William G Bradley, Jr., MD, PhD
Gary D Fullerton, PhD
John C Gore, PhD
Carlton T Hazlewood, PhD
R Edward Hendrick, PhD
Andre Luiten, PhD
William J McIntyre, PhD
Ray L Nunnally, PhD
Francis W Smith, MD
Luis E Todd, MD

Laurence P Clarke, PhD

Dr. Clarke is a Professor of Radiology and Physics in the Department of Radiology, College of Medicine, for the Center of Engineering and Medical Image Analysis, Colleges of Engineering and Medicine, University of South Florida, Tampa. He received his Bachelors and Masters Degrees in Physics at the National University of Ireland. Before moving to Tampa, Dr. Clarke served as Assistant Professor at the University of Miami; Medical Physicist, Dublin Institute of Technology, Ireland; and research Physicist at Sloan Kettering Institute in New York. He has been active in the SMRM, the AAPM, and IEEE Section in Engineering and Medicine and Biology.

His research emphasis is in MRI tissue characterization and 3D image segmentation using pattern recognition techniques, artificial and hybrid neural nets, fuzzy clustering techniques, image compression and computer assisted diagnosis (CAD) at central and remote locations. Dr. Clarke is author of over 80 technical papers and 200 scientific abstracts.

He has served as a member of the SMRI Board, the JMRI Editorial Board, and also as a JMRI reviewer, Annual Meeting Educational Program co-chairman and Scientific Program co-chairman.

John V Crues III, MD

Dr. Crues is Director of Magnetic Resonance, Musculoskeletal, and Emergency Imaging at Cedars-Sinai Medical Center in Los Angeles and is Assistant Clinical Professor of Radiology at UCLA School of Medicine. He obtained an AB in Physics from Harvard College, an MS in physics from the University of Illinois, and an MD from Harvard Medical School. An internship in internal medicine was completed at LAC-USC Medical Center. He completed residency training in internal medicine and radiology at Cedars-Sinai Medical Center. He has previously served as Medical Director of MR imaging at Cedars-Sinai and Santa Barbara Cottage Hospitals.

Dr. Crues' active research interests include MR applications in musculoskeletal imaging, MR microscopy, image processing and computer assisted image interpretation, electronic medical publishing, and electronic archiving and communication systems.

Dr. Crues has served as SMRI Secretary, President-Elect, member of the team which successfully obtained CME granting ability for the SMRI as well as serving an instrumental role in the formation of the SMRI. He is currently Vice President of the SMR.

Richard L Ehman, MD

Dr. Ehman is Associate Professor at Mayo Medical School and Chairman, Division of Research, Department of Diagnostic Radiology at Mayo Clinic and Foundation in Rochester. He received his BS in physics and an MD at University of Saskatchewan. Dr. Ehman has served as Assistant Professor, Mayo Clinic and Foundation; Fellow, Department of Radiology, Mayo Clinic and Foundation; Research Fellow, University of California at San Francisco and Resident in Diagnostic Radiology, University of Calgary. He is associated professionally with the SMRI, RSNA, SMRM, ACR, ARRS, Sigma XI, AMA and the Minnesota Radiological Society.

Dr. Ehman's research interests include clinical MRI, musculoskeletal, thoracicabdominal and vascular imaging. His active interests also include basic and technical areas for motion artifact correction techniques and flow assessment. He is the author of over 60 review scientific abstracts.

In SMRI, Dr. Ehman has served as a member of the Basic Science Council (Clinical Applications) and co-chairman of the SMR Scientific Program in 1994.

Norbert J Pelc, ScD

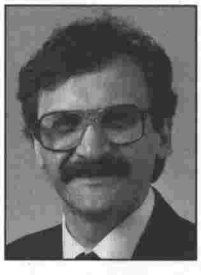

Dr. Pelc is Associate Professor of Radiology at Stanford University School of Medicine, Stanford, California. He received his BS in Applied Mathematic, Engineering and Physics at the University of Wisconsin, his MS in Medical Radiological Physics, Harvard University and ScD in Medical Radiological Physics, Harvard University with a dissertation topic entitled "A Generalized Filtered Backprojection Algorithm for Three Dimensional Reconstruction". Prior to coming to Stanford, Dr. Pelc has served as Senior Physicist and Manager of the Applied Science Laboratory at GE Medical Systems; Assistant Clinical Professor at the Department of Radiology, Medical College of Wisconsin; Visiting Professor at the Department of Biomedical Engineering at Duke University; Research Assistant at Massachusetts General Hospital Physics Research Laboratory; and, Research Assistant, University of Wisconsin Bone Mineral Laboratory.

He is active in the SMRM and AAPM. He is the author of numerous scientific articles and scientific abstracts in the area of image acquisition and reconstruction. Dr. Pelc has served as Scientific Program co-chairman of the SMRI.

Ronald R Price, PhD

Dr. Price is Professor and Director of the Division of Radiological Sciences, Department of Radiology and Radiological Sciences, Vanderbilt University Medical Center in Nashville. He received his PhD in Physics and Astronomy at Vanderbilt University. Dr. Price's background and experience include Associate Professor of Physics, Department of Physics and Astronomy, Vanderbilt University; Associate Professor of Radiology at Vanderbilt; Assistant Professor of Radiology, Instructor and Associate in the Division of Nuclear Medicine and Biophysics, Department of Radiology, Division of Nuclear Medicine and Biophysics, Department of Radiology, Vanderbilt.

Dr. Price's research interests include MRI quality assurance and quantitative methods for measuring tissue blood flow and diffusion using rapid MR Imaging. He is co-editor of 2 books on MRI and author of over 100 articles, 68 technical reports and over 100 abstracts.

He has served as a member of the SMRI Board of Directors; co-chairman of the Scientific Program Committee; co-chairman of the Educational Program Committee; on the Editorial Board of the Journal of Magnetic Resonance Imaging; Educational Program faculty, and a moderator at past Annual Meetings.

Stephen J Riederer, PhD

Dr. Riederer is Professor of Diagnostic Radiology and Director of the MR Laboratory at the Mayo Clinic in Rochester, MN. He received his BA and PhD from the University of Wisconsin - Madison. He previously was a faculty member of the Departments of Radiology and Biomedical Engineering at Duke University.

Dr. Riederer has been active in medical imaging for 20 years. In MRI he has made contributions to fast scan techniques including initial demonstration of vascular imaging with breath-hold acquisition times, recognition of the importance of the central phase encodings and development of the centric view order, interleaved echo-planar imaging, and continuous real-time imaging or "MR Fluoroscopy". He has applied many of these methods to abdominal MRI. He serves on the Editorial Boards of several journals, is a former member of the NIH Diagnostic Radiology Study Section, and has served as major advisor to over ten PhD students.

He has served the SMRI in several positions and is currently President of SMRI and President-Elect of the SMR.

Jeffrey S Ross, MD

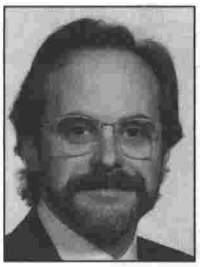

Dr. Ross is the Director of MRI, staff neuroradiologist at the Cleveland Clinic Foundation, and staff neuroradiologist at Lakewood Hospital in Lakewood, Ohio. He received his BS in Biology at the University of Akron and his MD at the Medical College of Ohio at Toledo. He serves as Assistant Professor of Radiology, Case Western Reserve University, staff neuroradiologist at University Hospitals of Cleveland, consultant radiologist at the Veterans Administration Medical Center at Wade Park Unit, Cleveland, and Assistant Clinical Professor of Radiology, University Hospitals of Cleveland.

Dr. Ross' research interests include MR imaging and correlated clinical evaluation of lumbar herniations and their natural history; prevention of postoperative peridural fibrosis and related symptoms following lumbar disc surgery evaluated with enhanced MR; and optimization of intracranial MR angiography and 3D imaging of the cervical spine. He has authored 70 referred publications, 29 technical publications, 15 book chapters, 1 book, 12 exhibits, and 83 scientific abstracts.

Dr. Ross has served as SMRI Education Program co-chairman and Scientific Program co-chairman. Also, Dr. Ross has served co-chairman for the SMRI Scientific and Educational Programs and on the SMRI Board of Directors.

Stephen R Thomas, PhD

Dr. Thomas is Professor of Radiology at the University of Cincinnati College of Medicine; Director of the Division of Medical Physics of the department of Radiology at the University of Cincinnati; and Adjunct Professor of Physics at the University of Cincinnati. He is also a member of the medical and dental staff at Children's Hospital Medical Center in Cincinnati. He received his BA in Physics at Williams College, Williamstown, Massachusetts, and MS in Physics and a PhD in Solid State Physics from Purdue University, West Lafayette, Indiana. His experience prior to joing the faculty of the University of Cincinnati in 1975 includes US Peace Corps in Ghana, West Africa; Assistant Professor of Physics at Kentucky Wesleyan College, Owensboro, Kentucky; and post doctoral fellow in Medical Physics at the University of Cincinnati.

Dr. Thomas' active interests include F-19 NMR in biomedical research with an emphasis on utilizing perfluorocarbon blood substitute materials as a monitor of pO_2 in vivo, and hardware and software component optimization for low field MRI systems. He is co-author of 78 scientific papers, 85 published abstracts, 19 book chapters, and is co-editor of 3 books. Dr. Thomas has served as SMRI AD Hoc ACCME Committee co-chair, Secretary, Basic Science Council chairman, Board of Directors member, faculty of the 8th and 9th Annual Meetings, abstract reviewer and moderator, as well as a member of the membership committee and founding JMRI Editorial Board member where he currently serves as a reviewer.

Stuart W Young, MD

Dr. Young is an Associate Professor and Director of MR Contrast Media Laboratory in the Department of Radiology at Stanford University Medical Center. He received his BA degree from DePauw University. He received his MD from Indiana University School of Medicine and an MBA from Stanford University. His experience includes Sloan Fellow at the Stanford School of Business, NIH Fellow and Cardiovascular Fellow in the Department of Radiology at Peter Bent Brigham and Women's Hospital and Harvard Medical School. He was a Naval Commander (Medical Research), intern and resident in Medicine in New York and Sloan Kettering Memorial Hospitals and a Ford Foundation Fellow.

Dr. Young has been the author of over 100 publications and patents, 87 abstracts, 10 scientific exhibits and 4 books. His current research interests include the application and development of targetable and tissue specific contrast agents. He has served on the NMR Directorate for the Stanford NMR Center and is currently interested in the economic aspects of the diffusion and operation of MRI technology.

In the SMRI, he served on the Board of Directors as chairman of the Reimbursement Committee, the Corporate Council, Program co-chairman of the MRI Economics Symposium, and moderator and participant in the post-graduate course, Evening Tutorial and Scientific Program.

Accreditation for Category I

The First Meeting of the Society of Magnetic Resonance (SMR) is accredited by the Society for Magnetic Resonance Imaging (SMRI) as providing continuing medical education for physicians. The Society for Magnetic Resonance Imaging (SMRI) is accredited by the Accreditation Council of Continuing Medical Education to sponsor Continuing Medical Education of Physicians.

The Society for Magnetic Resonance Imaging (SMRI) designates this continuing medical education activity of the Society of Magnetic Resonance (SMR) for a maximum of 36.5 credit hours in Category 1 of the Physician's Recognition Award of the American Medical Association (see Attendance Record below for accreditation procedures).

Accreditation for ECE

Technologists will receive 1994 SMRT Annual Meeting accreditation forms upon registering. Upon completion of the AnnualMeeting, return forms to the SMR Registration Desk located in the Chantilly Ballroom Foyer, Lobby Level. A record of these attendance forms will be forwarded to the ASRT for accreditation. Immediately following the SMRT Annual Meeting, a Certificate of Attendance will be forwarded to each attendee by the SMRT.

Announcement Board

An area is set aside in the Registration Area for posting announcements of future meetings and seminars and for publicizing events during the SMR Meeting. Announcements may not be larger than 8 1/2 x 11 inches.

Attendance Record

Personalized bar codes for use in tabulating individual CME credit will be distributed with registration credentials. Evaluation/CME Attendance Forms will be distributed at the beginning of each session; at the conclusion of each session, attendees are instructed to return completed Evaluation Forms (to which a personalized bar code is affixed so that CME credit may be received) to a Deposit Box located outside of each meeting room. Evaluations will be tabulated for use in future meeting planning while CME credits will be tabulated and forwarded to the Society for Magnetic Resonance Imaging (SMRI) to register each attendee's credit hours. **Please note**: the above instructions must be followed to receive CME credit.

Bank

The Loews Anatole Hotel will exchange foreign currency, cash guest's personal checks up to $150 per day and cash guest's traveler's checks up to $100 per day at no charge at the Front Desk. An automated teller machine (ATM) and Currency Exchange is available at Bank One, three blocks north of the hotel on Market Center Boulevard.

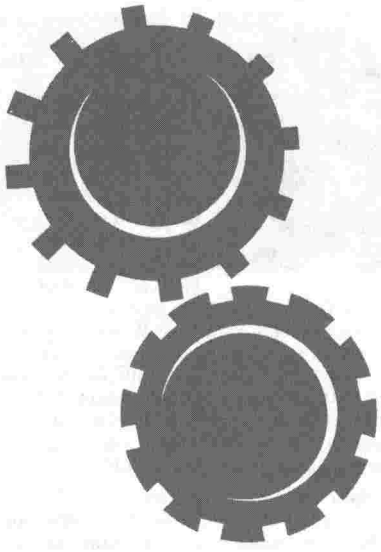

Business Center

The hotel Business Center, located on the Lobby Level between the Tower Convention Registration Desk and the Chantilly Ballroom (Hotel Guest Extension 7820), offers the following services: photocopying, FAX transmissions, Express Mail, DHL Worldwide Express, Federal Express (priority and economy), word processing and typing. The Business Center is open daily 7:00AM-11:00 PM.

Emergency Information

In case of an emergency, please contact the hotel Assistant Manager on any house telephone at extension 111.

Food Service

Complimentary pre-session coffee service is available in the Registration Area, 6:30 AM-7:30 AM. In addition, complimentary coffee breaks and luncheon service will be provided daily. Saturday's morning coffee and luncheon service and afternoon soda breaks will be provided in the Chantilly West Ballroom. Thereafter, all breaks will be in the Technical Exhibits Area. Please refer to the following **"Walk Through SMR '94"** for specific service schedules.

Job Bulletin

Technologist job listings may be posted in SMRT booth #507, the booth of the Combined Section of Magnetic Resonance Technologist (SMRT). All other job listings may be posted on the Job Bulletin Board in the Registration Area. Posted materials regarding positions available and positions sought may not exceed 8 1/2 x 11 inches.

Lost and Found

Lost and Found articles will be given to the Hotel Security service for safe-keeping. Please contact the Security Office on any house telephone at extension 7347.

Message Center

A Message Center Board is located in the Registration Area for posting messages during the SMR Annual Meeting. Notepads and pencils will be available for message deposit and retrieval.

Post Office

A stamp machine and mailbox are located in Atrium One, Lobby Level.

Presenters of Papers

- **Last minute concerns** about a presentation, call the SMR Central Office (Chicago location) at (312)751-2590 before March 2. After this date, call the Loews Anatole Hotel/SMR Registration area at 214/748-1200.

- **Contact authors** of abstracts listed in the Printed Program by writing to the SMR Central Office (Chicago location) at 213 West Institute Place, Suite 501, Chicago, Illinois, 60610. Requests will be forwarded to the author.

- **The Slide Preview Room** is located in the Coral Room, Lobby Level. The hours are as follows:

Saturday-Tuesday	6:30 AM - 6:00 PM
Wednesday	6:30 AM - 3:30 PM

Press Room

A Press Room will be located in the Ming Room, Mezzanine Level. Questions may be directed to Al Salerno 214/748-1200, Hotel Extension 5566. Press Room hours are as follows:

Friday-Wednesday 7:00 AM - 6:00 PM

Printed Program: A How To Guide

This Program contains a complete listing, with abstracts, of all scientific courses, sessions, and exhibits. Material is organized by category (Plenary Symposia, Proffered Papers, Scientific Poster Exhibits, etc.) and ordered chronologically within each category.

The Sections and Symbols throughout these pages are guides to locate information. Beginning with Plenary Symposia and continuing with Indices and Information, each section is preceded by a divider page. Please review the text on each divider page for important information and announcements relating to that section.

General Meeting Information

A designates an Award presentation. The Awards Ceremony will be held in the Chantilly West Ballroom, Lobby Level, Monday 8:00 AM-8:45 AM.

EP designates an Educational Session. Educational Program material will be distributed on-site to Educational Program attendees. The Educational Program will be presented in the Chantilly East Ballroom on Saturday and Sunday and the Wedgwood Ballroom on Monday.

P designates a Poster Scientific Paper. Poster Papers will be presented in the Poster Exhibit Area, located in the Trinity Exhibit Hall. Posters will be on display Sunday - Wednesday.

PS designates a Scientific Program Plenary Symposia. Plenary Symposia will be presented in the Chantilly West Ballroom.

Registration

All meeting registration will take place in the Chantilly Ballroom Foyer, located on the Lobby Level of the Loews Anatole Hotel, according to the following schedule:

Friday	2:00 PM - 6:00 PM
Saturday	6:30 AM - 5:00 PM
Sunday	7:00 AM - 6:00 PM
Monday	6:00 AM - 6:30 PM
Tuesday	6:00 AM - 6:00 PM
Wednesday	6:00 AM - 3:30 PM

Registration Entitlements

In completing the Registration Form, please use the following guide to select a Program to attend:

Educational Program

Entitled to attend the Educational Program (including the Economics Symposia) or SMRT Annual Meeting. Those wishing to attend only the Economics Symposia may register on-site.

Scientific Program

Entitled to attend the Scientific Program (including the MRI in a Quality and Cost-Conscious Environment Topical Conference and Morning Tutorial Program).

Scientific/Educational Program

Entitled to attend both Educational and Scientific Programs.

Schedule of Events

For alumni groups and other SMR-affiliated committees and organizations who have made meeting arrangements through the SMR Central Office (Chicago location), a schedule of events is available for review at the Registration Desk, Chantilly Ballroom Foyer, Lobby Level of the Loews Anatole Hotel.

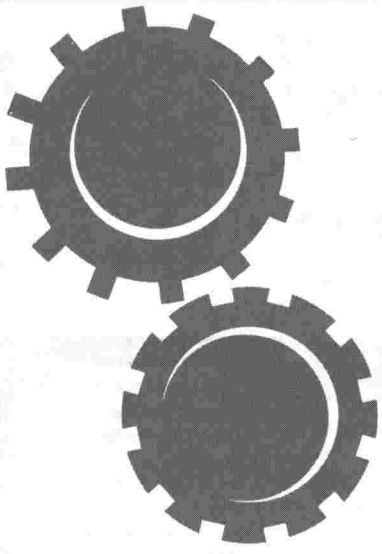

Scientific Poster Exhibit Hours

Scientific Poster Exhibits are located in the Trinity Exhibit Hall of the Loews Anatole Hotel. Exhibit hours are:

Sunday-Tuesday	8:00 AM - 8:00 PM
Wednesday	8:00 AM - 1:00 PM

SMR Membership Services

Membership applications will be available at the Registration Desk, Chantilly Ballroom Foyer, Lobby Level, for all non-member attendees wishing to join the Society. Due to the review process required, membership applications may not be approved on-site. However, you will be notified of your acceptance within six weeks following the Annual Meeting. Membership inquiries by current members may also be addressed at the Registration Desk.

SMR Business Meeting

All SMR members are encouraged to attend the Annual Business Meeting of the Society to be held Monday 10:15 AM-10:45 AM in the Chantilly West Ballroom.

SMR Publications

For subscription or manuscript information regarding the Journal of Magnetic Resonance Imaging (JMRI) or Magnetic Resonance in Medicine (MRM), visit booth #507 in the Technical Exhibits Area. Manuscripts for submission to JMRI may be submitted to the booth or forwarded to Gary D. Fullerton, PhD, JMRI Editor, University of Texas Health Science Center at San Antonio, Department of Radiology, 7703 Floyd Curl Drive, San Antonio, Texas 78284-7800. Manuscripts for submission to MRM may be submitted to the booth or forwarded to Felix W. Wehrli, PhD, MRM Editor, Hospital of the University of Pennsylvania, Department of Radiology, 3400 Spruce Street, First Floor Silverstein, Philadelphia, Pennsylvania, 19104.

Social Program

The SMR cordially invites all attendees (single day registrants must visit the Social Program Desk to purchase tickets) to join in an evening of fellowship at the following receptions:

SMR Technical Exhibits Opening Reception
Technical Exhibits Area
Saturday 5:00 PM - 7:00 PM

SMRT Poster Exhibit Reception
Poster Exhibit Area
Saturday 7:00 PM - 9:00 PM

SMR Poster Exhibit Reception
Poster Exhibit Area
Sunday 5:30 PM - 7:30 PM

SMR Gala Reception
Chantilly East Ballroom
Monday 7:30 PM - 10:30 PM

A Social Program Desk will be staffed in the Registration Area for participants wishing to purchase tickets for accompanying guests.

Technical Exhibits

The SMR Technical Exhibits Program will display the latest in MR equipment, supplies, and services in the Trinity Exhibit Hall, beginning with a reception on Saturday from 5:00 PM to 7:00 PM. Thereafter, the exhibits will be on display Sunday through Tuesday, 9:30 AM to 4:00 PM, and Wednesday, 9:30 AM to 1:00 PM.

Who's Who—Official Badges

Badges are color-coded as follows:

Blue: Member SMR/SMRT

Red: Non-member

Green: Press/Accompanying Guests

Brown: Technical Exhibitors

SAT 3/5

❑ **6:30 AM - 5:00 PM**
General Registration

Educational Program

8:15 AM - 9:45 AM
Intro to MRI Techniques in the CNS
- ❑ Image Contrast: Basic Factors
- ❑ Techniques for Mid & Low Field Neuro MRI
- ❑ Contrast Agents in CNS

9:45 AM - 10:15 AM
Break

10:15 AM - 12:15 PM
Stroke: Techniques & Diagnosis
- ❑ Gradient Echo Techniques for the CNS
- ❑ MRA of the CNS
- ❑ MRI of Cerebrovascular Disease
- ❑ CNS Hemorrhage

12:15 PM - 1:45 PM
Lunch

1:45 PM - 3:15 PM
Spine
- ❑ Optimizing Hybrid-RARE (Turbo-Spin Echo) for the CNS
- ❑ Degenerative Spine Disease
- ❑ Spine Tumors

3:15 PM - 3:45 PM
Break

3:45 PM - 5:15 PM
Brain
- ❑ Brain Tumors
- ❑ Periventricular and White Matter Disease
- ❑ CNS Infections

SMR TECHNICAL EXHIBITS RECEPTION
5:00 PM - 7:00 PM

SMRT Annual Meeting

7:00 AM - 7:45 AM
- ❑ k-Space for Technologists

8:00 AM - 9:30 AM
- ❑ MRI Safety
- ❑ *Proffered Papers*
- ❑ Virtual Reality and MRI
- ❑ *Proffered Papers*

9:30 AM - 10:00 AM
Break
SMRT Poster
Discussion Period

10:00 AM - 12:30 PM
- ❑ Proffered Papers
- ❑ MRI in Sports Medicine and Kinematics Applications
- ❑ Proffered Papers
- ❑ Tissue Suppression at High and Mid Field
- ❑ MRA/MTC in the Clinical Setting

12:30 PM - 1:30 PM
Lunch
SMRT Poster
Discussion Period

1:30 PM - 3:00 PM
Parallel Session
- ❑ Cardiac Tagging and Gating for Imaging of the Heart
- ❑ *Proffered Papers*

Parallel Session
- ❑ Breast Imaging: Current Understanding and Pitfalls
- ❑ *Proffered Papers*

3:00 PM - 3:30 PM
Break
SMRT Poster
Discussion Period

3:30 PM - 5:00 PM
Parallel Session
- ❑ Abdomen, Kidney, Liver, Spleen: What Makes a Good Exam?
- ❑ New Coil Technology
- ❑ Pediatric MRI

Parallel Session
- ❑ Fast Imaging: What Do All the Names Really Mean?
- ❑ MRI in Trauma Patients
- ❑ *Proffered Papers*

SMRT POSTER EXHIBIT RECEPTION
7:00 PM - 9:00 PM

SUN 3/6

❑ **7:00 AM - 6:00 PM**
General Registration

❑ **9:30 AM - 4:00 PM**
Technical Exhibits

❑ **8:00 AM - 8:00 PM**
Poster Sessions

Educational Program

8:15 AM - 10:15 AM
Abdomen & Pelvis
- ❑ Techniques for Body MRI
- ❑ Liver at Mid & High Fields
- ❑ Extra-Hepatic/Abdominal Uses of MRI Contrast Agents
- ❑ Gynecologic MRI

10:15 AM - 10:45 AM
Break

10:45 AM - 12:15 PM
Cardiovascular MR
- ❑ Cardiac & Chest
- ❑ Thoracic & Abdominal Aorta
- ❑ Body MRA: Peripheral Arteries & Veins

12:15 PM - 1:45 PM
Lunch
Scientific Poster
Discussion Period

1:45 PM - 3:15 PM
Lower Extremity
- ❑ Knee: Technical Considerations
- ❑ Knee: MRI Diagnosis
- ❑ Foot & Ankle

3:15 PM - 3:45 PM
Break

3:45 PM - 5:15 PM
Extremity/Other
- ❑ Shoulder
- ❑ Musculoskeletal Masses at Mid & High Fields
- ❑ Breast MRI: Clinical Update

5:15 PM - 5:30 PM
QUESTION & ANSWER SESSION

Scientific Program Topical Conference: MRI in a Quality and Cost-Conscious Environment

8:00 AM - 9:45 AM
Current Status of MRI: Resources, Applications & Research
- ❑ MRI Resources: A Global Inventory
- ❑ Perspectives on the Role of MRI in US Medicine
- ❑ Survey of Current Research Activity in MRI

9:45 AM - 10:15 AM
Break

10:15 AM - 12:00 PM
The Cost/Benefit Equation
- ❑ How Should the Benefits of an MRI Application be Assessed?
- ❑ How Much Should an MRI Examination Cost? Technical & Professional Components

12:00 PM - 1:30 PM
Lunch
Scientific Poster
Discussion Period

1:30 PM - 3:00 PM
Future MRI Technology
- ❑ Impact of Field Strength on Image Quality
- ❑ Magnetic Technology Update
- ❑ Gradient & RF Technology Update
- ❑ Panel: Future MR System Architectures

3:00 PM - 3:45 PM
Break

3:45 PM - 5:30 PM
- ❑ *Proffered Papers*

SMR POSTER RECEPTION
5:30 PM - 7:30 PM

SMRT Annual Meeting

8:00 AM - 12:00 PM
❑ ***Vendor Workshops***

General Electric Medical Systems, Inc.

Hitachi Medical Systems America, Inc.

Siemens Medical Systems, Inc.

Toshiba Medical Systems, Inc.

12:00 PM - 1:00 PM
Lunch
SMRT Poster
Discussion Period

1:00 PM - 3:00 PM
- ❑ Cardiac Flow
- ❑ Proffered Papers
- ❑ Clinton Health Care

3:00 PM - 3:15 PM
Break
SMRT Poster
Discussion Period

3:15 PM - 5:30 PM
- ❑ Proffered Papers
- ❑ ECE Update and Board Certification
- ❑ SMRT Business Meeting

MON 3/7

- ❑ **6:00 AM - 6:30 PM**
  General Registration
- ❑ **9:30 AM - 4:00 PM**
  Technical Exhibits
- ❑ **8:00 AM - 8:00 PM**
  Poster Sessions

Educational Program
Topical Conference: MRI Economics Symposium

8:00 AM - 10:15 AM
- ❑ MRI & the Overestimation of Disease
- ❑ Economic Implications of MRA
- ❑ Turf Issues in Cardiac MRI and Other Cardiac Imaging

10:15 AM - 10:45 AM
Break

- ❑ *SMR Business Meeting*
  Chantilly Ballroom

10:45 AM - 12:30 PM
- ❑ NIH Contrast Media Economics Consensus Conference–Implications for MRI Economics
- ❑ MRI: Technologic Change & the Timing of Technology Assessment

12:30 PM - 1:30 PM
Lunch
Scientific Poster Discussion Period

1:30 PM - 3:00 PM
- ❑ Beating the Competition, Cutting to the Bone on Price
- ❑ Managed Imaging: Contracting with Payors for Imaging Services

3:00 PM - 3:45 PM
Break

3:45 PM - 5:30 PM
- ❑ MR Diffusion in a Controlled Environment: The One Payor System & the Role of the MD in a Single Payor System
- ❑ Dealing with Uncertainty in MR

Scientific Program
Morning Tutorial

6:45 AM - 7:45 AM
- ❑ k-Space and Pulse Sequences
- ❑ Basic Clinical Interpretation for Physicists: CNS
- ❑ MRI of the Ankle

Scientific Program

8:00 AM - 8:45 AM
- ❑ Awards Presentation

8:45 AM - 10:15 AM
Fast Scan MRI
- ❑ Impact of Fast Scan Methods in Neuro MRI: Past, Present & Future
- ❑ Impact of Fast Scan Methods in Body MRI: Past, Present & Future
- ❑ Interventional MRI

10:15 AM - 10:45 AM
Break
SMR Business Meeting
Chantilly Room

10:45 AM - 12:30 PM
MRI of the Abdomen & Pelvis
- ❑ Gynecologic Malignancies of the Pelvis: Role of MRI–Clinician's & Radiologist's Perspective
- ❑ Panel Debate: Will MRI Replace CT for Upper Abdominal Imaging

12:30 PM - 1:30 PM
Lunch
Scientific Poster Discussion Period

1:30 PM - 3:00 PM
Neurological MRI
- ❑ Outcomes Research, Appropriateness & Pragmatism in Neuro MRI
- ❑ Clinical Applications of 3D Neuro MRI
- ❑ High vs. Low Field: The Debate Goes On

3:00 PM - 3:45 PM
Break

3:45 PM - 5:30 PM
- ❑ *Proffered Paper*

SMR GALA RECEPTION
7:30 PM - 10:30 PM

TUE 3/8

- ❑ **6:00 AM - 6:00 PM**
  General Registration
- ❑ **9:30 AM - 4:00 PM**
  Technical Exhibits
- ❑ **8:00 AM - 8:00 PM**
  Poster Sessions

Scientific Program:
Morning Tutorial

6:45 AM - 7:45 AM
- ❑ Understanding Gadolinium Contrast: Safety, Biodistribution, CNS Applications
- ❑ Basic Clinical Interpretation for Physicists: Outside the CNS
- ❑ MR Angiography

Scientific Program

8:00 AM - 9:30 AM
Update on Functional MRI
- ❑ Biophysical & Technical Basis for Functional MRI
- ❑ Potential Clinical Impact of Functional Neuroimaging
- ❑ Panel: Diverse Modalities for Functional Neuroimaging

9:30 AM - 10:30 AM
Break

10:30 AM - 12:15 PM
- ❑ *Proffered Papers*

12:15 PM - 1:30 PM
Lunch
Scientific Poster Discussion Period

1:30 PM - 3:00 PM
Musculoskeletal MRI
- ❑ Musculoskeletal Masses: Role of MRI
- ❑ Musculoskeletal Injuries: New Lessons for MRI
- ❑ Musculoskeletal MRI: Framework for Determining Cost Effectiveness

3:00 PM - 3:45 PM
Break

3:45 PM - 5:30 PM
- ❑ *Proffered Papers*

WED 3/9

- ❑ **6:00 AM - 3:30 PM**
  General Registration
- ❑ **9:30 AM - 1:00 PM**
  Technical Exhibits
- ❑ **8:00 AM - 1:00 PM**
  Poster Sessions

Scientific Program:
Morning Tutorial

6:45 AM - 7:45 AM
- ❑ Clinical Applications of Spectroscopy
- ❑ Fast Abdominal Imaging
- ❑ Flow Quantitation: Techniques & Applications

Scientific Program

8:00 AM - 9:30 AM
Cardiovascular MRI
- ❑ Cardiovascular Imaging Techniques: An Update
- ❑ Impact of MR Vascular Techniques in Clinical Practice
- ❑ Current Role of MRI in the Management of Cardiac Patients

9:30 AM - 10:30 AM
Break

10:30 AM - 12:15 PM
- ❑ *Proffered Papers*

12:15 PM - 1:00 PM
Lunch
Scientific Poster Discussion Period

1:00 PM - 2:30 PM
MRI of the Breast
- ❑ MR Evaluation of Breast Cancer: Specificity Issues
- ❑ Breast Cancer Staging
- ❑ MR Evaluation of Silicone Breast Implants

2:30 PM - 2:45 PM
Break

2:45 PM - 4:30 PM
- ❑ *Proffered Papers*

1994 SMRT Educational Program

SAT3/5

WEDGWOOD ROOM

7:00 AM - 7:45 AM
k-Space for Technologists
W Faulkner, BSRT

7:45 AM - 8:05 AM *Coffee Break*

8:05 AM - 8:30 AM
MRI Safety
F G Shellock, PhD

8:30 AM - 8:50 AM *Proffered Papers*

8:50 AM - 9:20 AM
Virtual Reality and MRI
R Kikinis, MD

9:20 AM - 9:30 AM *Proffered Papers*

9:30 AM - 10:00 AM *Coffee Break*

10:00 AM - 10:30 AM *Proffered Papers*

10:30 AM - 11:20 AM
MRI in Sports Medicine and Kinematics Applications
C Ho, MD

11:20 AM - 11:30 AM *Proffered Papers*

11:30 AM - 12:00 PM
Tissue Suppression at High and Mid Field
W G Bradley, Jr, MD, PhD

12:00 PM - 12:30 PM
MRA/MTC in the Clinical Setting
D Jarvis, RT

12:30 PM - 1:30 PM *Lunch*

GOVERNORS ROOM

1:30 PM - 2:15 PM
Cardiac Tagging and Gating for Imaging of the Heart
W Rogers, RT

2:15 PM - 3:00 PM
Proffered Papers

3:00 PM - 3:30 PM
Coffee Break

3:30 PM - 4:00 PM
Abdomen, Kidney, Liver, Spleen: What makes a good exam?
P Woodward, MD
B King, RT

4:00 PM - 4:30 PM
New Coil Technology
J Strandt, RT

4:30PM - 5:00PM
Pediatric MRI
R A Zimmerman, MD

SENATORS ROOM

1:30 PM - 2:15 PM
Breast Imaging: Current Understanding and Pitfalls
S E Harms, MD

2:15 PM - 3:00 PM
Proffered Papers

3:00 PM - 3:30 PM
Coffee Break

3:30 PM - 4:00 PM
Fast Imaging: What Do All the Names Really Mean?
G Wheeler, RT

4:00 PM - 4:30 PM
MRI of Trauma Patients
B Harte, MD

4:30 PM - 5:00 PM
Proffered Papers

SUN3/6

PARALLEL VENDOR WORKSHOPS

8:00 AM - 12:00 PM

MONET ROOM
General Electric Medical Systems, Inc.

METROPOLITAN ROOM
Hitachi Medical Systems America, Inc.

MIRO ROOM
Siemens Medical Systems, Inc.

MORROCCO ROOM
Toshiba America Medical Systems, Inc.

12:00 PM - 1:00 PM *Lunch*

WEDGWOOD ROOM

1:00 PM - 1:30 PM
Cardiac Flow
A Sawyer, RT

1:30 PM - 2:00 PM *Proffered Papers*

2:00 PM - 3:00 PM
Clinton Health Care
C Booth, JD

3:00 PM - 3:15 PM *Coffee Break*

3:15 PM - 3:55 PM *Proffered Papers*

3:55 PM - 4:30 PM
ECE Update and Board Certification
L Culbreth, MEd

4:30 PM - 5:30 PM
SMRT Business Meeting

SOCIETY OF MAGNETIC RESONANCE IN MEDICINE • SOCIETY FOR MAGNETIC RESONANCE IMAGING •
S M R T

SAT3/5

CHANTILLY EAST

CNS: INTRO TO MRI TECHNIQUES
Moderator: ***G C Hurst, MD***

8:15 AM - 8:45 AM
Image Contrast: Basic Factors
G C Hurst, MD

8:45 AM - 9:15 AM
Techniques for Mid/Low Field Neuro MRI
M A Solomon, MD

9:15 AM - 9:45 AM
Contrast Agents in CNS
W T C Yuh, MD, MSEE

9:45 AM - 10:15 AM *Coffee Break*

STROKE: TECHNIQUES AND DIAGNOSIS
Moderator: ***T J Masaryk, MD***

10:15 AM - 10:45 AM
Gradient Echo Techniques for the CNS
E K Fram, MD

10:45 AM - 11:15 AM
MRA of the CNS
R R Edelman, MD

11:15 AM - 11:45 AM
MRI of Cerebrovascular Disease
R N Bryan, MD

11:45 AM - 12:15 PM
CNS Hemorrhage
K R Thulborn, MD

12:15 PM - 1:45 PM *Lunch*

SPINE
Moderator: ***J S Ross, MD***

1:45 PM - 2:15 PM
Optimizing Hybrid-RARE for the CNS
G K Sze, MD

2:15 PM - 2:45 PM
Degenerative Spine Disease
J S Ross, MD

2:45 PM - 3:15 PM
Spine Tumors
D R Enzmann, MD

3:15 PM - 3:45 PM *Coffee Break*

BRAIN
Moderator: ***M N Brant-Zawadzki, MD***

3:45 PM - 4:15 PM
Brain Tumors
M N Brant-Zawadzki, MD

4:15 PM - 4:45 PM
Periventricular & White Matter Disease
W G Bradley, Jr, MD, PhD

4:45 PM - 5:15 PM
CNS Infections
J R Jinkins, MD

SUN3/6

CHANTILLY EAST

ABDOMEN AND PELVIS
Moderator: ***D G Mitchell, MD***

8:15 AM - 8:45 AM
Techniques for Body MRI
D G Mitchell, MD

8:45 AM - 9:15 AM
Liver at Mid and High Fields
D D Stark, MD

9:15 AM - 9:45 AM
Extra-Hepatic/Abdominal Uses of MRI Contrast Agents
R Semelka, MD

9:45 AM - 10:15 AM
Gynecologic MRI
L M Scoutt, MD

10:15 AM - 10:45 AM *Coffee Break*

CARDIOVASCULAR MR
Moderator: ***K M Link, MD***

10:45 AM - 11:15 AM
Cardiac and Chest
E A Zerhouni, MD

11:15 AM - 11:45 AM
Thoracic and Abdominal Aorta
K M Link, MD

11:45 AM - 12:15 PM
Body MRA: Peripheral Arteries and Veins
C E Spritzer, MD

12:15 PM - 1:45 PM *Lunch*

LOWER EXTREMITY
Moderator: ***J H Mink, MD***

1:45 PM - 2:15 PM
Knee: Technical Considerations
M P Recht, MD

2:15 PM - 2:45 PM
Knee: MR Imaging Diagnosis
J H Mink, MD

2:45 PM - 3:15 PM
Foot and Ankle
M E Schweitzer, MD

3:15 PM - 3:45 PM *Coffee Break*

EXTREMITY/OTHER
Moderator: ***P T Weatherall, MD***

3:45 PM - 4:15 PM
Shoulder
L S Steinbach, MD

4:15 PM - 4:45 PM
Musculoskeletal Masses at Mid and High Fields
P T Weatherall, MD

4:45 PM - 5:15 PM
Breast MRI: Clinical Update
C W Piccoli, MD

MON3/7

WEDGWOOD ROOM

EDUCATIONAL PROGRAM TOPICAL CONFERENCE: ECONOMICS SYMPOSIUM
Moderators: ***H L Abrams, MD***
S W Young, MD

8:00 AM - 8:45 AM
MRI and the Overestimation of Disease
W C Black, MD

8:45 AM - 9:30 AM
The Economic Implications of MR Angiography
S Baum, MD

9:30 AM - 10:15 AM
Turf Issues in Cardiac MRI and Other Cardiac Imaging
D C Levin, MD

10:15 AM - 10:45 AM *Coffee Break*

SMR Business Meeting:
Chantilly Ballroom

10:45 AM - 11:30 AM
NIH Contrast Medical Economics Consensus Conference - Implications for MRI Economics
F Shtern, MD

11:30 AM - 12:30 PM
MRI: Technologic Change & the Timing of Technology Assessment
H L Abrams, MD

12:30 PM - 1:30 PM *Lunch*

1:30 PM - 2:15 PM
Beating the Competition, Cutting to the Bone on Price
E J Potchen, MD

2:15 PM - 3:00 PM
Managed Imaging: Contracting with Payors for Imaging Services
P E Berger, MD

3:00 PM - 3:45 PM *Coffee Break*

3:45 PM - 4:45 PM
MR Diffusion in a Controlled Environ-ment: The One Payor System & the Role of the MD in a Single Payor System
D W MacEwan, MD

4:45 PM - 5:30 PM
Dealing with Uncertainty in Magnetic Resonance
S W Young, MD

SUN3/6

SCIENTIFIC PROGRAM: CHANTILLY WEST

TOPICAL CONFERENCE:
MRI IN A QUALITY AND COST-CONSCIOUS ENVIRONMENT

CURRENT STATUS OF MRI: RESOURCES, APPLICATIONS & RESEARCH
Moderator: ***R L Ehman, MD***

8:00 AM - 8:35 AM
MRI Resources: A Global Inventory
T Miller, PhD

8:35 AM - 9:10 AM
Perspectives on the Role of MRI in US Medicine
H Y Kressel, MD

9:10 AM - 9:45 AM
Survey of Current Research Activity in MRI
W R Brody, MD, PhD

9:45 AM - 10:15 AM *Coffee Break*

THE COST/BENEFIT EQUATION
Moderator: ***S W Young, MD***

10:15 AM - 11:00 AM
How Should the Benefits of an MRI Application Be Assessed?
E P Steinberg, MD, MPP

11:00 AM - 11:20 AM
How Much Should an MRI Examination Cost?
Technical Component
R A Bell, PhD

11:20 AM - 11:50 AM
How Much Should an MRI Examination Cost?
Professional Component
S W Young, MD

11:50 AM - 12:00 PM *Questions and Answers*

12:00 PM - 1:30 PM *Lunch*

MRI TECHNOLOGY: CHALLENGES & OPPORTUNITIES
Moderator: ***N J Pelc, ScD***

1:30 PM - 1:55 PM
Impact of Field Strength on Image Quality
B K Rutt, PhD

1:55 PM - 2:20 PM
Magnet Technology Update
G N Holland, M Phil

2:20 PM - 2:45 PM
Gradient and RF Technology Update
R E Kinsinger, PhD

2:45 PM - 3:15 PM
Panel: Future MR System Architectures
Session Faculty

3:15 PM - 3:45 PM *Coffee Break*

3:45 PM - 5:30 PM *Proffered Papers*

MON3/7

MORNING TUTORIAL PROGRAM

6:45 AM - 7:45 AM: MONET ROOM
k-space and Pulse Sequences
W Sattin, PhD

6:45 AM - 7:45 AM: METROPOLITAN ROOM
Basic Clinical Interpretation for Physicists: CNS
W Kucharczyk, MD

6:45 AM - 7:45 AM: MIRO ROOM
MRI of the Ankle
D Stoller, MD

SCIENTIFIC PROGRAM: CHANTILLY WEST

FAST SCAN MRI
Moderator: ***S J Riederer, PhD***

8:00 AM - 8:45 AM *Awards Presentation*

8:45 AM - 9:15 AM
Impact of Fast Scan Methods in Neuro MRI: Past, Present and Future
E K Fram, MD

9:15 AM - 9:45 AM
Impact of Fast Scan Methods in Body MRI: Past, Present and Future
S Saini, MD

9:45 AM - 10:15 AM
Interventional MRI
R B Lufkin, MD

10:15 AM - 10:45 AM *Coffee Break*

SMR Business Meeting: **Chantilly Ballroom**

MRI OF THE ABDOMEN & PELVIS
Moderator: ***J Heiken, MD***

10:45 AM - 11:15 AM
Gynecologic Malignancies of the Pelvis: Role of MRI/ Clinician's Perspective
J L Stern, MD

11:15 AM - 11:45 AM
Gynecologic Malignancies of the Pelvis: Role of MRI/Radiol-ogist's Perspective
H Hricak, MD

11:45 AM - 12:30 PM
Panel Debate: Will MRI Replace CT for Upper Abdominal Imaging?
J C Weinreb, MD, A J Megibow, MD

12:30 PM - 1:30 PM *Lunch*

NEUROLOGICAL MRI
Moderator: ***J S Ross, MD***

1:30 PM - 2:00 PM
Outcomes Research, Appropriateness & Pragmatism in Neuro MRI
M T Modic, MD

2:00 PM - 2:30 PM
Clinical Applications of 3D Neuro MRI
D N Levin, MD, PhD

2:30 PM - 3:00 PM
High vs. Low Field: The Debate Goes On
J V Zelch, MD , WG Bradley, Jr., MD, PhD

3:00 PM - 3:45 PM *Coffee Break*

3:45 PM - 5:30 PM *Proffered Papers*

TUE 3/8

MORNING TUTORIAL PROGRAM

6:45 AM - 7:45 AM MONET ROOM
Understanding Gadolinium
Contrast: Safety, Biodistribution, CNS Applications
E Kanal, MD

6:45 AM - 7:45 AM METROPOLITAN ROOM
Basic Clinical Interpretation
for Physicists: Outside the CNS
H Y Kressel, MD

6:45 AM - 7:45 AM MIRO ROOM
MR Angiography: Techniques & Applications
T M Grist, MD
C M Anderson, MD, PhD

SCIENTIFIC PROGRAM: CHANTILLY WEST

UPDATE ON FUNCTIONAL MRI
Moderator: ***C Jack, MD***

8:00 AM- 8:30 AM
Biophysical and Technical Basis for Functional MRI
M E Moseley, MD

8:30 AM - 9:00 AM
Potential Clinical Impact of Functional Neuroimaging
B R Rosen, MD

9:00 AM - 9:30 AM
Panel: Diverse Modalities for Functional Neuroimaging
A Evans, PhD, W W Orrison, Jr, MD
B R Rosen, MD, M E Moseley, MD

9:30 AM - 10:30 AM *Coffee Break*

10:30 AM - 12:15 PM *Proffered Papers*

12:15 PM - 1:30 PM *Lunch*

MUSCULOSKELETAL MRI
Moderator: ***J V Crues III, MD***

1:30 PM - 2:00 PM
Musculoskeletal Masses: Role of MRI
R A McLeod, MD

2:00 PM - 2:30 PM
Musculoskeletal Injuries: New Lessons from MRI
P J Tirman, MD

2:30 PM - 3:00 PM
Musculoskeletal MRI: Framework for Determining Cost Effectiveness
J V Crues III, MD

3:00 PM - 3:45 PM *Coffee Break*

3:45 PM - 5:30 PM *Proffered Papers*

WED 3/9

MORNING TUTORIAL PROGRAM

6:45 AM - 7:45 AM MONET ROOM
Clinical Applications of Spectroscopy
B Ross, MD, PhD

6:45 AM - 7:45 AM METROPOLITAN ROOM
Fast Abdominal Imaging: Pulse Sequences & Applications
J R Brookeman, PhD
E E De Lange, MD

6:45 AM - 7:45 AM MIRO ROOM
Quantification and Velocity Imaging
B K Rutt, PhD
P A Turski, MD

SCIENTIFIC PROGRAM: CHANTILLY WEST

CARDIOVASCULAR MRI
Moderator: ***R D White, MD***

8:00 AM - 8:30 AM
Cardiovascular Imaging Techniques: An Update
D L Parker, PhD

8:30 AM - 9:00 AM
Impact of MR Vascular Techniques in Clinical Practice
C E Spritzer, MD

9:00 AM - 9:30 AM
Current Role of MRI in the Management of Cardiac Patients
R D White, MD

9:30 AM - 10:30 AM *Coffee Break*

10:30 AM - 12:15 PM *Proffered Papers*

12:15 PM - 1:00 PM *Lunch*

MRI OF THE BREAST
Moderator: ***S E Harms, MD***

1:00 PM - 1:30 PM
MR Evaluation of Breast Cancer: Specificity Issues
M D Schnall, MD

1:30 PM - 2:00 PM
Breast Cancer Staging
S E Harms, MD

2:00 PM - 2:30 PM
MR Evaluation of Silicone Breast Implants
D P Gorczyna, MD

2:30 PM - 2:45 PM *Coffee Break*

2:45 PM - 4:30 PM *Proffered Papers*

1994 SMR Proffered Papers

SUN PM
3/6

Monet Room	**Metropolitan Room**	**Miro Room**	**Morrocco Room**	**Sapphire Room**
Papers 001-008	Papers 011-017	Papers 021-027	Papers 031-037	**Papers 041-047**
RAPID IMAGING	***INTERVENTIONAL MR***	***BRAIN I (GENERAL)***	***UPPER ABDOMEN I (HEPATIC, FAST)***	***FLOW QUANTITATION***
Moderators:	Moderators:	Moderators:	Moderators:	Moderators:
S Patz, MD	***R Kikinis, MD***	***R B Dietrich, MD***	***J P Mugler III, PhD***	***R B Buxton, PhD***
J Pauly, PhD	***R B Lufkin, MD***	***J S Ross, MD***	***P T Weatherall, MD***	***D Saloner, PhD***
001 **3:45 PM**	011 **3:45 PM**	021 **3:45 PM**	031 **3:45 PM**	041 **3:45 PM**
002 **3:57 PM**	012 **3:57 PM**	022 **3:57 PM**	032 **3:57 PM**	042 **3:57 PM**
003 **4:09 PM**	013 **4:09 PM**	023 **4:09 PM**	033 **4:09 PM**	043 **4:09 PM**
004 **4:21 PM**	014 **4:21 PM**	024 **4:21 PM**	034 **4:21 PM**	044 **4:21 PM**
005 **4:33 PM**	015 **4:33 PM**	025 **4:33 PM**	035 **4:33 PM**	045 **4:33 PM**
006 **4:45 PM**	016 **4:45 PM**	026 **4:45 PM**	036 **4:45 PM**	046 **4:45 PM**
007 **4:57 PM**	017 **4:57 PM**	027 **4:57 PM**	037 **4:57 PM**	047 **4:57 PM**
008 **5:09 PM**				

1994 SMR Proffered Papers

MON PM
3/7

Monet Room	**Metropolitan Room**	**Miro Room**	**Morrocco Room**	**Sapphire Room**	**Topaz Room**
Papers 101-107	Papers 111-116	Papers 121-126	Papers 131-137	Papers 141-147	Papers 151-156
CONTRAST AGENTS I	***BRAIN II (RAPID IMAGING)***	***PELVIS (FEMALE)***	***CARDIAC***	***SPECTROSCOPY I (TECHNIQUES)***	***IMAGING TECHNIQUES I***
Moderators:	Moderators:	Moderators:	Moderators:	Moderators:	Moderators:
R L Nunnally, PhD	***R L De La Paz,MD***	***J J Brown, MD***	***B Chen, MD***	***H C Charles, MD***	***C R Crawford, PhD***
D D Stark, MD	***F J Laine, MD***	***R C Smith, MD***	***E R McVeigh, MD***	***P A Narayana, PhD***	***J Listerud, MD, PhD***
101 **3:45 PM**	111 **3:45 PM**	121 **3:45 PM**	131 **3:45 PM**	141 **3:45 PM**	151 **3:45 PM**
102 **3:57 PM**	112 **3:57 PM**	122 **3:57 PM**	132 **3:57 PM**	142 **3:57 PM**	152 **3:57 PM**
103 **4:09 PM**	113 **4:09 PM**	123 **4:09 PM**	133 **4:09 PM**	143 **4:09 PM**	153 **4:09 PM**
104 **4:21 PM**	114 **4:21 PM**	124 **4:21 PM**	134 **4:21 PM**	144 **4:21 PM**	154 **4:21 PM**
105 **4:33 PM**	115 **4:33 PM**	125 **4:33 PM**	135 **4:33 PM**	145 **4:33 PM**	155 **4:33 PM**
106 **4:45 PM**	116 **4:45 PM**	126 **4:45 PM**	136 **4:45 PM**	146 **4:45 PM**	156 **4:45 PM**
107 **4:57 PM**			137 **4:57 PM**	147 **4:57 PM**	

1994 SMR Proffered Papers

TUE AM
3/8

Monet Room Papers 201-207 ***MAMMOGRAPHY (SILICONE)*** Moderators: ***P J Fritzsche, MD*** ***T A Spraggins, PhD***	**Metropolitan Room** Papers 211-217 ***FUNCTIONAL IMAGING*** Moderators: ***J A Helpern, PhD*** ***B R Rosen, MD***	**Miro Room** Papers 221-228 ***IMAGE QUALITY (MOTION & ARTIFACTS)*** Moderators: ***J A Sorenson, PhD*** ***M L Wood, PhD***	**Morrocco Room** Papers 231-237 ***SPECTROSCOPY II (BRAIN)*** Moderators: ***F Arias-Mendoza, MD, PhD*** ***I R Young, PhD***	**Sapphire Room** Papers 241-247 ***UPPER ABDOMEN II (HEPATIC, CONTRAST)*** Moderators: ***P L Choyke, MD*** ***R J Herfkens, MD***	**Topaz Room** Papers 251-258 ***VASCULAR IMAGING*** Moderators: ***M Bernstein, PhD*** ***D N Firmin, PhD***
201 **10:30 AM**	211 **10:30 AM**	221 **10:30 AM**	231 **10:30 AM**	241 **10:30 AM**	251 **10:30 AM**
202 **10:42 AM**	212 **10:42 AM**	222 **10:42 AM**	232 **10:42 AM**	242 **10:42 AM**	252 **10:42 AM**
203 **10:54 AM**	213 **10:54 AM**	223 **10:54 AM**	233 **10:54 AM**	243 **10:54 AM**	253 **10:54 AM**
204 **11:06 AM**	214 **11:06 AM**	224 **11:06 AM**	234 **11:06 AM**	244 **11:06 AM**	254 **11:06 AM**
205 **11:18 AM**	215 **11:18 AM**	225 **11:18 AM**	235 **11:18 AM**	245 **11:18 AM**	255 **11:18 AM**
206 **11:30 AM**	216 **11:30 AM**	226 **11:30 AM**	236 **11:30 AM**	246 **11:30 AM**	256 **11:30 AM**
207 **11:42 AM**	217 **11:42 AM**	227 **11:42 AM**	237 **11:42 AM**	247 **11:42 AM**	257 **11:42 AM**
		228 **11:54 AM**			258 **11:54 AM**

TUE PM
3/8

Monet Room Papers 301-306 ***PERFUSION AND FUNCTIONAL IMAGING*** Moderators: ***T J Brady, MD*** ***W T Dixon, MD***	**Metropolitan Room** Papers 311-317 ***CONTRAST AGENTS II*** Moderators: ***G D Fullerton, PhD*** ***S W Young, MD***	**Miro Room** Papers 321-327 ***MUSCULOSKELETAL I (JOINTS)*** Moderators: ***J V Crues III, MD*** ***E C Unger, MD***	**Morrocco Room** Papers 331-338 ***ABDOMEN AND MALE PELVIS*** Moderators: ***D G Mitchell, MD*** ***A Yang, MD***	**Sapphire Room** Papers 341-347 ***HEAD AND NECK*** Moderators: ***A N Hasso, MD*** ***K L Nelson, MD***	**Topaz Room** Papers 351-359 ***SPINE*** Moderators: ***M Rothmann, MD*** ***B D Flannigan-Sprague, MD***
301 **3:45 PM**	311 **3:45 PM**	321 **3:45 PM**	331 **3:45 PM**	341 **3:45 PM**	351 **3:45 PM**
302 **3:57 PM**	312 **3:57 PM**	322 **3:57 PM**	332 **3:57 PM**	342 **3:57 PM**	352 **3:57 PM**
303 **4:09 PM**	313 **4:09 PM**	323 **4:09 PM**	333 **4:09 PM**	343 **4:09 PM**	353 **4:09 PM**
304 **4:21 PM**	314 **4:21 PM**	324 **4:21 PM**	334 **4:21 PM**	344 **4:21 PM**	354 **4:21 PM**
305 **4:33 PM**	315 **4:33 PM**	325 **4:33 PM**	335 **4:33 PM**	345 **4:33 PM**	355 **4:33 PM**
306 **4:45 PM**	316 **4:45 PM**	326 **4:45 PM**	336 **4:45 PM**	346 **4:45 PM**	356 **4:45 PM**
	317 **4:57 PM**	327 **4:57 PM**	337 **4:57 PM**	347 **4:57 PM**	357 **4:57 PM**
			338 **5:09 PM**		358 **5:09 PM**
					359 **5:21 PM**

1994 SMR Proffered Papers

WED AM
3/9

Monet Room Papers 401-407 ***CARDIAC II (CORONARY IMAGING)*** Moderators: ***D Li, MS*** ***J D Pearlman, MD, PhD***	**Metropolitan Room** Papers 411-417 ***MR ANGIOGRAPHY I (NEURO)*** Moderators: ***C Dumoulin, PhD*** ***K R Maravilla, MD***	**Miro Room** Papers 421-427 ***MUSCULOSKELETAL II*** Moderators: ***J B Kneeland, MD*** ***S Marjumdar, PhD***	**Morrocco Room** Papers 431-437 ***IMAGING TECHNIQUES II*** Moderators: ***K Butts, PhD*** ***E M Haacke, PhD***	**Sapphire Room** Papers 441-448 ***IMAGE PROCESSING*** Moderators: ***J R MacFall, MD*** ***S Napel, PhD***
401 **10:30 AM**	411 **10:30 AM**	421 **10:30 AM**	431 **10:30 AM**	441 **10:30 AM**
402 **10:42 AM**	412 **10:42 AM**	422 **10:42 AM**	432 **10:42 AM**	442 **10:42 AM**
403 **10:54 AM**	413 **10:54 AM**	423 **10:54 AM**	433 **10:54 AM**	443 **10:54 AM**
404 **11:06 AM**	414 **11:06 AM**	424 **11:06 AM**	434 **11:06 AM**	444 **11:06 AM**
405 **11:18 AM**	415 **11:18 AM**	425 **11:18 AM**	435 **11:18 AM**	445 **11:18 AM**
406 **11:30 AM**	416 **11:30 AM**	426 **11:30 AM**	436 **11:30 AM**	446 **11:30 AM**
407 **11:42 AM**	417 **11:42 AM**	427 **11:42 AM**	437 **11:42 AM**	447 **11:42 AM**
				448 **11:54 AM**

WED PM
3/9

Monet Room Papers 501-507 ***MAMMOGRAPHY II (CONTRAST)*** Moderators: ***S E Harms, MD*** ***C L Partain, MD, PhD***	**Metropolitan Room** Papers 511-516 ***BRAIN III (CSF FLOW, OTHER)*** Moderators: ***W G Bradley, Jr., MD, PhD*** ***V M Runge, MD***	**Miro Room** Papers 521-527 ***MR ANGIOGRAPHY II*** Moderators: ***J E Siebert, MD*** ***S Wann, MD***	**Morrocco Room** Papers 531-537 ***SPECTROSCOPY III*** Moderators: ***D N Levin, MD*** ***M D Osbakken, PhD***	**Sapphire Room** Papers 541-547 ***DIFFUSION*** Moderators: ***J A Helpern, PhD*** ***R R Price, PhD***	**Topaz Room** Papers 551-558 ***OTHER (INSTRUMENTATION, SAFETY, RELAXOMETRY)*** Moderators: ***E Kanal, MD*** ***S R Thomas, PhD***
501 **2:45 PM**	511 **2:45 PM**	521 **2:45 PM**	531 **2:45 PM**	541 **2:45 PM**	551 **2:45 PM**
502 **2:57 PM**	512 **2:57 PM**	522 **2:57 PM**	532 **2:57 PM**	542 **2:57 PM**	552 **2:57 PM**
503 **3:09 PM**	513 **3:09 PM**	523 **3:09 PM**	533 **3:09 PM**	543 **3:09 PM**	553 **3:09 PM**
504 **3:21 PM**	514 **3:21 PM**	524 **3:21 PM**	534 **3:21 PM**	544 **3:21 PM**	554 **3:21 PM**
505 **3:33 PM**	515 **3:33 PM**	525 **3:33 PM**	535 **3:33 PM**	545 **3:33 PM**	555 **3:33 PM**
506 **3:45 PM**	516 **3:45 PM**	526 **3:45 PM**	536 **3:45 PM**	546 **3:45 PM**	556 **3:45 PM**
507 **3:57 PM**		527 **3:57 PM**	537 **3:57 PM**	547 **3:57 PM**	557 **3:57 PM**

SMR 1994: Meeting Overview

THE WEEK OF March 5–9, 1994, marks a historic time for the Society of Magnetic Resonance, representing its first scientific and educational meeting (formerly the 12th Annual Meeting of the Society for Magnetic Resonance Imaging). We present an overview of the exciting and informative events at this year's meeting, which is being held in Dallas. The format is similar to that of previous meetings, which has provided a comfortable yet stimulating forum for the exchange of ideas and information between clinicians, scientists, technologists, and everyone in between. The meeting consists of a Scientific Program, Poster Program, Morning Tutorial Program, Educational Program, Economics Symposium, combined Section of Magnetic Resonance Technologists (SMRT) annual meeting, and a technical exhibits program. The diversity of educational, scientific, and clinical topics have been designed to meet the continuing medical education goals of the Society. These programs are the result of extensive meetings during the year, starting at the 1993 Annual Meeting in San Francisco. Thanks go to Steve Harms, MD, for his diligence in coordinating the continuing medical education program.

The Scientific Program begins on Sunday, March 6th, and runs through Wednesday March 9th. It consists of a special topical symposium, plenary sessions, and proffered paper sessions. The topical symposium is on Sunday and this year will involve specifically organized interrelated sessions that include "Status of MRI: Resources, Applications and Research," "The Cost/Benefits Equation," and "Future MRI Technology," wherein the central theme of magnetic resonance imaging in a quality- and cost-conscious environment will be explored in depth, reflecting the concerns relating to the changing face of health care and its effect on research and development. The Scientific Program also includes related topics such as "Fast Scan MRI," "Outcomes Research in Relation to Neurological MRI," and "Current Role of MRI in Management of Cardiac Patients." The Scientific Program addresses basic research areas and includes topics such as "Update of Functional MRI," clinical practice topics such as "Musculoskeletal MRI," and new imaging protocols, as in "MRI of the Breast." We thank Richard Ehman, MD, and Norbert Pelc, ScD, for organizing the Scientific Program.

The Poster Program continues to be a vital way of conveying MR research, since certain work lends itself to this form of communication rather than as abstracts that can be presented within the limited time frame for proffered papers. Credit goes to Michael Moseley, MD, and Patrick Turski, MD, for organizing the Poster Program.

The Morning Tutorial Program has proved to be popular for more in-depth discussions of specific topics, both basic and advanced, and is scheduled for Monday through Wednesday. Topics this year include the ever popular k space, contrast materials, MR angiography, MR spectroscopy, and flow quantification, just to name a few. The program has been organized by Dwight Nishimura, MD, and Charles Spritzer, MD.

The Educational Program continues in its traditional form, occupying full days on Saturday and Sunday. Saturday topics include central nervous system techniques and evaluation of stroke, spine, tumors, and infections. Sunday topics include, in part, imaging of the abdomen and pelvis, cardiovascular system, and extremities. The Educational Program has been capably organized by Jeffrey Duerk, PhD, and Donald Mitchell, MD. Part of the Educational Program is the Economics Symposium. This symposium has been an important source of information on the rapidly changing world of reimbursement and utilization. Stuart Young, MD, and Herbert Abrams, MD, are to be congratulated on their fine contribution to the Annual Meeting.

The SMRT Educational Program, which is on Saturday and Sunday, continues its fine efforts in providing timely and important information of particular interest to MR technologists. This year's wide-ranging program includes presentations such as MR safety, MR angiography, cardiac imaging, fast imaging, and breast imaging, as well as nine proffered paper sessions and poster discussion periods. The SMRT Educational Program has been organized by Rodney Bell, BSRT, and Luann Culbreth, MEd.

Finally, congratulations and our thanks go to the SMR Chicago Central Office staff, Kristen Coe, Karen Bacidore, Kim Poff, and Peggy Lockrey, without whose diligent efforts the complexities of the Annual Meeting could not be accomplished.

Mark March 5–9, 1994, on your calendar. We look forward to seeing you in Dallas at the First Meeting of the SMR!

JEFFREY S. ROSS, MD
LAURENCE P. CLARKE, PhD
Co-Chairmen of the Annual Meeting Organizing Committee and Guest Editors

Index terms: Editorials • Radiology and radiologists, education • Society of Magnetic Resonance • Society of Magnetic Resonance, annual meeting

JMRI 1994; 4(P):19

SMR 1994: Scientific Program

ALTHOUGH NEW federal legislation has yet to be enacted, an accelerating process of health care reform in the United States has already resulted in new economically motivated restrictions on the use of magnetic resonance (MR) imaging as a clinical tool and a decrease in the resources that are available for further research and development in this area. It is disappointing to many in the diagnostic imaging community that MR imaging and other cross-sectional imaging modalities are so often depicted by the news media and by policymakers as prime examples of the type of high-tech medicine that has contributed to increasing costs. In fact, many pundits have expressed the view that the health care reform process will mandate decreased use of sophisticated medical imaging technology such as MR imaging in the care of patients.

These trends underscore the importance for physicians and scientists who work in the area of MR imaging to become actively involved in the health care debate. It is necessary to challenge some of the basic assumptions held by policymakers and even some leaders of organized medicine with regard to diagnostic imaging. We must point out that the goal of high-quality, cost-effective medical care may require *more* use of powerful diagnostic imaging technology rather than *less*. We must be sure that policymakers understand the profound impact that diagnostic imaging has had on medical care in the last few decades. It is not widely appreciated, for instance, that the availability of cross-sectional imaging modalities (ultrasound, computed tomography [CT], and MR imaging) and image-guided biopsy methods has led to the virtual disappearance of entire classes of previously common surgical procedures. Yet, the aggregate costs of these imaging modalities is less than 1% of total health care spending in the United States.

To a great extent, the future development of MR imaging will depend on our ability to show the the clinical importance of what has already been done and to show that further research is likely to yield the kinds of cost-effective applications that are appreciated by society.

The overall theme of the plenary sessions in the Scientific Program of this first SMR meeting is "MRI in a Quality- and Cost-Conscious Environment." As in previous years, the plenary sessions will focus on some of the most active areas of clinical and scientific activity in MR imaging. At the same time, the program has been designed to reflect the interest of the members of the Society in understanding these advances within the context of the overall health care system. The program will continue the trend in previous meetings to include more panel discussions and debate-style interchanges.

Three topical conference sessions on Sunday, March 6, 1994, will explicitly address the overall themes of quality, cost, and role. The first of these sessions will provide an overview of the global resources available for MR imaging, the current impact of MR imaging on the health care system, and the resources devoted to further research and development. The second session will address the issue of cost/benefit assessment in MR imaging. This session will provide perspectives on assessing the benefits of MR imaging and on developing a framework for the cost side of the equation. The final session on Sunday will focus on future MR imaging technology and will include a panel discussion on the potential effects of new system architectures on performance and cost.

On Monday, a plenary session on fast MR imaging will address the impact that rapid imaging techniques have had on neurologic and body MR imaging and on the anticipated progress in the future. This session will also present an update on interventional MR imaging. Other plenary sessions on Monday will present perspectives on the role of MR imaging in assessing gynecologic malignancies, a debate on the value of MR imaging versus CT for abdominal imaging, a discussion of outcomes research in neurologic MR imaging, and a review of the clinical applications of three-dimensional imaging and analysis. The final session on Monday will revisit the debate on the merits of high- versus low-field imagers. Plenary sessions on Tuesday and Wednesday will provide a similar type of emphasis in updates on functional neurologic, musculoskeletal, cardiovascular, and breast MR imaging.

For many attendees, the most important element of the program is the proffered papers. As in previous years, the Scientific Program will include multiple parallel sessions throughout the four days of the meeting. Here, we will have a chance to see the most up-to-date research results. Works-in-progress presentations will be incorporated into many of the scientific sessions, as well.

We are grateful to Jeffrey S. Ross, MD, Laurence P. Clarke, PhD, and William T.C. Yuh, MD (co-chairmen of the annual meeting and education coordination council); Stephen J. Riederer, PhD, President of the Society for Magnetic Resonance Imaging (SMRI); Karen Bacidore of the SMR Chicago Central Office; the many members of the Society who reviewed abstracts, the moderators, and invited speakers; and the scientific contributors for their help in creating an exciting Scientific Program for the 1994 meeting.

RICHARD L. EHMAN, MD
NORBERT J. PELC, PhD
Co-Chairmen of the Scientific Program

Index terms: Editorials • Radiology and radiologists, education • Society of Magnetic Resonance • Society of Magnetic Resonance, annual meeting

JMRI 1994; 4(P):20

Notes

Notes

Plenary Symposia

From the Cost-Conscious Topical Symposium on Sunday through the MRI of the Breast session on Wednesday, the Plenary Symposia, spaced throughout the week, highlight the Annual Meeting's scientific programming. The Plenary Symposia also provide the opportunity to recognize Society Award recipients and to honor individuals who have made important contributions to MRI.

SUNDAY, MARCH 6

8:00 AM - 9:45 AM
Current Status of MRI: Resources, Applications and Research

10:15 AM - 12:00 PM
The Cost/Benefit Equation

1:30 PM - 3:00 PM
Future MRI Technology

MONDAY, MARCH 7

8:00 AM - 10:15 AM
Awards Presentations
Fast Scan MRI

10:45 AM - 12:30 PM
MRI of the Abdomen and Pelvis

1:30 PM - 3:00 PM
Neurological MRI

TUESDAY, MARCH 8

8:00 AM - 9:30 AM
Update on Functional MRI

1:30 PM - 3:00 PM
Musculoskeletal MRI

WEDNESDAY, MARCH 9

8:00 AM - 9:30 AM
Cardiovascular MRI

1:00 PM - 2:30 PM
MRI of the Breast

1994 Young Investigator's Award

Isidor I Rabi Award

This award is named in memory of Isidor Isaac Rabi, physicist, statesman, and pioneer of modern science. During the 1930s Rabi and his co-workers at Columbia University developed and used nuclear magnetic resonance methods to measure, with extreme accuracy, the magnetic properties of nuclei. This work earned Rabi the 1944 Nobel prize in physics and directly stimulated research on collective nuclear magnetic resonance in solids and liquids, which has led to magnetic resonance spectroscopy and imaging. I. I. Rabi died in 1988 at the age of 89.

Douglas C Noll, PhD

1994 Rabi Award recipient

Dr. Noll is an Assistant Professor of Radiology and Electrical Engineering at the University of Pittsburgh and Visiting Assistant Professor in the School of Computer Science at Carnegie Mellon University. His current research projects in magnetic resonance imaging include image reconstruction and processing and the practical applications of MRI. He is part of an interdisciplinary team involving physicians and scientists in the Departments of Psychiatry, Neurosurgery, Radiology and Electrical Engineering seeking to apply newly developed MRI techniques for functional brain mapping. The concentration of these methods has enabled him to improve the efficiency and speed of these applications. His work also includes the application of high speed parallel computers to the processing of MRI data.

The Rabi Award recipient this year received his PhD in Electrical Engineering at Stanford University working in the magnetic resonance systems research laboratory under the direction of Dr. Albert Macovski in the area of rapid MRI techniques and image reconstruction algorithms. His PhD dissertation was entitled "Recognition Techniques for Magnetic Resonance Imaging". His earlier academic background includes a Bachelor of Science degree in Electrical Engineering, Summa Cum Laude, from Bucknell University in 1985 where he received the President's Award for Outstanding Academic Achievement and a Master of Science in Electrical Engineering from Stanford University in 1986. For two years, Dr. Noll was a member of the technical staff of the Applied Signal Processing Department of AT&T Bell Laboratories in Whippany, New Jersey where he served as a team leader for acoustic signal processing software and algorithm development.

Dr. Noll holds three patents related to magnetic resonance imaging, is a member of Tau Beta Pi, the Society of Magnetic Resonance and the Institute of Electrical and Electronic Engineers and has authored 13 scientific papers.

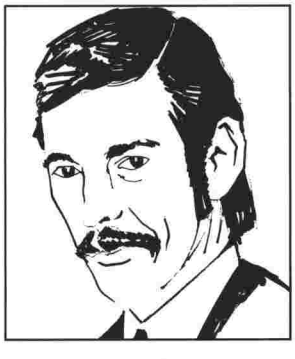

William S Moore Award

This award is named in memory of William Stanley Moore, physicist and Past President of the SMRI. William S. Moore was born in 1936 in Adrossan, Scotland and was educated at Merchiston Castle School in Edinburgh. He won an open scholarship to Caius College Cambridge where he was graduated with a BA degree in physics in 1958 and a MA in 1961. Thereafter, he moved to Nottingham University where he obtained his PhD for research in electron paramagnetic resonance. From 1961 to 1983, he served on staff at Nottingham University before moving to Boston as Director of NMR Physics at the Brigham and Women's Hospital. In 1984, Dr. Moore was elected President of the Society and died shortly afterwards on the 25th of March at the age of 47. A Young Investigator Award in clinical science will not be presented at the First Meeting of the SMR.

SMR '94 First Meeting of the SMR
Plenary Symposia

Sunday Morning • Chantilly West
Plenary Symposia 001–003

CURRENT STATUS OF MRI: Resources, Applications, and Research
MODERATOR: RL EHMAN, MD

PS 001 • 8:00 AM
A Global Inventory
TJ Miller
MR Division, Siemens AG, Erlangen, Germany

In the 12 years of the existence of commercial MR imaging, it has grown to where more than 7,000 systems are operating worldwide, sales of MR systems generate over $1.5 billion annually, and revenues from MR examinations top $2.0 million per working hour. In spite of this impressive business growth, the MR imaging industry now finds itself in the midst of cataclysmic change. The purchase and use of MR systems today is no longer simply influenced by the clinical needs of the radiologist. Rather, it is as greatly influenced by such factors as national health policy, the reimbursement limits of state and private health insurance, regulatory factors surrounding the development and permission for use of an MR system, and administrative and financing factors within the purchasing entity. In addition, the use of MR in medicine today is no longer exclusively seen as an example of the great benefits that technology has brought to patient care but is often used as an example of how technology has caused an explosion in health care costs to the detriment of the general populace. Since the MR systems of the future will, in great part, determine the use of MR imaging in the future, this lecture will describe the ways in which these new factors influence the decision processes governing the creation of new generations of MR systems for the worldwide market. We will also discuss our projections of what MR systems of the future may look like and what clinical, financial, and health care issues these new designs may address.
T.J. Miller is an employee of Siemens AG.

PS 002 • 8:35 AM
Perspectives on the Role of MR Imaging in Medicine in the United States
HY Kressel
Department of Radiology, Beth Israel Hospital, Boston, MA

In the more than 12 years since MR was introduced as a clinical tool, the number of units has burgeoned to over 3,000. In this presentation, we will attempt to review the current status of MR applications in the United States. We will attempt to assess national trends, identify regional differences, and review experience in an academic medical center over the years. Currently, newer applications, of course, remain the predominant focus of MR use in this country. In many centers, however, the number of brain and spine examination appears to have reached a plateau, or perhaps decreased somewhat over recent years. Musculoskeletal applications have grown considerably over the past years and, in many centers, may compose as much as 30% or more of the caseload. Applications in the abdomen and pelvis have been relatively slow to develop nationwide. This may relate to adequacy of other techniques for problem solving, lack of available imaging resources, and failure to educate clinicians appropriately. Vascular studies have increased dramatically over the past 3 years, although to some extent these have been dampened by regulatory issues. Cardiac applications currently await clinical validation and subsequent diffusion. Despite regional differences, and differences in regulatory environment, surprisingly rapid diffusion of MR technology has occurred nationwide. Further efforts in education and applications development would likely further extend applications diffusion.

PS 003 • 9:10 AM
Survey of Current Research Activity in MRI
WR Brody, MD, PhD
The Johns Hopkins Hospital, Baltimore, MD

Material unavailable at time of publication.

Sunday Morning • Chantilly West
Plenary Symposia 004–006

THE COST/BENEFIT EQUATION
MODERATOR: SW YOUNG, MD

PS 004 • 10:15 AM
How Should the Benefits of an MR Imaging Application Be Assessed?
EP Steinberg
Division of Internal Medicine, The Johns Hopkins University, Baltimore, MD

The purpose of this presentation is to (1) discuss the forces underlying increased interest in technology assessment, cost-effectiveness analysis, and "outcomes research"; (2) discuss the types of clinical evaluations of MR imaging that could be performed; (3) explain what is involved in performing a cost-effectiveness analysis; and (4) clarify the benefits and limitations of cost-effectiveness analysis.

PS 005 • 11:00 AM
How Much Should the Technical Component of an MR Imaging Examination Cost?
RA Bell
R.A. Bell and Associates, Olivenhain, CA

Determining the cost of the technical component of MR imaging requires multivariable analysis and many assumptions regarding future trends. This presentation discusses the application of sensitivity analysis to demonstrate which variables most strongly affect the bottom line and must, therefore, be considered with the greatest care. Conclusions are contrasted with historical data and with information drawn from a recent survey. Projections of future reimbursement trends and patient volume are also addressed.

PS 006 • 11:20 AM

Professional Component: Pricing MR Imaging

SW Young

Department of Diagnostic Radiology, Stanford University, Stanford, CA

What should MR imaging interpretation cost? Services are more difficult to price than manufactured products. For products, there is cost of goods, invention and development costs to be amortized over the life of a patent, and overhead. Profit margins should be sufficient to allow the company to perform enough research and development to invent the next product. Services are different. For example, why should a professional basketball player get $3 million per year and a college professor $60,000? The best answer is that this is the differential value the market has set for their services. One approach to this question is to treat MR imaging interpretation as if it were a manufactured product. Long-term average costs would include the costs of training the radiologists, and this cost would have to be amortized over the working life expectancy of the radiologists. Overhead expense could be calculated. A physician's profit margin is a dicey item for discussion these days, but physicians' economics must take into account opportunity cost. In some areas, plumbers make three-fourths as much as psychiatrists per hour, but they start practice 12 to 15 years sooner. Income potential must be high enough that talented individuals who have a choice of professions will still choose to enter radiology. Yet another way to price MR imaging interpretation is on the margin, or at marginal cost. In other words, what does it cost a radiologist who is already in practice and sitting at an alternator to read just one more scan? Marginal cost is always significantly less than long-term average cost.

Sunday Afternoon • Chantilly West
Plenary Symposia 007–009

MRI TECHNOLOGY: Challenges and Opportunities

MODERATOR: NJ PELC, SCD

PS 007 • 1:30 PM

Effect of Field Strength on Image Quality

BK Rutt

Department of Diagnostic Radiology, University Hospital, London, Ontario, Canada

As clinical MR imaging has evolved, there have been numerous arguments for the use of different field strengths. Those favoring high magnetic field strength (1.5 T and above) point to the advantages of higher signal-to-noise ratio, capability for MR spectroscopy and other forms of functional MR imaging, high-speed imaging, and high-resolution imaging. However, cost remains a significant limitation to the wider dissemination of high-field-strength MR imaging. There are definite cost advantages (capital, operating, siting) to the use of lower-field-strength MR imaging. In addition, there are some physiologic advantages to the use of lower-field-strength MR imaging, such as reduction in absorbed power in the patient. Much debate has occurred over the past decade regarding the relative diagnostic benefits of high-field-strength MR imaging versus lower-field-strength MR imaging. Given the intensity of this debate, it is perhaps surprising that there have been almost no randomized, controlled trials comparing the diagnostic accuracy of MR imaging at various field strengths. This presentation will review the physical principles of field strength and its relevance to MR image quality. The field strength dependence of signal intensity, noise, relaxation times, chemical shift, magnetic susceptibility effects, and other relevant physical parameters that affect MR images will be outlined. These parameters are combined with pulse sequence factors to produce the final image characteristics; appropriate examples for common field strengths and common imaging sequences will be given. As important as physical characterization of image quality—perhaps more important—is diagnostic information contained in MR images. The assessment of the importance of field strength in MR is incomplete without some analysis of diagnostic accuracy versus field strength. Such analysis is difficult to accomplish in an unbiased manner, and is not appropriate before technological advances at the various field strengths have stabilized. The use of receiver operator characteristic (ROC) analysis is probably the best available method of measuring diagnostic accuracy of various imaging methods without bias. An ROC study of diagnostic accuracy of 0.5-T versus 1.5-T MR imaging in examining several common clinical categories has recently been conducted at our institution. Results from this study demonstrate diagnostic equivalence between these two field strengths in at least two common clinical disease categories (multiple sclerosis and internal derangement of the knee). These results, as well as results from other clinical categories, will be discussed and related to results from previous field-strength studies.

PS 008 • 1:55 PM

Magnet Technology Update

GN Holland, S Pittard

Otsuka Electronics, Fort Collins, CO

Magnet technology has improved both the cost-effectiveness and performance of clinical MR imaging systems. This presentation summarizes recent developments and points the way for future technology trends. We focus on axial field superconducting magnets, which are used on the vast majority of clinical systems. Improvements have occurred in field homogeneity, magnet size and weight, and cryogen use. Improvement in the dimensions of the homogeneous volume relative to the diameter of the magnet bore has been achieved by improved magnet construction—essentially by reducing winding errors and, hence, impurities in the field—and by improved shimming methodology. Contemporary magnets may use a combination of active and passive shimming techniques, or may require passive shimming only with the exception of first order terms, which are provided as DC current from the gradient amplifiers. In passive shimming, a distribution of small metal slugs, determined from field plot analysis, is placed into an array of trays interior to the room-temperature bore. This approach allows the magnet to be rapidly shimmed, without requiring the complexity and expense of multiple room-temperature shim windings. Reduction in cryogen use has been achieved by better internal magnet mechanical design and improved thermal management. By incorporating two-stage refrigerators, most magnets use helium only to achieve boil-off rates of less than 0.1 L/h, whereas early magnets required a liquid nitrogen vessel surrounding the helium can. Also, with shielded gradients, energy deposition into the magnet windings from gradient eddy currents is vastly attenuated (generally by two orders of magnitude or more), which prevents raising the temperature of the windings and, therefore, increasing boil-off during imaging. Incorporation of shielded gradients has also allowed reduction in size and weight of the magnet assembly. Radiation shields within the magnet can be less massive because they are not required to prevent energy deposition from eddy currents in the magnet windings. Just as actively shielded gradients have played a part in the reduction of size and weight of the magnet assembly, active shielding of the magnet windings, where bucking coils outside of the main windings radically reduce the field beyond the cryostat, has been used to reduce weight of system shielding and size of system installation.

PS 009 • 2:20 PM

Gradient and RF Technology Update

RE Kinsinger

GE Medical Systems, Milwaukee, WI

Several recent and upcoming advances in gradient and RF subsystem design will be reviewed with primary emphasis on their implications for both system cost and operating performance. The specific topics to be highlighted will be (1) fast ramp/high peak gradient systems, (2) new techniques for gradient shielding, (3) local gradient and RF coils, (4) phased-

array RF coils, (5) RF coils for improved B_1 homogeneity, and (6) gradients and RF coils for open-imaging systems.
R.E. Kinsinger is an employee of GE Medical Systems.

Monday Morning • Chantilly West
Awards 001
Plenary Symposia 010–012

FAST SCAN MRI

MODERATOR: SJ RIEDERER, PHD

A 001 • 8:30 AM (I. I. Rabi Award)

Spiral K-Space MR Imaging of Cortical Activation

DC Noll, JD Cohen, CH Meyer, W Schneider
University of Pittsburgh, Pittsburgh NMR Institute, Pittsburgh, PA

Purpose: Functional MRI has shown promise as a tool for brain research and for the planning of interventional therapy in a clinical setting. We investigate fast spiral-scan imaging and compare this method with conventional spin-warp imaging.
Methods: A gradient-echo, T2*-weighted spiral k-space pulse sequence was implemented on standard unmodified 1.5-T clinical hardware. For comparison to spin-warp imaging, scan parameters were chosen so that echo time, resolution, theoretical SNR, and total imaging time were nearly matched. Functional scanning was performed in the primary visual cortex with a small stimulus (single characters), in the primary motor cortex with a fist clenching task, and in the prefrontal cortex.
Results: When spiral k-space imaging was compared with spin-warp imaging, the areas of statistically significant activation and the percentage change in those areas were similar for the two methods, though a measure of artifacts was smaller in spiral imaging, with $P < .025$ (df = 14). This artifact reduction is attributed to both a longer TR, reduced flow-related ghosting, and to the inherent motion robustness of spiral trajectories. Maps of activation were also generated in the prefrontal cortex by using verbal fluency and working memory tasks.
Conclusion: Spiral imaging is demonstrated as a robust functional MRI method, having a similar activation response but reduced variability across images when compared with spin-warp imaging. Also, because fewer excitations are required for image acquisition, the number of slices that can be examined in a fixed imaging interval was increased fourfold with spiral imaging.

PS 010 • 8:45 AM

Impact of Fast Scan Methods in Neurologic MR Imaging: Past, Present, and Future

EK Fram
Department of Neuroradiology, Barrow Neurological Institute, Phoenix, AZ

Fast scan techniques are not only improving existing clinical MR imaging applications but have the potential to create new ones. These techniques include fast spin-echo imaging, short TR gradient-echo imaging, and echo-planar imaging. Fast spin-echo imaging has changed the balance between SNR, imaging time, and resolution that exists for routine spin-echo imaging, the mainstay of brain MR imaging. The improved efficiency can be used to decrease examination time, acquire images with significantly increased resolution, and allow additional pulse sequences to be performed in a reasonable total examination time (eg, MR angiography). Perhaps more exciting than improved anatomic imaging are the functional applications that fast scan techniques may bring into clinical practice, including measures of blood flow, blood volume, perfusion, and diffusion. While conventional MR imaging provides exquisite anatomic information, it provides little information regarding brain function, a fact clear to anyone who has compared MR images of the a living brain with images of one fixed in formalin. Furthermore, the signal intensity changes that occur with disease are largely nonspecific. Virtually all pathologic processes are characterized by increased water content, with resulting prolongation of T2, as seen in tumor, infection, infarction, and demyelination. The brain is a highly complex and metabolically active organ. There are highly organized structure-function relationships and tight coupling of brain activity, metabolism, and blood flow. Despite PET's low resolution, the metabolic information it can provide has proved useful in the workup of multiple diseases, including seizure disorders, neurodegenerative diseases, and brain tumors. In fact, dramatic findings with PET may be seen in the face of either normal or nonspecific MR imaging findings. Fast scan MRI techniques may allow noninvasive evaluation of brain function on a routine clinical basis.

PS 011 • 9:15 AM

Impact of Fast Scan Methods in Body MR Imaging: Past, Present, and Future

S Saini
Department of Radiology, Massachusetts General Hospital, Boston, MA

Reduction in MR imaging time represents one of the principal areas of clinical research today. For body MR imaging, the primary motivating factor has been to improve image quality either by eliminating artifacts that arise due to physiologic motion or by increasing in-plane resolution. More recently, financial concerns have required development of imaging methods that reduce costs per examination by increasing patient throughput but without compromising patient care. In general, most patients can tolerate continuous imaging for 10–15 minutes. In the early 1980s, technical advances (reduction in $TE_{minimum}$) permitted improved image quality while maintaining these imaging times. For example, in liver MR imaging, inversion-recovery pulse sequences were replaced by multiaveraged short TR SE pulse sequences for obtaining T1-weighted images. In the mid-1980s, gradient-echo techniques were developed that permit image acquisition in a single breath hold. However, this technique has been limited by suboptimal SNR, and its use has been limited to post-Gd dynamic imaging. More recently, availability of fast SE pulse sequences has allowed acquisition of heavily T2-weighted images (longer TR) with a higher in-plane resolution (256^2 or 512^2) and with a modest reduction in imaging time. This methodology has been most effective in the pelvis. Application of echo-planar techniques is still under investigation. Although considerably more costly, this methodology remains the most powerful technique for obtaining motion-free images, particularly for evaluation of the heart. However, image resolution with echo-planar MR imaging remains inferior to that of conventional MR images. The availability of fast imaging techniques alone are likely to provide only a modest improvement in evaluation of "diseases." On the other hand, development of tissue-specific MR contrast agents is more likely to improve the efficacy of MR imaging as well as expand its application for diseases currently not evaluated with imaging. Hence, the combination of MR contrast media and fast imaging should allow development of efficacious and cost-effective MR examinations.

PS 012 • 9:45 AM

Interventional MR Imaging: A New Combination of Surgery and Radiology for the 21st Century

RB Lufkin
Department of Radiology, UCLA Medical Center, Los Angeles, CA

Although the concept of "interventional MR imaging" has always had a certain appeal, the clinical application of the technology and proof of concept has until very recently been impeded by the lack of MR instruments appropriate for invasive MR procedures. In late 1993, the first of a new generation of MR imagers specifically designed for MR-guided interventional procedures was introduced. Although so-called "open magnets" have been available for some time for diagnostic imaging, they were developed primarily for reducing claustro-

phobia in patients. They do not allow the degree of improved access that is possible with an interventional MR magnet and, thus, are not suitable for many advanced procedures. It is anticipated that other manufacturers will be producing interventional MR units in the near future as interest in the field grows. At least one major medical teaching hospital has announced the formation of a Center for Interventional Magnetic Resonance Imaging. Present applications of interventional MR imaging include a variety of approaches, including MR-guided aspiration cytology, electrophysiology, chemical ablation with alcohol, and thermal ablation with cryotherapy, lasers, radio-frequency energy, and focused US. Throughout the world, basic science and clinical series are now under way involving the brain, head and neck, breast, prostate, liver, and other body areas. This presentation will review the current state of the art of interventional MR imaging and explore possibilities for future development of this exciting technology.

Monday Morning • Chantilly West
Plenary Symposia 013–014

MRI OF THE ABDOMEN AND PELVIS

MODERATOR: J HEIKEN, MD

PS 013 • 10:45 AM

Gynecologic Malignancies of the Pelvis: Role of MR Imaging

H Hricak, JL Stern
Department of Radiology, University of California, San Francisco, San Francisco, CA

In this time of health care reform, the field of radiology needs to change as well. As radiologists, we need to take a more active part in decisions on patient management, be involved with consultations, and participate on tumor boards. To do so, however, our education must expand beyond film reading. The knowledge of the technical aspects of MR imaging—the use of proper sequences, planes of imaging, and the timely use of contrast media—is essential. In addition, our knowledge must expand to understanding of the pathophysiology of the disease, cancer prognostic factors, treatment options, and imaging findings that are crucial for treatment decisions. Only by speaking the same language as our colleagues in clinical services and understanding their needs will we be able to function as a valuable part of the team. In carcinoma of the cervix, the clinical questions of interest include tumor size, tumor location, depth of cervical stromal invasion, parametrial invasion, extension into the endometrial cavity, extension outside the uterus, presence of hydronephrosis, and lymph node metastasis. Therefore, all of these points must be evaluated and described in detail. With respect to lymph node metastasis, the exact location of the nodes and the number of nodes enlarged should be mentioned as well. In cancer of the endometrium, the emphasis is on depth of myometrial invasion, which will classify stage I disease into no myometrial invasion (IA), inner-half myometrial invasion (IB), or outer myometrial invasion (IC). For stage II disease, in addition to describing tumor extension into the endocervical canal, the statement of whether there is glandular invasion only (IIA) or stromal invasion as well must be assessed and described. Any mention of extension outside the cervix, as well as the previously described location and the number of nodes, should also be given. Encouraging teamwork and cooperation between radiologists and attending clinicians will foster the proper choice of imaging modality, the fastest route to diagnostic information, and, ultimately, better patient care.

PS 014 • 11:45 AM

Will MR Imaging Replace CT for Upper Abdominal Imaging?

JC Weinreb, AJ Megibow
Magnetic Resonance Imaging, New York University Medical Center, New York, NY

Despite numerous publications extolling the virtues of MR imaging compared with CT, the literature does not accurately reflect current clinical realities, and CT continues to be the mainstay for upper abdominal imaging. This is due to a number of factors, including cost, availability, labor intensity, expertise, and long-established practice patterns. This presentation will discuss the relative merits of state-of-the-art MR imaging and CT for specific upper abdominal applications. MR imaging is probably clinically significantly superior to CT for evaluation of the cirrhotic liver, adrenal masses, and some pancreatic tumors. MR imaging is competitive with CT for the diagnosis and staging of most pancreatic and renal neoplasms, hepatic metastases, and lymphadenopathy. CT is currently advantageous for screening, for guided intervention, trauma, and most gastrointestinal problems. Both MR angiography and CT angiography have technical limitations for abdominal applications, but MR is capable of providing a more global picture as well as supplemental information such as flow quantitation. Advances in MR technology, user interface, and contrast agents will be matched by progress in CT. Nevertheless, assuming that cost, availability, and user-friendliness are not major considerations in the future, MR imaging will likely assume much of the workload currently carried by CT for upper abdominal imaging. However, CT will not disappear. Rather, much abdominal imaging will remain in the purview of CT. Furthermore, the CT suite may become the x-ray room of the future and will replace conventional radiography for many applications.

Monday Afternoon • Chantilly West
Plenary Symposia 015–018

NEUROLOGICAL MRI

MODERATOR: JS ROSS, MD

PS 015 • 1:30 PM

Outcomes Research, Appropriateness, and Pragmatism in Neurologic MR Imaging

MT Modic
Division of Radiology, Cleveland Clinic Foundation, Cleveland, OH

The rising cost of health care and the current social-political environment have ushered in a new policy initiative known as "outcomes research" (also called appropriateness studies or efficacy research). The general intent of this initiative is to provide a more effective evaluation of the expected or potential outcomes of various diagnostic and therapeutic interventions. The imaging literature related to new technologies has been subjected to information synthesis to evaluate it for demonstration of clinical efficacy and found to be flawed in its methodology and statistics. Specifically, the literature is essentially descriptive, anecdotal, and relatively unscientific, especially as it relates to new technologies or contrast agents. Additionally, there is little, if any, methodologically sound research that studies the relationship between the employment of new developments and patient outcomes. While these criticisms are not unfounded, the reality is much more complicated. The imaging literature, while flawed as to outcome analysis, is not without value. There are problems related to radiologic research that are unique to diagnostic imaging. An experimental approach that optimizes the attainment of diagnostic information cannot readily provide simultaneous information on other indices such as patient treatment and patient outcomes. In addition, imaging usually produces intermediate data, not end points or final health outcome data. Linking intermediate data from imaging to the out-

comes of therapeutic interventions in some cases adds immeasurable complexity. This is further complicated in that we have done little to develop methods that will make evident the beneficial effects of imaging technologies on a patient's health, and existing models suffer from methodologic immaturity or infirmities. The goal of the presentation will be to provide a review of the literature, methodologies, and effect of outcomes research in neurologic MR imaging. This presentation will review a six-level efficacy model proposed by Fryback and Thornbury, with examples from the literature to illustrate both the difficulty and need for approaches such as this model. The issues of "appropriateness," health outcomes research problems, and potential compromise will be presented.

PS 016 • 2:00 PM

Clinical Applications of 3D Neurologic MR Imaging

DN Levin

Department of Radiology, University of Chicago Hospitals, Chicago, IL

This presentation will provide an overview of the role of 3D MR imaging of the brain in diagnosis and computer-assisted surgery. Three-dimensional images can aid diagnosis by making it possible to visualize complex anatomic structures. For example, abnormalities of the vascular tree are best detected with projection views (eg, maximum-intensity projection images), which are forerunners of more sophisticated 3D displays. Similarly, 3D imaging is the most reliable way of showing the relationship between lesions and specific gyral convolutions of the brain surface usually associated with movement, sensation, speech, and hearing. Three-dimensional brain models also provide a general anatomic framework for multimodality display of other diagnostic information, such as data from functional MR imaging, MR spectroscopy, PET, CT, radiography, electroencephalography, and magnetoencephalography. The fragmented data from multiple tests and scores of cross-sectional images are represented by these 3D models, which have a "natural" format appreciated by clinicians. Conventional surgical techniques use only a small fraction of available imaging data. However, technology is emerging that can bridge this wide gap between imaging and surgery. First, the craniotomy, cortical incision, and surgical "tunnel" can be planned by computer graphic manipulations of 3D models. Then, the actual operation can be performed with the aid of frameless stereotaxic devices that track surgical tools and display their positions on preoperative images. In the future, some operations may even be performed *inside* magnets specifically designed to provide real-time imaging during interventions. Experiments must be done to evaluate various advanced display technologies (eg, "heads up" or virtual reality methods) that might benefit these types of computer-assisted surgery. In short, brain surgery is on the threshold of a dramatic advance, which is being driven by developments in computer and imaging technology.

PS 017 • 2:30 PM

High- versus Low-Field MR Imaging: The Debate Goes On

JV Zelch

Regional MRI Centers, Cleveland, OH

High- versus low-field-strength MR imaging—the topic itself has confusing historical implications and very little application to present and future MR imaging discussions. High, mid, low, ultralow, and ultrahigh are arbitrary designations of magnetic field strength that have no basis in physics or scientific specifications. All clinical MR imaging systems are super high-field-strength systems as related to the magnetic field of the earth or ultralow as related to experimental systems designed with tesla ratings of 15 or higher. Field strength/tesla—so what! The tesla fixation of the 1980s paid tremendous dividends to equipment manufacturers and academic imaging specialists. The divisive debate should be eliminated and focused on reality and reaction, not words and influenced publications. In the words of Ross Perot, "We simply don't get it." Clinical MR imaging is a complex array of instruments and facilities that span the arena from echo-planar equipment in university research facilities to mobile units with antique 10-year old midfield systems. The issue is not field strength and tesla; the issue is performance and quality. The performance of MR imaging is in no way related to the strength, size, or cost of the magnet, nor is the quality of the procedure and the interpretation. The magnet is the torso, the gradients are the heart, the electronics allow the system to function, and the technologists and the physician direct the eventual output. It is inappropriate and inaccurate to separate the components of an MR imaging unit from each other and eliminate the human factor. Performance, performance, performance—what can the MR imaging system accomplish and at what quality? Dream procedures of high-field systems of the mid-1980s are standard applications of midfield units of today. Therefore, almost everything that was claimed to be in the high-field domain was an inaccurate representation. What about credibility? Let's begin an era in which our reports and publications will stand the test of time with scientific and clinical validity. Virtually all clinical MR imaging publications (thousands of them) issued prior to 1985 are completely worthless as reference sources for modern MR imaging. That's not right! Publications and presentations should represent scientific validity rather than "rush to publish" and the pursuit of academic escalation. MR angiography, MR mammography, MR oncology, dynamic/kinematic MR imaging, 3D with multiplanar, and so on—these are performance standards that are important in assessing a MR imaging system. Any reference to field strength/tesla represents an obsolete and archaic approach to a discipline that today is more dependent on electronics and gradients than it is on the raw magnetic field of the magnet. Manufacturers and those in academic positions supported by vendors will recall that General Electric and Siemens emphatically stated that quality MR imaging could not be performed at less than 1.0 T and that it was inconceivable to offer a unit at midfield strength. Unfortunately, the remarks were made in the mid-1980s and they now produce units at 0.5 or 0.2 T. Picker, a superconductive magnet advocate, now offers the Merit at 0.1 T. Many of the presenters at this conference advocate high field strength when lecturing and writing, yet are owners of 0.3-T systems and are consultants to major national companies and advise the acquisition of midfield MR imaging for community hospitals and imaging centers—a bit of misrepresentation by my standards. The issue is quality and fiscal responsibility, and they are measured in terms of performance, not field strength.

PS 018 • 2:30 PM

High- versus Low-Field MR Imaging: The Debate Goes On

WG Bradley, Jr

Memorial MR Center, Long Beach Memorial Medical Center, Long Beach, CA

The optimal field strength for a given site depends on anticipated patient volume and on how heavily certain outcome parameters are weighted, namely, return on investment and certainty of positive (or negative) diagnoses. High field strength is optimal for a high-volume site that places a greater premium on accuracy of diagnosis than on return on investment. On the other hand, a low-volume site (10 procedures a day or fewer) or one more interested in the economic bottom line can often provide "adequate" image quality with a low-field machine. The problem is that a study that may appear to be normal at low field strength might have been abnormal at high field strength. To compensate for a lower signal-to-noise ratio, low-field units must either reduce the bandwidth, increase voxel volume, or increase the number of excitations, any of which can potentially decrease detection of early disease. Low-bandwidth techniques typically have a relatively prolonged echo sampling time and thus a longer minimum TE and decreased T1 contrast. On T2-weighted images, the longer sampling time may limit the number of slices available for a given TR, decreasing coverage. Increasing excitations increases scan time and, potentially, motion artifacts, par-

ticularly for sick and claustrophobic patients. Increasing voxel volume decreases resolving power and increases partial volume artifacts, both of which reduce the detection of small, low-contrast lesions that are characteristic of early disease. In summary, the choice of the "optimal" field strength depends on exactly what is being optimized. As economic factors are weighted more heavily (relative to image quality), the optimum begins to shift toward lower field strengths. However, if the sole criterion is optimal detection of disease, high field strength clearly wins.

Tuesday Morning • Chantilly West
Plenary Symposia 019–021

UPDATE ON FUNCTIONAL MRI

MODERATOR: CR JACK, MD

PS 019 • 8:00 AM

Biophysical and Technical Basis for Functional MR Imaging

ME Moseley
Lucas MRS Center, Stanford University Medical Center, Stanford, CA

MR imaging has demonstrated noninvasive visualization of human brain function. Previously, the exclusive domain of PET technology, an important subset of "functional" MR imaging, task activation MR imaging (often denoted as fMRI) has shown the promise of allowing mapping of functional regions of the human cortex in real time for a large number of classical and novel "paradigms." This is achieved by using magnetic susceptibility as the contrast parameter and by the fact that deoxyhemoglobin in intact erythrocytes is paramagnetic whereas oxyhemoglobin is not. Regional blood oxygenation or deoxygenation in the brain can result from changes in local or global metabolic-related oxygen uptake and changes in blood flow. This is manifested as an increase or decrease in signal intensity on T2*-weighted images. The resulting variations in regional tissue oxygenation due to any and all cerebral perturbations (from apnea to word generation) could then be mapped by rapidly acquired MR images sensitive to T2* alterations. In addition to changing local magnetic susceptibilities, very small alterations in cerebral blood flow can give rise to observable in-flow effects on MR images. This can, in essence, allow mapping of regional arterial and venous demands in the brain. In a paradigm of mental activation, these two mechanisms work together, giving rise to a rapid and reversible increase in image intensity because of local increases in the arterial supply of oxygenated hemoglobin and in the accompanying increases in local blood flow and volumes. Aspects of technique development, improvement of image quality, refinement of the activation paradigms, and subject handling and positioning have been major components of the work being done in this field. The ability to repeatedly collect images every second or so over many minutes has allowed the design of paradigms that change during the examination to map the entire motor strip in a single examination or to track motional effects within the visual cortex.

PS 020 • 8:30 AM

Clinical Applications of Functional MR Imaging

BR Rosen, B Buchbinder, AG Sorensen, RG Gonzalez, R Bruning, RM Weisskoff, K Kwong, J Belliveau, TL Brady
NMR Center, Massachusetts General Hospital, Charlestown, MA

Fundamental aspects of brain function can be investigated by using the well-established interrelationship between cerebral activity, metabolism, and regional hemodynamics. Several techniques have been proposed to measure regional hemodynamics with MR imaging. These techniques can be applied in a wide variety of clinical applications in which characterizing functional attributes of pathologic tissue can enhance diagnostic and prognostic specificity, and in which definitive evaluation of adjoining eloquent cortex improves the safety of therapeutic intervention. Techniques using both exogenous and endogenous (deoxyhemoglobin) paramagnetic contrast agents have shown considerable promise in providing the ability to generate maps of hemodynamic parameters. Steady-state images of hemodynamic parameters (eg, CBV, CBF) can be made by following the first pass kinetics of injected paramagnetic chelates. These maps can be made with high SNR and are of value when evaluating pathologies characterized by resting perturbations in metabolism and function. Although of lower intrinsic sensitivity, endogenous flow or susceptibility contrast can be used to define regions of activated cortex by using the paradigm of paired task subtraction. Noninvasive measurement of these hemodynamic variables may have a significant effect on the diagnosis and management of patients with ischemia, epilepsy, neurodegenerative disorders, and cerebral neoplasms. Direct imaging of cortical activation opens new possibilities for presurgical planning, improved specificity in evaluating dementias, and providing quantitative tools for studying neuropsychiatric disorders at a functional level. The unique ability of MR to image tissue microvasculature may allow MR to directly image the phenotypic expression of tumor angiogenic growth factor genotypes. Microvascular insult may also lie at the heart of neurodegenerative disorders such as Alzheimer disease. With ischemic disease, functional MR data offer the potential to detect hypoperfusion well before conventional MR studies, to quantify the degree of hypoperfusion within the central lesion and the surrounding ischemic penumbra, and to evaluate cortical plasticity with recovery.

PS 021 • 9:00 AM

Panel Discussion: Functional Neuroimaging

CR Jack Jr, BR Rosen, W Orrison, A Evans, ME Moseley
Department of Diagnostic Radiology, Mayo Clinic, Rochester, MN

Functional neuroimaging is based on the observation that certain areas of the brain are activated by specific mental tasks. Task activation produces observable changes in local cerebral physiology above baseline rates in a number of parameters, such as blood flow, metabolism, neuronal firing rate, and others. A great deal of attention has been focused recently on three different neuroimaging modalities, all of which are used for imaging brain function: PET, magnetoencephalography (MEG), and functional MR imaging. In this panel discussion, an expert in each of these three functional neuroimaging modalities will describe the physics data processing strategies and the biologic basis underpinning their particular functional modality. Each will discuss the past, present, and what he believes the future holds for his particular modality in the areas of elucidating normal and abnormal mental function and in clinical applications. Attention will be focused on the potential (or lack thereof) of MR imaging and MEG to study specific primary sensory systems and higher cognitive domains as has been done with PET. Individual presentations will be followed by a panel discussion that will focus on the preceding individual presentations as well as approaches to cross-modality studies of brain function.

B.R. Rosen is an external advisory committee member for Sterling, Squibb Diagnostics, and Bracco, which support clinical trials.

Tuesday Afternoon • Chantilly West
Plenary Symposia 022– 024

MUSCULOSKELETAL MRI
MODERATOR: JV CRUES, III, MD

PS 022 • 1:30 PM
Musculoskeletal Masses: Role of MR Imaging
RA McLeod
Department of Diagnostic Radiology, Mayo Clinic, Rochester, MN

Musculoskeletal masses are uncommon and comprise a large number of heterogeneous lesions with widely divergent biologic capabilities and therapeutic requirements. This talk will address the contribution of MR imaging to the care of these patients, with emphasis on detection and characterization. The information in this presentation is based on the experiences and observations gleaned from a large clinical MR imaging practice containing many patients referred from a busy orthopedic oncology division. The plain radiograph is the least expensive and usually the most reliable for characterization of bone abnormalities. MR imaging, however, is useful in a number of situations, especially for lesions located in the medulla or on the bone surface, and for those that arise centrally or within abnormal bone altered by surgery, trauma, or preexisting disease. By observing MR imaging morphology and signal characteristics, certain characteristics of tissue can be inferred. This sometimes permits a diagnosis not otherwise possible. MR imaging is the examination of choice for detection and characterization of a soft-tissue mass. MR imaging findings permit distinction between benign and malignant processes in most cases. In many cases, a specific diagnosis may be suggested on the basis of the MR imaging appearance, and this is especially true when dealing with benign tumors or nonneoplastic conditions. For depiction and characterization of soft-tissue masses, MR imaging is unrivaled. For bone tumors, the plain radiograph is the initial study of choice, with MR imaging playing an important but secondary role.

PS 023 • 2:00 PM
Musculoskeletal Injuries: New Lessons from MR Imaging
PFJ Tirman, CG Peterfy
San Francisco Magnetic Resonance Center, San Francisco, CA

The purpose of this presentation is to document the effect MR imaging has had in advancing our understanding of pathophysiologic processes and directing change in the management of certain musculoskeletal injuries. A review of the literature and direct discussions with orthopedic surgeons were used to examine the ways MR imaging has influenced current treatment practices and patient outcome in a variety of specific disorders, including radiographically occult bone injuries, tendon and ligamentous degeneration, glenoid labral cysts and insufficiency, and articular cartilage injury. MR imaging is uniquely capable of identifying early stages of bone injury that are occult at plain radiography or CT. In cases of isolated trabecular injury or nondisplaced fracture, the use of MR imaging can obviate protracted diagnostic workup, expedite the initiation of appropriate therapy, and thereby limit the financial effect of these prevalent disorders. MR imaging is the only noninvasive method with any significant scope for directly visualizing articular cartilage in joint trauma and degeneration. Recent innovations in high-resolution imaging and novel pulse sequences now provide an unprecedented opportunity for examining the pathophysiology and treatment of cartilage disease. The recently recognized association between cysts about the glenoid labrum and shoulder instability has important implications both to surgical planning and evaluation of patients not initially thought to be unstable. The growing awareness of the role of glenohumeral instability in the pathophysiology of rotator cuff disease has fueled a renewed interest in detailed imaging evaluation of glenohumeral ligaments and the shoulder capsule. High-speed sequences have enabled these and other joints to be imaged during active movement. In contrast to cine images generated by means of passive positioning, truly dynamic joint imaging may be able to capture abnormal interactions between soft tissues that occur only transiently during joint loading. MR imaging has contributed significantly to our current understanding of pathophysiologic mechanisms of musculoskeletal disease, and will undoubtedly continue to play an instrumental role in the evolution of new approaches to combating some of these highly prevalent disorders.

PS 024 • 2:30 PM
Musculoskeletal MR Imaging: Framework for Determining Cost-Effectiveness
JV Crues, III
Cedars-Sinai Medical Center, Los Angeles, CA

The purpose of this talk is to define potential frameworks for experimental designs to determine the cost-effectiveness of MR imaging in clinical medicine. The American Academy of Orthopaedic Surgeons has commissioned a Task Force on Technology Assessment. Its first task was to evaluate the cost-efficacy of MR imaging of the knee. The choice of potential study designs and the results of this experiment will be reviewed. This study does show that cost-efficacy can be measured, and such measures can be used in clinical decision making and economic decisions. Many pitfalls are inherent in this type of study, and potential misinterpretations could have a significant negative effect on the quality of medical practice. Some assumptions inherent in cost-efficacy studies, such as the need to put a price on patient outcomes and the dependence of relative efficacy on payer or patient economic status, may be ethical dilemmas for physicians. Cost-efficacy studies will become a necessary component of medical practice in the future as a system is put in place nationally to require justification for medical reimbursement. Physicians, payers, patients, and the government must become more aware of potential pitfalls that could negatively effect the quality of medical practice.

Wednesday Morning • Chantilly West
Plenary Symposia 025–027

CARDIOVASCULAR MRI
MODERATOR: RD WHITE, MD

PS 025 • 8:00 AM
Cardiovascular MR Imaging Techniques: An Update
DL Parker
University of Utah School of Medicine, Department of Radiology, Salt Lake City, UT

Since the early days of MR imaging, there has been considerable interest in developing diagnostic applications in cardiovascular imaging. Such applications have included visualization of cardiac anatomy, cardiac dynamics, and regional blood flow, as well as blood vessel anatomy and blood flow. Anatomic and functional imaging of the beating heart itself is primarily limited by temporal resolution of current MR imaging systems. Although significant progress has been made in imaging stationary vascular anatomy by using both time-of-flight and phase-contrast techniques, these techniques fall short of the spatial resolution required for replacement of all functions performed by x-ray angiography, due at least in part to technical limitations of current MR imagers. Coronary artery MR imaging appears to require high temporal and spatial resolution and suffers from all of the technical limitations of current MR imagers. Several recent innovations have had a direct effect on cardiovascular imaging. Loss of blood signal from signal dephasing has been reduced with new acquisition techniques that make the echo time as short as possible. By reducing the repetition time and, thereby, the total imaging time, techniques have been developed for acquiring images within a single breath hold. Artifacts and signal loss due to

respiratory motion are, thereby, significantly reduced. Further increases in imaging speed can and will be obtained by the development of faster and stronger imaging gradients, as well as in the further development of special anatomically optimized receive-only and transmit/receive RF coils. Resonant echo-planar gradient systems that allow rapid echo-planar imaging are becoming widely used. Acquisition techniques developed by using such systems have already demonstrated excellent moderate-resolution images of cardiac anatomy. Current improvements to these gradient systems will allow their use as standard nonresonant gradient systems for most currently used pulse sequences. Finally, although MR imaging has generally been used as a noninvasive imaging modality, recent experiments have demonstrated that contrast agents can be used to significantly improve chamber visibility, provide additional functional information, and significantly increase the signal from small blood vessels. These improvements are especially true in the case of experiments performed with intravascular-only contrast agents. Significant improvements in various cardiovascular techniques can be expected when these latter contrast agents are approved for human use.

PS 026 • 8:30 AM

Impact of MR Vascular Techniques in Clinical Practice

CE Spritzer
Department of Radiology, Duke University Medical Center, Durham, NC

The widespread clinical utility of MR imaging is incontrovertibly associated with the sensitivity of the technique in visualizing flowing blood. From the earliest investigators to today's proponents of new MR angiography techniques, the ability to image and, if need be, quantify flow has been cited as a rationale for considering MR imaging as a primary means of evaluating multiple organ systems. This sensitivity, coupled with inherently superior soft-tissue contrast, cross-sectional imaging, and noninvasiveness, enables MR imaging to produce a comprehensive examination combining many of the best features of CT, US, and angiography. To date, literally hundreds of articles have been written demonstrating the utility of MR imaging to assess every major vascular structure in the body. However, in the coming years of stagnant or reduced medical expenditure, the precise role of MR imaging in the cardiovascular arena will undergo scrutiny. Somewhat surprising is the paucity of studies addressing the cost or benefit of using MR imaging to assess vascular problems. Traditional clinical judgment suggests that certain applications are clearly rational and cost-effective, such as the assessment of vessels and vascular abnormalities in the routine study of intracranial pathology. Similarly, other applications, such as assessment of sagittal sinus thrombosis or vascular extent of a renal tumor, may be justified. However, in many other applications, such as the assessment of portal vein patency and flow, most cardiac flow measurements, and carotid artery disease, it remains to be seen whether MR imaging is (*a*) a screening study or a definitive procedure, (*b*) efficacious, and (*c*) cost-effective. These issues will be discussed during this presentation.

PS 027 • 9:00 AM

Current Role of MR Imaging in the Management of Cardiac Patients

RD White, N Obuchowski
Cleveland Clinic Foundation, Cleveland, OH

Owing to its potential for evaluation of anatomic and physiologic aspects of cardiovascular disease, MR imaging has become an important modality in the management of patients with disease of the heart, surrounding structures, or great vessels. While the role of cardiovascular MR imaging appears to be great, it is best assessed by outcomes analysis based on parameters addressing patient satisfaction, safety, cost, and diagnostic yield. Unfortunately, such studies are detailed, laborious, and difficult to implement at the present time (eg, because of difficulties with randomization of patients to different imaging modalities). Experience with use of cardiovascular MR imaging in a large routine clinical and clinical research practice will be discussed, and preliminary data from outcome studies will be presented.

Wednesday Afternoon • Chantilly West
Plenary Symposia 028–030

MRI OF THE BREAST

MODERATOR: SE HARMS, MD

PS 028 • 1:00 PM

MR Evaluation of Breast Cancer: Specificity Issues

MD Schnall
Department of Radiology, Hospital of the University of Pennsylvania, Philadelphia, PA

MR imaging has been shown to have the capability of demonstrating breast lesions that are mammographically and clinically occult. This is particularly true in women with dense breasts. However, the major finding that is considered suspicious for carcinoma—enhancement after gadolinium injection—is known to be nonspecific. The enhancement time course after the administration of gadolinium has been suggested as a method of improving MR specificity. Although early studies have reported this to be an effective way of classifying enhancing lesions as benign or malignant, more recent studies have demonstrated significant overlap. The architecture of lesions detected with MR imaging may also present a clue to lesion origin. The presence of internal septation and lobulation suggest the lesion represents a fibroadenoma, while border irregularity and rim enhancement are very suggestive of cancer. Thus far it appears that no technique will allow one to identify all enhancing lesions as either benign or malignant. However, some improvement in the specificity of the MR breast examinations may be achieved by considering multiple features.

PS 029 • 1:30 PM

Breast Cancer Staging

SE Harms
MRI Department, Baylor University Medical Center, Dallas, TX

The availability of and participation in breast cancer screening programs result in detection of smaller tumors, thus increasing potential for breast conservation surgery. The shift in surgical treatment toward lumpectomy emphasizes more accurate staging of breast disease. The rate of repeat surgery due to inadequate margins in lumpectomy patients approaches 50%. Undetected multifocal/multicentric disease at mammography is as high as 60%. Breast MR imaging may answer many of the clinical needs for a better staging method. Technical requirements for a staging method are more rigorous than for other breast MR applications because *all* cancer must be detected, not just the lesions seen at mammography. Fat suppression, T1 weighting, and 5-minute imaging time or less is needed in addition to high spatial resolution. Because breast cancers infiltrate surrounding normal tissue, the contrast between enhancing tumor and fat or ductal tissue will determine the spatial resolution needed for adequate tumor demonstration. The RODEO method provides robust fat suppression with heavy T1 weighting for a 128 × 256 × 256 3D image set in 5 minutes. Staging methods cannot be validated at biopsy because the remainder of the breast is not sampled. The presence of missed lesions is generally determined by using serial sectioned mastectomy analysis. For 30 patients imaged with RODEO with subsequent mastectomy analysis, a 94% sensitivity resulted. Multicentric disease not detected at mammography was seen in 30% of cases and 70% of those had involvement of more than one quadrant. Rigorous validation of MR methods is needed because, ultimately, MR staging will be employed in minimally invasive therapy for breast cancer.

PS 030 • 2:00 PM

MR Imaging Evaluation of Silicone Breast Implants

DP Gorczyca

Department of Radiological Sciences, UCLA Medical Center, Los Angeles, CA

Silicone breast implants have been surgically placed in nearly 2 million women for augmentation mammoplasty or reconstruction after mastectomies. Because of concerns about the potential dangers of rupture and leakage of gel implants, radiologists are often requested to evaluate the integrity of silicone implants. MR imaging has proved to be an excellent imaging modality for locating free silicone and evaluating an implant for rupture, with a sensitivity of approximately 95% and specificity of 97%. Silicone has a unique MR frequency and long T1 and T2 values that allow several MR sequences to provide excellent diagnostic images. The most commonly used sequences include T2-weighted, STIR, and chemical shift imaging. The T2-weighted and STIR sequences are commonly used in conjunction with chemical water suppression. The most reliable findings at MR imaging for detection of implant rupture include identification of the collapsed implant shell (linguine sign) and free silicone within the breast parenchyma. Unreliable MR findings for implant rupture include implant herniations, prominent radial folds, or fluid surrounding the implants. The different MR sequences, reliable MR findings, and potential pitfalls in evaluation of silicone breast implants will be discussed in this session.

MResource Guide Order Form

SMRI

the critical link between science and the clinical application of medicine, provides yet another important and helpful tool...
the MResource Guide

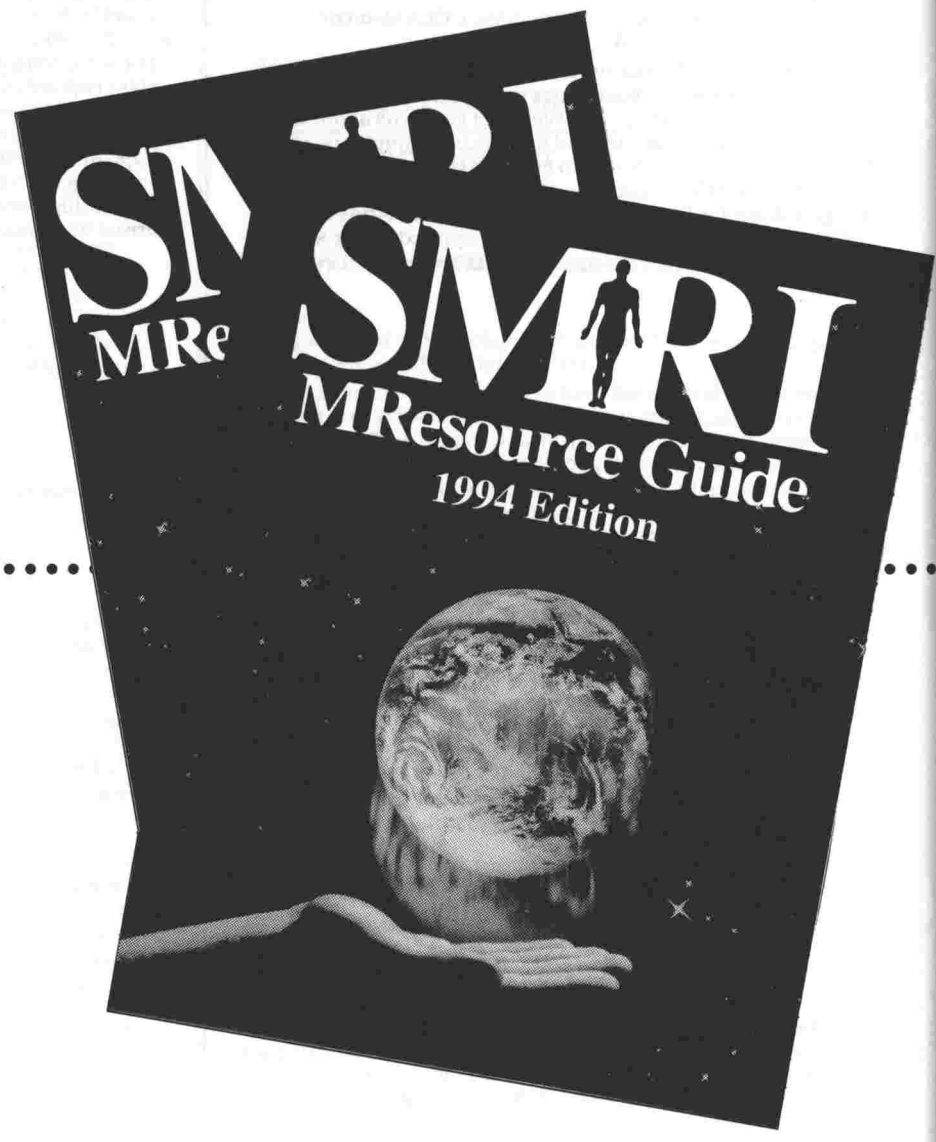

Photo by Al Francekevich

The second edition of the MResource Guide will be published inside the JMRI November/December 1993 issue. Additional copies of the Guide will be available and may be ordered by faxing this Order Form to the **SMRI** Central Office at 312/951-6474. If questions, call 312/751-2590.

Take control of a critical variable in magnetic resonance...order your MResource Guide today.

Name _____

Address _____

_____

City/State/Zip Code _____

Country _____

Phone _____ **FAX** _____

Number of MResource Guides:

☐ **1992 Edition** **@ $15.00 each**

☐ **1994 Edition** **@ $15.00 each**

$ _____ ***Total***

Payment enclosed (U.S. Funds only) ☐

MasterCard/Visa ☐

Name _____

Account #/Exp. date _____

Society for Magnetic Resonance Imaging

213 West Institute Place, Suite 501, Chicago, Illinois, 60610, Phone: 312/751-2590 FAX: 312/951-6474

Notes

Notes

Proffered Papers

The SMR Scientific Program Committee has assembled a fine selection of scientific paper presentations from more than 390 abstracts submitted this year. The final program offers a total of 244 papers in 34 parallel sessions during the week. Additional Works-in-Progress will also be presented; they may be found in the Works-in-Progress Supplement to be distributed on-site.

Seating for the scientific sessions is on a space-available basis. You are invited and encouraged to move from one meeting room to another during a time block to hear different presentations. Please, however, be sensitive to the presenter and the other attendees while implementing your itinerary.

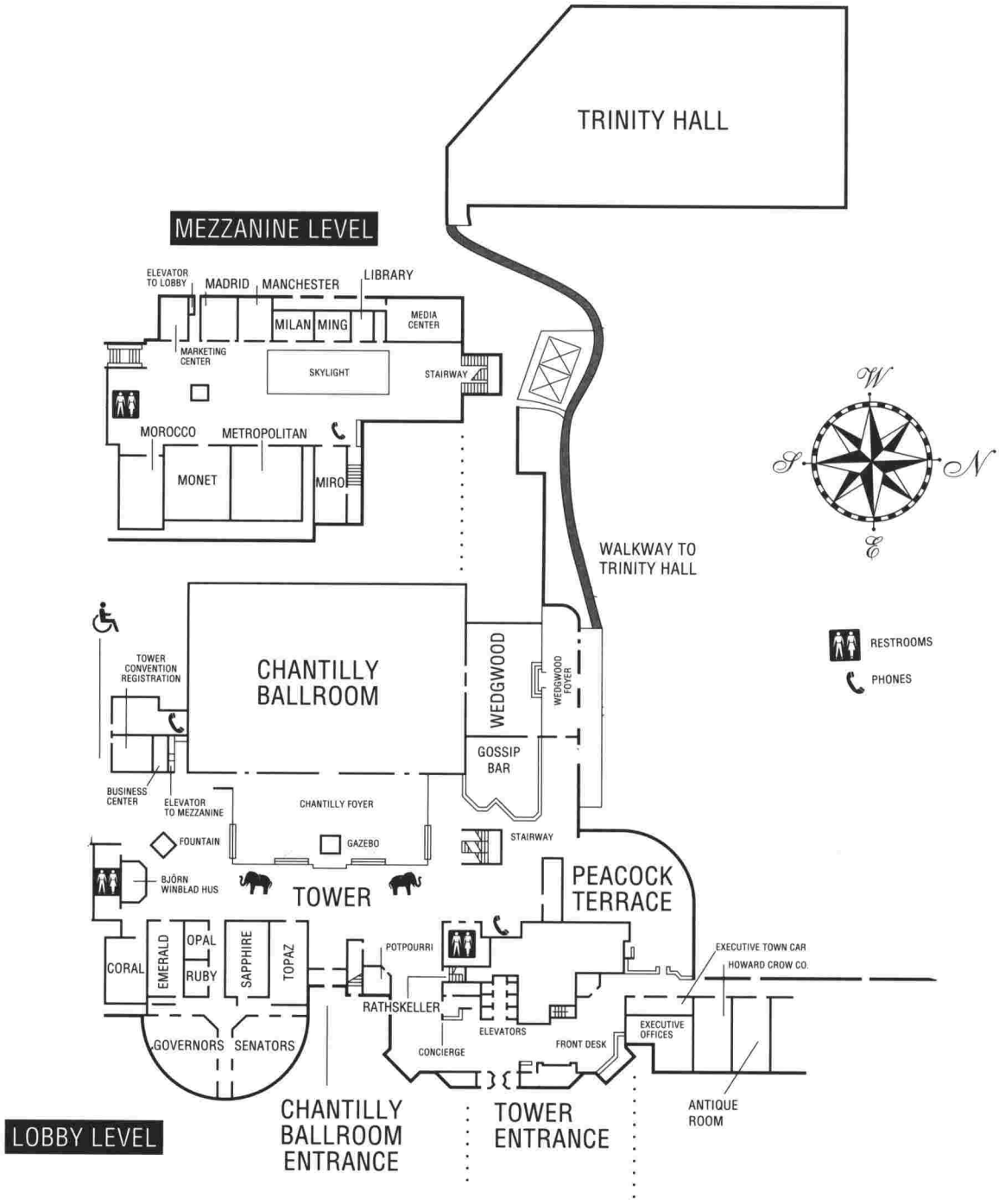

LOEWS ANATOLE
HOTEL

2201 STEMMONS FREEWAY DALLAS, TEXAS 75207
TEL 214 . 748 . 1200 FAX 214 . 761 . 7520

1994 Scientific Abstract Reviewers

S W Atlas, MD
Hospital of the University of Pennsylvania

W G Bradley, Jr., MD, PhD
Long Beach Memorial Medical Center

M N Brant-Zawadzki, MD
Newport Harbor Radiology

J J Brown, MD
Mallinckrodt Institute of Radiology

R N Bryan, MD, PhD
Johns Hopkins Hospital

M H Buonocore, MD, PhD
U C Davis Medical Center

R K Butts, PhD
Mayo Clinic

T Ceckler, PhD
National Institutes of Health

H C Charles, PhD
Duke University

B Chen, PhD
University of Southern California

M S Cohen, PhD
UCLA Medical Center

C L Crawford, PhD
General Electric Medical Systems

J V Crues III, MD
Cedars-Sinai Medical Center

R B Dietrich, MD
UC, Irvine

W P Dillon, MD
UC, San Francisco

W T Dixon, PhD
Emory University

J L Duerk, PhD
MetroHealth Medical Center

C Dumoulin, PhD
General Electric R & D

R R Edelman, MD
Beth Israel Hospital

J Frahm, PhD
Max-Planck Institut für Biophysikalische Chemie

P J Fritzsche, MD
Riverside MRI

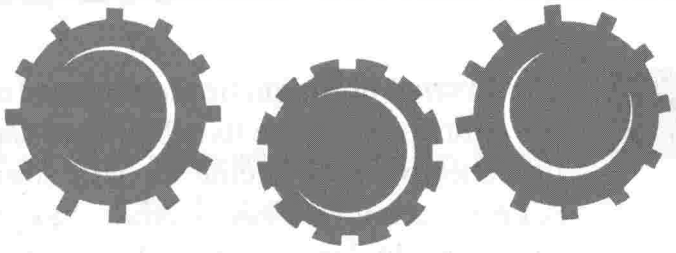

G D Fullerton, PhD
UT Health Science Center at San Antonio

E M Haacke, PhD
Mallinckrodt Institute of Radiology

S E Harms, MD
Baylor University Medical Center

A N Hasso, MD
Loma Linda Medical Center

R M Henkelman, PhD
Sunnybrook Health Science Centre

R J Herfkens, MD
Stanford University

C B Higgins, MD
UC, San Francisco

R Kikinis, MD
Brigham and Women's Hospital

J B Kneeland, MD
Hospital of the University of Pennsylvania

R J Kurland, MD
Geisinger Medical Center

J Listerud, MD, PhD
Hospital of the University of Pennsylvania

R B Lufkin, MD
UC, Los Angeles

J R MacFall, MD
Duke University

K R Maravilla, MD
University of Washington

S McCarthy, MD, PhD
Yale University

E R McVeigh, MD
Johns Hopkins Medical Center

D G Mitchell, MD
Thomas Jefferson University Hospital

M T Modic, MD
Cleveland Clinic Foundation

O Nalcioglu, PhD
UC, Irvine

P A Narayana, PhD
UT Health Science Center at Houston

K L Nelson, MD
Clarkson Hospital

D G Nishimura, PhD
Stanford University

R L Nunnally, PhD
Molecular Biosystems, Inc.

M D Osbakken, MD, PhD
Bristol-Meyers Squibb

S Patz, PhD
Brigham and Women's Hospital

S B Peterman, MD
Emory University

B D Pressman, MD
Cedars-Sinai Medical Center

R R Price, PhD
Vanderbilt University Medical Center

S J Riederer, PhD
Mayo Clinic

P A Rinck, PhD
University of Trondheim

B R Rosen, MD, PhD
Massachusetts General Hospital

J S Ross, MD
Cleveland Clinic Foundation

M Rothman, MD
University of Maryland

V M Runge, MD
University of Kentucky

B K Rutt, PhD
University Hospital, London Ontario

P Schmalbrock, PhD
Ohio State University

F G Shellock, PhD
Tower Imaging

J E Siebert, MD
Michigan State University

M S Silver, PhD
Philips Medical Systems

O P Simonetti, PhD
Siemens Medical Systems

W R K Smoker, MD
Medical College of Virginia

J A Sorenson, PhD
University of Wisconsin

H D Sostman, MD
Duke University Medical Center

C E Spritzer, MD
Duke University Medical Center

D D Stark, MD
University of Massachusetts Medical Center

S R Thomas, PhD
University of Cincinnati Medical Center

E C Unger, MD
University of Arizona Health Science Center

V Waluch, MD
St. Vincent Medical Center

S Wann, MD
St. Luke's Medical Center

M L Wood, PhD
Sunnybrook Health Science Centre

A Yang, MD
University Memorial Hospital

I R Young, PhD
Hammersmith Hospital

S W Young, MD
Stanford University

W T C Yuh, MD, MSEE
University of Iowa

Contrast Agent Special Issue Call for Papers

Intent:

The **Journal of Magnetic Resonance Imaging (JMRI)** provides a scientific forum where its subscribers may focus their attention on the collective work of clinical, basic science and commercial laboratories, each investigating areas of promise for exceptional clinical impact. In doing so, these developments will be advanced by unifying input from all components of MR research. **JMRI**'s contribution? **...the Contrast Agent Special Issue.**

Guest Editors:

David D. Stark, MD
William T.C. Yuh, MD, MSEE

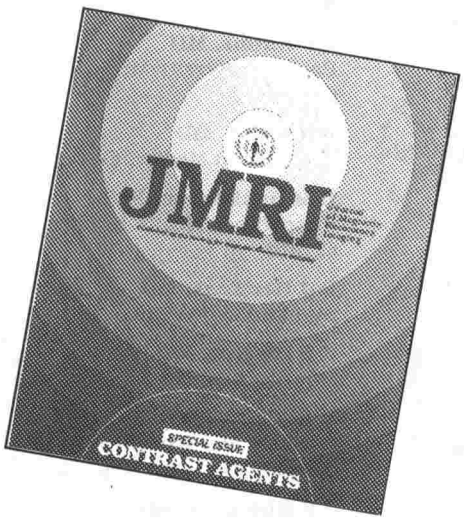

Schedule:

May/June 1994

Size:

240 pages + (double issue)

Content:

This issue will contain proffered basic science and clinical research papers specifically devoted to contrast agent-related topics, as well as 3-5 invited reviews of the field with multiple, focused analyses of subtopics. The reviews section is designed to extend and update topics from the 1993 edition.

Format:

The majority of the issue will be devoted to peer-reviewed contrast agent papers on extra-cellular agents (preclinical), intracellular agents (preclinical), and clinical applications of contrast agents.

Call for Papers:

JMRI invites authors of manuscripts in preparation on MR imaging contrast-related topics to submit their work for publication in the special topic issue. Submit all material to:

Gary D. Fullerton, PhD
Editor-in-Chief, **JMRI**
University of Texas Health Science Center at San Antonio
Department of Radiology
7703 Floyd Curl Drive
San Antonio, TX 78284

Questions: Call the JMRI Editorial Office at 210/567-5550

SMR '94 First Meeting of the SMR
Scientific Paper Abstracts

Sunday Afternoon • Monet Room
Papers 001–008

RAPID IMAGING
MODERATORS: S Patz, MD
J Pauly, PhD

001 • 3:45 PM
Turbo Spiral Sequence for Fast Imaging
AB Ken, JM Pauly, CH Meyer, DG Nishimura
Stanford University, Stanford, CA

Purpose: To develop a short TR, fast imaging sequence by using spiral readouts.
Methods: Most spiral sequences have interleaved multiple spirals that are rotated with respect to one another. Our technique acquires concentric segments (rings) of a single spiral, with one ring per TR. Any amplitude modulation of the MR signal between successive TRs caused by imaging before steady state is reached will then weight k-space in a smooth annular fashion, giving desirable impulse response characteristics. To reduce undesired modulation of the MR signal and to maximize SNR, a train of progressively increasing flip-angle RF excitation pulses are designed (1).
Results: The sequence was implemented on a standard 1.5-T GE Signa system. A 64-turn spiral was broken into 16 rings of 8 ms each to give a 32-cm FOV and resolution of 3 mm. The TR for the sequence was 16 ms, resulting in a total scan time of only 256 ms. Good quality images of phantoms were acquired, showing the feasibility of this approach. Ungated cardiac images were also acquired, demonstrating the insensitivity to flow and motion. A segmented k-space version was also implemented to give a 24-cm FOV and 1-mm resolution. This sequence used 8 interleaved spirals, each broken into 8 concentric rings, with one complete spiral acquired per heart cycle.
Conclusion: The feasibility of a turbo spiral sequence has been demonstrated. Good quality, moderate resolution images have been acquired in only 256 ms.
1. A. Kerr et al. 12th SMRM 1993; 1189.

002 • 3:57 PM
Three-dimensional K-Space Trajectory for Fast Volumetric Imaging
P Irarrazabal, DG Nishimura
Stanford University, Stanford, CA

Purpose: To design and implement a fast sequence for 3D acquisition with efficient use of gradients on standard hardware.
Methods: After experimenting with several 3D k-space trajectories, we chose one that we call the "yarn" trajectory because it resembles the way yarn is rolled into a ball. It is a continuous curve that traverses semicircles perpendicular to the $k_x - k_y$ plane. Each semicircle has the least curvature possible to minimize the slew rate and maximum gradient requirements. Interleaving provides a means to shorten the readout. Two types of interleaving are performed: angular (with respect to k_z) and radial (spherical shells). The nonuniformly sampled data are compensated for k-space density and gridded to a Cartesian grid for the image reconstruction.
Results: A sequence was implemented by using the yarn trajectory for a 3D FOV of 20 cm with isotropic resolution of 3 mm. The slew-rate limit is 2 G/cm/ms and the maximum gradient amplitude is 1 G/cm. A total scan time of 9 s was achieved with 300 interleaves (10 shells, 30 rotations), TR of 30 ms, and 16 ms readouts. A prototype RARE version of the sequence using 180° pulses was also implemented to further reduce the scan time.
Conclusion: We demonstrated the feasibility of imaging a volume with reasonable FOV (20 cm) and resolution (3 mm) in a short time (9 s).

003 • 4:09 PM
Effect of High-Speed Gradients on SNR in Ultrafast Gradient Echo Imaging
SB Reeder, ER McVeigh
Johns Hopkins University, Baltimore, MD

Purpose: The purpose of this work was to calculate the expected improvement in signal-to-noise (SNR) ratio obtained with high-speed imaging gradients (10 G/cm/ms, 2 G/cm maximum amplitude) versus that obtainable with conventional gradient hardware (1.7 G/cm/ms, 1 G/cm maximum amplitude). The improvements were also compared with those that would be obtained from an "ideal" gradient probe that has infinite slew rate and infinite available gradient strength.
Methods: Equations were derived for the SNR obtained with spoiled GRASS (SPGR), and Bloch equation simulations were performed to determine the SNR obtained with GRASS. Experiments were performed to validate the equations and simulations. The effects of slice selection, phase spoiling, and the approach to steady state were accurately modelled. The relative SNR of the two pulse sequences was evaluated for the three gradient performance levels, and T1 = 875 ms and T2 = 60 ms.
Results: Complete descriptions of the tradeoffs between maximum slew rate and amplitude were calculated. It was found that rapid switching was more important than maximum available amplitude for improving SNR. As an example, the relative SNRs for SPGR at a TR of 5.5 ms (minimum achievable with conventional gradients) were 0.55, 0.90, and 1.0 for the conventional, high-speed, and ideal gradient probes, respectively. For GRASS with the same TR, the relative SNR values were 0.56, 0.85, and 1.0.
Conclusion: It was found that optimal SNR was achieved by minimizing the bandwidth and dead times through rapid gradient switching. For both SPGR and GRASS, the high-speed gradient system yielded approximately 65% improvement in SNR, and the relative SNR achieved was approximately 90% of the maximum possible.

004 • 4:21 PM
Fast T1-Weighted Imaging with Multiexcitation EPI
K Oshio, FA Jolesz
Department of Radiology, Brigham & Women's Hospital, Boston, MA

Purpose: The current technique of choice for fast T1 imaging is either RF-spoiled GRASS (SPGR) or T1-weighted RARE. The main drawback of the SPGR sequence is that contrast to noise has to be compromised for speed. The speed advantage of the T1 RARE sequence is not as dramatic as in T2 imaging, since the echo train length is limited to keep the effective TE short. The purpose of this work is to show that the multiexci-

tation EPI sequence is a good alternative for clinical fast T1 imaging.
Methods: Multiple gradient echoes are collected following the excitation and the refocusing pulses. The Hahn spin-echo position is set to the first gradient echo, and half Fourier phase encoding is used. This sequence is particularly suitable for multislice dynamic examination. Breath-hold imaging is possible (around 10 seconds) with multislice capability. Echo position shifting was used to reduce ghosting artifact due to field inhomogeneity or chemical shift. The pulse sequences were implemented on a commercial scanner (1.5-T Signa) without hardware modifications.
Results: Phantom images, as well as images from healthy volunteers, were obtained. Typical imaging time was 12 seconds for 10 slices with a 500 msec TR and 256 × 120 imaging matrix. Image contrast is essentially the same as with the spin-echo sequence.
Conclusion: The multiexcitation echo-planar sequence tailored for fast, high quality T1 imaging, rather than ultrafast imaging, can be a good alternative for clinical T1 imaging.

005 • 4:33 PM
Random Phase Encoding for Continuous Image Updating
T Parrish, X Hu
Department of Radiology, University of Minnesota Medical School, Minneapolis, MN

Purpose: To develop a technique that allows for faster image updating in dynamic imaging by using random phase encoding.
Methods: Using an ultrafast sequence (TR/TE/α = 8/4/10°), consecutive frequency-encoded gradient echoes are sampled, each with a phase-encoding step from a random table. The table is randomized such that the k-space coverage is statistically equivalent at any time. To insure that an image can be obtained at any time, the low k-space lines are repeated more frequently in the table. In this implementation, on the average for each repetition of the high k-space lines, the central (0) line is repeated 5 times, ±1 lines 4 times, ±2 lines 3 times, ±3 lines 2 times, and ±4 lines 2 times. The reconstruction starts by selecting data in a window centered around the desired time with width determined by the matrix size. For the repeated lines, the one closest to the center of the window is used. The data are then reordered and Fourier transformed to form an image. The window is moved along the time axis to generate images at other times. We have applied this technique to phantoms and in the heart of volunteers.
Results: Images of the phantom depicting its movement were obtained. These images exhibited "continuous" motion of the phantom with negligible blurring. An effective temporal resolution of 15 frames/sec was achieved. Continuous images from the volunteer, adequately depicting the heart and chest motion were obtained.
Conclusion: We have developed and demonstrated a new technique capable of faster image updating for dynamic imaging.

006 • 4:45 PM
Local Look (LOLO): Zoom Fluoroscopy of a Moving Target
JJ van Vaals, GH van Yperen, TLM Hoegenboom, MJ Duijvestijn
Philips Medical Systems, Best, The Netherlands

Purpose: Recently, MR has been developing toward a real-time imaging modality with special high-performance hardware and methods like EPI. We present a method that, with a standard commercial scanner with prototype software, allows real-time imaging and viewing of a zoomed area, repositionable on the fly.
Methods: We used a turbo spin-echo sequence with an echo spacing of approximately 6 ms on a standard 1.5-T Philips ACS-II. The FOV in the phase-encoding direction is zoomed to reduce scan time. Backfolding of tissue signal outside the reduced FOV is eliminated by slice selection applied during the excitation pulse, perpendicular to the refocusing pulse slice selection. The position and angulation of the observed slice, and also scan parameters such as the frame rate, can be interactively changed on the fly.
Results: A time resolution could be achieved of up to 10 frames per second (fps) for a 128 matrix with a zoomed FOV in the phase-encoding direction with a factor of 8. The SNR depends strongly on the frame rate, where fewer fps allows more relaxation between shots and, therefore, increased SNR. Typically, for 4 fps the SNR decreased from the initial image to subsequent ones by a factor of 2, and by changing to 10 fps, SNR decreased by another factor of 2.
Conclusion: The Local Look (LOLO) method allows fluoroscopic imaging of a zoomed FOV, which can be adjusted on the fly to follow a moving target. Possible applications are following catheter or biopsy needles in interventional MR, and interactive slice positioning in cardiac MR.
J.J. van Vaals is an employee of Philips Medical Systems.

007 • 4:57 PM
Dynamically Adaptive MRI Method Using SVD
GP Zientara, LP Panych, DO Kuethe
Department of Radiology, Brigham and Women's Hospital, Boston, MA

Purpose: Dynamic applications in MRI, such as the real-time monitoring of some surgical procedures, require rapid, continuous updating of image data. We are developing an adaptive pulse sequence and data acquisition technique that uses prior image information and scaling to dynamically specify the image encoding and acquisition strategy for greater efficiency in acquiring MR images.
Methods: The previous image acquired in a series, at the original resolution or scaled, is used as the current image estimate to determine an "optimal" MR encoding scheme utilizing the selective RF excitation encoding technique. The image estimate is processed to obtained its singular value decomposition (SVD), and the SVD is used to specify the next set of RF excitations for dynamic image refreshment. RF pulses are shaped to generate a reduced number of excitation profiles that are equivalent to a small subset of the most significant SVD basis vectors that encode image features. Changes in the newly acquired image relative to the estimate are accommodated by scaling, repeating the SVD, and acquiring only new uniquely encoded image data. Acquired SVD-encoded data are applied within the simultaneous iterative reconstruction technique (SIRT), which enforces self-consistency between computed and acquired image data. The technique is adaptive, since the encoding strategy in each time interval is based on the image estimate from the previous time interval.
Results and Conclusion: Studies of SVD transformation of MR images indicate that image detail can be adequately encoded by a compact set of SVD singular vectors. Our simulations of MR imaging show that only a fraction of encodes are necessary when continuously updating images with this dynamic multiscale SVD technique. The method is currently being simulated with images obtained with a 1.5-T GE Signa imaging system.

008 • 5:09 PM
Keyhole Sequence in Two Dimensions for High-Speed Fluoroscopic Imaging on Ultra-Low-Field MR Systems
M Busch, MH Friebe, S Hellwig, H Lerchner, DHW Grönemeyer, RMM Seibel
University of Witten/Herdecke, Bochum, Germany

Purpose: Currently, rapid sequences implemented on low-field MR systems are, because of their low signal/noise ratio, low voxel resolution, and insufficient contrast differentiation, not usable in many clinical applications requiring near real-time imaging capabilities. To correct these problems we developed a new imaging technique that acquires the image k-space data in the form of a cross around the center of the matrix by using two keyholes in both the phase-encoding (PE) and frequency direction.
Methods: We implemented the keyhole technique in a standard 2D SE sequence, acquiring only 64 PE steps around k-space and, after rotation of frequency and PE direction, another 64 PE steps. The remaining points of the k-space data

matrix were filled with zeros. Actual data are therefore collected only in a cross with a width of 64 points. This sequence does not, therefore, require a reference image as in standard keyhole acquisitions and still acquires all the relevant data. We dubbed this new sequence PHREAK (PHase Read Exch-Ange Keyhole). The MR system used was a 0.064-T Toshiba ACCESS.
Results: We obtained high quality (high S/N ratio, good contrast) images with a 2D SE sequence (3 slices, TR = 0.1 sec, TE = 20 msec, 1.0 mm × 1.0 mm × 5 mm, 256 × 256 matrix) in less than 13 seconds, a speed increase of a factor of two compared with a 256-step SE sequence.
Conclusion: The results show this new imaging technique offers sufficient speed and image quality for ultra-low-field MR imaging. PHREAK can be implemented on any commercial scanner and with virtually any imaging technique currently used, reducing the acquisition time by factors of two to four.

Sunday Afternoon • Metropolitan Room Papers 011–017

INTERVENTIONAL MR

MODERATORS: R Kikinis, MD
RB Lufkin, MD

011 • 3:45 PM
Low Back Pain Treatment with Interventional MRI Guidance

DHW Grönemeyer, RMM Seibel, G Schmid, M Deli, M Friebe, M Busch
University of Witten/Herdecke, Mühlheim, Germany

Purpose: CT-guided pain therapy treatments are routine techniques in our department. Interventional magnetic resonance imaging is helpful in the therapy of facet and iliosacral joints.
Methods: For interventional procedures, a 0.064-T open designed MRI scanner and, for comparison, a helical CT scanner were used. For the treatment, self-developed nitinol, titanium, or stainless steel (18G) instruments were used. Local anesthetic and cortisone, as well as 1.0 mL of 50% ethanol, for the therapy of chronic facet joint pain, were injected.
Results: Results of 20 interventional MRI- and CT-guided facet joint therapies and 20 iliosacral joint infiltrations were compared. There is a lack of ionization and possibility of 3D localization with MRI. An open access allows nearly real-time guidance of instruments. In CT the tip of the instruments is easy to define, especially if the guidance direction is oblique, but the patient has to be moved in and out of the gantry several times. In open MRI the treatments were done inside the gantry, and tissue contrast changes with ethanol treatment are visible without contrast media injection.
Conclusion: MRI-guided techniques are helpful for interventions in low back pain therapy, when there are no important structures such as motor nerves to damage. The infiltration of ethanol can be documented without contrast media.

012 • 3:57 PM
Interventional MRI Guidance: Competition with CT in the Field of Microtherapy?

DHW Grönemeyer, RMM Seibel, M Deli, M Busch, MH Friebe, L Kaufman, M Stehling, D Boyd
University of Witten/Herdecke, Mülheim, Germany

Purpose: Interventional computed tomography/fluoroscopy (I-CT/F)-guided microsurgery for biopsies, sympathectomies, cancer therapy, diskectomies, and pain therapy are increasingly used for minimally invasive therapy. Interventional magnetic resonance imaging (I-MRI) is a new monitoring tool in this environment.
Methods: For I-MRI, two systems were used: a 0.064-T open scanner and a 1.0-T scanner. For monitoring the interventional procedures, fast MRI fluoroscopy and keyhole sequences were used. Self-developed biopsy instruments made of nitinol, titanium, or stainless steel (18G) and microendoscopes (0.3–1.2 mm) were used for comparison with CT-guided interventions with a helical CT scanner (1 slice per second) and an ultrafast CT scanner (up to 17 slices per second).
Results: Results of 30 interventional MRI- and CT-guided soft-tissue biopsies and endoscopies of animals and humans were compared. The average inaccuracy in determining the true location of the tip of the instruments with MRI was 0.6–2.5 mm. The combination of acquisition and reconstruction time was faster with MRI than with CT. Best feedback times between repositioning of the patient couch and patient access were found with the open low-field MRI scanner.
Conclusion: MRI-guided techniques are helpful for biopsies and interventions in soft-tissue regions of more than 1.0 cm diameter, as in intratumoral therapies, and if the treatment is time consuming. I-CT/F guidance still is the standard for high accuracy in treatments, as in percutaneous diskectomies, sympathectomies, or for biopsies in high risk areas.

013 • 4:09 PM
Ultrasonic Neurowand for Interventional MR and Interactive Frameless Stereotaxis

DW Kormos, CP Steiner, GH Barnett, DW Piraino, J Weisenberger, C Wood, JM McNally
Department of Neurosurgery, Cleveland Clinic Foundation, Cleveland, Ohio

Purpose: To develop an interactive and frameless means of stereotaxic localization for interventional MR procedures inside and outside the imaging suite.
Methods: A 3D ultrasonic digitizer system (Science Accessories) was interfaced to a ViStar medical graphical supercomputer (Picker International). Custom "neurowands" were built as digitizer pointing devices. Spherical fiducials filled with an MR visible solution were attached to the patient. A volume gradient-recalled echo sequence was used to image the patient and fiducials. By using the neurowand and fiducials, scan data were registered to patient anatomy. Once registered, multiplanar reformatting software locates axial, sagittal, and coronal planes selected with the neurowand tip. Oblique planes normal to and inclusive of the neurowand axis were presented. Surface rendering of patient MR data provided orientation.
Results: The described system has been successfully used in over 160 craniotomies, neurosurgical biopsies, spinal instrumentation cases, and CT-table–guided biopsies at the Cleveland Clinic Foundation. The mobile system's accuracy is comparable with that of traditional framed-based stereotaxic methods. Results of its use outside the MR suite as well as strategies for its use proximal to the MR scanner will be presented.
Conclusion: A user-friendly, hand-held "neurowand" has been developed as an interface between clinicians and a state-of-the-art graphics supercomputer. It provides near real-time interactive visualization for interventional MR and CT procedures and stereotaxic surgery. This system has the potential to significantly shorten procedure times, thereby reducing costs.
This research was supported in part by Picker International.

014 • 4:21 PM
Temperature–Signal Intensity Correlation for FSE Imaging of in Vitro Laser Irradiation

SG Hushek, PR Morrison, GE Kernahan, MP Fried, FA Jolesz
Department of Radiology, Brigham & Women's Hospital, Boston, MA

Purpose: Dynamic imaging of interstitial laser irradiation in vitro was performed to compare image-derived temperatures to measured temperatures. Successful correlation of signal intensity (SI) to temperature would enable intraoperative images to predict postoperative effects on tissue.
Methods: The study tested a fast spin echo (FSE) sequence for monitoring temperature changes. The sequence used TR = 300 msec, TE = 18 msec, echo train length of 4, and 128 × 256 matrix to yield a total acquisition time of 10 sec-

onds. Repeated imaging of the same plane monitored the changing spatial profile of the SI during the laser exposure. Temperatures were recorded during a 1-second delay between successive images. The plane imaged contained the Nd:YAG laser fiber inserted into the polyacrylamide gel and the thermocouples used to measure the temperatures. SIs from circular ROIs were sampled on all the images; the SIs were normalized and multiplied by the Δ°C/%ΔSI (a linear coefficient from prior work) to produce "derived temperatures." The results were graphed separately as SI and derived and measured temperatures versus time.
Results: Results showed approximately a 1% change in SI per degree centigrade. Image-derived temperatures were consistently higher than measured temperatures, often by as much as 10°C, but the shapes of the plots were very similar.
Conclusion: The results are encouraging and quantify the intraoperative image in a parameter important to the tissue (ie, temperature). A possible source of error could be T2 variation or convective flow due to temperature gradients, as will be discussed.

015 • 4:33 PM
Dynamic Diffusion-weighted Snapshot FLASH Sequence for Interventional MR Applications
U Sinha, S Sinha, A Huang, R Lufkin
Department of Radiological Sciences, University of California at Los Angeles, Los Angeles, CA

Purpose: To measure spatial distribution of temperature and temperature transients during and after RF ablation in ex vivo bovine muscle and in vivo pig and rabbit brain by using diffusion-sensitized fast imaging sequences.
Methods: Diffusion-sensitive gradients were added to the preparatory pulse of a T2-magnetization–prepared snapshot FLASH sequence (TE/TR = 2/5 ms). Gradient pulses were 9 mT/m in strength and 20 ms in duration. A 5° flip angle minimized T1 effects. Two sequences, one with the diffusion gradients on and the other without were acquired to calculate diffusion maps every 2 s. An RF probe for delivery and monitoring of RF power (developed here and reported at the last SMR meeting) was used with an RF generator (Radionics, Burlington, Mass) on a Siemens 63SP Magnetom.
Results: RF ablation for 60–90 s elevated the temperature as sensed by the probe to 80°–90°C. Diffusion maps could be calculated every 2 s, and were acquired at intervals of 5 s during and 5 min after the RF ablation. Temperature variations calculated from the diffusion maps agreed well with the temperature readings of the generator as well as maps generated by fiberoptic temperature sensors.
Conclusion: The diffusion-weighted snapshot FLASH sequence provides a robust and fast imaging scheme that has sufficient sensitivity to reflect temperature changes during RF ablation. Efforts are underway to incorporate specially designed RF pulses to reduce the artifact from the RF needle, which is significant in these gradient-recalled images.

016 • 4:45 PM
High-Resolution MR Imaging and Quantification of Laser-induced Thermal Injury in the Vascular Wall
A Ahmad, C Roberts
Ohio State University, Columbus, Ohio

Purpose: To achieve quantitative correlation between T1-weighted images of laser-induced thermal injury in human aorta (in vitro) and the corresponding histology in order to verify the extent of injury and serve as a base from which to guide future in vivo studies.
Methods: Thermal injuries were produced by using a continuous wave broadband argon ion laser. Injuries were produced remotely by using an optical fiber delivery system. High-resolution images (256 × 256 matrix, 40-mm FOV, 0.7-mm section, NEX = 2) were obtained at 1.5 T with a 3D time-of-flight sequence (TE/TR = 18/86 msec, flip angle = 45°) with a specifically designed (1-inch diameter, receive only) surface coil. Each sample was imaged first in the uninjured state and then reimaged after laser injury without physical movement of the sample within the magnet. The samples were then fixed and assessed histopathologically by using Masson trichrome and H and E stains.
Results: T1-weighted MR images clearly showed residual thermal injury, typically as a region of high signal intensity relative to the surrounding undamaged tissue. By using spatial resolution of 156 μm, even subtle thermal injuries were detected. Quantitative correlations between thermal injury on MR images and the corresponding histologic sections, and quantification of thermal injury by subtraction of pre- and postinjury images will be presented.
Conclusion: Evaluation of high-resolution pre- and postinjury images clearly demonstrated the capability of MRI to map thermal injuries in the vascular wall, as supported by the corresponding histology.

017 • 4:57 PM
Reduction of Susceptibility Artifacts from RF Probes in Interventional MR Imaging
A Huang, S Sinha, U Sinha, R Lufkin
Department of Radiological Sciences, University of California at Los Angeles, Los Angeles, CA

Purpose: To reduce the significant susceptibility artifacts that arise from differences in susceptibility between the RF delivery probe and surrounding biologic tissue in applications where MR is used for visualizing RF hyperthermia.
Methods: Magnetic field distortions caused by RF needles are calculated from known values of susceptibility of the needle and surrounding tissue. A tailored RF excitation pulse is designed to minimize the spin dephasing in the slice-select direction and the consequent signal loss. Such tailored RF pulses can then be tagged onto any imaging pulse sequence that uses gradient-recalled echoes. Biopsy needles, 22 gauge, made of the same material as an RF delivery probe developed at our site and used with a Radionics (Burlington, Mass) generator, were used in different phantom material to test the efficacy of the sequence.
Results: These tailored RF pulses were incorporated in 2D FLASH sequences on a Siemens 63SP Magnetom, for imaging a water phantom containing $NiCl_2$, ex vivo chicken muscle, and in vivo pig brain. Reductions of 17%–35% in the size of the needle artifact were observed in all three.
Conclusion: This technique has proved useful in reducing the signal void around RF needles. The artifact can be reduced further by lowering the TE, while regions heated by RF can be visualized better with diffusion imaging. Hence, we are in the process of combining this technique with fast gradient-echo sequences (TE = 2 ms) with magnetization-prepared diffusion weighting to provide real-time imaging of the region of heating during an RF ablation procedure.

Sunday Afternoon • Miro Room
Papers 021–027

BRAIN I: General
MODERATORS: RB Dietrich, MD
JS Ross, MD

021 • 3:45 PM
Childhood Cerebral Form of Adrenal Leukodystrophy: Contrast-enhanced versus Nonenhanced Brain MR Imaging in Patients following Bone Marrow Transplantation
W Bula, DJ Loes, A Stillman, E Shapiro, L Lockman, R Latchaw, W Krivit
University of Minnesota, Minneapolis, MN

Purpose: The purpose of the study was to compare contrast-enhanced axial T1 images with nonenhanced T1 and T2 MR images in patients with the childhood form of cerebral adrenal leukodystrophy (COCALD) following bone marrow transplantation.
Methods: Seven boys with COCALD (mean age, 8 years 10 months) have undergone successful BMT at our institution. Initial diagnosis was based on positive biochemical test re-

sults, abnormal neurophysiologic test results, and positive brain MR imaging findings. Serial post-BMT MR scans were performed on a 1.5-T Siemens magnet. All studies included routine sagittal T1-weighted and axial protein-density/T2-weighted sequences. Of the 26 post-BMT MR studies, 19 included contrast-enhanced axial T1-weighted images. An MR severity score (0.5–34) based upon disease location and the presence or absence of focal and/or global atrophy was calculated for each patient.
Results: Twenty-six post-BMT brain MR examinations were available for review in the seven patients. The mean post-BMT MR follow-up was 19 months. Based upon MR severity scoring, post-BMT images showed improvement in 2 patients, stabilization in 3 patients, and progression in 2 patients. None of these studies demonstrated any abnormal contrast enhancement. One of the patients with progressive disease had a pre-BMT MR study that did show enhancement.
Conclusion: Contrast agent use does not appear to be of clinical importance in routine MR follow-up of post-BMT COCALD patients. MR disease progression may occur without corresponding abnormal contrast enhancement.

022 • 3:57 PM
Diagnosis of Liquor Fistulas with a 3D PSIF Sequence
KEW Eberhardt, HP Hollenbach, M Gjuric, WJ Huk
Department of Neuroradiology, University of Erlangen, Erlangen, Germany

Purpose: Posttraumatic and postoperative liquor fistulas are at high risk of developing an endocranial infection. In former studies, we demonstrated that there is a correlation between the width of a skull base fracture and a dural lesion. Therefore, it is necessary to examine all skull base fractures with a critical width of fracture slit of about 2 mm.
Methods: In 30 patients with posttraumatic liquor fistulas, we compared the sensitivity of a new MR method with CT cisternography. The results were confirmed with intraoperative findings. The MR examinations were performed with a 1.0-T whole-body MR system (Siemens Magnetom Impact). A strongly T2*-weighted 3D PSIF sequence (TR/TE = 17/7, flip angle = 80°) and a 3D CISS sequence (TR/TE = 14/6, flip angle = 70°) were applied in a coronal orientation by using a circularly polarized head coil. The spatial resolution in both sequences was 0.98 × 0.98 × 1.00 mm. To reduce artifacts due to eye motion, the patients had to wear pinhole blinders. The measurement time was about 8 minutes.
Results: In all cases it was possible to visualize the exact location of the dural lesions. The sensitivity was higher with the MR technique compared with CT cisternography. MR cisternography was also possible in patients without rhinoliquorrhea.
Conclusion: The MR technique has advantages over CT cisternography, which is reflected in the higher sensitivity as well as in the short measurement time when evaluating dural lesions.

023 • 4:09 PM
Influence of Immunosuppressive Therapy on the Extent of White Matter Lesions in the Brain of Heart Transplant Patients
J Reinhardt, NJ Shah, G Notohamiprodjo, R Koerfer
Herz-und Diabeteszentrum NRW, Bad Oeynhausen, Germany

Purpose: Neurotoxicity of cyclosporine has been reported in heart transplant patients (HTX) with a suspected incidence of 25%. We present the results of MRI examinations of the brain in a large population of HTX patients and examine whether the extent of prevalent leukoencephalopathy increases with duration of immunosuppressive therapy.
Methods: MR images of the brain were obtained by using the spin-echo technique with T1 weighting (TE/TR = 20/720), and a dual-echo sequence for proton-density and T2 weighting (TE/TR = 20,100/3,000). Eighty-five HTX patients with double immunosuppressive therapy (cyclosporine A and azathioprine) or with additional corticoid therapy of duration ranging from 0 to 75 months have been reviewed. The concentrations of the immunosuppressive agents were titrated to maintain the required plasma concentrations, which were monitored regularly. The degree of periventricular demyelination, lacunary lesions, and cerebral atrophy was correlated with the duration of immunosuppressive therapy and patient age. The study will be continued with preoperative and 1-year follow-up patients.
Results: We found no dependence of white matter lesions or periventricular demyelination on the duration of immunosuppressive therapy or on additional corticoid application; the frequency of these lesions matches the numbers known from previous reports and correlates well with patient age. We found that 44% of the patients showed slight, and 25% distinct, cerebral atrophy, indicated by widening of the external and internal CSF space. Only one patient had acute leukoencephalopathy, which may be related to therapy.
Conclusion: Preliminary results lead to the conclusion that there are no visible long-term white matter effects caused by immunosuppressive therapy, and the amount of acute leukoencephalopathy in HTX patients seems to be largely overrated. Repetitive long-time cerebral hypoperfusion due to periods of cardiac decompensation may explain the unusually large incidence of cerebral atrophy seen in HTX patients.
N.J. Shah is an employee of Picker International.

024 • 4:21 PM
MRI of the Brain in Boxers: Comparison with a Normal Control Population and Correlation with Boxing History
CJ Hoffman, K Soila, TR Struhl, JJ Sheldon, M Viamonte Jr, RA Labrie
Department of Radiology, Mount Sinai Medical Center, Miami, FL

Purpose: To determine differences in MRI findings between a group of professional boxers and controls, and to correlate the MRI findings in boxers with details of boxing history.
Methods: MRI of the brain was performed in 62 boxers and 32 normal control subjects. Dual-echo T2-weighted coronal and axial images were obtained. The images were evaluated for atrophy and for parenchymal abnormalities. In addition, a quantitative atrophy assessment was performed with selective measurements used in neurodiagnostic imaging: ventricular size index (VSI), intercaudate distance (ICD), and third ventricular width (TVW). The width of the cavum septum pellucidum (CSP) was measured. The findings were correlated with the atrophy analysis and boxing history parameters.
Results: Assessment of quantitative measurements reveals significantly higher values of VSI and TVW among boxers ($P < .001$). VSI proves to be the most important predictor of atrophy. Discriminant analysis identifies boxers from control subjects with greater than 80% accuracy. The incidence of CSP in the boxing population is 31% (risk ratio, 6.6) versus 2% in the control group ($P < .01$). Subjective diagnosis of atrophy on the images shows significant correlation with the measured indices VSI, ICD, and TVW. Focal white-matter signal abnormalities are identified in 16% of the boxers. No correlation is found between the details of boxing history and MRI findings.
Conclusion: In our study, boxers unequivocally demonstrate evidence of generalized atrophy and have a greater incidence of CSP. Surprisingly, in our sample group of boxers, there is no correlation between the details of boxing history and the abnormalities found at MRI.

025 • 4:33 PM
Imaging Features of Cavernous Angiomas of the Pituitary and Cavernous Sinus
AT Watanabe, GS Meyers, J Ahmadi, HD Segall
Neuroradiology Section, University of Southern California, Los Angeles, CA

Purpose: We report the clinical and imaging findings of three patients with cavernous angiomas in extremely unusual locations: the pituitary and cavernous sinus. The MRI findings are characteristic and, to our knowledge, have not been previ-

ously reported. Distinguishing these lesions from other pathologies is important for surgical planning and clinical management.
Methods: All of the patients underwent MRI. Catheter angiography and computed tomography were also performed. The diagnoses were confirmed in all three patients by means of open surgical biopsy. The clinical presentations and clinical follow-up were obtained for correlation. Follow-up was obtained over a 3–10-year period.
Results: Two of the patients presented with symptoms related to subarachnoid hemorrhage. The third patient presented with a third nerve palsy. There was hemorrhage within the lesions at MRI in all cases. The natural history of these lesions is relatively benign with stability in size on follow-up examinations performed over 3–10 years.
Conclusion: Cavernous angiomas of the pituitary and parasellar region are rare benign lesions. However, preoperative differentiation of sellar angiomas from pituitary adenomas is important because radical resection of a sellar angioma may result in massive hemorrhage. MRI, due to its exquisite sensitivity to blood products, is the modality of choice for diagnosing these lesions.

026 • 4:45 PM
MR Findings of Fat Embolism Syndrome in Brain
S Suzuki, M Ohbuchi, K Takizawa, S Hasebe, T Takagi, M Yamada, Y Kuniyasu, Y Osakabe
Showa University, Fujigaoka Hospital (Radiology Department) Yokohama, Kanagawa, Japan
Purpose: To report and discuss MRI findings of fat embolism syndrome in brain.
Methods: A total of 13 brain MR studies were performed in five patients with fat embolism syndrome in their early clinical courses. A 0.5-T superconductive MR system was used. All five patients had a long bone fracture caused by a motor vehicle accident, and all met Gurd criteria for fat embolism syndrome. All patients exhibited neurologic deterioration after a latent period after the accident; MRI studies were then performed.
Results: In the first week, T2-weighted images of all patients showed spotty or patchy high signal intensity lesions that were distributed throughout the gray and white matter in the cerebrum, cerebellum, and brain stem, whereas T1-weighted images showed some of these lesions as low signal intensity spots. From the second to fourth weeks, T2-weighted images demonstrated subsiding and disappearance of these lesions, followed by neurologic improvement. Disappearance of these high signal lesions occurred more quickly in the cerebellum than in the cerebrum.
Conclusion: T2-weighted images clearly showed the brain abnormalities of fat embolism syndrome; additionally, disappearance of these lesions at MRI correlated well with the improvement of clinical features.

027 • 4:57 PM
Correlation of Meningeal Morphology with Etiology and Clinical Findings
J Soto, AR Gillams, M Carroll, V De Carvalho, AP Carter
Boston University Medical School, Boston, MA
Purpose: Gadolinium-enhanced MRI provides a unique opportunity to evaluate and characterize meningeal disease. The meningeal changes associated with meningioma and carcinomatosis are well described, but other meningeal pathologies have not been studied in detail. Our aim was to correlate morphologic MR features with etiology and clinical outcome.
Methods: All cases of meningeal pathology (excluding meningioma) depicted at MRI over a 12-month period were collected. T1-weighted coronal/sagittal images were obtained both before and after administration of standard-dose gadolinium. The images were interpreted "blindly" by 2 experienced radiologists. Meningeal enhancement was classified as dural/leptomeningeal/both, focal/diffuse, or smooth/nodular and graded for severity from 1 to 3. Related abnormalities were noted and the findings correlated with clinical and CSF analysis.
Results: Twenty-two patients (14 women, 8 men), mean age, 39 years (range, 2–67 years), had meningeal pathology. Nine had infectious meningitis (2 pyogenic and 2 aseptic, 4 had TB, and 1 had toxoplasmosis), 4 had carcinomatous disease, 6 had "chemical" meningitis, and 3 had neurosarcoid. There were 4 cases of isolated leptomeningeal disease, including 2 of 3 patients with neurosarcoid. Four patients had pure dural involvement, including 2 of 6 with "chemical" meningitis. Fourteen of 22 had involvement of all meningeal layers. Nodularity was rare but had no distinct diagnostic value. Predominantly basal meningeal involvement was seen in patients with TB; pyogenic meningitis was characterized by marked meningeal enhancement over the convexities. Milder degrees of severity were seen in patients with neurosarcoid and aseptic meningitis; more severe involvement was seen in those with TB and pyogenic meningitis. Hydrocephalus was seen only in patients with severe meningeal enhancement.
Conclusion: Anatomic distribution, severity, and isolated leptomeningeal involvement had etiologic and prognostic significance. Nodularity had no diagnostic value; the predominant picture was of involvement of all layers, and this was seen in all diagnostic categories.

Sunday Afternoon • Morrocco Room
Papers 031–037

UPPER ABDOMEN I: Hepatic, Fast
MODERATORS: JP Mugler, III, PhD
PT Weatherall, MD

031 • 3:45 PM
High-Speed T2-Weighted Imaging of the Liver with Single-Shot GRASE (TGSE)
DA Feinberg, B Kiefer, JC Weinreb, N Rofsky, C Mercado, J Safir, J Stevenson
Department of Radiology, New York University, New York, NY
Purpose: GRASE (or turbo gradient spin echo [TGSE]) uses multiple gradient refocusings during each spin-echo period of a CPMG spin-echo train. GRASE images can be made with one echo train (single shot) so that T2-weighted images can be produced in less than 1 second. The purpose of this study was to implement single-shot GRASE on a commercial 1.0-T MR system and to evaluate this sequence for hepatic imaging.
Methods: The GRASE sequence of 115 echoes in 330 msec was altered such that the center of k space was moved from a central location (58th echo) to an earlier location (28th echo) to obtain a TE of 75–80 msec. TR was infinite. A commercially available scanner (Impact 1.0 T, Siemens), with 15 mT/M gradients at 1-msec ramp time, was used to acquire 1-cm-thick axial sections with 128 × 128 or 128 × 256 matrices in 20 patients referred for hepatic MRI. Images of the entire liver (15 slices) were obtained in a 5-second breath hold. The images were evaluated and compared quantitatively and qualitatively to other T2-weighted images.
Results: The images exhibited excellent lesion-liver and spleen-liver contrast and were free of respiratory motion artifacts. There was no appreciable geometric distortion secondary to magnetic field inhomogeneities.
Conclusion: Single-shot GRASE has been implemented on a 1.0-T MR system and can provide a T2-weighted image of the liver in a third of a second. With further refinements, this sequence could be useful for clinical abdominal imaging.
B. Kiefer is a research scientist for Siemens Medical Systems.

032 • 3:57 PM
Flow-compensated Fast Spin Echo Sequence with Respiratory Gating in Detection and Characterization of Hepatic Lesions
M Keogan, C Spritzer, J MacFall, J Dahlke
Department of Radiology, Duke University Medical Center, Durham, NC
Purpose: The purpose of this study is to determine the role

of fast spin echo (FSE) imaging with flow compensation (FC) and respiratory gating in hepatic imaging by comparison with standard T2-weighted spin-echo imaging.
Methods: Images were obtained on a 1.5-T Signa system. Thirty patients with suspected hepatic pathology were studied with the following protocol: (*a*) FSE: respiratory gated; FC (slice selection); TR/TE, 4,000/102 ef; echo train, 8; matrix, 256 × 256 and (*b*) T2-weighted spin echo: respiratory compensation; FC; TR/TE, 2,500/40,80; matrix, 128 × 256. Both sequences employed spatial presaturation and slice thickness/gap of 7/3 mm. Images were analyzed objectively by using signal-to-noise values and objectively by means of assessment of image quality (artifact and lesion conspicuity).
Results: Approximate imaging time for the FC FSE sequences with respiratory gating was 3–4 minutes compared with 12.5 minutes for the T2-weighted spin echo sequence. The FC FSE sequences with respiratory gating achieved superior lesion-to-liver contrast compared with the T2 sequence, and facilitated anatomic localization of detected lesions. Artifact related to respiratory and cardiac motion was almost completely absent on the gated FC FSE sequences.
Conclusion: FC FSE sequences with respiratory gating are comparable with T2-weighted spin-echo sequences in terms of signal-to-noise values and are superior in terms of lesion-to-liver contrast. The shorter acquisition of the FSE sequences represents a significant advantage over standard T2-weighted spin-echo sequences.

033 • 4:09 PM
Fast Spin-Echo Imaging of the Abdomen: Contrast Optimization and Artifact Reduction
RN Low, RS Hinks, G Alzate, A Shimakawa
Sharp and Children's MRI Center, La Jolla, CA

Purpose: To examine the effects of various FSE imaging parameters and artifact reduction techniques on FSE image contrast and quality.
Methods: We performed 166 abdominal MR studies comparing the standard FSE images (TR/TE, 4,900/85; 2 NEX; ETL, 8; E-space, 17 msec; ±16 kHz bandwidth) with FSE images with an ETL of 16 (n = 22) or a reduced E-space of 11–16 msec (n = 54). FSE artifact reduction techniques were evaluated with spectral fat saturation (n = 40) or with a new flow-compensation FSE sequence (n = 50). Images were reviewed qualitatively and with CNR measurements of liver lesions.
Results: Decreasing the time of echo-train sampling produced superior image quality with increased anatomic sharpness, less image artifacts, and improved hepatic lesion CNR. The images obtained with an ETL of 8 showed a 25% improvement in relative contrast and CNR for liver tumors. Images obtained with ETL of 16 showed more image blurring with loss of small hepatic lesions in six patients. A reduction in E-space increased image sharpness, reduced vascular pulsation artifacts, and decreased background noise by 12%. Artifact reduction with fat saturation or flow compensation produced a decrease in background noise with 39% and 20% increase in liver tumor CNR, respectively. FSE images with fat saturation or flow compensation showed less ghosting artifact and superior overall image quality.
Conclusion: To provide images with excellent depiction of hepatic disease, FSE image quality and contrast can be optimized by the careful selection of imaging parameters (ETL and E-space) and the use of artifact reduction techniques such as fat saturation and flow compensation.

034 • 4:21 PM
Optimizing FSE Acquisition for Hepatic Imaging
CE Spritzer, M Keogan, J MacFall, J Dahlke
Department of Radiology, Duke University Medical Center, Durham, NC

Purpose: The purpose of this study is to determine what modifications to a standard fast spin-echo (FSE) sequence will result in improved image quality. Specifically, will flow compensation (FC), randomized phase encoding (RPE), and respiratory tract (RT) and ECG triggering (ECGT) result in improved motion reduction with a long-range objective of improving lesion detection?
Methods: Images were obtained on a 1.5-T Signa system. One of the authors (J.D.) constructed a device that allows data acquisition based on RT, ECGT, and both RT and ECGT. With this device, with a flow-compensated FSE database, the following sequences were tested in five volunteers: (*a*) FSE without FC (NFC FSE); (*b*) FSE with FC (FC FSE); (*c*) RPE with NFC FSE; (*d*) RPE with FC FSE; (*e*) FC FSE, RPE, and RT; (*f*) NFC FSE, RPE, and RT; and (*g*) FC FSE, RPE, RT, and ECGT.
Results: Use of RPE reduced apparent ghosts with either FC or NFC FSE sequences. FC FSE reduced coherent ghosting due to motion or flow compared with NFC FSE. Use of RT reduced coherent ghosts and blurring for both FC and NFC FSE sequences, albeit with an increase in scan time (4.5 min vs 7–8 min). Incorporation of both ECGT and RT resulted in further reduction of blurring, albeit with a time penalty (7 vs 10 min).
Conclusion: The simultaneous use of RPE, FC, and respiratory triggering with FSE sequences produces excellent image quality in times less than that of standard spin-echo imaging.
This research was supported in part by GE Medical Systems.

035 • 4:33 PM
Optimized Tissue Characterization with Fast Spin-Echo Imaging at 1.5 T
TH Rijcken, A Davidoff, J Mukai, J Colby, DA Davidson, SA Afonso, DD Stark
Department of Radiology, University of Massachusetts Medical Center, Worcester, MA

Purpose: Fast spin-echo (FSE) imaging offers limited parameter choice because tau values and echo train length are fixed on most commercial systems. Contrast weighting is achieved by reordering phase encoding, placing k-space contrast emphasis (null phase-encoding gradient) at the selected TE. Spatial frequency resolution is shuffled to remote (shorter and longer) TE values. We investigated the impact of these constraints on the choice of contrast and results in detection and characterization of focal liver lesions. Our goal was to validate substitution of conventional spin echo (SE) with FSE in routine clinical practice and further optimize T2-weighted FSE through more rational parameter selection.
Methods: One hundred patients with hepatic metastases or cavernous hemangiomas were studied at 1.5 T with SE and FSE sequences varying TE (or effective TE) from 30 to 300 msec. Tissue signal intensities and background noise were measured and SNR, CNR, and SIR (tissue-tissue signal intensity ratios) were calculated by using conventional methods.
Results: Time normalized data showed that FSE images at a TE of 117 or 195 (effective) outperformed SE 80 images. Longer SE TE images produced lower CNR, principally due to motion artifact degradation. Longer TE FSE at fixed tau distorted TE effective, with no gain in contrast and only loss of SNR as TE effective exceeded 200 msec. SE CNR for metastases was 6.32 ± 4.7 while FSE was 12.05 ± 8.8. Hemangioma SE CNR was 12.8 ± 7.2 and FSE CNR was 24.9 ± 11. Thus, FSE produced more lesion-liver contrast for detection and more hemangioma versus metastasis contrast for characterization.
Conclusion: FSE outperforms SE for purposes of T2-weighted imaging of the liver with respect to both lesion detection and characterization. SE is limited by motion artifact at longer TE, while FSE can be further improved by reduction in tau to fit k-space sampling within 100 msec at TE in excess of 200 msec.

036 • 4:45 PM
Value of Flow Compensation in Postcontrast T1-weighted Spin-Echo Pulse Sequences of the Liver
C Reinhold, PM Bret, L Rohoman, T Denton
McGill University, Montreal General Hospital, Department of Radiology, Montreal, Quebec, Canada

Purpose: To determine the effect of adding flow compensation (FC) in postcontrast-enhanced T1-weighted sequences in the liver on image quality and lesion detection.
Methods: Both FC and no flow compensation (NFC) postcon-

trast T1-weighted sequences were obtained in 40 patients undergoing MR imaging of the liver, between 8–12 minutes after IV injection of gadolinium DTPA. The sequence order (FC/NFC) was assigned by using a randomization table. The following parameters were used: TR, 400 ms; TE, 11 ms (NFC), 21 ms (FC); matrix, 256 × 192; 2 NEX. The images were filmed without imaging parameters and evaluated side by side independently in a blinded fashion by two reviewers.
Results: Flow artifacts were markedly diminished in all FC cases. Lesion conspicuity and characterization were improved with the application of FC. Vessels appeared hyperintense on the FC images compared with the NFC images; however, this did not impede lesion detection in the study. Increasing the TE in the FC sequence decreased neither lesion detection nor characterization.
Conclusion: FC should be used routinely in T1 postcontrast pulse sequences in the liver.

037 • 4:57 PM
Musculoskeletal and Abdominal MR Findings in Patients with Type 1 Gaucher Disease
MR Terk, J Esplin, JM Tyszka, G Magre, PM Colletti
LAC/USC Imaging Science Center, Los Angeles, CA

Purpose: Gaucher disease is an autosomal recessive genetic disease characterized by a deficiency of the enzyme glucocerebrosidase (glucosylceramidase). As a result of the enzymatic defect, highly insoluble glucocerebroside accumulates in body tissues. Type 1 disease is the most common and is distinguished by sparing of the central nervous system. Recently, effective enzyme replacement therapy (alglucerase) has become available, creating a need for a means of following and quantitating disease manifestations. The purpose of this study was, therefore, to quantitate liver and splenic volumes and to correlate these changes with the osseous findings.
Methods: Twenty consecutive patients entering the system for Gaucher disease assessment were referred for MR evaluation. There were 14 female and 6 male patients with an age range from 10 to 70 years. Imaging was performed on a 1.5-T 5× Signa magnetic resonance imaging system. Breath-hold fast SPGR images were obtained of the abdomen and used for calculation of liver and spleen volumes. Calculation was performed by summing the areas within manually drawn regions of interest and multiplying by the slice thickness plus gap. Extremities were evaluated in the coronal plane with T1- and T2*-weighted images. Because it was necessary to use a large field of view, the matrix was increased to 512 × 256 to limit pixel size. A classification (class 0–class 3B) for skeletal changes was applied and correlated against visceral volume measurements.
Results: Eight patients underwent splenectomy, two had splenic nodules, and three showed esophageal varices. Four patients had avascular necrosis of the femoral head, and of these, two had splenic nodules. In both cases the splenic nodules had a characteristic MR appearance. There did not appear to be a correlation between splenectomy and other features. Liver and spleen volumes appeared to vary independently of osseous changes. The distribution of marrow changes was approximately equal among the 4 grades defined.
Conclusion: Volume measurement of liver and spleen provides an objective MR measurement of the extent of visceral involvement. This measurement appears independent of musculoskeletal changes. Application of this method to patients post enzyme replacement therapy may provide an objective and reproducible method for following treatment results.

Sunday Afternoon • Sapphire Room
Papers 041–047

FLOW QUANTITATION
MODERATORS: RB Buxton, PhD
D Saloner, PhD

041 • 3:45 PM
Influence of Respiratory Motion on Cine Phase-Contrast–based Flow Measurements
JF Debatin, H Wegmueller, BS Bowman, FG Sommer, NJ Pelc, RJ Herfkens
Department of Diagnostic Radiology, Stanford School of Medicine; University Hospital Zurich, Zurich, Switzerland

Purpose: Abdominal arterial vasculature is subject to different degrees of respiratory motion. The length of standard CPC imaging precludes breath holding. This study assessed the influence of respiratory motion on flow measurements.
Methods: An 8-cm segment of harvested human carotid artery was connected to tygon tubing and embedded in a container filled with nickelous agarose gel. The proximal tubing was linked to a pulsatile pump (60 beats per minute), calibrated to deliver 970, 720, 490, and 250 mL/min. Flow was monitored with an ultrasonic flow probe. The container was placed in the body coil of a 1.5-T MR system (Signa) and could be moved perpendicular to its axis by a computer-driven motion device. With a TR/TE of 24/9, 45° flip angle, 5-mm section, 128 × 256 matrix, 20-cm FOV, 1 NEX, R/L flow encoding, and v_{enc} of 100 cm/sec, 16-frame CPC acquisitions were obtained for all four flow settings with and without simulated respiratory motion (12 10-mm excursions per minute). At 720 mL/min, flow motion excursions of 5 and 15 mm were also evaluated.
Results: CPC-based measurements without motion were accurate ($r > .95$). The presence of motion caused overestimation of flow. The relative degree of overestimation was dependent on flow volume and degree of pulsatility. It ranged from 19.1% for the 970 mL/min flow setting to 80.4% for the 250 mL/min flow setting. As motion excursion increased, overestimation of flow increased: 10.8% for 5 mm and 56.3% for 15 mm. Flow overestimation seems to be due to partial volume effects: the apparent vessel size increased from 55 mm^2 (no motion) to 115 mm^2 (15 mm motion).
Conclusion: To avoid flow overestimation, quantification of abdominal vasculature subject to respiratory motion requires breath-hold data acquisition. Initial in vitro and in vivo experience with rapid breath-hold PC techniques have been encouraging.

042 • 3:57 PM
Breath-hold Phase-Contrast MR Quantification of Renal Arterial Blood Flow
JF Debatin, RH Ting, H Wegmueller, FG Sommer, JO Fredrickson, TJ Brosnan, BS Bowman, NJ Pelc
University Hospital Zurich, Zurich, Switzerland

Purpose: Respiratory motion can cause overestimation of cine phase-contrast (PC)–based renal flow measurements. We evaluated two breath-hold PC imaging strategies: single-frame 2D PC and 6-frame TRIADS (time resolved imaging by automatic data segmentation) PC.
Methods: In vitro flow measurements were performed in the body coil of a 1.5-T MR system (Signa) across a segment of harvested human artery embedded in agarose gel and linked to a pulsatile pump (60 beats per minute), calibrated with an ultrasonic flow meter to deliver 970, 720, 490, and 250 mL/min. Single-frame 2D PC (imaging time, 9 sec), and 6-frame TRIADS PC (imaging time, 37 sec) employed identical parameters: TR/TE of 24/9, 45° flip angle, 5-mm section, 128 × 256 matrix, 20-cm FOV, 1 NEX, R/L flow encoding, v_{enc} of 100 cm/sec. Five subjects with recent PAH-clearance flow data were also evaluated with both techniques in suspended respiration as well as with standard non-breath-hold 16-frame cine PC imaging. PC imaging was performed in a plane perpendicular to the renal arteries identified by means of a double oblique localizing strategy.

Results: In vitro single-frame 2D PC imaging underestimated true flow in the phantom experiment with errors ranging from 23% for the 970 mL/min flow setting to 70% for the 250 mL/min flow setting. TRIAD PC (6 frame) showed good correlation between measured and true flow ($r > .9$). Breath-hold 6-frame TRIADS PC imaging showed excellent agreement between left renal arterial and venous flow. Total renal artery flow correlated well with PAH-clearance flow ($r > .9$). Standard non-breath-hold 16-frame cine PC techniques overestimated renal flow by as much as 30% and was significantly less accurate than breath-hold TRIAD PC flow measurements ($P < .001$).
Conclusion: To prevent respiratory motion-induced overestimation of flow, data acquisition in suspended respiration appears imperative. Single-frame 2D PC imaging can underestimate pulsatile flow. Six-frame TRIADS PC measurements were accurate both in vitro and in vivo.

043 • 4:09 PM
Phase-Contrast Velocity Measurements with Increased Signal-to-Noise Ratio
AT Lee, NJ Pelc
Department of Radiology, Stanford University School of Medicine, Stanford, CA

Purpose: The signal-to-noise ratio of phase-contrast MRI increases linearly with the applied first moment but is limited in practice by the need to avoid aliasing. The authors examine unwrapping high-moment (or low v_{enc}) phase-contrast measurements by comparison with a low-moment (or high v_{enc}) data set that does not include any phase wraps. The gain in SNR with this strategy is much greater than with simple averaging.
Methods: Unwrapped velocities are given by $v = v_{low\text{-}venc} + 2*n*v_{enc}(low)$, where $n = round\{(v_{high\text{-}venc} - v_{low\text{-}venc})/(2*v_{enc}(low))\}$ and v_{enc} = velocity producing a phase change of π. The SNR is that of the low v_{enc} measurement. A steady-flow phantom ($v \sim 18$ cm/s) was imaged with v_{enc} = 20, 15, 10, 5, and 1 cm/s. The v_{enc} = 20 cm/s data set was used to unwrap each of the others.
Results: The SNR increased inversely with v_{enc} down to v_{enc} = 5 cm/s. At v_{enc} = 1 cm/s, the SNR decreased near the tube wall due to intravoxel dephasing, and the unwrapping algorithm incorrectly estimated the number of phase wraps for some pixels because $v_{enc}(low)$ was comparable to the velocity noise in the high v_{enc} data.
Conclusion: The required number of measurements can be reduced to three by using one common zero-moment phase reference for the two flow-encoded measurements. In this case, the 400% SNR increase of the present experiment would require an increase in scan time of only 50% compared to conventional measurements. The improved SNR should significantly improve the quality of phase-contrast angiograms and the precision of flow quantification.

044 • 4:21 PM
Flow Quantification with a Complex-Difference Technique
MT Alley, JA Polzin, FR Korosec, TM Grist, CA Mistretta
Departments of Medical Physics and Radiology, University of Wisconsin, Madison, WI

Purpose: Phase-contrast flow quantification with the phase-difference (PD) image is subject to error due to partial volume effects at the vessel edge (1–3). We have developed an analysis technique that exploits the currently unused information inherent in the complex-difference (CD) image. Because the signal from a given voxel in a CD image is proportional to the density of flowing spins and the sine of the velocity-induced phase, flow measurements are not affected by signal from stationary tissue.
Methods: Our technique uses information from the vessel center in the PD image to correct for saturation and other signal modifying effects, thereby transforming the CD image into a flow map. Computer simulations were performed to model through-plane flow along with the effects of noise, intravoxel phase dispersion, saturation, and plug versus laminar flow profiles. Flow data were also obtained on a GE 1.5-T MR system with a product vascular phase-contrast sequence and an anthropomorphic flow phantom.
Results: Simulations and flow phantom studies have shown that in nearly all cases systematic measurement errors were both smaller and less susceptible to parametric variation in the CD technique as opposed to the standard PD analysis.
Conclusion: The CD-based flow analysis promises more accurate flow measurements, particularly in small vessels such as the coronary arteries, where partial volume effects tend to be significant.
1. Pelc NJ, Herfkens RJ, Shimakawa A, Enzmann DR, Magn Reson Quart 1991; 7:229. 2. Tang C, Blatter DD, Parker DL, JMRI 1993; 3:377. 3. Wolf RL, Ehman RL, Riederer SJ, Magn Reson Med 1993; 30:82.

045 • 4:33 PM
Blood Velocity Measurement of Portal Vein Improved with DANTE Pulse
J Mao, JJ Steinbach
Department of Radiology, University of Florida, Gainesville, FL

Purpose: To improve the measurement accuracy of blood velocity for the portal vein.
Methods: A Siemens 1.0-T SP system was used. A DANTE sequence was used to replace a commercially available presaturation pulse and to mark the blood of the portal vein before a FLASH pulse sequence. There were three consecutive data acquisitions in the same FLASH pulse sequence. In other words, three gradient echos were acquired after each excitation. The time interval between two acquisitions was 20.4 ms. The shortest TE was 10 ms. TR was 71 ms. The FLASH sequence was used in a breath hold of 16 seconds to eliminate the artifacts due to chest motion. The total length of the DANTE sequence was 2.56 ms. The DANTE sequence consisted of 16 rectangular pulses, each of which had the same amplitude and the same length. The interval between two rectangular pulses was the same. The length of each rectangular pulse was one-seventh of the length of the interval between two rectangular pulses. The flip angle of the whole DANTE sequence was 120°. Three images were obtained at each scan. Any two images can be used to determine the blood velocity; usually the first image and the third image are used. The blood velocity was determined by the ratio of the displacement between two corresponding blood marks in the first image and the third image to the time interval of 40.8 ms (2*20.4).
Results and Conclusion: The length of the blood marks obtained with the DANTE sequence presaturation was about one-eighth of that obtained with the commercially available presaturation pulse. The edge of the blood mark obtained with the DANTE sequence was sharper than that obtained with the commercially available presaturation pulse. The accuracy determining the displacement between two blood marks was thus increased. Therefore, the accuracy of the velocity measurement was increased.

046 • 4:45 PM
Simultaneous Calculation of Flow and Diffusion Sensitivity in SSFP
H Gudbjartsson, S Patz
Brigham & Women's Hospital, Boston, MA

Purpose: Steady-state free precession (SSFP) has long been known to be sensitive to diffusion and has been used for fast diffusion imaging (1–6). SSFP is also sensitive to bulk flow and has been used to image slow flow (7–13). Analytical expressions have been derived for the diffusion sensitivity of SSFP (1,5,6) but not for its flow sensitivity, although a gradient-dependent scale-invariant parameter has been derived (8). The aim here is to quantitatively evaluate the combined effect of both diffusion and flow in pulsed gradient SSFP.
Methods: A partition analysis was used to get a fourth order (in E2) approximation to the signal used in an echo SSFP sequence. The flow was considered constant and uniform over the whole sample, and Brownian motion was superimposed on the bulk flow.
Results: The diffusion attenuation in SSFP is found to de-

pend on the flow and vice versa. The partition analysis gives an expression that is a function of flip angle, flow, bD, T1, T2, and TR. The maximum error in the approximation, compared with the exact solution with no flow (6) and 20° flip angle, is 13% for a TR/T2 ratio of one-half and 5% for a TR/T1 ratio of one. The relative error is less for most cases of interest.

Conclusion: We have found a way to simultaneously quantify flow and diffusion dependency in SSFP for a range of TR/T2 ratios and shown that attenuation caused by flow and diffusion in SSFP are not independent processes. Future work will use numerical simulation to verify the results and to look for the general analytical solution to the Bloch equation in SSFP, with flow and diffusion terms.

1. R. Kaiser, E. Bartholdi, R. R. Ernst. J. Chem. Phys. 8, 2966 (1974). 2. R. C. Hawkes, S. Patz, Magn. Reson. Med. 4, 9 (1987). 3. K. D. Merboldt, W. Hanicke, M. L. Gyngell, J. Frahm, H. Bruhn, J. Magn. Reson. 82, 115 (1989). 4. D. Le Bihan, R. Turner, J. R. MacFall, Magn. Reson. Med. 10, 324 (1989). 5. E. X. Wu, R. B. Buxton, J. Magn. Reson. 90, 243 (1990). 6. R. B. Buxton, J. Magn. Reson. Med 29, 235 (1993). 7. S. Patz, R. C. Hawkes, Magn. Reson. Med. 4, 140 (1986). 8. S. Patz, Magn. Reson. Imag. 6, 405 (1988). 9. S. Patz, S. T. S. Wong, M. S. Roos, Magn. Reson. Med. 10, 194 (1989). 10. M. E. Stromski, H. R. Brady, S. R. Gullans, S. Patz, Magn. Reson. Med. 20, 66 (1991). 11. M. Tyszka, R. C. Hawkes, L. D. Hall, J. Magn. Reson. 92, 183 (1991). 12. M. Tyszka, R. C. Hawkes, L. D. Hall, Flow Meas. Instum. 2 (1991). 13. M. Tyszka, R. C. Hawkes, L. D. Hall, J. Magn. Reson. B 101, 158 (1993).

047 • 4:57 PM

MRA and Computer Simulation of Blood Flow in Near-90° Arterial Branches

S Vinitski, HV Ortega, EK Outwater, SH Faro, FB Mohamed, S Seshagiri, DG Mitchell, S Albert
Department of Radiology, Thomas Jefferson University Hospital, Philadelphia, PA

Purpose: To investigate blood flow behavior in the presence of sharp (close to 90°) arterial branches with computer simulation of blood flow, color Doppler, and phase-contrast (PC) MRA.

Methods: In vitro experiments were performed with a Plexiglas phantom of a 90° arterial branch and a pulsatile flow pump. The blood-mimicking fluid was a solution of carboxymethylcellulose yielding 3.6-cp viscosity (T1 = 1,750 msec, T2 = 350 msec). Arteries with near-90° branches, such as renal arteries, celiac trunk, and femoral branches, were scanned in normal volunteers with color Doppler and gated PC MRA. Blood-flow computer simulation was carried out by finite element analysis (1). Non-Newtonian viscosity of blood was taken into account in this analysis (2). Local wall shear stress was also calculated as a function of a cardiac cycle.

Results: Computer simulation demonstrated flow separation at the proximal origin of the branch with an increase of shear stress and reversal into the main branch during the early deceleration period of systole. Color Doppler and MRA both showed reversal of flow at the level of the branch due to high resistance and an area of flow separation at the origin. Results of phantom experiments correlated well with that of the in vivo studies. Despite substantial changes in the flow pattern and sharp curvature of vessels, these results were in accord with those obtained previously in the carotid arteries.

Conclusion: The behavior of flow demonstrated by the computer model identified the area(s) most likely to develop stenosis. This model allows better understanding of the signal loss demonstrated in imaging of near-90° arterial branches at MRA.

1. Vinitski S, Ortega HV, et al. Proc IEEE Eng Biol Med 1992; 14:1974. 2. Cho YI, Kensey KR. Adv Bioeng 1989; 15:147.

CONTRAST AGENTS I

MODERATORS: RL Nunnally, PhD
DD Stark, MD

101 • 3:45 PM

Clearance Rates of Gadolinium Chelates with Dialysis: Clinical Implications

PL Choyke, ME Girton, E Vaughn, H Austin, JA Frank
National Institutes of Health, Bethesda, MD

Purpose: Gadolinium (Gd) chelates are routinely used in patients with compromised renal function and in patients with renal failure on dialysis. Two small clinical studies have shown that Gd-DTPA can be dialyzed; however, the rate of plasma clearance has not been determined. We compare the in vitro plasma clearance of the three FDA-approved Gd chelates—Magnevist, ProHance, and Omniscan—with urea, creatinine, and vitamin B12, all well-studied markers of dialysis efficiency.

Methods: Human plasma was doped (0.75 mL Gd chelate/1,500 mL plasma) with one of three agents: Magnevist (Berlex), ProHance (Squibb), and Omniscan (Sanofi-Winthrop). A Cobe dialyzer with a Baxter 12-11 capillary flow filter was employed. Pre- and postdialysis samples of the Gd chelate were determined at flow rates of 0–400 mL/min in 50 mL/min increments. The clearance rate (CR) for each agent was calculated by using standard formulas. The CRs for urea, creatinine, and vitamin B12 were also determined. These CRs were compared with those obtained with Gd chelate in saline.

Results: At dialyzer flow rates of 300 mL/min, the urea, creatinine, and vitamin B12 CRs were 200, 165, and 40 mL/min, respectively. The CRs for Magnevist, ProHance, and Omniscan were 70, 74, and 78 mL/min, respectively, and were not statistically different. CRs for the same agents in saline were 95, 97, and 96 mL/min, respectively.

Conclusion: The CRs of FDA-approved Gd chelates were uniformly lower than expected based on early clinical experience. Plasma protein binding and molecular size probably account for lower extraction rates. Hemodialysis sessions should either be extended or grouped more frequently to clear Gd chelates by means of dialysis.

102 • 3:57 PM

Complete Elimination of Gd-EOB-DTPA in Hepatic or Renal Dysfunction

A Mühler, I Heinzelmann, HJ Weinmann
Schering AG, Berlin, Germany

Purpose: Gd-EOB-DTPA is a hepatobiliary MR contrast agent with dual elimination by means of the kidneys and the liver. The study was designed to investigate (*a*) whether the dysfunction of either one of the elimination pathways can be fully compensated by the remaining and (*b*) whether the elimination of Gd-EOB-DTPA is complete in hepatic or renal dysfunction.

Methods: The study was performed in two groups of rats: group A with ligation of common bile duct ($n = 11$) and group B with ligation of renal blood vessels ($n = 8$). A dose of 0.1 mmol/kg Gd-EOB-DTPA or Gd-DTPA (control) was injected via a tail vein. Bile or urine were collected in fractions of 0–1 h, 1–2 h, 2–4 h, and 4–8 h following administration of either contrast agent. At the end of the experiments, detainment of the contrast agents in the carcass was determined by measurement of gadolinium concentrations (by means of ICP-AES at a wavelength of 342.247 nm).

Results: Most of the Gd-EOB-DTPA was rapidly cleared from the body: 89.4% ± 7.5 of the injected dose within 4 hours following bile duct ligation (group A) and 87.0% ± 6.0 within 1 hour following ligation of renal vessels (group B). At 8 hours following injection of Gd-EOB-DTPA, 3.0% ± 2.4 of the administered dose of this contrast agent was found in the carcasses of group A, and 1.3% ± 0.6 in the carcasses of group B. By comparison, at this time point 1.9% ± 3.2 of the injected Gd-DTPA was found in the carcasses of group A (no

statistically significant difference compared with Gd-EOB-DTPA), and 96.3% ± 3.3 in the carcasses of group B.
Conclusion: On the basis of the rat model, it is expected that the MRI contrast agent Gd-EOB-DTPA is rapidly and effectively eliminated in patients with severely impaired liver or kidney excretory function by virtue of its dual elimination pathway. The dysfunction of liver or kidney may be fully compensated by the remaining elimination pathway.
A. Mühler, I. Heinzelmann, and H.J. Weinmann are employees of Schering AG.

103 • 4:09 PM

Nephrotoxicity of High-Dose Gadopentetate Dimeglumine Compared with Iodinated Contrast Agent

MR Prince
Department of Radiology, University of Michigan, University of Michigan Hospitals, Ann Arbor, MI

Purpose: To determine if high-dose gadopentetate dimeglumine (Gd) causes less nephrotoxicity than iodinated contrast agent.
Methods: Serum creatinine was evaluated pre- and postcontrast administration in 23 patients who received both high-dose Gd (0.2–0.3 mmol/kg) and iodinated contrast agent (> 100 mL) on separate days for MRA and conventional angiography. None of the 23 patients had any other renal stress (ie, CHF, vascular surgery, or nephrotoxic medication) at the time of either Gd or iodinated contrast agent administration, and all patients were appropriately hydrated at the time of iodinated contrast agent administration. The mean patient age was 65 years, ranging from 4 to 87 years.
Results: The mean change in serum creatinine following Gd was 0.06 mg/dL, from 2.33 mg/dL ± 1.5 to 2.39 mg/dL ± 1.5. No patient had contrast-induced renal failure following Gd administration. By comparison, the mean change in serum creatinine in the same patients following iodinated contrast agent was 0.67 mg/dL, from 2.00 mg/dL ± 1.1 to 2.67 mg/dL ± 2.0 ($P > .3$). Five of the 23 patients had iodinated contrast-induced renal failure (> 1.0 mg/dL rise in serum creatinine).
Conclusion: High-dose Gd shows no evidence of nephrotoxicity in a population of patients that is at high risk for contrast-induced renal failure.

104 • 4:21 PM

Lack of Evidence for in Vivo Decomplexation of Gd-EOB-DTPA following Repeated Intravenous Injection

A Mühler, HJ Weinmann
Schering AG, Berlin, Germany

Purpose: Clinical MR contrast agents like Gd-DTPA show high thermodynamic and conditional stability given the conditions in the extracellular space, and decomplexation with release of free gadolinium will not occur. Gd-EOB-DTPA, a liver-directed derivative of Gd-DTPA, is taken up intracellularly into hepatocytes. The excess to the intracellular compartment may bring higher risks for decomplexation or long-term storage of gadolinium. The study was designed to prove whether Gd-EOB-DTPA may be completely eliminated following repeated IV application.
Methods: Rats were injected with 50 μmol/kg radioactive ^{153}Gd-EOB-DTPA for 5 consecutive days (total dose: 0.25 mmol/kg). Measurement of gadolinium concentrations in blood, liver, spleen, kidneys, lungs, heart, bone (femur), and carcass were measured at days 3, 7, 14, and 21 after the final application of the contrast agent. Additionally, urine and feces were collected to show recovery of the injected amount of ^{153}Gd. Five rats were used per time point, and the results are expressed in percentage of total dose per organ.
Results: The measurements of gadolinium concentrations were accurate; the recovery of gadolinium ranged from 99.8% to 100.2%. At 3 days following the last injection, less than 0.5% of the injected dose could still be detected in the body. The whole body burden of gadolinium decreased to 0.24% at day 7, to 0.13% at day 14, and to 0.07% at day 21. Twenty-one days post injection, the liver contained 0.01%, the spleen 0.004%, the kidneys 0.002%, the lungs 0.0002%, the heart 0.0001%, and the carcass 0.07% of the injected dose. The femur gadolinium concentration at day 21 was 0.0006 μmol/g wet weight.
Conclusion: Based on the presented rat data, no evidence could be found for either decomplexation of Gd-EOB-DTPA in vivo or long-term gadolinium storage following repeated doses of the contrast agent. The current data for Gd-EOB-DTPA are virtually identical with those of Wedeking (Magn Res Imaging, 1992, 10:641–648) for Gd-DTPA, Gd-DOTA, and Gd-HP-DO3A.
A. Mühler and H.J. Weinmann are employees of Schering AG.

105 • 4:33 PM

Gd-EOB-DTPA–enhanced MRI in Rats with Selective and Total Bile Duct Obstruction: Chronological Correlation of MRI, Serology, Microcholangiography, and Histology

Y Ni, G Lukito, G Marchal, A Mühler, J Yu, AL Baert
Department of Radiology, University Hospitals, Leuven, Belgium

Purpose: To evaluate the safety of hepatobiliary contrast agent Gd-EOB-DTPA in long-term biliary obstruction and the potential of this agent for mapping local and total cholestasis.
Methods: A total of 44 rats were used; selective biliary obstruction (SBO) was created in 20, total biliary obstruction (TBO) was created in 14, and 10 underwent sham operation. During both acute (10 hours) and chronic (1 to 4 weeks) phases, serial T1-weighted SE images were obtained before and after Gd-EOB-DTPA (30 μmol/kg) intravenous injection. Serum bilirubin, alkaline phosphatase, and alanine aminotransferase (ALT) were measured sequentially. Postmortem microcholangiography and histology were further correlated.
Results: In SBO, a significantly prolonged enhancement of ligated liver lobes with no obvious serologic change was found during the acute phase. No difference in enhancement between ligated and unligated lobes occurred during the chronic phase due to bile collateral formation. In TBO, during the acute phase, only a minimal liver enhancement was seen due to hepatic injury and cholestasis, as evidenced by elevation of ALT and bilirubin values. Gd-EOB-DTPA was then efficiently eliminated through the kidneys. However, a normal liver enhancement with an enhanced common bile duct appeared sooner or later during the chronic phase, due to restoration of bile drainage through newly developed collaterals, as proved at microcholangiography and histology.
Conclusion: Gd-EOB-DTPA is a safe contrast agent even in long-term cholestasis. The distinction between obstructed and unobstructed liver at enhanced MRI implies a novel application of the agent for visualizing cholestasis.
This research was supported in part by Schering AG.

106 • 4:45 PM

Preclinical Evaluation of Gadolinium [III] Texaphyrin: A New Cancer Selective Paramagnetic Contrast Agent for MRI

SW Young, MK Sidhu, HH Muller, JD Mutch, JL Sessler, RA Miller
Department of Radiology, Stanford University School of Medicine, Stanford, CA

Purpose: Gadolinium III texaphyrin (Gd-Tex), a cancer-selective MRI contrast agent, was evaluated in these preclinical studies.
Methods: Relaxivity and signal intensity were measured in serial dilutions of Gd-Tex, and MRI of normal and tumor-bearing nude mice, rats, and rabbits was performed following IV doses of Gd-Tex at 1.5 T. Subchronic toxicity study: 120 normal rats, 2–20 μmol/kg, 3 days per week IV for 3 weeks.
Results: R1 = 19, R2 = 22; maximum signal intensity occurred at a dose of 1 μmol. Gd-Tex is stable in D5W. The toxicity study revealed no abnormalities. MRI in normal ($n = 34$) and tumor-bearing ($n = 4$) rats and normal ($n = 8$) and tumor-bearing ($n = 19$) rabbits revealed significant ($P < .05$) contrast enhancement (% E) of liver and kidney following 17 to 1 μmol Gd-Tex/kg IV. Significant ($P < .05$) increases in

% E and contrast to noise were observed following 2.5 μmol for V2 carcinoma (in liver, $n = 8$); 5 μmol (V2 in bilateral thigh, $n = 22$); 17 μmol/kg of Gd-Tex in fibrosarcoma-bearing rats ($n = 4$) up to 24 hours; and nude mice with human colon cancer ($n = 5$).
Conclusion: Gd-Tex appears to be an excellent, stable, and safe liver- and cancer-targetable MRI contrast agent.
S.W. Young, R.A. Miller, J.L. Sessler, and J.D. Mutch have an equity position with Pharmacyclics, Inc.

107 • 4:57 PM
Contrast-enhanced MR Imaging with a New Synthesized GD Complex as Contrast Agent: Experimental Study in Rats and Rabbits
GK Schneider, J Otto, K Urbschat, M Uder, H Sperber, D Gohl, B Kramann
University of Saarland, Homburg, Germany
Purpose: In this experimental study, a new Gd complex was tested for its imaging properties in enhancing general and local blood-brain-barrier (BBB) disruption and focal and diffuse liver lesions.
Methods: The new contrast medium consists of a neutral gadolinium BP-DTTA complex, eliminated by renal and hepatobiliary excretion. MRI was performed with a 1.0-T magnet (Siemens Magnetom) with T1- and T2-weighted SE sequences. Investigations of contrast enhancement in regions with disrupted BBB were performed by using rats and rabbits with general osmotic BBB disruption, experimentally induced brain infarction, and experimental brain abscess. To investigate imaging qualities in enhancing focal and diffuse liver lesions, rats with experimentally induced micronodular liver cirrhosis, acute hepatocyte necrosis, and hematoma of the liver were used. MR images were compared with corresponding histologic preparations.
Results: In general osmotic BBB disruption, injection of the new Gd complex leads to an increase in SI of up to 21%, and contrast-enhanced T1-weighted images of cerebral insult show SI increase of up to 32% in the surrounding edema with clear delineation from the central core of the infarction. Models with experimental brain abscess demonstrate strong SI enhancement of up to 54% in the abscess area after administration of the new Gd complex. SI in liver parenchyma of animals without pathologic alterations increased 40%–50%, whereas in models with experimentally induced focal and diffuse liver lesions, a good delineation of focal alterations with SI increases of 0%–20% and an enhancement up to 80% in acute liver necrosis were observed.
Conclusion: The new Gd complex can be categorized as a potential new contrast agent for MRI of local BBB disruption and for focal and diffuse liver lesions.

Monday Afternoon • Metropolitan Room
Papers 111–117

BRAIN II: Rapid Imaging
MODERATORS: RL De La Paz, MD
FJ Laine, MD

111 • 3:45 PM
High-Resolution Imaging of the Brain with GRASE (TGSE)
DA Feinberg, B Kiefer, A Litt, R Hausmann
Department of Radiology, New York University, New York, NY
Purpose: GRASE (turbo gradient spin echo [TGSE]) is a fast imaging technique based on the CPMG spin-echo sequence. The purpose of this study was to evaluate an improved high-resolution version of this sequence for T2 brain imaging.
Methods: Two methods of increasing GRASE spatial resolution were implemented. In method 1, a slight overlap of phase-encoding pulse and read-gradient pulse (200 μsec of the 5-msec read period) increased phase encoding for 20% higher in-plane resolution. The so-altered outer edge (4%) of k space was a potential source of artifact. Images were acquired with a 512 × 512 matrix and 240-mm field of view (FOV) compared with a 290 mm FOV without method 1 (TR/TE, 3,500 msec/110 msec; 16 sections at 5-mm thickness; 2 signals averaged in 2 min 50 sec). A Siemens Impact 1.0 T with 15 mT/m gradients was used. Method 2 simply used stronger gradients, 25 mT/m on a prototype 1.5-T Siemens Magnetom. Images were obtained with a 1,024 × 1,024 matrix with a 320-mm FOV (TR/TE, 5,000/140 for 19 images in 6 min 45 sec). In-plane resolution was 0.31 mm.
Results: The high-resolution 512-matrix images made with method 1 showed no distortions or artifacts related to overlapping gradients. There was reduction in the previously noted ringing artifacts. The 1024-matrix images demonstrated substantially higher brain detail. In all cases the normal gray-white contrast was preserved.
Conclusion: High-resolution GRASE T2-weighted imaging has been implemented in 512 × 512 and 1024 × 1024 matrices in rapid scan times.
B. Kiefer and R. Hausmann are research scientists for Siemens Medical Systems.

112 • 3:57 PM
Comparison of the Clinical Efficacy of Post-gadolinium FMSPGR and Spin-echo T1-weighted Imaging of the Brain
JK Curé, HP Clark, P Van Tassel
Department of Radiology, Medical University of South Carolina, Charleston, SC
Purpose: Before implementation of fast spin-echo (SE) techniques, T2-weighted SE sequences were the most time-consuming segment of a typical MR brain examination. Now T1-weighted (T1W) SE sequences are often the longest series. We evaluated the possibility of substituting fast, multiplanar spoiled grass (FMSPGR) for SE T1W imaging after gadolinium administration.
Methods: One hundred patients were studied with both FMSPGR and SE T1W sequences after administration of gadopentetate dimeglumine, 0.1 mmol/kg. Patients were studied on a 1.5-T system (Signa, GE Medical Systems, Milwaukee, Wis). The order of the sequences was varied. Patient's FMSPGR and SE studies were mixed and reviewed without comparison with each other by two neuroradiologists. Because of characteristic appearances of SE versus FMPSPGR images, it was impossible to "blind" the neuroradiologists to the technique used. Image quality was rated as unacceptable or acceptable, and sites of abnormal enhancement were graded as subtle, moderate, or intense. Scan times and artifacts were recorded. Artifacts were judged as diagnostically significant or not.
Results: FMSPGR proved as sensitive for abnormal enhancement as SE T1W imaging, and was far less sensitive to CSF and vascular flow artifacts, at significantly reduced scan times. Susceptibility artifacts were noted despite the short TE of the FMSPGR sequence; some were diagnostically significant.
Conclusion: The results of this small series support use of FMSPGR sequences in place of SE sequences for most post-contrast T1W brain imaging. Caution should be exercised when intracranial metal is present, as pathology in its immediate vicinity may be obscured.

113 • 4:09 PM
Comparison of EP Imaging and FSE for Clinical Brain MR Imaging
RL De La Paz, G Krol, B O'Malley
Department of Radiology, Memorial Sloan-Kettering Cancer Center, New York, NY
Purpose: Comparison of T2-weighted (T2W) echo-planar (EP) and fast spin-echo (FSE) brain MRI.
Methods: Eighty-four patients were studied. Image data sets of 20 EP images were obtained with an upgrade to a GE 1.5-T system (Advanced NMR) in 49 seconds with TR of 4,000 ms; TE of 75 ms; matrix of 512 × 128 (pixels, 0.8 × 1.5 mm); 5 mm thick; 2.5-mm gap; 4 NEX; and "mosaic" k-space mapping. Matched FSE images were obtained in 3:03 minutes

with a TR of 3,650 ms; TE of 102 ms; ET, 8; matrix, 256 × 192 (pixels, 0.9 × 1.1 mm); 5 mm thick; 2.5-mm gap; and 1 NEX. Three neuroradiologists compared films on a 10-point scale by using a randomized, blinded paradigm to assess lesion detection and specificity, image quality, anatomic resolution, tissue contrast, and artifacts.
Results: T2W EP and FSE images were equal in lesion detection, lesion specificity, image quality, anatomic resolution, and tissue contrast scores, although FSE images were considered "sharper," and chronic hemorrhage was more prominent on EP images. Ferromagnetic and skull base magnetic susceptibility artifacts were more prominent on EP images (subfrontal greater than petrous). Motion artifacts were more frequent and more prominent on FSE images, especially vascular and CSF phase ghosting and gross patient motion degradation. Good quality EP images were obtained in cases where patient motion artifact produced nondiagnostic FSE images.
Conclusion: T2W EP images were diagnostically equivalent to T2W FSE images. EP images were inferior in cases with prominent ferromagnetic or magnetic susceptibility artifacts, and superior when substantial patient motion was present.

114 • 4:21 PM
Imaging of the Internal Auditory Canal with MPRAGE with Spectral Selective Excitation
EA Knopp, AW Litt
New York University Medical Center, Brooklyn, NY

Purpose: To determine if the MPRAGE sequence with a novel approach to achieve rapid fat suppression could improve the post-gadolinium imaging of the internal auditory canal (IAC).
Methods: Forty patients referred for IAC evaluation were studied following the intravenous administration of 0.05 mmol/kg of gadolinium. Routine coronal T1 SE and axial fat-suppressed T1 SE scans were followed by an MPRAGE sequence with spectral selective excitation (MPRAGE-SSE) (TR/TE/flip angle/FOV/acquisition time: 14/4/15°/200/6:18) through the IACs. To achieve fast fat suppression in the MPRAGE sequence, a spectrally selective 1-1 binomial excitation pulse was substituted for the imaging pulse, allowing only water protons to be excited while minimizing fat signal. The interpulse delay and TR were reduced by applying a phase shift to the second component of the 1-1 pulse.
Results: In all cases, MPRAGE-SSE allowed greater depiction of the components of the neurovascular bundle, as well as better definition of the vascular anatomy of the posterior fossa (arterial and venous). Of the 12 enhancing lesions seen, MPRAGE-SSE was superior in five and T1 SE imaging was better in two. Vascular pulsation artifacts within the posterior fossa were less apparent at MPRAGE-SSE. In three patients white matter changes not seen at standard T1 SE imaging were appreciated at MPRAGE-SSE.
Conclusion: MPRAGE-SSE permits rapid fat suppression with overall better resolution of the neurovascular bundle. There is also less artifact, and better tumor and white matter pathology visualization.

115 • 4:33 PM
Dynamic High-Resolution Subtraction Imaging of the Pituitary
EA Knopp, AW Litt
New York University Medical Center, Brooklyn, NY

Purpose: To evaluate the utility of an image subtraction technique for high-resolution dynamic turbo T1 spin-echo (SE) imaging of the pituitary gland.
Methods: Ten patients with no clinical evidence of pituitary dysfunction and 10 patients referred for evaluation of the pituitary were studied. Following routine 4-mm sagittal T1 SE and 3-mm coronal T1 SE scans, 6 sets of dynamic 3-mm coronal turbo T1 SE (TR/TE eff/FOV: 385 msec/15 msec/200 mm) images were obtained, each set taking 39 seconds. One set was acquired before and 5 after bolus and flush injection of 0.05 mmol/kg of gadolinium. The standard coronal T1 SE sequence was then repeated. Subtraction images were postprocessed using an algorithm that calculates the absolute value of signal intensities, on a pixel-by-pixel basis, of each dynamic turbo T1 SE image minus its baseline turbo T1 SE image. Five subtraction images for each of the seven coronal slices were obtained.
Results: In both normal subjects and those with suspected pituitary pathology, dynamic subtraction imaging showed better depiction of the pituitary vascular "tuft" and infundibulum compared with standard techniques. There was also a differential enhancement pattern between the gland and the adjacent cavernous sinuses. This difference clearly demarcated the lateral margin of macroadenomas.
Conclusion: High-resolution dynamic subtraction imaging of the pituitary is a simple technique with the advantage of better depiction of the pituitary vascular anatomy and the relationship of the cavernous sinus to the intrasellar contents.

116 • 4:45 PM
Comparison of Half-Fourier Transform Single-Shot Spin-Echo and Turbo Spin-Echo T2-weighted Sequences in Evaluation of the Brain
JL Port, JS Ross, PM Ruggieri, JA Tkach, TJ Masaryk
Department of Radiology, Cleveland Clinic Foundation, Cleveland, Ohio

Purpose: To evaluate the clinical utility of a recently developed heavily T2-weighted rapid spin-echo MR pulse sequence with half-Fourier reconstruction for use in routine clinical brain imaging by comparison with conventional rapid scan technique.
Methods: Lesion conspicuity, artifacts, CSF-brain and gray-white matter contrast were compared on HASTE (half-Fourier transform, single shot turbo spin echo) and routine TSE (turbo spin echo) pulse sequences in 27 patients on a 1.0-T MR (Siemens) unit. A total of 20 images were obtained in 40 seconds with a 240 × 256 matrix using a single excitation with half-Fourier reconstruction, an effective TE of 74 msec, echo train length of 128, and an interecho spacing of 9.2 msec. This was compared with 19 images obtained in 1:38 minutes with a hybrid RARE technique (TSE) using an effective TE of 90 msec, echo train length of 7, and interecho spacing of 22.5 msec. Images were interpreted independently by two neuroradiologists.
Results: Lesion conspicuity was consistently reduced in the HASTE images both on lesion contrast and definition. Some lesions seen on TSE images were absent on the HASTE images. Although CSF-brain contrast compared favorably with that of the TSE sequence, gray-white differentiation varied from very poor to indistinguishable. Magnetic susceptibility effects were diminished on HASTE images in comparison with TSE, and the quality of HASTE images was degraded by prominent areas of artifactual bandlike hypointensity adjacent to CSF spaces.
Conclusion: Diagnostically reliable information cannot be ascertained from brain images obtained with the HASTE pulse sequence in its current form. The combination of acquiring a reduced number (approximately half) of phase-encoding steps, prominent T2 filtering effects, and high bandwidth significantly degrade the signal-to-noise ratio and resolution, resulting in markedly decreased lesion conspicuity and parenchymal contrast. CSF-brain contrast remains high. Magnetic susceptibility effects are profoundly reduced due to the very short interecho spacing, and artifactual areas of low signal may be related to the half-Fourier reconstruction.

117 • 4:59 PM
Dynamic Fast Spin-Echo Imaging of Brain Tumors
JD Hazle, NE Leeds
Department of Diagnostic Radiology, University of Texas M.D. Anderson Cancer Center, Houston, TX

Purpose: The extent of vascularity of intracranial lesions is believed to be an indicator of malignancy. The purpose of this study was to determine if fast spin-echo techniques sensitive to contrast agent uptake or perfusion could assist in the differentiation of benign from malignant brain disease.
Methods: All images were acquired on 1.5-T General Electric Signa scanners. Following routine precontrast examination,

the anatomy of interest was identified and three axial planes through the region prescribed. Acquisition parameters were typically 600/20-ms TR/TE, 20–24-cm FOV, 256 × 128 matrix, 5-mm slice thickness with 2.5-mm gaps, and an echo train length (ETL) of 4. The time points were acquired at the rate of one per 25 seconds. Images were acquired at the time of bolus and approximately every 25 seconds thereafter for 5 minutes. Software developed in house was used to produce maximum difference and slope images. Maximum difference images were generated by sampling all images in each plane pixel-by-pixel and determining the maximum difference from all images. Slope images were produced by calculating the uptake slope as the change in relative intensity as a function of time for each pixel in the three scan planes. Tools were developed for plotting the uptake curves as well.

Results: As predicted, the contrast uptake slopes of active tumors were found to be significantly higher than those of normal brain or necrotic tissues. Maximum difference images emphasized the regions of maximum contrast uptake, while the slope images accentuated the regions of more rapid uptake.

Conclusion: Both the maximum difference and slope images have a role in the study of contrast uptake and were good predictors of malignant disease. These techniques may be applied to other clinical situations where perfusion can be used for differential diagnosis.

Monday Afternoon • Miro Room
Papers 121–127

PELVIS: Female

MODERATORS: JJ Brown, MD
RC Smith, MD

121 • 3:45 PM

Staging of Endometrial Carcinoma: Comparative Study Using Endovaginal US and MR Imaging with and without Gadolinium Enhancement

C Reinhold, AE Aldis, M Atri, R Zakarian, PM Bret
Department of Radiology, McGill University, Montreal General Hospital, Montreal, Quebec, Canada

Purpose: To prospectively evaluate the accuracy of endovaginal sonography (EVS) and MRI in staging endometrial carcinoma, and to evaluate whether gadolinium improves the accuracy of MRI staging.

Methods: We studied 32 consecutive women with proved endometrial carcinoma. MRI was performed with a pelvic multicoil. All studies were interpreted in a double-blind fashion. Diagnostic examinations were obtained in 28 EVS and 30 MRI studies; in addition, 22 patients were injected with gadolinium.

Results: At pathology, 2 carcinomas were confined to the endometrium (stage 1A); 26 demonstrated superficial (stage 1B) and 4 demonstrated deep (stage 1C) myometrial invasion. The overall accuracy of EVS in staging endometrial carcinoma was 71% (20 of 28), and EVS successfully differentiated stage 1A/1B from stage 1C in 93% (26 of 28). The overall accuracy of MRI in staging endometrial carcinoma was 87% (26 of 30), and MRI differentiated stage 1A/1B from stage 1C in 93% (28 of 30). MRI with gadolinium correctly staged endometrial carcinoma in 82% (18 of 22) compared with 91% (20 of 22) for MRI alone.

Conclusion: MRI was superior to EVS in the overall staging of endometrial carcinoma; however, MRI was equal to EVS in differentiating stage 1A/1B from stage 1C. The administration of gadolinium did not improve the accuracy of MR staging.

122 • 3:57 PM

High-Resolution in Vitro and in Vivo MRI of the Uterine Cervix with an Intravaginal Coil

NM DeSouza, JE Schwieso, IC Hawley, WP Soutter, DJ Gilderdale
Department of MRI, Royal Postgraduate Medical School, Hammersmith Hospital, London, England

Purpose: The low anatomic resolution of MRI in cervical neoplasia with a body coil limits its sensitivity, particularly in the detection of parametrial extension. High-resolution images of the normal cervix in vitro and in vivo with detailed histologic correlation were, therefore, obtained by using an intravaginal coil to establish a baseline for diagnosis of early malignancy.

Methods: Nine premenopausal women were imaged with an enveloping solenoidal intravaginal coil. Five were nulliparous and all had normal cervical smears. T1W SE and T2W SE axial scans were obtained in the follicular phase of the cycle in six subjects and in the luteal phase in three. Five in vitro premenopausal uterine surgical specimens were similarly imaged and comparison made with histologic appearances.

Results: On both in vivo and in vitro studies, the normal cervix comprises an outer high signal intensity zone, an inner low signal intensity zone, and a higher signal intensity rim around the endocervical canal. In the parous cervix, this innermost rim is prominent and irregular and represents deep infolding of the mucosa at histology. The inner zone corresponds to densely packed fibroblasts and composes approximately 30% of the cervical area. The outermost zone contains high signal intensity foci corresponding to vascular bundles in histologic specimens. In vivo, these foci are highlighted on single-slice scans due to inflow effects. Up to three small parametrial lymph nodes (< 1 cm) were seen in some subjects. There were no visible differences between the follicular and the luteal phase images.

Conclusion: Dedicated cervical imaging delineates zonal differentiation, vascularity, and parametrial anatomy and may be valuable for recognizing early invasive disease.

123 • 4:09 PM

Prospective Comparison of MRI and Transvaginal Sonography for the Diagnosis of Adenomyosis

SM Ascher, LL Arnold, RH Patt, AS Bagley, JJ Schruefer, RCR Semelka, RK Zeman, JA Simon
Department of Radiology, Georgetown University Hospital, Washington, DC

Purpose: We prospectively evaluated MRI and TVS for the diagnosis of adenomyosis.

Methods: Twenty women (mean age, 36.6 years) with clinically suspect adenomyosis were studied. MRI was performed with a 1.0-T (12 patients) or a 1.5-T (8 patients) magnet (Magnetom, Siemens, Iselin) by employing T1-, T2-, T2-turbo (T2-TSE), and post-Gd-DTPA T1-weighted spin-echo techniques. TVS was performed with a 5.0-MHz probe (General Electric, Milwaukee). MR and TVS images were blindly interpreted by two separate investigators for the presence of adenomyosis by using published criteria. MR images were evaluated as individual sequences as well as collectively. Surgical pathology was obtained in all cases. Statistical analysis was by means of χ^2.

Results: Seventeen of the 20 patients had pathologic proof of adenomyosis. Adenomyosis was correctly diagnosed at MRI in 15 of 17 patients (88%). There were 2 false-negative and 1 false-positive diagnoses at MRI. Nine of 17 patients (53%) had adenomyosis correctly diagnosed at TVS. There were 8 false-negative and 1 false-positive diagnoses at TVS. The most frequent cause of false-negative diagnoses at TVS was the misinterpretation of adenomyomas as leiomyomas (7 cases). MRI was significantly better than TVS in the diagnosis of adenomyosis ($P < .02$). T2 and T2-TSE sequences were comparable in imaging adenomyosis. Contrast-enhanced T1-weighted sequences were superior to unenhanced T1-weighted sequences for depicting adenomyosis, but inferior to T2 and T2-TSE sequences.

Conclusion: MRI is superior to TVS in the diagnosis of adenomyosis.

124 • 4:21 PM

Comparison of Fatsat Fast Spin-Echo and Spiral Spin-Echo Imaging of the Pelvis

KC Li, ME Yacoe, L Cheung, M Hollett, C Meyer, FG Sommer, R Herfkens, RB Jeffrey Jr
Department of Radiology, Stanford University Medical Center, Stanford, CA

Purpose: To compare conventional fast spin-echo with fatsat (FSE) and spiral spin-echo techniques in imaging of the pelvis.
Methods: Sixteen patients undergoing pelvic MR imaging were evaluated with FSE (TR/TE, 4,000/102; 256 × 192 matrix, 4 NEX, fat saturation) and spiral spin-echo (TR/TE, 2,000/70, 30 interleaves, 256 × 256 matrix, 4 NEX) techniques at identical image locations on a 1.5-T GE Signa imager. The FSE and spiral images were independently compared for fat suppression, anatomic detail, image quality, and lesion detectability by three independent radiologists.
Results: Fat suppression in the spiral images, obtained with a spectral-spatial water selective excitation pulse, was superior to that of the FSE images. The anatomic details and image quality were better in the spiral images due to better motion suppression and flow-compensation characteristics. Minor problems encountered with the spiral technique included spiral motion artifacts and blurring from off-resonance effects.
Conclusion: Compared with FSE images, spiral images provide more uniform fat suppression and better motion suppression and flow-compensation characteristics and have great potential in increasing our accuracy of staging pelvic neoplasms.

125 • 4:33 PM

MR Imaging of Hydrosalpinx and Hematosalpinx

EK Outwater, DG Mitchell
Department of Radiology, Thomas Jefferson University Hospital, Philadelphia, PA

Purpose: To elucidate the MR appearance of dilated fallopian tubes, with particular regard to hematosalpinx, and to study the frequency of association with other pelvic pathology.
Methods: A search of surgical and MR records disclosed 11 patients with surgically proved dilated fallopian tubes who had MR studies performed. MR studies were obtained at 1.5 T with the body coil ($n = 4$) or pelvic array coil ($n = 7$) and short TR/TE and long TR/TE sequences in 2 or more planes. Studies were reviewed retrospectively with rating of signal intensity on a 5-point scale.
Results: A total of 13 dilated tubes were found surgically. Four patients had endometriosis, 2 had acute PID, and 1 had ovarian torsion. Dilated tubes appeared on long TR/TE MR images as high (fluid) signal intensity structures with a thin low signal intensity wall. Two or more long TR/TE images were frequently necessary to demonstrate their tubular configuration. MR evidence of hematosalpinx (signal intensity of the fluid greater than that of the myometrium on short TR/TE images) was seen in 5 of 13 tubes, 3 of which were in patients with endometriosis. Six patients had free fluid in the pelvis.
Conclusion: Long TR/TE images in multiple planes can demonstrate dilated fallopian tubes. Hematosalpinx at MR imaging is associated with endometriosis and is not diagnostic of ectopic pregnancy.

126 • 4:45 PM

MR Imaging of the Fetus: Current Concepts and a Review of 56 Cases

PM Colletti, PB Sylvestre, JM Tyszka, MR Terk
LAC/USC Imaging Science Center, Los Angeles, CA

Purpose: We reviewed the MR results of 56 cases of ultrasonographically detected fetal anomalies.
Methods: Upon IRB approval, MRI was performed in 56 pregnant patients with sonographically detected fetal anomalies; 35 studies were performed at 0.5 T and 21 at 1.5 T. Sagittal, axial, and coronal short TR/TE images required 3–6 minutes. Seven of the cases had gradient echo sequences performed with subsecond image acquisitions. Finally, sequential acquisition and cine display of GRASS and spoiled GRASS images were performed.
Results: There were 32 fetal CNS lesions: Chiari malformation, agenesis of the corpus callosum, acrania, Dandy Walker, spinal defect, and teratoma. Twenty-four non-CNS abnormalities included hydronephrosis, gastroschisis, omphalocele, hernia, dwarfism, and limb anomalies. All lesions were demonstrated at MR imaging. MR imaging provided information additional to that of ultrasound in 7 of 56 cases (12.5%). Fast spoiled GRASS was superior to GRASS and was at least equal to T1 spin-echo imaging. Fetal vessels with flow show high signal intensity. Fetal MRA was possible. Fetal motion can be demonstrated at sequential fast imaging.
Conclusion: Fetal MR imaging demonstrates sonographically detected gross fetal anomalies. Currently available fast imaging can allow improved results in the active fetus.

CARDIAC

MODERATORS: B Chen, MD
ER McVeigh, MD

131 • 3:45 PM

Motionless Movies of Myocardial Strain Rates by Means of a Stimulated Echo

VJ Wedeen, RM Weisskoff, GM Beache, TG Reese, BP Poncelet, BR Rosen, EE Dinsmore
Department of Radiology, MGH-NMR Center, Massachusetts General Hospital, Charlestown, MA

Purpose: To resolve the time course of contraction of individual tissue elements within the heart, we have developed a method to acquire movies of the myocardial strain-rate tensor field, in which gross cardiac motion is completely suppressed.
Methods: Myocardial velocity is phase encoded at an early point in the cardiac cycle, stored by a stimulated echo, and then read out at a later time in the cardiac cycle. If the cardiac delay before the velocity encode is incremented with successive heartbeats, and the cardiac delay to spatial selection and encoding is held constant, a movie results in which the heart appears motionless but cardiac phases evolve to show the velocity history of each element of tissue seen in the image. By using a stimulated-echo echo-planar MRI acquisition, the two in-plane velocity components are encoded and motionless movies of the myocardial strain-rate tensors are obtained at 4–8 cardiac delays, in a breath-hold acquisition of <30 seconds (1).
Results: Eigenimage analyses of motionless strain-rate movies indicate that $>95\%$ of the systolic motion (velocity variance) in normals is described as a single spatial pattern of contraction that progresses at variable speeds. In hypertrophic cardiomyopathy, focal intramural dyssynchrony has been demonstrated in diastole.
Conclusion: Stimulated-echo acquisition makes possible movies of the myocardial strain-rate tensor in which the confounding effects of in-plane and through-plane cardiac motion are entirely removed (2,3). This technique may facilitate quantitative study of the temporal dimensions of myocardial function.
1. Wedeen VJ. Magn Reson Med 27, 52–67 (1992). 2. Rogers WJ, et al. Circulation 84, 721–723 (1991). 3. Pelc NC, et al. Magn Reson Q 7, 229–254 (1991).

132 • 3:57 PM

Physiologic Exercise Testing and Cardiac MRI with a Newly Developed MR Cardiac Ergometer

RW de Boer, JW Vermeulen, A de Roos
MR Clinical Science, Philips Medical Systems, Best, The Netherlands

Purpose: Dynamic stress testing is commonly accepted as the most efficient method to increase cardiac oxygen demand and to detect myocardial ischemia. Isometric hand grip and plantar flexion exercises cause only a modest increase in coronary blood flow. Also, pharmacologic stimulation (intravenous dipyridamole) does not substantially increase the myocardial oxygen demand and is considered a nonphysiologic load on the heart. We experimented with a newly developed MR-compatible cardiac ergometer that allows physiologic exercise testing with the major upper leg muscles.
Methods: Cardiac MR images during exercise (supine position) were obtained with a Philips Gyroscan T5-II. Subjects' feet were strapped to pedals and cyclelike movements were used to drive the electromechanically braked ergometer. Workload (watts) and pedal frequency were computer controlled. The exercise protocol consisted of 3 levels of 5 minutes of steady-state exercise (heart rate: 80, 110, and 140 bpm) at the subject's preferred individual cycling rhythm. The control unit dynamically adjusted the absolute workload to maintain the desired heart rate level. A standard cardiac-triggered multislice, multiphase gradient-echo sequence was used for imaging (short-axis view, 6 slices, 8 phases, TR/TE/flip angle = RR interval/9.4/40°).
Results: Initial experiments with 5 volunteers showed images with a clear delineation of myocardial wall, papillary muscles, and ventricular blood volumes, even at heart rates of 140 bpm. The critical factor for image quality turned out to be a proper fixation of the subject's shoulder and waist.
Conclusion: The MR cardiac ergometer allows controlled exercise with the major upper leg muscles (increasing heart rate up to 140 bpm) while obtaining cardiac-triggered series of MR images without distortion. Optimized MR protocols and patient testing are currently being evaluated.
R.W. de Boer is an employee of Philips Medical Systems.

133 • 4:09 PM

Rapid Multiphase Imaging with Progressive Fourier Interpolation

EG Walsh, M Doyle, GG Blackwell, GM Pohost
University of Alabama at Birmingham, Birmingham, AL

Purpose: The keyhole technique is based on the acquisition of the central portion of k space for a time series of images (typically for first-pass tracer studies). However, when applied to multiphase cardiac imaging, the keyhole images appear blurred. A method is presented that extends the coverage of k space for a keyhole scan, which allows better definition of edges.
Methods: Analysis of a multiphase cardiac image set shows that the central portion of k space changes most rapidly, while regions more distant from the center vary at progressively slower rates. This is exploited in our acquisition scheme: the central k-space portion is sampled for each image, while the regions either side of center are sampled in alternate images, the skipped points being generated with Fourier interpolation (this is valid since the temporal variations occur at less than the Nyquist rate). Regions farther out are sampled every fourth image and so on. Computer simulations (with use of patient images) were conducted to compare the acquisition of a quarter of a k-space matrix for the conventional keyhole technique with that for the progressive interpolation technique.
Results: When compared with the keyhole scan, the Fourier interpolated images represented moving cardiac walls and details such as valves with markedly better edge definition. Additionally, edge definition in the Fourier interpolated images compared well with the original images.
Conclusion: By using Fourier interpolation in reduced acquisition scans, a greater portion of k space can be covered compared with direct substitution of the central lines.

134 • 4:21 PM

Regional Myocardial Blood Volume Estimated with MR First-Pass Imaging and Polylysine-Gd-DTPA in the Dog

N Wilke, K Kroll, H Merkle, Y Xu, Y Zhang, J Bassingthwaighte
Department of Radiology, University of Minnesota, Center for Magnetic Resonance Research, Minneapolis, MN

Purpose: Regional myocardial blood volume (MBV) was estimated by using a new approach: MR first-pass (MRFP) imaging after a bolus injection of the intravascular contrast agent polylysine Gd-DTPA (molecular weight 80 kd). This measurement was compared with MR measurements in the steady state (MRSS).
Methods: MBV was estimated by using MRFP imaging (TurboFLASH, TR/TE/TI = 5.9/3/10 msec) on a commercially available imager at 1.5 T to determine the ratio of the areas under tissue region-of-interest (ROI) ($n = 18$) and blood pool signal intensity time curves during bolus injections (0.07 mmol/mL) in instrumented dogs. MRSS estimates of MBV were obtained by measuring the same ratio after stable signal intensity levels at least 5 minutes after injecting higher concentrations of polylysine Gd-DTPA. The MR data were compared with radiolabeled albumin (Alb) measurements in corresponding ROIs.
Results: MBV was estimated to be 0.11 ± 0.011 (mean ±

SEM, $n = 18$), 0.097 ± 0.021 ($n = 9$) and 0.073 ± 0.0097 ($n = 9$) mL/g, on the basis of MRFP, MRSS, and Alb, respectively. Alb measurements of MBV were highly correlated with those obtained by using MRFP ($r = .94$) and MRSS ($r = .82$) measurements. In addition, MRFP and MRSS estimates of MBV correlated with each other ($r = .89, .83$).
Conclusion: MRFP imaging provides quantitative estimates of MBV in less than 1 minute, while a perfusion study might be accomplished simultaneously. The next step is the application of mathematical model analysis to derive myocardial blood flow, on the basis of data obtained with the MRFP technique. (Supported by NIH grants RR01243, and RR08079.)

135 • 4:33 PM
Accurate Cardiac Volume Measurement with Automated Border Detection and Partial-Volume Correction on Contiguous Multislice Turbo-FLASH and EP MR Images
ML Chuang, JD Pearlman
Department of Radiology, Beth Israel Hospital, Boston, MA

Purpose: The goal was to examine the potential for increased accuracy of left ventricular (LV) volume measurements by means of comprehensive 3D image stack acquisition, with automatic computer analysis providing correction of partial-volume errors.
Methods: Heart volumes of patients undergoing gated blood pool studies (MUGA) and Yorkshire pigs were analyzed with standard area-length, bullet, and Simpson rule formulas, and with integrated continuous section (ICS) by using CUBE software (UMS, Brookline, Mass). Image analysis, including border recognition and correction of partial volume, was automatic, proceeding from a single "mouse click" near the LV border. Imaging was performed on a 1.5-T EPI system (Siemens, Erlangen, Germany). Phantoms (casts of porcine heart at diastolic arrest) were also measured by means of volume displacement.
Results: Agreement between ICS and true volume measurements (by displacement of cast hearts) was excellent (mean difference, 0.6%). This represents an order of magnitude improvement over bullet or area-length formulas; in an example of LV aneurysm (pig with chronic infarction), LV volume was measured as 64.46 mL (area-length) vs 43.67 mL (ICS/CUBE). True diastolic-arrest volume was 43.33 mL. With automatic partial-volume correction, transverse stack volume agreed well with true short axis (mean difference, <4%) in humans.
Conclusion: Contiguous image stacks do not depend on assumptions about LV geometry that may be invalid for diseased patients. Fast imaging techniques (EP imaging, Turbo-FLASH) allow acquisition of the large number of images needed in reasonable time. ICS with automated optimal statistical border detection and partial-volume correction in CUBE reduce LV volume error to less than 1%, an order of magnitude improvement over existing methods.
J.D. Pearlman is the founder of UMS.

136 • 4:45 PM
Dipyridamole Cine MR Stress Imaging in Assessment of Patients with Ischemic Heart Disease
M Ahmad, D Dornfest, GR Hillman
University of Texas Medical Branch, Galveston, TX

Purpose: The superior resolution of MR imaging offers advantages in assessing left ventricular (LV) wall motion at rest and during stress intervention. The present study examined the feasibility of performing cine myocardial MR imaging during intravenous infusion of dipyridamole (Dip-Cine MRI).
Methods: Dip-Cine MRI was performed on a General Electric 1.5-T Signa 5 X system by using gated multiphase gradient-echo imaging. The pulse sequence technique included a 20° flip angle with minimum TE per RR cycle. Image slice thickness was 10 mm and the acquisition matrix was 256 × 192 pixels. Images were recorded in LV short-axis and four-chamber views. In all patients, an intravenous line was placed, along with a 12-lead electrocardiograph, and blood pressure was monitored. After the baseline study, dipyridamole was infused intravenously at a dose of 0.56 mg/kg, and the image sequence was repeated. Cine MR images were analyzed for changes in segmental LV wall motion.
Results: Thirteen patients (age range, 35–65 years) underwent Dip-Cine MRI. Twelve patients had coronary artery disease, and one patient was without coronary artery disease. Two patients developed angina and ischemic ST segment changes after dipyridamole infusion. There was a significant increase in heart rate: 78 ± 17 at rest and 89 ± 11 after dipyridamole infusion (mean ± SD; $P < .05$). The changes in blood pressure were not significant. LV wall motion was normal at rest in 5 patients and abnormal in 8 patients. New LV wall-motion abnormalities after dipyridamole were detected in 4 of 8 patients with abnormal resting LV wall motion.
Conclusion: These data suggest that Dip-Cine MRI is feasible and may be valuable in assessing LV wall motion in patients with ischemic heart disease.

137 • 4:57 PM
Simulations of Signal Dynamics during Contrast-enhanced First-Pass Cardiac MRI Studies
M Jerosch-Herold, N Wilke, M Deimling, AE Stillman
Department of Radiology, Center for Magnetic Resonance Research, University of Minnesota, Minneapolis, MN

Purpose: There is considerable interest in analysis of the MR signal time course (STC) during bolus injection of a contrast agent (CA) when using ultrafast MRI. Our simulations suggest a solution for the key step of transforming an STC into a concentration time curve (CTC).
Methods: A gamma variate function was used to describe the CTC of a bolus. The inflow and outflow characteristics and blood pool concentration of the bolus can be freely varied. The simulation of the STC is carried out with a TurboFLASH sequence with an inversion recovery as preparation. All sequence parameters are provided as input to the simulation program. The simulation uses stepwise solutions of the Bloch equations and derives, for the CTC of a bolus, the time dependence of the signal and relaxivities. The simulated STCs were compared with the experimental STCs measured in instrumented dogs.
Results: The simulation program provides the STC and also the T1 and T2 curves for any CA and concentration. The variation of the STC for a large range of concentrations could be simulated. At higher concentrations, a nonlinear relationship between the STC and the CTC can be observed in the simulations. These observed STCs were reproduced in dog experiments. We used an experimentally measured STC with a nonlinear fitting algorithm to calculate the true CTC curve. This proved to be particularly useful at higher CA concentrations.
Conclusion: The simulation allows one to numerically deduce the CTC from a measured STC for a wide range of CA concentrations. CTC can then be processed by using complex model analysis to derive quantitative perfusion data.

Monday Afternoon • Sapphire Room
Papers 141–147

SPECTROSCOPY I: Techniques
MODERATORS: HC Charles, MD
PA Narayana, PhD

141 • 3:45 PM
Eddy-Current Correction in Volume-Localized MR Spectroscopy
C Lin, AD LeBlanc, HJ Evans, RE Wendt, RM Rowe
Department of Medicine, Baylor College of Medicine, Houston, TX

Purpose: To obtain accurate MR spectra from a gradient-localized volume, the distortion caused by eddy currents needs to be corrected. Eddy-current correction is currently done during postprocessing by using a single-frequency reference FID acquired with the same sequence. Collection of this

reference FID internally is not always possible, and the use of an external phantom results in other errors. We investigated a new method based on gradient inversion that does not require a reference FID.
Methods: This technique employs two FIDs from the same selected volume by using two sequences with opposite gradient waveforms. By multiplying these two FIDs, the phase distortions due to the eddy currents are canceled. The square root of this product is then Fourier transformed to produce the final spectrum. We tested this method in a phantom of corn oil and water that simulated fatty bone marrow. Normal and gradient-inverted STEAM sequences with 12 msec TE and 4 mT/m gradients were used to collect FIDs on a clinical imager.
Results: The effect of eddy currents is completely removed in the final spectrum. All peaks are correctly registered, including the one from -CH=CH- protons, which, otherwise is undetectable. Their relative intensities match those measured with a high-resolution spectrometer.
Conclusion: Eddy-current correction with gradient inversion offers many advantages over the current methods that use a reference FID. The principles of eddy-current correction with gradient inversion may be applied to correct eddy-current artifacts in other types of MR imaging.

142 • 3:57 PM
Quick Proton Shimming for MR Studies
WR Riddle, SJ Gibbs, MR Willcott
Department of Radiology, Vanderbilt University Medical Center, Nashville, TN

Purpose: An essential component of MRS studies and a desirable component of MRI studies is a magnet shimmed to minimize static field inhomogeneities. Investigators often shim the magnetic field by using ad hoc techniques or an algorithm such as multiparameter simplex. Either method requires up to 15 minutes and is susceptible to local maxima. We have developed an iterative, deterministic algorithm for adjusting the shim currents, which converges rapidly.
Methods: The integral of a free induction decay increases with field homogeneity. Since the integral is directly proportional to T2*, maximizing the integral will maximize T2*. Plots of shim current versus integral for the X, Y, Z, and Z^2 coils are approximately Gaussian, while plots of shim current versus 1/integral are approximately parabolic. A procedure was written that determines the integral at three different shim currents. Reciprocals of these three points define a parabola ($ax^2 + bx + c$) with a minimum at $x = -b/2a$. This minimum is the new shim current.
Results: Since the assumption of a parabolic function for the X, Y, Z, and Z^2 coils is approximate and the coils are not completely independent, it is necessary to iterate this optimization. With a phantom and starting from zeroed initial shim currents, two iterations produce an optimal global shim. With humans and single-voxel spectroscopy, an optimal localized shim is obtained within one to two iterations.
Conclusion: Shimming with this algorithm is quick (less than 4 minutes) and provides optimal results. It makes all MRS and high-precision MRI observations more convenient and precise.

143 • 4:09 PM
Dynamic Chemical Shift Imaging
RV Mulkern, J Meng, HS Lilly, K Oshio
Department of Radiology, Children's Hospital, Boston, MA

Purpose: To demonstrate a method for spatially mapping proton spectra at time resolutions, permitting the study of dynamic processes.
Methods: Experiments were performed with a 1.5-T Signa imaging system (General Electric, Milwaukee, Wis). Inner volume spectroscopic rapid acquisition relaxation enhanced (RARE) sequences have been developed that are capable of yielding 32 Hz/pixel proton spectra from 128 locations along a 20 cm long, 5 × 5 mm cross-sectional column in 15 seconds (TR/TE = 600/144). Serial spectroscopic interrogation of the column allows the study of differential transport of spectroscopically distinct species along the column.
Results: To demonstrate the technique, the gravity-driven separation of oil and water after mixing was spectroscopically imaged at 15-second intervals. The spectral separation of water and (-CH_2-) groups allowed distinct visualization of the spatial distribution of each component along the column, with the largest changes occurring over the first minute.
Conclusion: Accessing the spectroscopic dimension with MRI is generally a time-consuming process. Therefore, the very concept of "dynamic" chemical shift imaging and potential applications have rarely been addressed. We have demonstrated one method for performing rapid, high-spatial-resolution, moderate-spectral-resolution mapping of a selected column. Potential applications include dynamic monitoring of ethanol distribution during ethanol treatment therapy of tumors or ethanol uptake within brain. The methods may ultimately prove useful for increasing temporal/spatial resolutions with which ^{31}P chemical shift differences between long T2 PCr and Pi spectral peaks can be measured, facilitating dynamic studies of pH changes in muscle during exercise.

144 • 4:21 PM
Reduced K-Space Acquisition of Spectroscopic Images
M Doyle, EG Walsh, HP Hetherington, GM Pohost
University of Alabama, Birmingham, AL

Purpose: A method is presented that allows the acquisition time for spectroscopic imaging (SI) studies to be reduced by 50%. Typically, about 50% of the SI phase-encoding steps contain predominantly noise. Data acquired before the SI acquisition can be used to determine which points contain significant information, allowing the nonsignificant points to be omitted.
Methods: Typically, the water image is highly correlated with the less abundant metabolite images. Thus, the k-space map of the water image can be used as a mask to determine which k-space points are significant. To account for imaging gradient imperfections, the water image should be acquired by using the same phase-encoding scheme (but not necessarily the same repetition rate) as used for the SI acquisition. A water image (to form the mask) and a proton spectroscopic image of the brain (resolution, 32, 32, 1,024) were acquired on the UAB/Philips 4.1-T system. With use of the water data (obtained independently of the SI data), 50% of the SI data points (FIDs) were set to zero.
Results: Spectra from the full matrix and the 50% set were analyzed by using a paired *t* test (9 representative volumes were chosen, 4 from gray matter and 5 from white matter, and the resonance areas of choline, creatine, and NAA were selected). A *P* value of .86 indicated that the spectra were not significantly different. Setting substantially greater fractions of points to zero results in degradation of the SI data.
Conclusion: SI acquisition times can be halved without degrading the resolution by using the information obtained from a scout image.

145 • 4:33 PM
Single-Voxel Proton MR Spectroscopy: Accuracy and Reproducibility
MR Willcott, WR Riddle, KM Cecil, SJ Gibbs
Department of Radiology, Vanderbilt University Medical Center, Nashville, TN

Purpose: N-acetylaspartate (NAA), choline (Cho), and creatine (Cr) are present in virtually all proton MR spectra of human brain. Single-voxel spectroscopy (SVS) estimates concentrations of these and other metabolites. We have used solutions of known compositions of these compounds to ascertain accuracy and reproducibility of SVS.
Methods: Aqueous solutions were prepared: NAA, 15 mM; Cho, 5 mM; and Cr, 15 mM. In addition, a single solution containing all three compounds, at the above concentrations, was prepared. Spectra were obtained by using a standard technique on a high-resolution analytical spectrometer (400 MHz, 9.2 T). Localized spectra of these solutions were obtained at 1.5 T (64 MHz), by using both STEAM (TE = 20 msec, 1.5 × 1.5 × 1.5 cm) and double spin echo (DSE) (TE = 135 msec, 2 × 2 × 2 cm). Spectra were scaled to the

intensity of the NAA methyl resonance. Response factors (observed:expected intensity) were calculated for all peaks from spectra of solutions.
Results: Response factors relative to NAA methyl from the analytical spectrometer were between 0.97 and 1.03. From SVS at 1.5 T, they ranged from 0.5 to 1.25. This deviation from unity depended on pulse sequence (STEAM vs DSE), TE, TR, and technique. With proper care, reproducibility was within 5% for these solutions.
Conclusion: Deviation from unity of response factors is an artifact of the SVS technique. These response factors can be used as calibration for human spectroscopy when it can be assured that T1 and T2 for these solutions and for human brain tissue are approximately equal.

146 • 4:45 PM
Evaluating Changes in Murine Tumor Oxygenation in Response to Nicotinamide by Using F-19 Echo-Planar Imaging and Spectroscopy
BJ Dardzinski, CH Sotak
Department of Biomedical Engineering, Worcester Polytechnic Institute, Worcester, MA

Purpose: To map murine tumor oxygen tension in vivo by using F-19 inversion-recovery echo-planar imaging (IR-EPI) of sequestered perfluorocarbon (PFC) emulsions and evaluating changes in tumor oxygenation in response to nicotinamide administration.
Methods: Coronal projection IR-EPIs of perfluoro-15-crown-5-ether emulsion sequestered in RIF-1 tumors of C3H mice were obtained at 2.0 T every 15 minutes for 2.75 hours. A 3-parameter nonlinear fitting algorithm was used to calculate the relaxation rate (R_1) on a pixel-by-pixel basis. The R_1 values and the corresponding Po_2 values were then displayed as a map that allows the spatial distribution of oxygen tension to be visualized. T1 was also calculated by using IR spectroscopic techniques within this 15-minute period. Nicotinamide (1,000 mg/kg) or a saline sham was injected i.p. 1 hour after start of measurements.
Results: Preliminary spectroscopic results indicated an increase in ΔPo_2 of 4.2 torr ± 2.8 (mean ± SEM) 1 hour after injection in nicotinamide-treated animals ($n = 8$) and no change (ΔPo_2 of −1.1 torr ± 1.1) 1 hour after injection of saline shams ($n = 3$). Oxygen tension maps provided similar mean changes although localized variations can be visualized.
Conclusion: IR-EPI of PFCs provides a fast and accurate method for spatially mapping murine tumor oxygenation. Po_2 maps can be produced to monitor the temporal evolution of spatial variations in oxygen tension in response to radiosensitizers. This work is being extended to study the response of other chemical adjuvants and radiation therapy. Funding for this work by the Whitaker Foundation is gratefully acknowledged.
C.H. Sotak is a consultant for Hemagen.

147 • 4:57 PM
Detection and Quantitation of Free Silicone with MR Spectroscopy in a Breast Phantom and an Animal Model
HHL Shih, HM Do, DP Gorczyca, LW Bassett
Department of Radiological Sciences, UCLA Medical Center, Los Angeles, CA

Purpose: Detection of microscopic residual silicone after removal of a breast implant is difficult with current MR imaging methods. MR spectroscopy (MRS) provides a potentially more sensitive method for detection and separation of silicone signal intensity from the dominant lipid signal intensities. By using phantom and animal model studies, we propose to determine the sensitivity of MRS for detecting small amounts of silicone embedded in fat.
Methods: From 0.5 to 10 cm^3 of free silicone was embedded into the phantoms and rabbits. MRS was performed on a 1.5-T GE Signa MR imager by using the knee coil. Localization was achieved with a PRESS sequence at 2,000/272 (TR/TE). Both lipid-suppressed and nonsuppressed spectra were obtained for each model.
Results: The silicone signal intensity could be clearly separated from the lipid signal intensities when there was more than 1 cm^3 of silicone polymer per 500 cm^3 of fat. There was good correlation between signal intensity and silicone concentration in the phantom. The rabbit model also demonstrated this relationship.
Conclusion: MRS is a potentially more sensitive method for detecting small or microscopic amounts of residual silicone after removal of silicone breast implants. The limit of detection with a clinical imager is approximately 1 cm^3 of silicone per 500 cm^3 of fatty tissue in both phantom and rabbit models. Semiquantitative measurement is possible.

Monday Afternoon • Topaz Room
Papers 151–156

IMAGING TECHNIQUES I
MODERATORS: CR Crawford, PhD
J Listerud, MD, PhD

151 • 3:45 PM
Use of Prior Knowledge of Human Anatomy to Guide the Acquisition and Reconstruction of MR Brain Images
Y Cao, DN Levin
Department of Radiology, University of Chicago, Chicago, IL

Purpose: In feature-recognizing (FR) MRI, training images of many subjects are used to reconstruct images of similar subjects from a subset of the usual phase-encoded (PE) signals, optimally scattered in k space. The FR method, previously tested in small phantoms (1), is now applied to human brain images.
Methods: A 1.5-T whole-body imager was used to collect T1-weighted training images from a group of normal and abnormal subjects and to image "unknown" subjects. In one experiment, 75 64 × 64 training images were used to reconstruct 64 × 64 brain images of "unknown" subjects from 32 or 40 measured PE signals. In a second experiment, 140 128 × 128 training images were used to reconstruct 128 × 128 "unknown" images from 64 or 80 PE signals. In each experiment, a simulated annealing algorithm was applied to the training data to determine how to distribute the measured PE signals in k space so that image reconstruction would be optimized (2). During image reconstruction, an effort was made to avoid possibly ill-conditioned steps in the algorithm.
Results: In both experiments, brain images reconstructed with the FR method had much less truncation artifact than Fourier reconstructions from the same number of signals. The FR method was not very sensitive to the TR or TE of the training images or unknown images.
Conclusion: The FR MRI algorithm can be used to reconstruct brain images from a small number of PE measurements collected with a clinical imager. This technique can be used to reduce truncation artifacts in image reconstruction from a given number of phase encodings or to reduce imaging time without increasing truncation artifacts.
1. Cao Y and Levin DN. Magn. Reson. Med. 1993, 30:305.
2. Cao Y and Levin DN. JMRI 1993, 3(P):111.

152 • 3:57 PM
MR Imaging of the Signal Intensity on a Known Curved Line or Surface
L Yao, Y Cao, DN Levin
Department of Radiology, University of Chicago, Chicago, IL

Purpose: To demonstrate a new technique for efficiently acquiring and reconstructing images of the signal intensity distribution on a curved line or surface with a known configuration.
Methods: If an MR signal originates from a curved line or surface with a given geometry, the spatial distribution of the signal intensity can be reconstructed from a small number of signals (the number required to image either an equivalent

straight line or flat slice) by utilizing a curvilinear coordinate system in which the curved line or surface is locally "straightened (flattened)." Images can be reconstructed from an optimal subset of the usual 2DFT or 3DFT signal array, chosen by minimizing the propagation of noise into the image. The technique was applied to signals from known curved lines in a plane, produced by numerical simulation and also by imaging slices of fruit with a 1.5-T whole-body machine.
Results: By using prior knowledge of the curve shape and only a small portion of the data points needed for 2DFT MRI, images were reconstructed with good signal-to-noise ratio and without significant loss of resolution. In typical cases, we were able to use signals within a 16 × 16 array in the center of k space to reconstruct images similar to conventional 256 × 256 images.
Conclusion: Prior knowledge of the geometry of a curved line or surface can be used to increase the efficiency of imaging the signal from that structure. Velocity imaging of curvilinear blood vessels and functional imaging of brain cortex can benefit from this technique.

153 • 4:09 PM
Fast Spectrally Selective Excitation in 3D Gradient-Echo Imaging
DM Thomasson, DE Purdy, JP Finn
Siemens Medical Systems, Iselin, NJ

Purpose: Conventional fat suppression in short TR sequences results in a disproportionate penalty in imaging time. Spatial-spectral pulses of durations on the order of 20 msec do not alleviate this problem. Consequently, the present study implements a fast spectrally selective excitation for rapid gradient-echo imaging.
Methods: Measurements were performed on a 1.0-T Magnetom Impact. A standard 3D Flash sequence with an echo time of 11 msec and a minimum TR of 20 msec was used. A modified 1:1 binomial nonspatial selective, spectrally selective excitation scheme was employed for fat suppression. The modified 1:1 scheme used a reduced interpulse spacing by appropriate phase modulation of the second pulse in the 1:1 pulse pair. Three phase offset measurements were compared with a conventional chemical shift selective acquisition; an alpha(x)-alpha(x) with a 3.35-msec interpulse interval, an alpha(x)-alpha(y) with a 1.175-msec interval, and an alpha(x)-alpha(x, y; 45° phase rotation) with a 0.588-msec interpulse interval. Care was taken to set up the acquisition matrix so as not to receive signal from undesired anatomy.
Results: All sequences showed a decrease in fat signal intensity. A small SNR decrease was observed at the small interpulse delays, but tissue contrast was otherwise equivalent. The total examination time was reduced to 50% of that of the equivalent off-resonance pulse method. There was no significant overlap of undesired anatomy with this nonselective 3D technique.
Conclusion: Fast spectrally-selective excitation provides effective fat suppression with a substantial savings in imaging time when used in a nonselective 3D gradient-echo acquisition.
D.M. Thomasson is an employee of Siemens Medical Systems.

154 • 4:21 PM
Driven Equilibrium Gradient-Echo Sequence for Orthopedic Imaging
DM Thomasson, DE Purdy, JP Finn
Siemens Medical Systems, Iselin, NJ

Purpose: A driven equilibrium FISP type sequence structure was developed to improve the contrast between fluid, cartilage, meniscus, and bone marrow in orthopedic imaging. A driven equilibrium condition is established by adding an alpha pulse at the end of the data acquisition with a 180° phase relative to the initial excitation pulse. This pulse restores some of the magnetization vector back to the +z axis prior to the next excitation and therefore increases the signal from long T1 (fluid) tissues.
Methods: Measurements were performed on a 1.0-T Magnetom Impact. A standard 3D FISP sequence with a TE of 9 msec, bandwidth of 130 Hz/pixel, and a minimum TR of 18.1 msec was used. This was a nonselective sequence with 200 μsec rectangular alpha pulses used for excitation and restoration. A normal volunteer underwent clinical knee imaging. The amount of signal was measured from muscle, marrow fat, fluid, and meniscus when the sequence was used both with and without the restoration pulse.
Results: Images acquired with this technique show an increase in fluid signal intensity and a decrease in both cartilage and menisci signal intensities compared with the same sequence run without the restoration pulse. There was also a significant decrease in muscle tissue. The fluid/cartilage contrast as determined with simple ratios increased from 1.76 to 3.25.
Conclusion: A driven equilibrium condition can be established by using a restoration pulse at the end of a normal FISP type data acquisition. A significant improvement in fluid/cartilage contrast is obtained when using this type of sequence structure.
D.M. Thomasson is an employee of Siemens Medical Systems.

155 • 4:33 PM
MT Studies of Chemical Models for Atherosclerotic Plaque
J Hua, GC Hurst, AM Cohen, JJ Piotrowski, S Shah
Department of Radiology, MetroHealth Medical Center, Cleveland, OH

Purpose: This study seeks to determine if magnetization transfer (MT) MRI sequences could be useful for the study of atherosclerotic plaque. This potential application is suggested by (*a*) the known correlation of MT effect with cholesterol content of lipid/water mixtures and (*b*) observations that normal and diseased arterial wall components are well distinguished with conventional long TE, long TR T2-weighted sequences, which have contrast that is often similar to that due to MT.
Methods: Lipid/water model mixtures were composed from the known chemical composition of human atherosclerotic plaque; 11 combinations of phospholipid, cholesterol, cholesteryl ester, and triglyceride were chosen to represent stages I–III disease. MRI data were obtained by using a 1.5-T clinical whole-body MRI system. MT M_s/M_0 ratios were measured by using MT sequences composed by adding off-resonance Gaussian pulses to conventional 2DFT gradient echoes. Bulk spin $T1_a$ and $T2_a$ were measured by means of standard inversion-recovery and spin-echo methods.
Results: $T1_a$ varied from 560 to 955 msec; $T2_a$ varied from 95 to 195 msec. With adjustment for field strength, these values are similar to reported measurements in ex vivo lesion samples. The MT M_s/M_0 values of stage I lesion models monotonically decreased from 0.92 to 0.55; however, for later stage lesion models, the MT effect was relatively small, even at the highest cholesterol levels.
Conclusion: Although MT may not provide a direct, quantitative index of lesion stage, it may nonetheless be useful in sequences with less motion sensitivity than conventional T2-weighted sequences.

156 • 4:45 PM
Quantitative Prediction of Magnetization Transfer in Conventional and Fast Spin Echo
J Listerud
Department of Radiology, Hospital of the University of Pennsylvania, Philadelphia, PA

Purpose: Although magnetization transfer (MT) has been proposed as a clinical MRI technique in its own right (1), a significant amount of MT has been qualitatively observed in conventional spin echo (~10%) and in fast spin echo (FSE) (~30%) (2,3). We propose a quantitative algorithm for predicting the degree of MT in conventional MRI (4). The algorithm is based on three observations concerning the magnetization transfer contribution (MTC) of a prior RF pulse to the total MT observed in an image: (*a*) MTC decays exponentially with temporal gap between pulse and image (5), (*b*) its base value at zero gap depends on the frequency difference be-

tween the pulse and image (an "effective Z curve"), (*c*) the MTC of multiple pulses can be added to obtain total MT observed (the "infinitesimal limit").
Methods: A single-slice, multiphase FSE pulse sequence was modified to precede each sequence by an ensemble of RF pulses: the number, spacing, frequency, and temporal gap between pulse ensemble and image may be incrementally varied with "phase." Meat, oil, and water sample volumes were imaged under a variety of clinical imaging protocols by using conventional spin echo and FSE in which the following parameters were varied: TE, TR, number of slices, number of echoes, slice spacing, bandwidth of RF pulses.
Results: The multiphase, single-slice FSE sequence was used to acquire an effective Z curve and an exponential decay constant for the MTC of a single RF pulse in meat. This effective Z curve, when normalized for power per pulse or for number of pulses per ensemble, was found to be independent of either of these quantities, supporting claim (*c*).
Conclusion: With use of the derived data, the total observed MT in the center slice of the conventional multislice acquisitions was predicted on the basis of knowledge of the slice excitation pattern. Correlation with observed MT for FSE exceeded $r = .95$. The MT observed in conventional imaging may be quantitatively predicted.
1. E. Outwater, M.D. Schnall, L.E. Braitman, B.J. Dinsmore and H.Y. Kressel. *Radiology* 182, pp 535–540 (1992). 2. W.T. Dixon, H. Engels, M. Castillo and M. Sardashti *MRI* 8, pp 417–422 (1990). 3. P.S. Melki and R.V. Mulkern, *Mag. Res. in Med.* 24, pp 189–195 (1992). 4. J. Listerud, S. Einstein, E. Outwater and H.Y. Kressel *MRO* 8(4), pp 199–244 (1992). 5. R.T. Constable, A.W. Anderson, J. Zhong and J.C. Gore *MRI* 10, pp 497–511 (1992).

Tuesday Morning • Monet Room
Papers 201–207

MAMMOGRAPHY: Silicone

MODERATORS: PJ Fritzsche, MD
TA Spraggins, PhD

201 • 10:30 AM

Dynamic Multislice TurboFLASH MR Mammography for Pharmacokinetic Mapping

MV Knopp, T Hess, U Hoffmann, H Junkermann, G Brix, D von Fournier, WJ Lorenz, G van Kaick
Department of Radiology, German Cancer Research Center, Heidelberg, Germany

Purpose: To introduce clinically a dynamic MR mammography (MRM) technique that fulfills the following requirements: (*a*) complete detection in both breasts, (*b*) good temporal resolution for dynamic analysis, (*c*) acceptable spatial resolution, (*d*) feasibility of automatic pharmacokinetic analysis resulting in projection images.
Methods: Thirty-seven patients (age range, 30–68 years) with subsequent histologically confirmed breast cancer were included in the initial evaluation. All imaging was performed on a 1.5-T Siemens Magnetom SP with use of a standard double breast coil. A specially designed T1-weighted saturation recovery TurboFLASH sequence (TR = 8 msec, TE = 2.7 msec, TI = 125 msec, $\alpha = 12°$, 128 × 128 matrix) was used, which permited acquisition of 15 adjacent images within 20 seconds. By repeating this for 32 cycles, the contrast enhancement can be monitored for each individual cross section over 10.5 minutes. A dose of 0.1 mmol Gd-DTPA per kg body weight was administered over 1 minute by using an infusion pump (PIM 717; Doltron AG, Switzerland). On the basis of a pharmacokinetic model, a pixel-by-pixel analysis of each cross section was performed on a workstation (VAX 3100, DEC). The pharmacokinetic parameters amplitude and distribution time were color coded, and three projection images in the anteroposterior, craniocaudal, and mediolateral plane were calculated. These projection images guide the detailed analysis of individual enhancing lesions by using a cine display of the 32 images in each plane and analysis with a region-of-interest technique.
Results: The introduced procedure fulfills the clinically desired requirements. In this initial study, all 37 lesions were visualized on the pharmacodynamic projection maps. Patient motion caused artifacts in 12 studies, which were identified as such by using this cine display. The pharmacokinetic parameters correlate with the previously used single-slice spin-echo sequence.
Conclusion: The introduced dynamic multislice technique enables a complete automated pharmacokinetic analysis of Gd-DTPA uptake within both breasts in a study time of 15 minutes. The color-coded projection images visualized all histologically confirmed lesions in this study. This technique appears clinically useful and facilitates standardized image analysis of MRM.

202 • 10:42 AM

Turbo Inversion Recovery MRI of Breast Implants: Initial Clinical Experience

NR Bucciarelli, WG Bradley, Jr, D Atkinson, S Roux
Memorial MR Center, Long Beach Memorial Medical Center, Long Beach, CA

Purpose: To determine the sensitivity and specificity of turbo inversion recovery (IR) MRI for the detection of intra- and extracapsular ruptures of silicone implants.
Methods: One hundred fifteen patients with 221 implants were evaluated by using turbo IR MRI. All studies were performed on Siemens SP4000 1.5-T MR imager with use of a dedicated bilateral breast coil. A turbo IR 3,300/18 and 93 sequence with an inversion time of 100 msec was used to null fat. A turbo IR 5,200/16 sequence with an inversion time of 400 msec was used to null silicone. Both techniques were applied over a 350-mm field of view (FOV) with a 256 × 512 matrix. Two interleaved 5-mm acquisitions were obtained for a total acquisition time of 9 minutes. In addition, a 3D PSIF 17/7/70° sequence was applied in the coronal plane using a 160 × 512 matrix over a 320-mm FOV with a partition thickness of 1.5 mm. Surgical follow-up was obtained in 52 implants. All studies were reviewed prospectively (at the time of examination) and retrospectively as a group, with the reviewers blinded to the surgical results.
Results: Of the 221 implants studied, 44 ruptures were diagnosed, 37 of which were intracapsular and 7 extracapsular; 39 of the ruptures were of single-lumen silicone implants, 4 were of double-lumen implants, and 1 was of a saline implant. Of the 39 single-lumen silicone implants, 9 were subpectoral and 30 were subglandular. Of the 52 implants with surgical follow-up, there were 19 true positives, 30 true negatives, 2 false positives, and 1 false negative. This led to a retrospective sensitivity, specificity, and accuracy of 93.3% with a positive predictive value of 87.5% and a negative predictive value of 96.6%.
Conclusion: Turbo IR techniques offer excellent tissue characterization for evaluation of suspected implant rupture.
This research was supported in part by Siemens Medical Systems.

203 • 10:54 AM

MR Imaging of Silicone Breast Implants: Use of 3-Point Dixon Chemical Shift and Inversion Recovery Fast Spin-Echo Techniques

HB Borofsky, DM Ikeda, RJ Herfkens, A Sawyer, W Whitney, GH Glover
Department of Radiology, Stanford University School of Medicine, Stanford, CA

Purpose: To evaluate modified 3-point Dixon chemical shift (1) and inversion recovery fast spin echo (IRFSE) techniques in imaging silicone breast implants for rupture, and to compare these results with findings at mammography and sonography.
Methods: Twenty-two patients with suspected implant rupture were referred for MRI, sonography, and mammography. MRI was performed on a 1.5-T GE Signa imager with the patient prone, with use of a breast surface coil (GE Medical Systems). Each breast was imaged separately, sagittally and axi-

ally, by using 4-mm-thick slices, 20-cm field of view, and 256 × 192 matrix. Three-point Dixon acquisitions were obtained with TR/TE of 400–600/25 with the center frequency on silicone. IRFSE acquisitions were obtained with TR/TE of 3,500–5,000/102Ef and TI of 140 msec. MR images were prospectively evaluated by a radiologist blinded to findings at mammography and sonography.

Results: Of 44 breast implants imaged, 20 had MRI evidence of rupture. Sonography and mammography were negative in 7 and 13 of these 20 cases, respectively.Three-point Dixon resulted in silicone-only images with suppression of fat and water, limited by artifacts caused by mismapping at borders of susceptibility differences. IRFSE resulted in silicone and water sensitive images with fat suppression, particularly useful in depicting water droplets and reactive fluid, and more sensitive in depicting radial folds and "linguine" (2).

Conclusion: Our preliminary results show 3-point Dixon and IRFSE are useful and complementary in evaluating silicone breast implants for rupture and may be more sensitive than sonography and mammography.

1. Schneider E, Chan TW. Selective MR imaging of silicone with the 3-point Dixon technique Radiology 1993; 187(1):89–93. 2. Gorczyca DP, Sinha S, Ahn CY, DeBruhl ND, Hayes MK, Gausche VR, Shaw WW, Bassett LW. Silicone breast implants in vivo: MR imaging. Radiology 1992; 185(2):407–410.

204 • 11:06 AM

Detection of Implant Leaks from Residual Gel Volume Estimates and Silicone-enhanced MRI: Combined 3D and 2D Approach

SN Sarkar, G Halvas, C Kirby, M Calderon
Houston Imaging Center, Houston, TX

Purpose: A simple, accurate test exists for implant leakage detection and volume measurements that uses fast 3D MRI. Another effective, modified 2D sequence for partial suppression of adipose tissue with enhancement of silicone has also been used.

Methods: About 35 oblique/sagittal 3D slices per implant were collected with an under-the-breast surface coil, with gradient moment nulling and presaturation to suppress chest motion. Optimum parameters were TR of 31 msec, TE of 9 msec, flip angle of 10°–25° for small to large breasts, and total time of 1–2 minutes. Double-lumen bags required a longer TE (>30 msec). Three-dimensional reconstructions and residual gel volume were quantitated by multiplying implant area and thickness for each slice. An optimal fat- and water-suppressed 2D sequence was constructed with simultaneous T1 and T2 weighting guided by in vivo relaxation data.

Results: Volumes measured from 2–3-mm 3D slices are in agreement with actual gel volumes in phantoms and in five symptom-free volunteers, to within 98%. Application to 25 patients with a variety of symptoms showed measurable volume loss in 16 subjects (32 implants) with leaks further confirmed by isolated gel globules and linguine signs in fat-suppressed 2D sequences. Five subjects with single-lumen bags and 4 subjects with double-lumen bags had negligible silicone loss.

Conclusion: Motion-compensated, fast 3D MRI with presaturation gives high-quality axial and sagittal images for accurate volume determination of residual silicone in implants. Silicone enhancement is possible by means of fat and water suppression in 2D sequences with moderate T1 and heavy T2 weighting.

205 • 11:18 AM

Normal Breast in MR Imaging: Two Years Later

M Megido-Ravid, Y Itzchak
Sheba Medical Center, Tel Hashomer, Tel-Aviv, Israel

Purpose: To follow up women with normal MR imaging examinations and try to assess the time interval for new tumor formation as detected with MR imaging with Gd-DTPA.

Methods: During the last 4½ years, 391 women between the ages of 20 and 89 years with suspicious mammograms underwent MR imaging followed by either open or closed core needle biopsy. All women with normal MR examinations were reexamined with MR imaging either 1 or 2 years after the initial examination. Images were obtained with the Elscint Gyrex 2-T instrument. Field strength was 1.9 T. A transmitter/receiver H-1 surface coil specially designed for breast examination was used. Spin-echo pulse sequences were applied. Gd-DTPA was administered intravenously at a dose of 0.1 mmol/kg.

Results: After injection of Gd-DTPA, no shortening of T1 was noted in 164 patients, and their examinations were considered and histologically proved to be normal. T1 was shortened in 127 patients: The findings were recognized as and histologically proved to be carcinoma in 58 patients, premalignant changes such as papillary hyperplasia or apocrine metaplasia in 32 patients, and fibroadenomas in 37 patients. Follow-up of the normal breast (164 cases) after 1 year in 92 women and 2 years in 97 women showed no shortening of T1, which meant no malignant tumor or premalignant changes.

Conclusion: Although with screening mammography, 1 year is considered as the time interval for detecting a new tumor; with MR imaging this period is prolonged and may exceed 2 years. This may be related to the ability of the technique to help exclude the premalignant changes in a very early stage. This might be important when considering the control of health care costs.

206 • 11:30 AM

Quantitative Analysis of MR Breast Tissue Parameters and X-ray Mammograms

SJ Graham, MJ Bronskill, JW Byne, MJ Yaffe, NF Boyd
Department of Medical Biophysics, University of Toronto, Sunnybrook Health Science Centre, Toronto, Ontario, Canada

Purpose: The correlation between MR breast tissue parameters (relative water content and T2 relaxation times) and quantitative x-ray mammographic parameters was investigated to estimate the relative sensitivity of the MR parameters for assessing risk of breast cancer.

Methods: Forty-two subjects with no history of breast cancer and 5 subjects with previous breast cancer but no clinical signs of recurrence were examined. Relative water content was measured from one-dimensional profiles of the breast by using a hybrid Dixon technique (TE/TR = 20/5,000 msec); T2 measurements used a CPMG train of hard pulses (TE/TR = 8/5,000 msec, 140 echoes), preceded by saturation pulses that suppressed unwanted signal from the chest wall and torso. The MR methods were carefully validated in phantoms and volunteers. Mammograms were acquired within 12 months before MR measurements and then digitized. The percentage of mammographic dysplasia was determined by using computer-aided classification.

Results: Significant differences were found in the relative water content of subjects at low and high risk of breast cancer. Relative water content correlated strongly with the percentage of mammographic dysplasia, when measured in the right, left, or both breasts, and displayed comparable sensitivity to breast cancer risk. T2 values were complicated and more difficult to interpret.

Conclusion: New MR methods have been developed permitting accurate measurement of relative water content and T2 values within 30 minutes. These methods correlate well with previous MR methods and with quantitative x-ray measures of mammographic dysplasia, and offer a noninvasive assessment of breast cancer risk.

207 • 11:42 AM

Exploiting the FSE Bright Fat Phenomenon for Silicone-Fat Differentiation in Breast Imaging

H Hiramatsu, K Oshio, DF Adams, ED Waitzkin, DS Williamson, NE O'Connor, FA Jolesz, RV Mulkern
Department of Radiology, Brigham and Women's Hospital, Boston, MA

Purpose: To demonstrate differentiation of fat from silicone in breast imaging by using the echo spacing dependence of fat signal in FSE sequences.

Methods: Studies were performed with 1.5-T Signa imagers (GE Medical Systems). Phantom studies of vegetable oil and

silicone implants and in vivo studies of patients with silicone implants were performed. Two separate FSE sequences were applied, one with one-half the echo spacing and twice the number of echoes as the other (16 vs 8). Effective TEs were identical for both sequences. Echo spacing pairs studied were 12/24 msec and 16/32 msec. TRs were 2.5 seconds with 192 phase encodes sampled. Imaging times were 1 and 2 minutes for short and long echo spacing sequences, respectively.

Results: Vegetable oil and fat had approximately twice the signal intensity on short echo spacing FSE images as on long echo spacing FSE images. Signal intensity from silicone was not dependent on echo spacing. The ratio of fat signal intensity on long versus short echo spacing images provided a scale factor for postprocessing images to generate pure silicone/water and pure fat images. Signal from fat or silicone was suppressed to the noise level homogeneously over the entire FOV.

Conclusion: The fat/silicone differentiation technique described is dependent on the special properties of fat signal in FSE sequences, properties not shared by silicone or water. Unlike with other methods, B_1 and B_0 inhomogeneities play no role in the suppression technique, making the method extremely useful in breast imaging, in which both factors can impede conventional frequency-selective suppression pulses.

Tuesday Morning • Metropolitan Room
Papers 211–217

FUNCTIONAL IMAGING

MODERATORS: JA Helpern, PhD
BR Rosen, MD

211 • 10:30 AM

Functional MRI: Promising Approach for the Evaluation of Visual Pathway Abnormalities Associated with Albinism

S Lai, P Hedera, EM Haacke, AJ Lerner, AL Hopkins, JS Lewin, RP Friedland
Physics Department, Case Western Reserve University, Cleveland, OH

Purpose: To examine the potential of functional MRI to evaluate visual pathway abnormalities associated with albinism.

Methods: Studies were done in three albino patients and six healthy volunteers on a clinical 1.5-T Siemens Magnetom with a surface coil. Every subject underwent a series of randomly ordered binocular and monocular (left or right eye) photic stimulations at 8 Hz provided with LED goggles. A susceptibility-sensitized 2D FLASH sequence was developed to detect stimulation-induced signal changes in a 4-mm-thick slice covering the superior and inferior lips of the calcarine fissure.

Results: Photic stimulation-induced signal enhancements in visual cortex were observed in all subjects. Areas showing large percentage signal changes were found to be correlated with sulci, in which there exist superficial veins. Smaller signal changes were observed in regions in which we proposed that there are smaller blood vessels (eg, venules). In all normal subjects, both binocular and monocular stimulations caused near-symmetric patterns of activation in two hemispheres in the visual cortex, extending from the occipital pole to the deep parts of the calcarine fissure. All three albino patients showed consistently that monocular stimulation caused predominant contralateral activation accompanied by a much smaller, well-delineated area of enhancement in the ipsilateral hemisphere in the anterior part of the calcarine fissure, which is due to residual ipsilateral projection of the outermost parts of the temporal retina. Binocular stimulation caused a near-symmetric activation pattern. But neither binocular nor monocular stimulation caused signal enhancement in the most superficial parts of the occipital lobe.

Conclusion: Our observations were consistent with known anomalies of retina-calcarine projections in albinism. This suggests that functional MRI is a promising approach for evaluating visual pathway abnormalities associated with albinism.

212 • 10:42 AM

Functional MRI Localization of Hand Motor Cortex in Patients with Neonatal Focal Brain Injury

Y Cao, EM Vikingstad, PR Huttenlocher, DN Levin
Department of Radiology, University of Chicago, Chicago, IL

Purpose: To use functional MR imaging (FMRI) to localize the hand motor cortex in children and young adults with neonatal brain injury.

Methods: A conventional 1.5-T imager was used to obtain a series of T2*-weighted gradient-echo images during a baseline period and during several alternating periods of rest and motor task performance (finger opposition). Significant functional signals were identified by applying paired *t* tests to signals in the baseline and task images. Cross-correlation coefficients between the time course of the FMRI signals and a sinusoidal wave function were calculated and were used to remove some false-positive signals in the functional images (1). We studied seven patients (age range, 14–22 years) with focal unilateral brain damage and contralateral hand weakness.

Results: Movement of the normal hand in the seven patients was associated with functional signals observed near the contralateral central sulcus, supplementary motor area, and anterior frontal areas. In nine trials in five patients, movement of the weak hand was associated with bilateral functional signals; the volume ratio of ipsilateral to contralateral signals was 2.8, nine times larger than that observed previously in normal subjects (2,3). In three of these patients, movement of the weak hand was accompanied by minor, involuntary "mirror" movement of the strong hand.

Conclusion: FMRI may be used to study the spatial reorganization of the motor cortex after focal brain injury. Initial data suggest changes in functional localization after perinatal brain lesions, presumably related to plasticity of the immature brain (4).

1. Bandettini P, Jesmanowicz A, Wong EC, and Hyde JS. *Magn. Reson. Med* 30:161, 1993. 2. Cao Y, Towle VL, Levin DN, and Blater JM. *J. Magn. Reson. Imag.*, 1993 (in press). 3. Kim SG, Ashe J, Georgopoulos AP, Merkle H, Ellemann JM, Menon RS, Oguwa S, and Ugurbil K. *J. Neurophysiology* 69:297, 1993. 4. Huttenlocher PR and Raichelson RM. *Developmental Brain Research* 47:59, 1989.

213 • 10:54 AM

Discrimination of Large Veins in Time-Course Functional Neuroimaging with Spiral K-Space Trajectories

AT Lee, CH Meyer, GH Glover
Department of Radiology, Stanford University School of Medicine, Stanford, CA

Purpose: Stimulus-induced contrast changes in T2*-weighted images result from blood oxygenation changes in a range of vessel sizes. We examined the time course of each pixel in a set of T2*-weighted images by using periodic visual stimuli to determine if signals that result from large vessels are time-delayed compared with those from smaller vessels.

Methods: Volunteers were imaged with a 1.5-T Signa whole-body imager, with a 5-inch-diameter local receive coil. Each image consisted of 20 interleaved spiral acquisitions. Gradient echoes were acquired with TE = 40 msec, TR = 75 msec, FOV = 20 cm, 188 × 188 image matrix, and slice thickness = 5 mm (plane parallel to calcarine fissure). One image was acquired every 1.5 seconds with an in-plane resolution of 1.06 mm. The efficiency of spiral k-space readouts allows both high temporal and spatial resolution with conventional gradients. Spiral readout images also have high immunity to brain motion artifacts, since the center of k space is acquired with each interleave. Volunteers were presented with 18 seconds of a ~10 Hz full-field flashing checkerboard pattern alternating with 18 seconds of dark field. Time-course data for each pixel were correlated with a sinusoid (period = 36 seconds).

Results: Comparison of the correlation maps with T1-weighted images shows that regions of high correlation occur both in cortical gray matter and pixels containing large veins. The pixels that corresponded to the large vessels had a larger temporal phase shift (6–14 seconds) compared with the phase of the stimulus in regions corresponding to cortical gray matter (3–7 seconds). Error in the temporal phase was ~ 1 second, for a correlation of 0.4.
Conclusion: Large veins can carry oxygenated blood that originates far from the vessel location in the imaging slice. The transit time of the oxygenated blood from the site of metabolism to where it affects image contrast manifests itself as a temporal phase lag, which can be used to discriminate the vessel.

214 • 11:06 AM
Evidence for Stimulus-correlated Motion in Functional Neuroimaging Experiments
JV Hajnal, R Myers, A Oatridge, GM Bydder, IR Young
The Robert Steiner MR Unit, Hammersmith Hospital, London, England

Purpose: To investigate the degree to which subject movements correlate with the stimulus in functional neuroimaging studies. Such stimulus-correlated motion may result in signal changes that mimic brain activity (1).
Methods: Conventional gradient-echo (TR = 150 msec, TE = 100 msec, flip angle = 65°) images of a single brain slice of normal male volunteers were repeatedly acquired during four motor and four hemifield visual activation studies. Image coregistration (2) was then used to retrospectively track the subject's change in position through the studies. This information was analyzed for its frequency content by calculating power spectra and autocorrelation function.
Results: In all eight studies performed, subject motion that correlated with the stimulus cycle was detected. In three of four visual stimulus studies and two of four motor studies, these power spectra showed peaks at the stimulus cycle frequency that were larger than any other peaks. Peaks were seen at harmonics two and four of the stimulation frequency on at least one axis on all visual stimulation studies and at the second harmonic in three of four subjects for the motor stimulation studies. These harmonics reflect the basic structure of the four-part stimulation cycle used for the visual studies and the two-part stimulation cycle used for the motor studies.
Conclusion: Stimulus-correlated motion was found to be a routine component of the functional imaging studies performed. Such motion can result in signal changes at tissue interfaces or where there are high or low signals produced by flow effects.
1. Hajnal JV, Oatridge A, Schwieso J, Cowan FM, Young IR, Bydder GM. Cautionary remarks on the role of veins in the variability of functional imaging experiments. Book of Abstracts, SMRM 1993 p 166. 2. Woods RP, Cherry SR, Mazziota JC. J Comput Assist Tomogr 1992; 16:620–633.

215 • 11:18 AM
Functional MRI of Alternating Hyperventilation and Apnea
K Ying, DW Chakeres, P Schmalbrock
MRI Facility, Ohio State University, Columbus, OH

Purpose: The goal of this study was to evaluate if susceptibility-weighted gradient-echo images depict blood flow and oxygenation changes for altered respiration in a similar fashion as motor cortex activation and if this technique is potentially useful for brain perfusion studies.
Methods: Axial images of the motor cortex region and 2D TOF angiograms were acquired in six healthy volunteers at rest, during alternating hyperventilation (20s) and breath holding (40s) (at apnea) and during motor cortex activation (1.5-T GE Signa, 2D SPGR, TR/TE/α = 45/35/30°, 1 NEX, 1 × 2 × 5 mm voxel volume, flow compensation, head coil or bilateral dual phased array). Visual inspection, image subtraction, correlation with the task pattern, Fourier transformation, and ROI measurements were employed for data analysis.
Results: Alternating signal intensity was observed in all cortical vessels (low after hyperventilation and high after breath holding). The signal intensity in the superior sagittal sinus altered with opposite phase. No correlated signal changes were observed for brain tissue. Motor activation led to typical alternating signal intensity in the motor area.
Conclusion: Physiologic respiratory variations (apnea) induce transient hypercapnia and secondary universal increase in blood flow and vessel signal intensity. This demonstrates rapid autoregulation of cerebral blood flow. The opposite phase of the superior sagittal sinus signal intensity may reflect deoxyhemoglobin. The lack of overall brain signal changes suggests that this technique is not applicable for perfusion studies. However, it emphasizes important differences between physiologic changes induced by respiratory variations and changes due to neural activation.

216 • 11:30 AM
Functional MR Imaging at 1.5 T: Findings in Schizophrenic Patients Receiving Neuroleptic Medication
F Wenz, MV Knopp, LR Schad, KT Baudendistel, J Schröder, F Flömer, G Van Kaick
Department of Radiology, German Cancer Research Center, Heidelberg, Germany

Purpose: Measurement and quantification of cerebral activation patterns during motor task performance in schizophrenic patients receiving neuroleptic medication.
Methods: A modified FLASH sequence (first order flow rephased, fat suppression, reduced bandwidth, 120 repetitions) on a standard 1.5-T imager was used to study 10 schizophrenic patients receiving clozapine and 10 healthy volunteers. All subjects were right-handed. Quantification was performed by using a grid overlay on statistical parametric maps based on the Student *t* test.
Results: Global quantification revealed significantly ($P \leq .003$) lower mean *t* values in patients. Selective evaluation demonstrated an increased mean *t* value during left hand movement in volunteers. In patients, a decreased mean *t* value and a reduced ipsilateral coactivation in the dominant left hemisphere was found.
Conclusion: We conclude that the detection of a drug-induced global reduction in cortical activation in these patients is possible by using functional MRI. Differences in right and left hemispheric balance may be caused by a disturbed interhemispheric interaction in schizophrenic patients.

Tuesday Morning • Miro Room
Papers 221–228

IMAGE QUALITY: Motion and Artifacts
MODERATORS: JA Sorenson, PhD
ML Wood, PhD

221 • 10:30 AM
Motion Artifacts in Fast Spin-Echo Imaging
B Madore, RM Henkelman
Sunnybrook Health Science Center, North York, Ontario, Canada

Purpose: Motion artifacts in fast spin-echo (FSE) imaging usually appear less structured than the usual ghost pattern seen in spin echo. The purpose of this work is to provide a good understanding of the structure of these "strange looking" artifacts and to communicate the mathematical expression for the point spread function (PSF) of a moving point imaged with the FSE technique. This information should help eliminate or at least reduce the intensity of these artifacts.
Methods: First, the equation for the phase of the signal in FSE acquisitions from a moving point was derived, and a simulated k space was calculated with a Sun Sparcstation. Then, a 1.5-mm-diameter sphere of 0.23 mM $MnCl_2$ solution (T2 = 70 msec, and T1 = 500 msec) was imaged by using a

transmit-receive coil with a diameter of 7 mm. The sample and the coil were moved inside a 1.5-T General Electric imager by a stepping motor that approximates harmonic motion.
Results: Comparison between the simulated and the experimental images showed excellent agreement.
Conclusion: The PSF of a moving point in FSE is calculable and corresponds to experimental results. Sometimes the result is simply a band pattern, but two different band patterns may convolve together to yield an apparently complicated and rich structure.

222 • 10:42 AM
Real-Time Reduction of Motion Artifacts in Spiral MRI by Using Navigators
TS Sachs, CH Meyer, BS Hu, DG Nishimura, A Macovski
Stanford University, Stanford, CA
Purpose: Our previous studies have demonstrated the feasibility of detecting the presence of corruptive motion in real time during a scan, and accepting or rejecting a data line based on that detection. We now apply this technique to a spiral sequence. Success in this sequence allows abdominal and cardiac imaging with reduced motion artifacts.
Methods: A sequence was designed that traverses k space through a series of interleaved spirals. After each interleaf, a one-dimensional navigator echo is acquired. Before the next spiral acquisition, this navigator is tested against a reference navigator for motion. A motion threshold is set based on the index of the peak of the cross correlation of the two navigators. If the motion falls below the threshold, the next interleaf is acquired during the next acquisition. If it is above the threshold, the same interleaf is reacquired.
Results: Preliminary experiments have demonstrated clear reduction of motion artifacts by using this acceptance/rejection algorithm. Through-plane or in-plane motion can be detected by using one navigator, or both by using two navigators.
Conclusion: Real-time motion detection, and subsequent acceptance or rejection of data, has been demonstrated to be a viable way of reducing motion artifacts in MRI. Specifically, it can be used in conjunction with a spiral sequence to yield images of the abdomen and heart (including coronary arteries) that have reduced motion artifacts.

223 • 10:54 AM
Clinical Trial of Adaptive Correction of Motion in Shoulder MR Imaging
JZW Fu, DJ Burkart, JP Felmlee, RC Grimm, RL Ehman
MRI Research Laboratory, Mayo Clinic, Rochester, MN
Purpose: High-resolution T2-weighted MR imaging of the shoulder is motion sensitive. The purpose of this work was to develop an adaptive motion correction technique clinically suitable for reducing motion blurring (caused predominantly by respiratory movements) in shoulder MRI examinations.
Methods: A T2-weighted spin-echo pulse sequence with an interleaved navigator echo for imaging of the shoulder was generated. The navigator echo was used to monitor motion along the superior/inferior direction. A least-squares difference algorithm was used to process the navigator echo data to extract a record of motion. Errors in individual slice motion measurements were minimized by correlating the motion seen in all the acquired slices. The measured displacements were used to adaptively correct the image echo data during image reconstruction.
Results: Review of the navigator echo data from 20 patients (acquired with a 16-cm FOV) revealed that 8 examinations showed significant displacements (1–3 mm) with corresponding degraded image quality. By utilizing the technique described above, all of the blurred images were substantially improved. Further improvement in the sharpness of the image was obtained by using additional techniques, including subtraction of the projection of the static part of an image from the navigator echo data.
Conclusion: In our 20-patient clinical trial, 40% of the shoulder MR images contained significant motion, and these degraded images were substantially improved by the adaptive motion correction technique.

224 • 11:06 AM
Comparison of Two Breath-Hold Feedback Techniques for Reproducible Breath Holds in MRI
YL Liu, PJ Rossman, RC Grimm, JP Debbins, RL Ehman, SJ Riederer
MRI Research Laboratory, Mayo Clinic, Rochester, MN
Purpose: Breath-hold acquisition has been effectively used in many applications, but performance could often be improved if the acquisition were extended over several breath holds. The purpose of this work was to compare two techniques for providing reproducible breath holding.
Methods: Both techniques indicate to the patients their instantaneous respiratory position, and enable MRI data acquisition to be initiated once the desired position is attained. The "bellows" method displays the respiratory bellows signal to the patient before and during breath-hold image acquisition. The "navigator" method uses a 2D RF navigator acquisition to continuously monitor the superior/inferior (S/I) position of the diaphragm before each breath-hold image acquisition. For both techniques, the respiratory position is displayed to the patient by using an LED panel. The two techniques were evaluated by using the range of S/I positions of the diaphragm as the index for breath-hold reproducibility. The navigator technique was also incorporated into a multiple breath-hold 3DFT cardiac imaging pulse sequence.
Results: We have previously demonstrated that the average range of S/I diaphragm positions acquired for normal volunteers is 8.2 mm without any feedback. Here we show that the average range is reduced to 2.7 mm with the "bellows" feedback technique, and to only 1.3 mm with the navigator technique. There is no chest wall misregistration ghost in a multiple breath-hold 3DFT cardiac acquisition.
Conclusion: The reproducibility of breath holding is significantly improved when feedback techniques are used. The navigator feedback gives the highest reproducibility, while the bellows feedback might be more readily implemented.

225 • 11:18 AM
MR Imaging of Moving Objects with Segmented Cine Sequences
PA Hardy, A Lingamneni, RD White
Department of Radiology, Cleveland Clinic Foundation, Cleveland, OH
Purpose: To assess the image degradation when imaging moving objects by using segmented cine acquisition.
Methods: Images of a rotating phantom were made with segmented cine sequences by using five different numbers of lines per segment (ie, 1, 3, 5, 7, and 9) and two different matrix sizes of 256 × 128 and 256 × 256. The degree of blurring that resulted from segmented acquisition was assessed by imaging sharp SPAMM lines. The phantom used rotated at a constant speed with a maximum tangential velocity typical of cardiac contraction. Short-axis images of the heart of volunteers were also acquired by using the same sequences.
Results: Blurring of the SPAMM lines was assessed qualitatively on the moving phantom as well as on the human images. Blurring was only present when the SPAMM lines moved in the phase-encode direction, and the blurring increased with the number of lines per segment and the tangential velocity. In the case of images made with 9 lines per segment, the apparent width of the SPAMM lines doubled. The blurring diminished with increasing matrix size. The observations from the phantom experiments were confirmed with human studies. A decrease in the image acquisition time to less than 20 seconds permitted the volunteers to hold their breath during the acquisition. Images acquired in breath hold had superior edge definition even when acquired with large segmentation factors.
Conclusion: Imaging of moving objects with segmented sequences results in blurring of sharp edges (eg, blood-myocardium) because of acquiring different parts of k space with the object in different positions. Segmented acquisition de-

creases imaging time and the available number of phases of cine images.

226 • 11:30 AM

Correction for Planar Rigid-Body Movements during MRI

ML Wood, PL Stanchev, MJ Shivji
Department of Imaging Research, University of Toronto, Sunnybrook Health Science Centre, Toronto, Ontario, Canada

Purpose: We demonstrate a method of correcting MR images for rigid-body motion in the imaging plane.
Methods: Two sets of k-space data are acquired by using a pulse sequence that interchanges the phase-encoding and frequency-encoding directions. These data provide 1D projections onto both directions of the imaging plane, from which displacements are estimated. Translation alters the center of 1D projections, while rotation alters their width and shape. The k-space data are phase shifted to correct for translation. Data to be corrected similarly for rotation are copied to an empty array the same size as k space. This array is given Hermitian symmetry by synthesizing the opposite half of k space and adding it to the array. The data are transformed to the spatial domain, rotated, transformed back to k space, and then added to a new array. After all of the data have been rotated as desired, a complementary step is to replace corrupted data with any corresponding uncorrupted data from the other side of k space. Finally, the two sets of corrected data are combined and then reconstructed into an image.
Results: It was possible to measure the width of 1D projections for every k_y. The correction reduced the ghosts and blurring in a transverse image of a patient nodding his head in the transverse plane.
Conclusion: Rigid-body movements of certain structures can be detected from k-space MR data, which then can be corrected to reduce the associated ghosts and blurring.

227 • 11:42 AM

Nonsusceptibility Effects of Metallic Implants in MR Imaging

CR Camacho, RM Henkelman, DB Plewes
University of Toronto, North York, Ontario, Canada

Purpose: Local artifacts produced by nonferromagnetic metal implants degrade MR image quality. In this study, we investigated and proposed corrections for artifacts resulting from RF-induced eddy currents in the metal.
Methods: A circular copper wire loop was used to provide a simple eddy-current pathway with minimal susceptibility effects. The loop was placed in an $MnCl_2$ solution and imaged by using various clinical pulse sequences in a 1.5-T imager with both linearly and circularly polarized RF coils. A change in the orientation and location of the copper loop allowed independent investigation of eddy currents induced by either RF pulses or field gradients. The effects of RF eddy currents on the transmit/receive sensitivity of the RF coil were quantified by analyzing the variation in MR signal as a function of transmit gain to the RF coil. These effects were also simulated numerically for both RF polarizations.
Results: We observed no artifacts due to field gradients. However, RF-induced eddy currents produced substantial artifacts in the vicinity of the loop. These artifacts were shown to be caused by the spatial variation of the transmit/receive sensitivity of the RF coil that resulted from the RF eddy currents. Simulations of this variation agreed with experimentally obtained values, which confirmed our understanding of its cause.
Conclusion: This study explains the basis of RF eddy-current artifacts that exist whenever good conductors are imaged. An understanding of this basis suggests several methods for artifact minimization. For example, GRE sequences are less sensitive than spin-echo to RF transmit nonuniformity and show reduced artifacts.

228 • 11:54 AM

Excitation of a 1-mm-Diameter Beam with Response Modulated Excitation

TJ Wieczorek, JD Pearlman
Beth Israel Hospital, Boston, MA

Purpose: To confine magnetic excitation to a 1-mm-diameter beam deep inside a target.
Methods: A response modulated excitation (RME) algorithm was implemented to calculate an RF pulse and gradient trajectory designed to excite a beam of magnetization with a diameter of 1 mm and an axial length of 5 mm. A square beam cross section was prescribed to maximize the sharpness of the cutoff between the beam and the background. The RME algorithm was fine-tuned with an FFT-based simulation of magnetization excited by the prescribed RF and gradient waveforms. An analog filter was used to minimize stray excitation in one direction perpendicular to the beam. Experiments were performed in a water phantom with a Siemens 1.5-T EPI scanner using a blipped EPI excitation with an excitation time of 8 msec.
Results: A 1-mm beam was obtained with signal dropoff to less than 12% of the peak height over a distance of 1 mm in either of two directions perpendicular to the beam axis. Mean signal magnitude outside the beam in a 65-mm square was .00151, with a standard deviation of .00628, compared with a normalized magnitude of 1 inside the beam.
Conclusions: Magnetization may be confined so that MR signal is obtained from a precisely localized region deep within an excitation target. Confinement of magnetization to narrow beams opens up the possibility for precise M-mode imaging of valve motion in the human heart, small field-of-view imaging without aliasing, and magnetic "tagging" of small moving structures.

Tuesday Morning • Morrocco Room
Papers 231–237

SPECTROSCOPY II: Brain

MODERATORS: F Arias-Mendoza, MD, PhD
IR Young, PhD

231 • 10:30 AM

Measurement of Metabolite Concentrations and T2 in Brain with Proton MRS: Increased Choline T2 of Meningiomas

M Lowry, DJ Manton, SJ Blackband, A Horsman
Centre for MRI, Hull Royal Infirmary, Hull, England

Purpose: To obtain estimates for T1, T2, and concentrations of choline, creatine, and N-acetylaspartate (NAA) in normal brain and meningiomas.
Methods: Thirty volunteers and 8 patients were examined with a GE 1.5-T Signa. Voxels (8 mL) were placed in white matter, gray matter, cerebellum, and meningioma. Spectra were acquired by using STEAM with a TR of 0.8–10 seconds and TE of 30–272 msec. Water reference spectra were also acquired for each TE. Concentrations were calculated by using the method of Barker et al (1).
Results: Compared with white matter, meningiomas were characterized by the absence of NAA, increased choline/creatine area ratio (5.6 ± 3.2 vs 1.3 ± 0.2, mean ± SD), and the presence of alanine in spectra acquired at TE = 272 msec. Values of T2 for choline, creatine, and NAA in white matter were 223 msec ± 96, 154 msec ± 30, and 447 msec ± 114, respectively. The T2 of NAA was significantly less in gray matter (320 msec ± 52, $P < .05$) and cerebellum (335 msec ± 75, $P < .05$), while choline T2 of meningiomas (381 msec ± 66) was greater than that in any region of normal brain ($P < .05$). Calculated white matter metabolite concentrations were 3.3 μmol/g ± 0.7, 13.2 μmol/g ± 1.9, and 13.4 μmol/g ± 1.4 fresh weight for choline, creatine, and NAA, respectively. Choline and creatine concentrations in meningiomas were 4.5 μmol/g ± 1.1 and 9.4 μmol/g ± 2.7, respectively.

Conclusion: The high choline/creatine peak area ratio seen in meningioma spectra is mainly due to a longer choline T2. This difference in T2 may reflect alterations in the relative proportions of choline compounds. The data indicate that individual measurements of relaxation parameters are important for long echo spectra and may reveal important metabolic information.

1. Barker, P.B. et al (1993). NMR Biomed. 6:89–94.

232 • 10:42 AM

Use of Proton MR Spectroscopy in the Follow-up of Patients with Primary Brain Tumors

MM Mengeot, D Elias, TK Helenowski, K Cramer, JE Leestma, J Moskal, G Rosseau, LJ Cerullo, M Mikhael
Chicago Institute of NeuroSurgery and NeuroResearch, Chicago, IL

Purpose: To evaluate the usefulness of proton MR spectroscopy (MRS) in following the response of astrocytomas in patients who have undergone radiosurgery with a Leksell Gamma unit.
Methods: Fifty patients with histologically diagnosed astrocytomas grade 2–4 were examined with single voxel proton MRS on a 1.5-T Siemens Magnetom. Fifteen patients underwent serial studies. We use an SE-PRESS sequence with TE of 135 msec. Calibration with an instrumental factor allows quantitative comparison of the spectra. We also present our initial results with two-dimensional chemical shift imaging.
Results: Plots of concentrations or metabolite ratios show wide ranges. Also, voxels in different parts of large tumors exhibit very different spectra. Tumor heterogeneity is a major obstacle, and the heterogeneity revealed with MRS does not closely match that shown on images. Enhancing rim areas usually display marked reduction in N-acetylaspartate (NAA) and creatine (Cr) and an increase in choline (Cho) by up to a factor of three; nonenhancing central regions sometimes show no measurable signal from the three major metabolites, while lactate (Lac) is present; after treatment, peaks often appear in the lipid region at 0.9 and 1.3 ppm.
Conclusion: "Extreme" cases appear to allow clinical correlation: a pattern of elevated Cho (higher than twice the norm), reduced Cr, and very reduced NAA is compatible with viable tumor; low levels of all three metabolites is compatible with some form of necrosis or radiation changes (however, an increase in metabolite levels after irradiation occurs in the nonenhancing core of some tumors); a continued decrease in all metabolite levels after treatment correlates with tumor control. To evaluate spectra with intermediate metabolite levels, we are attempting to utilize (*a*) volumetry of the imaging compartments (normal, enhancing, nonenhancing core, edema, etc); (*b*) regular serial studies; and (*c*) timing of the postradiation decrease in Cho and increase in lipid peaks.

233 • 10:54 AM

Brain [Mg^{2+}] in Cancer Cachexia

F Arias-Mendoza, T Greenberg, R Stoyanova, F Ottery, T Brown
NMR Department, Fox Chase Cancer Center, Philadelphia, PA

Purpose: To use the magnesium-sensitive chemical shift of the β-nucleotide triphosphate (β-NTP) in ^{31}P MRS to measure localized [Mg^{2+}] with three-dimensional chemical shift imaging (3D-CSI) in the brain of cachectic patients and to examine the effect of nutritional repletion on brain [Mg^{2+}].
Methods: ^{1}H decoupled ^{31}P 3D-CSI spectra from the brain of 7 healthy volunteers and 13 cachectic patients were acquired with a spectrometer at 1.5 T. The β-NTP position was measured by referencing its chemical shift to that of the phosphocreatine resonance in each brain spectrum. [Mg^{2+}] was then calculated by using the Henderson-Hasselbach equation.
Results: Eight of 10 cachectic patients before nutritional repletion were found to have abnormally high levels of brain [Mg^{2+}] (0.18 mM ± 0.07 vs. 0.12 mM ± 0.04, $P < .036$). Two patients who had normal levels of brain [Mg^{2+}] had in common an obstruction of the gastrointestinal (GI) tract. Three of 4 patients observed during replenishment had high brain [Mg^{2+}] levels, while the 3 fully repleted patients showed normal levels.
Conclusion: One possible explanation for the high brain [Mg^{2+}] in cachectic patients before repletion is that [Mg^{2+}] extrusion from the brain may be impaired because of a lack of energy to transport it out of the cell. This process is presumably restored after repletion, since brain [Mg^{2+}] levels then return to normal. However, it is important to determine why some patients have normal levels before replenishment. The finding of GI obstruction in cachectic patients with normal [Mg^{2+}] is interesting, but it requires more observations before any explanation can be provided. In any case, [Mg^{2+}] levels may provide a quantitative method of determining successful nutritional replenishment.

234 • 11:06 AM

Single-Volume H-1 Spectroscopy as an Index of Neural Degeneration in Alzheimer Disease

JP Kesslak, D Atkinson, D Drost, J Bowler, M Brant-Zawadzki, R Sauter
I.R.U. in Brain Aging, Biological Sciences II, University of California, Irvine, CA

Purpose: Alzheimer disease (AD) is characterized by progressive neural degeneration that clinically produces a variety of behavioral deficits. Hydrogen-1 MR spectroscopy (MRS) provides a novel means of detecting biochemical changes in AD brain pathology in vivo. This study examined the relative amounts of N-acetylaspartate (NAA) as an index of neural density, and the metabolites creatine (Cr) and choline (Cho) as neural and nonneural components.
Methods: Thirty AD patients (70 ± 9 years of age) with diagnosis according to NINCDS-ADRDA guidelines were compared with 10 age-matched controls (64 ± 9 years of age). MRS (SE 135, TR 1,600) was done within 4 weeks of clinical evaluations on a 1.5-T Siemens Magnetom 63/84 SP system and head coil. Placement of a 2 × 2 × 2 cm volume of interest in the parietal and temporal cortices was done with coronal, sagittal, and axial images. Peak areas for NAA, Cho, and Cr were integrated and ratios calculated.
Results: Analysis of the ratios for NAA, Cr, and Cho indicated that in the parietal lobe the AD group had lower levels of NAA/Cr, a trend toward decreased levels of NAA/Cho and no difference in Cho/Cr. A similar but nonsignificant trend for NAA/Cr was observed in the temporal lobe. There did not appear to be any age-related differences in this small sample of normal controls; however, it should be noted that variability did increase with age. Automated time-of-flight spectra analysis from one test site indicated a larger significant difference between groups compared with the manual integral analysis. Analysis of the distribution of gray and white matter in the VOI indicated a higher correlation for NAA/Cr and NAA/Cho levels in control subjects compared with the AD group.
Conclusion: These results may indicate that a decrease in NAA levels relative to Cr and Cho may be consistent with the cell-loss characteristic of AD pathogenesis. This is further supported by the observation of lower correlation with NAA ratios in the gray and white matter of AD patients compared with controls.
D. Atkinson is an employee of Siemens Medical Systems.

235 • 11:18 AM

H-1 MRS in Patients with Metastatic Brain Tumors: Multicenter Study

MV Knopp, AE Stillman, PE Sijens, A Brunetti, JA Sanders, H Kett, R Sauter
Department of Radiology, German Cancer Research Center, Heidelberg, Germany

Purpose: To evaluate in a multicenter trial (6 participation sites) the clinical applicability of single-volume proton MR spectroscopy and its utility (*a*) to study metastatic brain tumors, (*b*) to quantitate the metabolite levels, and (*c*) to determine variation and agreement of proton MRS data obtained in different MR centers using the same technique.
Methods: Single-volume proton MR spectroscopy was performed by using a double spin-echo localization sequence on

Siemens Magnetom SP systems (Erlangen, Germany) with a voxel size of 2 × 2 × 2 (or 1.5 × 1.5 × 1.5) cm. The voxel was placed so that the metastasis covered at least 50% of the volume. Reference voxels were placed in the contralateral occipital lobe or in the contralateral site. Follow-up studies were obtained if clinically feasible. Standard MR imaging results as well as patient history were sent to the coordinating site for reference. Metabolite levels were quantified by each individual site by using a manual technique and in a central site by Marquardt fit and Wigner distribution fit.

Results: Eighty-five patients were included in this multicenter trial within a 6-month period. The histologic findings of the metastatic lesions included a large variety, with the largest groups being 31 lung cancers, 17 melanomas, and 16 breast cancers. About two-thirds of the examinations were performed with the 8 cm^3 and one-third with the 3.375 cm^3 voxel size. Subgroup specific data analysis is currently being performed.

Conclusion: The trial has shown that compatible results can be obtained when applying a standardized single-volume proton spectroscopy sequence at different MR sites. Furthermore, excellent agreement was observed between the quantification at each individual site and a central site, as well as between the different techniques. The data will facilitate further detailed studies of specific histologic entities and the use of this technique to noninvasively monitor therapy response.

236 • 11:30 AM

Single-Voxel Spectroscopy of the Cerebellum: Baseline Study in Normal Volunteers

SJ Gibbs, WR Riddle, MR Willcott
Department of Radiology, Vanderbilt University Medical Center, Nashville, TN

Purpose: Application of single-voxel proton MR spectroscopy (SVS) to the study of human disease requires baseline data from normal volunteers. We present here such data for the cerebellum, which we have been unable to find in the published literature.

Methods: SVS was performed by using a double spin-echo technique, TE = 135 msec, 2 × 2 × 2 cm voxel, with 256 acquisitions at TR = 1.5 seconds, and data collected as 1,024 complex pairs in 1.024 seconds, with a Siemens Magnetom SP. Magnetic field homogeneity was optimized within the volume of interest. Time-domain data were subjected to eddy-current correction, zero-filled to 2,048 points, and treated with a 2 Hz Gaussian line-broadening filter. After Fourier transform, spectra were phased manually, and an independent cubic spline baseline correction was applied. All post-processing used software supplied by the magnet manufacturer. Peak intensities were determined by means of the integrated area.

Results: Peak ratios were determined for the methyl singlet resonances, with N-acetylaspartate (NAA) as the reference, for choline (Cho:NAA) and creatine (Cr:NAA). The Cho:NAA ratio was 0.65 ± 0.1 and Cr:NAA was 0.72 ± 0.1. Variance was primarily the result of variation between subjects. Reproducibility between repeated measurements of a single subject was generally better than 5%.

Conclusion: These values characterize the cerebellum for the technique employed. These values differ significantly from those for other parts of the brain, as reported by other investigators.

237 • 11:42 AM

Localized H-1 MR spectroscopy for Noninvasive Differentiation of Cerebral Tumors

TJ Vogl, O Söuner, R Felix
Department of Radiology, Free University of Berlin, Berlin, Germany

Purpose: To analyze the correlation between H-1 spectroscopy, CT imaging, MR imaging, histology, and in vitro MRS of the tumor tissue for evaluation of the vascularization and metabolic state of metastasis and gliomas.

Methods: Fifty-seven patients (32 men and 25 women) with different cerebral tumors were examined. Histology was obtained in all patients except two. The tumors included meningiomas (n = 18), gliomas grade I–II (n = 14), gliomas grade III and anaplastic astrocytomas (n = 5), gliomas grade IV (n = 14), and metastasis (n = 6). The MR and MR spectroscopy (MRS) examinations were performed on a whole-body 1.5-T Magnetom (Siemens, Erlangen, Germany) with a circular polarized head coil. A volume of interest (VOI) varying in size from 8 to 16 cm^3 was positioned. ^1H MRS was performed by using spin-echo (SE) sequences (TE, 135 and 270 msec) and stimulated echo (STEAM) sequences (TE, 20 msec) with water selective presaturation. The detected metabolites of the proton spectra of 30 volunteers and 57 patients were Ins at 3.56 ppm, Cho at 3.22 ppm, Cr at 3.03 ppm, NAA at 2.02 ppm, Ala at 1.47 ppm, and Lac at 1.31 ppm.

Results: In comparison with the spectra of healthy control subjects, the ^1H spectra of gliomas demonstrated some common features including the reduction of the NAA/Cho ratio and the Cr/Cho ratio. The Ins/Cho ratio increased with the grade of malignancy of gliomas. The spectra of all metastatic tumors contained reduced Cr signals and NAA resonances but exhibited strong contributions from cholin-containing compounds and from mobile free fatty acids. ^1H MR spectra of all meningiomas were mainly characterized by a reduction of the Cr/Cho ratio, missing NAA signal, and an increased Ala resonance signal. The evaluation of in vitro MRS demonstrated an increase of glutamate and free fatty acids, which influence the NAA signal. These metabolites were higher in high-grade gliomas with large necrotic areas, as opposed to low-grade gliomas with small or no necrosis.

Conclusion: The results of this study confirm that all tumor spectra are remarkably different from those of normal brain tissue. The malignancy of gliomas can be assessed with the Cr/Cho and Ins/Cho ratios. The diagnostic quality of the NAA signal in evaluation of malignancy is limited according to the results of in vitro MRS. However, localized ^1H MRS is a valuable aid in the differential diagnosis of human brain tumors in combination with MRI.

Tuesday Morning • Sapphire Room
Papers 241–247

UPPER ABDOMEN II: Hepatic, Contrast

MODERATORS: PL Choyke, MD
RJ Herfkens, MD

241 • 10:30 AM

MR Imaging with and Elimination of Gd-EOB-DTPA in Transport-Deficient Mutant Rats: Experimental Study of a Condition Resembling the Human Dubin-Johnson Syndrome

A Mühler, RPJ Oude Elferink, HJ Weinmann
Contrast Media Research, Schering AG, Berlin, Germany

Purpose: Gd-EOB-DTPA is a hepatobiliary MR contrast agent with dual elimination by the kidneys and by the liver. Mutant Wistar rats (transport-deficient rats) are known for their deficiency of the canalicular transport system of the liver, which is used by Gd-EOB-DTPA for biliary secretion. This study was designed to investigate whether Gd-EOB-DTPA can be completely eliminated in transport-deficient rats despite absence of the biliary elimination route, and to show the MR imaging characteristics of Gd-EOB-DTPA in these mutant rats.

Methods: Biliary excretion rates of 0.05 mmol/kg Gd-EOB-DTPA were determined in transport-deficient rats (n = 3) and in control rats (n = 3). The whole-body retention of the contrast agent was investigated 1 day and 7 days after administration of the dose of 0.25 mmol/kg (n = 3 transport-deficient rats, n = 3 control rats). Gadolinium concentrations of bile, liver, kidneys, and carcass were measured by ICP-AES (λ = 342.247 nm). MR imaging was performed at 2 T by using a T1-weighted SE sequence (250/15/4, 256 × 256). Images were acquired before and after injection of 0.025 mmol/kg Gd-EOB-DTPA.

Results: In transport-deficient rats, only insignificant biliary

excretion was shown to occur (2.4% ± 0.4). However, body gadolinium retention was less than 2% at 1 day and less than 0.7% at 7 days after intravenous injection. By comparison, in control rats the majority of the Gd-EOB-DTPA was eliminated via the biliary route (80.3% ± 3.9), and body containment of the contrast agent was comparable to that in mutant rats. During MR imaging, strong initial liver enhancement was observed in both rat strains after injection of Gd-EOB-DTPA. Liver signal intensities returned to preinjection values in 6 hours (control rats) or within 24 hours (mutant rats).
Conclusion: The hepatobiliary MR contrast agent Gd-EOB-DTPA is completely removed from the body even in the case of severely impaired biliary secretion. The remaining urinary elimination pathway can fully compensate for the hepatic dysfunction. The uptake of Gd-EOB-DTPA into the liver cells of transport-deficient rats was shown to be unaffected despite congenital hyperbilirubinemia.
A. Mühler, R.P.J. Oude Elferink, and H.J. Weinmann are employees of Schering AG.

242 • 10:42 AM

Enhancement in Primary Liver Tumors with the Superparamagnetic MRI Contrast Agent AMI-25: In Vivo–in Vitro Correlation

TJ Vogl, R Hammerstingl, C Bergman, W Pegios, J Hölzl, B Wössmer, R Felix
Department of Radiology, Free University of Berlin, Berlin, Germany

Purpose: In a phase III trial, the specific contrast enhancement of primary and secondary liver tumors, especially FNH versus adenoma and HCC, with the superparamagnetic iron oxide AMI-25 was evaluated.
Methods: Eighteen patients were prospectively investigated using T2- (TR/TE = 2,000/90) and T1-weighted (550/15) spin-echo (SE), FLASH 2D gradient-echo (GRE), and fat-suppressed (fatsat) sequences before and after administration of AMI-25 (concentration: 0.2 mmol Fe/mL, dose: 15 μmol/kg bw). Six patients underwent in vivo–in vitro correlation 30 minutes after sequential or lobar resection with use of a special probe coil.
Results: Primary liver tumors were histopathologically proved in 10 patients with FNH (n = 6), HCC (n = 3), and adenoma (n = 1), as were secondary liver tumors such as metastases from colorectal carcinoma (n = 6) and endocrine tumors (n = 2). Contrast-enhanced studies allowed detection of more lesions in 3 of 10 patients with primary and 4 of 8 patients with secondary liver tumors. Primary tumors showed significant negative enhancement (FNH, −44.8%; HCC, −8.5%; adenoma, −37.1%) on proton-density-weighted SE images and could be differentiated from secondary tumors, which showed only minimal enhancement (colorectal, 8.4%; endocrine metastases, −6.2%). In 6 patients with 9 lesions of FNH, a capsule was seen in 11% plain and 33% enhanced, enhancement of the capsule in 1 case of 9, scar tissue in 22% plain, 56% enhanced, and enhancement in 2 cases, whereas in patients with HCC a capsule was seen in only 1 case enhanced, and no scars were seen. In the patient with adenoma, a capsule with contrast enhancement was seen, but no scar was detected. In vitro examinations in FNH (n = 2), adenoma (n = 1), and metastases (n = 3) enabled detection of a larger number of lesions versus the in vivo studies.
Conclusion: The use of the superparamagnetic iron oxide AMI-25 allows differentiation of primary and secondary liver tumors on the basis of contrast enhancement. FNH can be differentiated versus HCC and adenoma by using contrast-enhanced sequences. The existence and specific enhancement of capsule or scar enables detection of a more focal lesion after administration of AMI-25. The preliminary results of in vivo–in vitro correlation demonstrate some limitations of in vivo liver MRI.

243 • 10:54 AM

MR Imaging of Liver Metastatic Disease: Efficacy and Technique as Evaluated in an Experimental Model

VM Runge, JE Kirsch, JW Wells, JN Dunworth, CE Woolfolk
University of Kentucky, Lexington, KY

Purpose: The detectability of liver metastases was evaluated in a rabbit model, with attention to MR pulse technique and contrast medium dose.
Methods: Seven New Zealand white rabbits were studied at 1.5 T 2 weeks after implantation of multiple 2-mm^3 tumor nidi (adenocarcinoma). T1, fat-saturated T1, T2, breath-hold fast T2, breath-hold T1 spin-echo, and breath-hold T1 TurboFLASH images were obtained before administration of contrast medium. After bolus IV contrast injection (gadoteridol), breath-hold T1 images were acquired dynamically at 1-minute intervals, for a duration of 5 minutes. Non-breath-hold T1 images were then obtained. Each animal was scanned twice, on consecutive days, comparing doses of 0.1 and 0.3 mmol/kg.
Results: Liver-lesion contrast (signal difference/noise) was 32 ± 7 (T1), 30 ± 5 (fat-saturated T1), 28 ± 8 (T2), 23 ± 5 (breath-hold fast T2), 12 ± 4 (breath-hold T1 spin-echo), and 16 ± 3 (breath-hold T1 TurboFLASH) before injection; and 17 ± 20 (T1) and 27 ± 11 (breath-hold T1 spin-echo) after injection of the 0.3 mmol/kg dose. Among postcontrast images, lesion conspicuity was greatest at 1 minute. Liver-lesion contrast was not improved statistically by using the 0.1 mmol/kg dose.
Conclusion: Lesion detectability, as evaluated with SD/N measurement, is lower on breath-hold images (T1 or T2), whether acquired before or after injection of contrast medium, when employing a dose of 0.1 mmol/kg. High-dose (0.3 mmol/kg) breath-hold imaging, however, demonstrates equivalent efficacy to that of non-breath-hold precontrast T1 and T2 imaging.

244 • 11:06 AM

Comparison of MR, CT, and Angiography for the Assessment of Hepatocellular Carcinoma Treated with Transcatheter Arterial Emolization

JP Goldman, JC Weinreb, NM Rofsky, A Goldenberg, A Megibow, R Rosen
Department of Radiology–MRI, New York University Medical Center, New York, NY

Purpose: To compare CT, MR, and angiography for the assessment of hepatocellular carcinoma treated with transcatheter arterial embolization (TAE).
Methods: Fifteen patients underwent MRI, CT, and angiography before and one or more times after TAE (total, 35 MRI/CT/angiograms). MRI consisted of (*a*) T1-weighted breath-hold FLASH (TR = 160, FA = 70, TE = 4) preinjection and dynamic (5 time points) postinjection (gadolinium) sequences, and (*b*) T2-weighted TSE (TR = 3,500–5,000, TE = 120) with and without fat suppression. In many cases, postprocessed images were obtained by subtracting preinjection data from postinjection data. CT was performed with and without intravenous contrast medium. TAE was performed with a combination of adriamycin and ethiodized oil emulsion. The studies were evaluated retrospectively for lesion detection, assessment of viable (ie, vascularized) tumor, and depiction of ethiodized oil emulsion. Phantom studies of varying concentrations of adriamycin/ethiodized oil were correlated with the MR findings.
Results: MRI depicted hepatomas (especially very small ones) better than did CT or angiography. CT depicted areas of ethiodized oil depostion, but the very high attenuation on CT scans did not correlate with areas of tumor death and obscured areas of viable tumor demonstrated with MRI and angiography. Although the ethiodized oil demonstrated high signal intensity on T1- and T2-weighted images of phantoms, it did not appreciably affect tumor signal intensity in vivo. Areas of tumor necrosis were best demonstrated with MRI. Dynamic postcontrast images more clearly defined viable tumor than did individual postcontrast images. The subtracted im-

ages improved depiction of areas of necrosis and viable tumor.
Conclusion: Contrast-enhanced MRI is better than CT for the pre- and posttreatment assessment of hepatocellular carcinomas treated with TAE.

245 • 11:18 AM
Comparison of Fat-Suppression Techniques for Hepatic MR Imaging: Turbo-SE, Breath-Hold Turbo-SE, GRASE, and Turbo STIR
NM Rofsky, JC Weinreb, J Safir, C Mercado, JP Goldman, AJ Megibow
Department of Radiology–MRI, New York University Medical Center, New York, NY
Purpose: Fat-suppression techniques have been reported to result in improved contrast and to facilitate the detection of hepatic lesions. This study was performed to compare different rapid fat-suppressed T2-weighted MR techniques for hepatic imaging.
Methods: Thirty patients referred for abdominal MRI were assessed with the following sequences: (*a*) Turbo-STIR (TR/TI/TE = 5,690/140/60; 18 slices/04:04; matrix = 154*256; NSA = 3), (*b*) fat-suppressed Turbo-SE (1-3-3-1 prepulse, TR/TE = 5,000/120; 18 slices/02:35; matrix = 150*256; NSA = 3), (*c*) fat-suppressed breath-hold Turbo-SE (1-3-3-1 prepulse, TR/TE = 2,152/120; 8 slices/00:23; matrix = 150*256; NSA = 1), and (*d*) fat-suppressed breath-hold GRASE (1-3-3-1 prepulse, 2,300/140; 8 slices/00:18; matrix = 132*256; NSA = 2). Subjective image preferences and CNR analyses were performed.
Results: The Turbo-STIR images provided the most uniform fat suppression. Lesion conspicuity was best overall with the Turbo-STIR sequence. Average values for liver-spleen CNR: (*a*) = 37.4, (*b*) = 19.7, (*c*) = 13.4, (*d*) = 17.7.
Conclusion: Each of the sequences generated high-quality images. The Turbo-STIR sequence was best for lesion detection. Breath-hold sequences minimized motion-related artifacts and occasionally depicted lesions not appreciated with the other sequences.

246 • 11:30 AM
Comparison Between In-Phase and Opposed-Phase T1-weighted Breath-Hold FLASH Sequences for Hepatic Imaging
J Safir, JC Weinreb, N Rofsky
Department of Radiology–MRI, New York University Medical Center, New York, NY
Purpose: Some users are employing opposed-phase sequences for breath-hold T1-weighted imaging of the liver, primarily because the shorter TE permits more slices (and thus better hepatic coverage) per unit time. The purpose of this study was to compare in-phase and opposed-phase sequences for contrast, liver lesion detection, and image quality for breath-hold hepatic imaging.
Methods: Non-contrast-enhanced in-phase and opposed-phase breath-hold images were obtained in 35 consecutive patients referred for abdominal MRI at 1.0 T. For both sequences, the TR (160), FA (70), matrix (128 × 256), FOV (350 mm), slice thickness (1 cm), gaps (2 mm), measurements (1), and BW (130) were kept constant. The in-phase sequence used a TE of 6 msec and provided 11 slices in 22 seconds. The opposed-phase sequence used a TE of 4 msec and provided 16 slices in 22 seconds. No presaturation pulses were employed. Images were compared quantitatively (liver/spleen and liver/lesion CNR) and qualitatively (artifacts, lesion detectability, intra- and extrahepatic anatomy).
Results: The in-phase sequence had higher CNR for liver/spleen (mean, 18.2 vs 12.5) and liver/lesion (mean, 18.1 vs 13.4) in all patient groups, especially patients with fatty infiltration. Qualitative indices also favored the in-phase sequence.
Conclusion: The results of this study demonstrate advantages for in-phase breath-hold gradient-echo imaging of the liver. A complete assessment of the liver with MR should include both in-phase and opposed-phase imaging.

247 • 11:42 AM
MRI of Benign and Malignant Hepatic Lobar Atrophy
ES Siegelman, E Outwater, DG Mitchell
Department of Radiology, Thomas Jefferson University Hospital, Philadelphia, PA
Purpose: To describe the MR findings of hepatic lobar atrophy.
Methods: The authors reviewed MR liver examinations obtained from their teaching files and from a computer search of MR imaging reports. The plane of the middle hepatic vein was located on the axial image that showed maximal liver volume. We defined lobar atrophy as a ratio of the angle subtended by the line joining the IVC and middle hepatic vein with both the right and left liver margins of <0.5 or >2. Eight patients, 4 with cholangiocarcinoma and 4 with benign etiologies, were thus identified as having lobar atrophy. MR imaging at 1.5 T included TOF, T1- and T2-weighted SE sequences. Gd-DTPA–enhanced images were obtained in 6 patients. We evaluated the signal intensity of the atrophic lobe and for the presence of an apical mass, portal vein patency, and biliary dilatation.
Results: The atrophic lobe had lower T1 and higher T2 signal intensity compared with that of the remainder of the liver for all 8 patients. Areas of increased enhancement were present in the atrophic lobes in 5 of 6 patients. Only 1 patient showed patent portal vein branches to the atrophic lobe. Biliary dilatation was present in 1 benign and 3 malignant cases. An apical mass was identified in only 1 patient, who had benign lobar atrophy.
Conclusion: Atrophic lobes have suggestive MR findings that are similar for both benign and malignant etiologies. The atrophic hepatic parenchyma demonstrates signal intensity characteristics similar to malignant hepatic lesions.

Tuesday Morning • Topaz Room
Papers 251–258

VASCULAR IMAGING
MODERATORS: M Bernstein, PhD
DN Firmin, PhD

251 • 10:30 AM
Cine Phase-Contrast MRI Assessment of Pedal Blood Flow
JF Debatin, R Dalman, RJ Herfkins, NJ Pelc, EJ Harris
MRI Center, Zurich University Hospital, Zurich, Switzerland
Purpose: The objective relationship between pedal blood flow and rest pain or ischemic ulceration has not been reliably established. We used cine phase contrast (CPC) to assess pedal blood flow in normal subjects and patients with limb-threatening ischemia before and after surgical revascularization.
Methods: The feet of 5 healthy volunteers (age range, 20–37 yrs) were imaged with a quadrature head coil in a 1.5-T MR-system (Signa) on 4 separate occasions. Oblique axial CPC images were obtained at the level of the tibiotalar joint by using a TR/TE of 25/8, 45° flip, 5-mm section, 256 × 256 matrix, 20-cm FOV, 2 NEX, of S/I flow encoding, Venc of 60 cm/sec, and 16 phases/RR interval. With use of identical imaging parameters (except Venc = 40 cm/sec), 8 patients with lower-extremity ischemic ulceration were evaluated before and after surgical revascularization (ax-bifem grafting [$n = 2$]; fem-pop/tibial grafting [$n = 6$]). Total pedal blood flow was calculated by summing flow of all visualized vessels.
Results: Intrasubject variability in arterial flow measurements was considerably lower than intersubject variability ($P < .001$), which revealed relative consistency of pedal flow measurements over time. Normal arterial flow patterns were consistently triphasic in character. CPC-measured pedal flow of chronically ischemic limbs (bilateral [$n = 2$]; unilateral [$n = 6$]) ranged from 0 to 27.3 mL/min. Waveforms were

nontriphasic due to ischemia-induced maximal vessel dilatation. Revascularization increased flow in affected limbs between 51% and 630%. In limbs not affected by surgical revascularization (n = 6), measured flow changed only minimally. ***Conclusion:*** The ability to quantitate ischemic levels of pedal blood flow and subsequent revascularization-induced increased flow promises to be useful in identifying optimal treatment options and monitoring treatment results.

252 • 10:42 AM

Segmented Traveling Saturation with Cardiac Triggering: Improved Peripheral MR Angiography

DE Purdy, OP Simonetti, JP Finn
Siemens Medical Systems, Iselin, NJ

Purpose: In 2D time-of-flight peripheral arteriography, effective elimination of venous signal mandates the use of traveling saturation pulses. However, these saturation pulses can lead to ghost artifacts and signal loss when the flow is pulsatile. The combination of a segmented acquisition with cardiac triggering optimizes the flow enhancement of the traveling saturation sequence while almost eliminating ghosting.
Methods: Measurements were performed in the legs of volunteers by using a 1.0-T imaging system with 15 mT/m gradients. A 2D RF-spoiled FLASH sequence was used with a saturation band eight times the thickness of the imaged slice and a gap of one slice thickness. Nineteen data lines were acquired within a 550-msec window centered in systole. A 228-line matrix was generated by interleaving the data from 12 heartbeats.
Results: The cardiac-triggered leg images showed more than twice the arterial blood contrast-to-noise ratio of the untriggered sequence, while virtually eliminating the ghost artifacts.
Conclusion: A substantial improvement in peripheral angiograms is obtained by restricting the data acquisition to a period of high flow in the cardiac cycle. Besides the obvious increase of inflow enhancement, an additional gain results from the recovery of signal ordinarily displaced to the multiple ghosts usually observed in leg arteriograms.
D.E. Purdy is an employee of Siemens Medical Systems.

253 • 10:54 AM

Three-dimensional Phase-Contrast MR Angiography of the Renal Arteries: Evaluation for Donor Nephrectomy

SP Meyers, SL Talagala, S Totterman, MVU Azodo, E Kwok, L Shapiro, R Shapiro, RC Pabico, GR Applegate
University of Rochester Medical Center, Rochester, NY

Purpose: The purpose of this study was to assess the capability of 3D phase contrast (PC) magnetic resonance angiography (MRA) in visualizing renal arteries in potential donors as compared with conventional arteriography (CA).
Methods: Blinded retrospective reviews of the CA and 3D PC MRA studies of 17 patients were performed by two experienced radiologists with regard to the number, length, and configuration of renal arteries. The acquired MR data were postprocessed by using maximum-intensity-projection (MIP) and surface rendering (SR) techniques.
Results: MRA clearly depicted all 34 dominant renal arteries but only 8 of 10 accessory arteries. One of the nonvisualized accessory arteries was located within the imaged volume, and the other arose from the distal aorta and beyond the imaged regions. Postprocessing with MIP and SR techniques yielded the same number of renal arteries, although SR was superior in separating overlapping veins and visualizing the renal artery origins.
Conclusion: These results suggest that 3D PC MRA is a reliable method for demonstrating dominant renal arteries, but future technical improvements will be necessary for the visualization of all accessory renal arteries.

254 • 11:06 AM

2D MRA of Renal Arteries with Segmented Breath-Hold Acquisitions

AJ Duerinckx, DJ Atkinson, A Alim, U Sinha, E Grant
Radiology Service, MRI, Veterans Affairs Medical Center, West Los Angeles, Los Angeles, CA

Purpose: To evaluate ECG-gated segmented breath-hold 2D MRA of the renal arteries.
Methods: Normal volunteers and patients with angiographically proved renal artery stenoses (50%–90%) were studied. Images were acquired on a 1.5-T imager (Magnetom SP, Siemens) with an EKG-triggered flow-compensated cine gradient-echo (2D TurboFLASH) sequence with breath holding. K-space data acquisition allowed for up to eight cardiac phases. Fat suppression was used to suppress perirenal fat and to enhance the visualization of renal arteries. MR angiograms (MRAs) were reconstructed for several phases of the cardiac cycle.
Results: All images were judged to be diagnostic. MRAs obtained at different points in the cardiac cycle demonstrated the pulsatile motion at the origin of the renal arteries. Coronal plane 2D MR images obtained with this technique were superior to 2D TOF or 3D TOF angiograms in the visualization of the renal artery origin. Clear visualization of the middle and distal renal arteries was also possible.
Conclusion: Two-dimensional MRA of renal arteries to alleviate respiratory and cardiac motion shows great promise as an accurate, noninvasive imaging method for the evaluation of renal arteries.
D.J. Atkinson is an employee of Siemens Medical Systems.

255 • 11:18 AM

MR Angiographic Evaluation of Vascular Anastomoses after Liver Transplantation

E Squillaci, F Maspes, M Crecco, Q Marignetti, G Tisone, A Orlacchio, CU Casciani, G Simonetti
Department of Radiology, University of Rome, Rome, Italy

Purpose: To assess the reliability of magnetic resonance angiography (MRA) in evaluating vascular anastomoses after liver transplantation.
Methods: Twenty consecutive adult patients were prospectively studied with MRA and presaturation pulses during workup after liver transplantation, for assessment of vascular anastomoses (portal vein, hepatic artery, and venae cavae [superior and inferior]). Coronal 2D TOF MRA was performed at 1.5 T. The ability to visualize anastomosis with MRA was evaluated as good, poor, or not visualized. Duplex ultrasound was performed in all patients for correlation.
Results: Technically satisfactory MR angiograms were obtained in all cases. Among 80 anastomoses evaluated, the visualization was considered good in 78% of cases and poor in 14% of cases. Six anastomoses (8%), all of the hepatic artery, were not visualized. One case of severe stenosis of the portal vein was correctly evaluated with MRA. Two small no-signal spots, due to surgical wire, allowed exact localization of the anastomosis. An experimental model will be presented to demonstrate this new semiological sign. There was full agreement between duplex ultrasound and MRA in assessing flow direction.
Conclusion: MRA is an extremely accurate, noninvasive, and complete means of evaluating vascular anastomoses after liver transplantation.

256 • 11:30 AM

Experimental Blood Pool Agent: Polylysine-Gd-DTPA

A Mühler, H Schmitt-Willich, H Vogler, B Radüchel, T Frenzel, HJ Weinmann
Schering AG, Berlin, Germany

Purpose: Several blood pool agents for MR imaging are currently in preclinical development. Among them, polylysine-Gd-DTPA has successfully been used in rodent models to show the specific requirements and potential applications of blood pool agents for extracranial MR imaging. The current communication summarizes those data about pharmacoki-

netics, tolerance, and imaging applications for the experimental blood pool agent polylysine-Gd-DTPA.
Methods: The blood pool agent (MW ≈ 50 kd) was synthesized by covalently binding DTPA monoanhydride to poly-L-lysine (>95% derivatization) and complexation with gadolinium. Polylysine-Gd-DTPA was characterized by relaxometry (0.47 T, 39°C), concentration-time profile in blood plasma (dose of 0.1 mmol/kg, blood sampling interval 5 minutes to 5 hours [n = 6]), acute toxicity (LD_{50}, 3 dose groups per 3 rats), and elimination from the body (dose of 0.2 mmol/kg, 7 days p.i. [n = 5]). Gadolinium concentrations were measured by ICP-AES (λ = 342.247 nm). MR angiography was performed with 2D-IR Snapshot-FLASH (2 T/TR 4.5 msec/TE 2.2 msec/TI 180 msec/flip angle 20/Nex 4/6 images per minute) after administration of 20 μmol/kg polylysine-Gd-DTPA and Gd-DTPA.
Results: The R1 relaxivities were measured to be 13.1 L/mmol*s in water and 13.9 L/mmol*s in plasma. In rats, blood half-life was 1.4 hours and the distribution volume was 0.06 L/kg, which corresponds to the blood space of the body. The LD_{50} should be in the range of 17 mmol/kg. Of the injected dose, 88.1% was excreted via the urine and 2.8% via the feces, which left 9.1% of the gadolinium remaining in the body at 7 days p.i. In extracranial MR angiography, vessel-to-background contrast after administration of the blood pool agent polylysine-Gd-DTPA was shown to be superior (6 times higher) and longer lasting (up to 15 minutes) compared with extracellular Gd-DTPA.
Conclusion: Availability of blood pool agents like polylysine-Gd-DTPA may boost the interest in perfusion imaging, MR angiography, and tumor imaging (imaging of leakiness).
A. Mühler, H. Vogler, B. Radüchel, T. Frenzel, and H.J. Weinmann are employees of Schering AG.

257 • 11:42 AM
Phase Contrast–based MR Flow Visualization by Means of Moving Artificial Particles
M Kouwenhoven, J De Becker, M Fuderer
Philips Medical Systems, Best, The Netherlands
Purpose: Phase contrast angiography (PCA) allows in vivo measurement of 3D velocity vector fields of flowing blood in a 3D volume. A convenient technique to visualize this large amount of data is crucial to give good insight into the nature of the blood flow. Most 3D PCA images are obtained without cardiac triggering, so that the acquired velocity is more or less time averaged. If PCA is combined with cardiac gating, the acquired velocity is time averaged only over the width of the gate.
Methods: Given the PCA data of the blood flow and the vessels, simulated seed particles are positioned in one or more vessels, and their trajectories inside the vessel structures are calculated according to the acquired velocity field. Projecting the positions of these particles for successive simulation time steps on a projection image (eg, the MIP) gives the observer a semiquantitative motion impression of the blood flow behavior in the vessels of interest.
Results: Both cardiac-gated and ungated PCA images have been acquired in several anatomic areas. The visualization technique has proved to be very effective in giving a semiquantitative overall impression of the flow in the volume of interest.
Conclusion: The proposed flow visualization method is valuable in evaluating complex flow in a 3D volume. Potential application areas are mainly in the head and liver and include AVMs, fistulas, shunts, circle of Willis, carotid arteries, and tumor vascularization. The visualization technique can in principle be extended to cardiac-triggered PCA acquisitions, so that the pulsatile nature of the flow is also shown.
M. Kouwenhoven is an employee of Philips Medical Systems.

258 • 11:54 AM
Hand MRA with a Designated Transmitter/Receiver Coil
DJ Roach, SM Totterman, MG Spencer, J Hornak
University of Rochester Medical Center, Rochester, NY
Purpose: MR angiography has been used in the evaluation of the carotid, intracerebral, pelvic, and lower extremity arteries. However, the signal-to-noise ratio requirement has limited its use in the hand and wrist. The purpose of this study was to evaluate the capability of 3D TOF MR angiography for visualizing the arteries of the hand by using an asymmetric single-turn solenoid hand coil.
Methods: Volunteers were imaged on a GE Signa 1.5-T clinical imager using an asymmetric single-turn solenoid coil as a transmitter and receiver, 8-cm FOV, 2-mm slice thickness, 59-msec TR, 69-msec TE, 30° flip angle, and fat-saturation pulses. Saturation pulses were used to suppress venous flow. The images were postprocessed with the interactive vascular imaging (IVI) package (GE).
Results: The 3D TOF technique with a high-Q single-turn solenoid coil enabled visualization of ulnar, radial, and digital arteries. The palmar arch arteries were difficult to visualize because of the direction of flow. This transmitter/receiver coil did not significantly suppress venous flow; however, use of the IVI enabled us to eliminate the superficial veins.
Conclusion: By using a designated transmitter/receiver coil, the vasculature of the hand and wrist can be visualized.

Tuesday Afternoon • Monet Room
Papers 301–306

PERFUSION AND FUNCTIONAL IMAGING
MODERATORS: TJ Brady, MD
WT Dixon, MD

301 • 3:45 PM
Noninvasive Mapping of Cerebral Perfusion by Using EPISTAR MR Angiography
RR Edelman, B Sievert, P Wielopolski, J Pearlman, S Warach
Department of Radiology, Beth Israel Hospital, Boston, MA
Purpose: We describe a new method, called EPISTAR, that noninvasively depicts cerebral perfusion without the limitations of previous methods.
Methods: A single 180° radio-frequency pulse is applied inferiorly to the inflowing arterial spins, followed after a variable delay by acquisition of a flow-compensated echo-planar image. This image is subtracted from a similarly acquired image without inversion to produce a "perfusion" angiogram. The method was validated in a pig model, volunteers, and patients with cerebrovascular disease.
Results: Progressive delays between the inversion prepulse and the image readout produced a series of images successively showing enhancement of proximal arteries, arterial branches, and cortex. Inhalation of CO_2, intravenous injection of acetazolamide, or visual stimulation, standard paradigms for increasing global or focal brain perfusion, produced increases in cortical signal intensity and decreases in the delay time for maximal cortical enhancement. In patients with internal carotid artery occlusions, delays were observed in the time to enhancement of normal cortex ipsilateral to the occlusion, and there was virtually no enhancement of chronic infarctions. The results were comparable or superior to those of perfusion techniques with gadolinium injection or single photon emission tomography. Unlike BOLD, activation studies with EPISTAR were not degraded by cortical vein activity, which permitted better localization.
Conclusion: These preliminary results indicate that the EPISTAR method depicts cerebral perfusion. This noninvasive technique has the potential to show cerebral localization based on perfusion changes and abnormalities in cerebrovascular circulation. Future work will be directed toward quantification of cerebral blood flow with this method.

302 • 3:57 PM

MR Mapping of Cerebral Perfusion: New Sensitivity to Mild Cerebral Ischemia

TP Roberts, ZS Vexler, N Derugin, ME Moseley, J Kucharczyk
Department of Radiology, University of California, San Francisco, San Francisco, CA

Purpose: Echo-planar MR imaging (EPI) was used in conjunction with bolus administration of an intravascular magnetic susceptibility contrast agent, Dy-DTPA-BMA (S043 injection, Nycomed-Salutar Inc; Sprodiamide, Sterling-Winthrop) to assess cerebral blood supply during cerebral ischemia. Maps of bolus-peak arrival time and relative cerebral blood volume (rCBV) were compared during variable degrees of stenosis of the middle cerebral artery (MCA).
Methods: Subtotal stenosis of the MCA was induced in 10 cats. EPI was used after 1 hour to track a bolus of Dy-DTPA-BMA, injected intravenously. Pixel-by-pixel variations in $\Delta R2^*$ were derived. With use of the time integral of $\Delta R2^*$, maps of rCBV and bolus-peak arrival time were generated.
Results: In cases of near-total stenosis ($n = 3$), both rCBV and bolus-peak arrival time maps clearly demarcated perfusion deficits within the MCA vascular territory. This territory also shows a reduced apparent diffusion coefficient and abnormal histologic (TTC) staining. With milder flow perturbation ($n = 7$), rCBV maps demonstrated no significant difference ($P > .05$) between ipsi- and contralateral tissues. However, the bolus-peak arrival time map clearly indicated ($P < .05$) delayed blood supply to the MCA vascular territory.
Conclusion: Bolus tracking of magnetic susceptibility contrast agents allows mapping of parameters related to cerebral perfusion. In addition to rCBV, which is sensitive to severe cerebral ischemia, the delay in arrival of the bolus peak allows detection of minor perturbations in cerebral blood flow and collateral flow recruitment, which are not easily visible with other imaging techniques.

303 • 4:09 PM

Parametric T2* Imaging in Ischemia and Stroke

RR Price, H Lee, DR Pickens, TC Larson, J Creasy, CL Partain
Department of Radiology, Vanderbilt University Medical Center, Nashville, TN

Purpose: It has been demonstrated previously that blood itself becomes an intravascular bulk magnetic susceptibility contrast agent when deoxygenated (1). The hypothesis is that signal decrease during ischemia or hypoxia is directly related to the deoxyhemoglobin content of the tissue. In this work, we investigated changes as measured by T2*-weighted gradient-echo sequences after flow alterations in the brain.
Methods: All experiments were performed by using a 4.7-T 40-cm bore SISCO imager/spectrometer with standard unshielded gradients. Small-vessel ischemia was induced in six adult dogs in one cerebral hemisphere by injection of 150–250 μm polyvinyl alcohol particles into the ICA. A series of nine gradient-echo images (FLASH, TR = 40 msec) with TEs ranging from 12 to 28 msec were acquired, followed by a dynamic contrast-enhanced susceptibility study. The nine gradient-echo images were reduced to a parametric image of R2*. Similarly, a susceptibility blood-volume parametric image was derived from the dynamic contrast-enhanced study.
Results: Gradient-echo images of ischemic lesions showed an accelerated decrease in signal intensity with increased TE relative to normal brain tissue. R2* value derived from manually selected symmetric regions from each hemisphere were compared. The mean R2* value (sec^{-1}) for the ischemic side was 0.054 ± 0.014, as opposed to the normal side, which was 0.021 ± 0.003. R2* images were found to be correlated with regional blood-volume images derived from the dynamic contrast-enhanced study.
Conclusion: Parametric T2* images in brain ischemia and stroke have been found to be correlated with relative blood-volume images from the dynamic contrast-enhanced study.
1. Turner R., et al., *Magn Reson Med* 22, 159 (1991).

304 • 4:21 PM

Dynamic Regional Cerebral Blood Volume Imaging by Using Echo-Planar Sequences with Conventional Imaging Gradients

X Wan, WL Davis, GT Gullberg, DL Parker
Department of Radiology, University of Utah School of Medicine, Salt Lake City, UT

Purpose: Dynamic regional cerebral blood volume imaging has been accomplished by using fast gradient-echo pulse sequences with conventional gradients or by using single-shot echo-planar pulse sequences with special gradient hardware. The purpose of the current study is to show that the kinetic study of contrast agents can be performed by using an echo-planar technique that can be implemented on most clinical imagers without adding any special hardware.
Methods: Dynamic studies were performed in several patients with a standard GE 1.5-T Signa clinical system with conventional gradients. An echo-planar pulse sequence, which acquired data during both the ramping and constant portion of the readout gradient, was used for the study. A 128×64 image matrix can be acquired within 98 msec. The injection of 12 mL of Gd-DTPA (0.1 mmol/kg) in a dorsal vein of the hand was performed over a period of 10 seconds. At the start of the injection, the pulse sequence acquired one image of a 10-mm slice every 1 second, for a total of 120 images.
Results: The regions of interest were defined for gray and white matter and time-contrast curves were obtained. As expected, the image intensity decreased a short time after the injection due to the T2* effect and gradually increased back to the baseline as the Gd-DTPA washed out of the selected blood volume. There was increased susceptibility contrast material in the gray matter compared with white matter, which is indicative of the larger blood volume in gray matter.
Conclusion: The results demonstrate the ability to study the time course of a contrast agent through the brain with conventional MR imagers.

305 • 4:33 PM

Recording of an Electroencephalogram during Functional MRI Studies

S Warach, JR Ives, F Schmitt, DL Schomer, RR Edelman
Department of Neurology, Beth Israel Hospital, Harvard Medical School, Boston, MA

Purpose: Our goal was to simultaneously record an EEG while obtaining artifact-free functional MR images as a means of correlating brain electrical activity with functional MRI data.
Methods: Functional echo-planar imaging (EPI) was performed at 1.5 T by using a BOLD technique with an FID sequence and TE of 60 msec. Patients undergoing continuous long-term EEG monitoring and several normal volunteers (total subjects, $n = 10$) were studied while wearing an 18-channel EEG telemetry system; several subjects had minisphenoidal electrodes placed.
Results: No adverse experiences occurred in any subject. With the subject lying in the magnet, EEG recordings were of good quality and enabled identification of generalized and focal epileptiform discharges, electrical seizures, and sleep stages. During gradient switching, EEG was unusable due to artifact. With proper selection of electrode materials and placement of the telemetry preamplifier outside of the CP head coil, images were obtained without artifact due to metallic material. Noise spikes on EPI images were eliminated by placing the EEG equipment entirely in the imaging room and switching off the EEG only during image acquisition (less than 100 msec for EPI images).
Conclusion: Good quality EEG telemetric recordings and EPI BOLD images were obtained within a single functional MRI session. Although EEG equipment must be briefly switched off immediately before an EPI acquisition, triggering of an EPI BOLD image with EEG output was feasible, and therefore direct correlation of brain electrical activity with functional MRI is possible.

306 • 4:45 PM

Reduction of Signal Fluctuation in Functional MRI with a Navigator Echo

X Hu, I-G Kim
Department of Radiology, University of Minnesota Medical School, Minneapolis, MN

Purpose: To develop a method that utilizes a "navigator" echo to monitor and subsequently compensate for signal fluctuations due to physiologic motion.
Methods: With a FLASH sequence, the technique acquires as the navigator signal a single data point before the application of the phase-encoding and readout gradients. The phase correction required to bring all the navigator signal to a common phase (zero) is then applied to the phase of the corresponding phase-encoded imaging data. This technique was implemented on a 4-T whole-body system. To validate the technique, consecutive gradient-echo images were acquired with a TR/TE of 45/30 msec, FOV of 18 × 18 cm, matrix of 128 × 64, and flip angle of 22° and were reconstructed with and without the navigator echo correction, respectively; temporal variations of these images were analyzed and compared. Furthermore, motor and visual activation studies were performed by using the technique with similar imaging parameters; functional images, generated with and without the navigator correction, were obtained and compared.
Results: Temporal variation in the images obtained with the navigator echo correction were reduced by a factor of 2 relative to that in images obtained without correction. The reduction in signal fluctuation was not uniform and was greater in the parenchyma. Functional images obtained from corrected images exhibited additional areas of activation with smaller signal changes.
Conclusion: We have developed and demonstrated a simple and robust noise reduction technique for functional imaging. Our results demonstrate that the technique is capable of providing greatly improved functional images.

Tuesday Afternoon • Metropolitan Room
Papers 311–317

CONTRAST AGENTS II

MODERATORS: GD Fullerton, PhD
SW Young, MD

311 • 3:45 PM

Characterization of an Organ-specific Contrast Agent for Adrenal MR Imaging

A Mühler, J Platzek, H Vogler, B Radüchel, T Frenzel, C Heyer, HJ Weinmann
Schering AG, Berlin, Germany

Purpose: In nuclear medicine, derivatives of cholesterol have been widely used for adrenal imaging. The purpose of this study was to investigate whether the principle of targeting the adrenal cortex with cholesterol may be transferred to MR imaging by using a derivatized gadolinium complex.
Methods: The gadolinium complex of the macrocyclic chelator DO3A was derivatized with cholesterol via a spacer and was then characterized by relaxometry (0.47 T, 39°C) and by ultrafiltration in bovine serum through a 20 kd membrane (15 minutes at 1,200*g*). Tissue gadolinium concentrations were determined in liver, kidneys, adrenal glands, and blood at 2 hours and at 24 hours after injection of 0.05 mmol/kg Gd-DO3A-cholesterol. Gadolinium concentrations were measured with ICP-AES at a wavelength of 342.247 nm. MR imaging was performed at 2 T (SISCO animal imager) by using T1-weighted SE sequences (250/15/8/256 × 256). Enhancement of tissues was compared after administration of 0.05 mmol/kg Gd-DO3A-cholesterol and Gd-DTPA-albumin, a blood pool agent.
Results: The R1 of Gd-DO3A-cholesterol was found to be 17.9 L/mmol*sec in water and 21.2 L/mmol*sec in plasma. More than 99% of the contrast agent was protein bound in serum. The gadolinium concentrations in adrenal glands were about equal to that in blood at 2 hours p.i. (0.7–1.0 mmol/L) but were about 10 times higher at 24 hours p.i. (adrenal gland: 0.48 mmol/L, blood: 0.05 mmol/L). Liver gadolinium concentrations have consistently been lower than those in adrenal glands. During MR imaging, renal medulla (270%) and renal cortex (170%–180%) showed virtually the same peak enhancement after administration of Gd-DO3A-cholesterol and Gd-DTPA-albumin. However, adrenal glands enhanced about 160% after injection of the cholesterol derivative but less than 60% after injection of the blood pool agent.
Conclusions: The study shows that a cholesterol derivative of a gadolinium complex may accumulate in the adrenal glands, making it an organ-specific contrast agent for adrenal MR imaging.
A. Mühler, J. Platzek, H. Vogler, B. Radüchel, T. Frenzel, C. Heyer, and H.J. Weinmann are employees of Schering AG.

312 • 3:57 PM

3D-TOF MR Angiography with Gd-DTPA-Polyethylene Glycol Polymers: Effect of Increasing Dose

TS Desser, DL Rubin, F Ching, HH Muller, KE Kellar, JA Wellons, DL Ladd, JL Toner, RA Snow
Department of Radiology, Stanford University School of Medicine, Stanford, CA

Purpose: To quantitate dose response in 3D-TOF MRA with the macromolecular contrast agent Gd-DTPA-PEG (MW = 20.2 kd) in a model designed to elicit maximal saturation effects.
Methods: Twenty-one normal New Zealand white rabbits were injected with increasing doses of Gd-DTPA-PEG (Sterling-Winthrop) ranging from 0.02 to 0.4 mmol Gd/kg. 3D-TOF MRA of abdominal vasculature was performed at 1.5 T (GE, Signa) before and 5 and 15 minutes after administration of contrast material, with 30° and 90° flip angles and a large (24-cm) slab thickness to maximize saturation effects. Region-of-interest measurements were obtained in the proximal and middle inferior vena cava and in stationary tissue.
Results: At 30° flip angles, vessel signal intensity and contrast with background reached a plateau at the 0.1 mmol Gd/kg dose. With 90° flip angles, signal intensity continued to increase with dose. Significantly greater contrast between vessels and background was achieved with 90° flip angles versus 30° flip angles for doses ≥ 0.06 mmol Gd/kg.
Conclusion: Gd-DTPA-PEG polymers can be used in MRA to minimize effects of spin saturation in large imaging volumes. Excellent vessel-background contrast can be achieved by imaging at 90° flip angles with doses ≥ 0.06 mmol Gd/kg.
This research was supported by Sterling Winthrop, Inc.

313 • 4:09 PM

Optimizing Flip Angle in 3D-TOF MRA with a Blood-Pool Contrast Agent

TS Desser, DL Rubin, F Ching, S Khodor, KE Kellar, JA Wellons, DL Ladd, JL Toner, RA Snow
Department of Radiology, Stanford University School of Medicine, Stanford, CA

Purpose: To identify the optimum flip angle for 3D-TOF MRA with a blood-pool contrast agent.
Methods: Sixteen normal New Zealand white rabbits underwent 3D-TOF MRA at 1.5 T (GE, Signa). Imaging of abdominal vasculature was performed before and 5 and 15 minutes after injection of 0.06, 0.08, 0.2 or 0.4 mmol/kg Gd-DTPA-PEG, MW = 20.2 kd (Sterling-Winthrop,Inc). Rabbit whole blood 1/T1 was measured before and after injection. On the basis of the 5- and 15-minute whole blood T1s, The Ernst angle and differential T1 contrast angle were calculated for each dose. 3D-TOF MRA sequences were performed at 30°, 90°, the Ernst angle, and the differential T1 contrast angle. Region-of-interest measurements were performed in the proximal and middle IVC and background muscle.
Results: At all doses, contrast between IVC and background muscle was maximal at 90° flip angles, rather than at the differential T1 contrast angle. At lower doses, IVC signal inten-

sity was maximized at the lowest flip angle used, rather than at the Ernst angle. At the two highest doses, IVC signal was greatest at the Ernst angle.
Conclusion: Maximal vessel signal intensity and contrast in 3D-TOF MRA with Gd-DTPA-PEG are not solely predicted by the Ernst and T1 contrast angles, likely due to flow effects.
This research was funded by a grant from Sterling-Winthrop, Inc. K.E. Kellar, J.A. Wellons, D.L. Ladd, J.L. Toner, and R.A. Snow are employees of Sterling Winthrop, Inc.

314 • 4:21 PM
Experimental Study in Rats and Rabbits with a New Manganese Complex as an MRI Contrast Agent
GK Schneider, K Urbschat, H Sperber, J Otto, M Uder, R Kubale, D Gohl, B Kramann
Department of Radiodiagnostics, University of Saarland, Homburg, Germany

Purpose: This experimental study investigates imaging qualities of a new manganese complex for the detection and enhancement of blood-brain-barrier (BBB) disruption and focal or diffuse liver lesions.
Methods: MRI was performed with a 1.0 T magnet (Siemens, Magnetom) by using T1- and T2-weighted SE sequences. The new manganese complex represents an ionic Mn-BP-DTTA complex, eliminated by renal and hepatobiliary excretion. Local BBB disruption was investigated in rabbits with experimentally induced brain infarction or brain abscess. The potential for enabling the detection of liver lesions was tested in rats with experimentally induced liver infarction, acute liver necrosis, and liver abscess. MR images were compared with histologic specimens.
Results: In experimentally induced brain abscess, T1-weighted images showed an increase in signal intensity (SI) of up to 45% in the abscess area after injection of the new manganese complex. In experimentally induced brain infarction, contrast-enhanced images showed significant increase in SI of up to 27% in the surrounding edema, and so the edema could be clearly delineated from the central core of the infarction. Both animal models demonstrated good correlation between histological specimen and MRI. Liver parenchyma of animals without pathologic alterations showed an increase in SI between 40% and 50%. In experimentally induced focal liver injury, a good delineation of liver lesions with an increase in SI of 0%–20% could be observed, whereas in acute liver necrosis, an increase of up to 80% was measured.
Conclusions: The new manganese complex tested in this study shows a clear increase in SI in regions with disrupted BBB. Additionally, SI in liver parenchyma shows a clear increase, and the detectability of liver lesions significantly improves. On the basis of these results, the new manganese complex has potential as a new contrast agent for MR imaging of the central nervous system and the liver.

315 • 4:33 PM
Intravenous MR Lymphography with Iron Oxide Particles: Interlymphonodal Distribution in Different Animal Species
D Pfefferer, S Wagner, M Kresse, M Taupitz, W Ebert
Institute for Diagnostic Research, Berlin, Germany

Purpose: MR studies of interlymphonodal distribution of intravenously administered superparamagnetic iron oxide particles (SIP) and dextran-formulated SIP (DSIP) in mice, rats, and rabbits.
Methods: MRI at 1.5 T with SE 2,000/15 and GRE 135/15/15° was performed 24 hours after intravenous administration of 200 μmol Fe/kg SIP—dextran-stabilized monodisperse iron oxides ($r_1 = 22.9$, $r_2 = 54.2$ l * [mmol*s]$^{-1}$ at 0.47 T, 37°C)—or DSIP (postsynthetic formulation of SIP with dextrans [1, 10, or 70 kda]). The interlymphonodal distributions of SIP and DSIP were studied ex vivo (agarose embedded) in rats and mice and in vivo in rabbits.
Results: In rats, SIP showed the highest signal loss in mesenteric lymph nodes. DSIP (dextran ≥ 10 kda) were inversely distributed (ie, faintly detectable in mesenteric but strongly accumulated in peripheral lymph nodes), whereas DSIP (1 kda-dextran) showed a uniform interlymphonodal accumulation with supersaturation effects in both sequences. In mice, the distribution of SIP and all DSIP was similar and comparable to SIP in rats. In contrast to SIP and DSIP (≥ 10 kda), the interlymphonodal distribution of DSIP (1 kda-dextran) was homogeneous, producing supersaturated signal loss in all lymph nodes.
Discussion: The interlymphonodal distribution of SIP in rats can be influenced by dextran but may be due to the well-known immunosensitivity of rats to dextran. Because interlymponodal DSIP distributions in rats could not be verified in other species (mice, rabbits), the distribution patterns of dextran-coated or grafted colloidal contrast agents should be carefully verified in *different* species.

316 • 4:45 PM
Evaluation of Two Metalloporphyrin Agents as Potential Tumor-Specific MRI Contrast Media: MRI-Microangiographic-Histologic Correlation Study in Rats with Primary and Secondary Liver Tumors
Y Ni, G Marchal, G Lukito, W Ebert, W Semmler, CS Hilger, FK Maier, X Zhang, J Yu, et al
Department of Radiology, University Hospitals, Leuven, Belgium

Purpose: To investigate the potential of two patented metalloporphyrins, gadolinium hematoporphyrin (Gd-HP) and manganese tetraphenylporphyrin (Mn-TPP), as tumor-specific MRI contrast agents.
Methods: A total of 20 rats were used, of which 12 had chemically induced multiple hepatocellular carcinoma and 8 had implanted Novikoff hepatoma. Gd-HP (0.1 mmol/kg) and Mn-TPP (0.05 mmol/kg) were tested in separate groups of rats, and both were compared with the tissue-nonspecific agent Gd-DTPA (0.3 mmol/kg). T1-weighted SE images before and up to 48 hours after administration of contrast agents were obtained and were further correlated with the corresponding microangiograms and histologic specimens.
Results: At the early phase after administration, both metalloporphyrins functioned as nonspecific agents similar to Gd-DTPA and enhanced the tumor by perfusion and diffusion. However, during the delayed phase (2–48 hours), a reverse enhancement between different compartments in some tumors dramatically occurred with both agents. After matching the MR images with microangiograms, macroscopic specimens, and light microscopy, the compartments that showed delayed enhancement were actually nonviable tumoral components such as necrosis, thrombosis, and cystic secretion.
Conclusion: The current metalloporphyrins can label certain tumoral components on delayed MR images, though they cannot be regarded as highly tumor specific in the investigated models. The mechanisms of this labeling and the potential use in other tumor models need further investigation.
This research was supported in part by the Institut für Diagnostikforschung GmbH.

317 • 4:57 PM
Comparative Transmetallation Kinetics and Thermodynamic Stability Studies of Gd-DTPA-bisglucosamide
WA Gibby, NR Puttagunta
Department of Radiology, Utah Valley Regional Medical Center, Provo, UT

Purpose: To assess the transmetallation kinetics and relative thermodynamic stability of Gd-DTPA-bisglucosamide in relation to the existing MR contrast agents Gd-DTPA-BMA, Gd-DTPA, and Gd-HP-D03A.
Methods: The given gadolinium chelate was mixed with equimolar Zn citrate, DTPA, or EDTA at pH 7.4, chromatographed with HPLC, and detected with fluorescence. The transmetallation of the chelates was visualized by means of the progressive change in relative concentrations of various Gd-ligand species.
Results: The ratio of relative Gd-ligand/EDTA thermody-

namic stability for Gd-DTPA-Gluc was 1.6, and for Gd-DTPA-BMA was 0.9. The ratios of Gd-ligand/DTPA at equilibrium for Gd-DTPA-Gluc was 0.4 and for Gd-DTPA-BMA was 0.2. Gd-HP-DO3A did not show observable ligand exchange with either EDTA or DTPA. Zn transmetallation kinetics with Gd-BMA and Gd-DTPA versus Zn citrate showed 50% and 45%, respectively, of Gd exchange within 20 minutes. The Gd-Bis-Gluc showed no detectable transmetallation for the first 60 minutes. Gd-ligand/Gd citrate equilibrium ratios of Gd-DTPA-Gluc, Gd-DTPA, and Gd-DTPA-BMA were 1.3, 1.1, and 0.2, respectively, in the presence of Zn citrate. Gd-HP-DO3A did not show observable Zn-ligand exchange.
Conclusion: Gd-DTPA-Gluc exhibits higher kinetic stability in Zn transmetallation as well as ligand exchange reactions compared with Gd-DTPA-BMA. It has slower Zn exchange rates than do Gd-DTPA-BMA and Gd-DTPA. Gd-HP-DO3A is the most stable of the chelates studied.
W.A. Gibby is a stockholder of and medical adviser for Medical Advances, Inc.

Tuesday Afternoon • Miro Room
Papers 321–327

MUSCULOSKELETAL I: Joints

MODERATORS: JV Crues, III, MD
EC Unger, MD

321 • 3:45 PM

Dynamic MRI in Ulnar Wrist Pain

W Judmaier, M Lener, M Gabl, M Hackl, A Dessl, K Strasser, R Knapp, K Wicke, S Pechlaner
Department of Magnetic Resonance Imaging, University of Innsbruck, Innsbruck, Austria

Purpose: To demonstrate the utility of dynamic MRI in wrist movement disorders that could possibly lead to degenerative changes and tears of the triangular fibrocartilage complex (TFCC).
Methods: Seventy-three patients with ulnar wrist pain were examined at 1.5 T with a surface coil. Twenty-seven patients (37%) did not have a history of trauma. The hands were strapped onto a device that allowed an abduction movement in 12 steps of 5°. A T2*-weighted GE sequence (FLASH, TR = 0.102 seconds, TE = 18 msec, α = 20°) allowed three coronal slices in every position. These images were evaluated individually and on a 3D workstation in a continuous loop.
Results: Thirty patients (41%) showed an impingement of the TFCC in three variants: (1) disk impingement between the ulnar head and the triquetrum in ulnar abduction (n = 12), (2) between the lunate and ulnar head in radial abduction (n = 12, three also belonged to group 1), and (3) impingement of ligaments of the TFCC between the os triquetrum and dorsal edge of the radial notch during ulnar abduction (n = 9). Among these patients, 70% had ruptured disks and 30% showed signs of degeneration. Four patients with impingement showed no morphologic changes to the disk.
Conclusions: In ulnar wrist pain of both traumatic and atraumatic origin, MRI can depict an impingement syndrome in almost 50% of patients. There is evidence that this condition leads to degeneration and subsequent tearing of the TFCC. Early detection of these movement disorders with MRI could lead to early treatment, thus preventing irreversible damage to the TFCC.

322 • 3:57 PM

Correlation between Signal Intensity Pattern and Operative Findings in Adults with Supraspinatus Tendon Injury

SK Goergen, J Liu, WG Bradley, Jr, JK Tam, MD Dubin, PJ Pema, JE Jordan, LM Teresi
Memorial MR Center, Long Beach Memorial Medical Center, Long Beach, CA

Purpose: To determine the incidence of surgically confirmed supraspinatus tendon tears that mimic tendinitis on MR images.
Methods: The MR studies of 43 consecutive patients who had supraspinatus tendon tears at surgery were retrospectively reviewed. Imaging was performed at 1.5 T in the axial, coronal, and sagittal planes with proton-density and T2-weighted sequences (SE 2,000/30,80) at 4-mm intervals. The images were reviewed by one radiologist who was blinded to the operative findings. The supraspinatus muscle and tendon were inspected for abnormal signal intensity and morphology on both the first and second echo images. This signal abnormality was characterized either as (*a*) fluid intensity or (*b*) "slightly increased" on the second echo.
Results: Of 43 suprapinatus tendon tears, 11 (25.6%) demonstrated "slightly increased" signal intensity, and partial tears were found at surgery. One of these 11 patients also had a partial (25% thickness) tear of the infraspinatus tendon, and another had a partial tear of the biceps tendon associated with annular fraying (type 2 SLAP lesion). The remaining 32 shoulders demonstrated fluid-intensity suprapinatus tears. In 2 cases, partial-thickness tears were discovered at surgery, but 30 of 32 tendons (94%) had full-thickness tears or ruptures. Seventeen of 32 (53%) patients also had infraspinatus tendon injury, 5 of these also had teres minor tears and 8 had biceps tendon tears or ruptures.
Conclusions: Partial supraspinatus tendon tears that have fluid intensity on long TR/TE MR images are common, may be indistinguisable from tendinitis, and are rarely associated with injuries elsewhere in the rotator cuff and biceps. Focal areas of fluid intensity in the supraspinatus tendon on long TR/TE images almost always represent full-thickness tears or complete tendon ruptures, more than half of which have associated injuries elsewhere in the rotator cuff and biceps tendon.

323 • 4:09 PM

Improving the Diagnostic Accuracy of MRI in the Detection of Infraspinatus Tendon Injuries

SK Goergen, J Liu, WG Bradley, Jr, MD Dubin, PJ Pema, JE Jordan, LM Teresi, D Morrisson
Memorial MR Center, Long Beach Memorial Medical Center, Long Beach, CA

Purpose: To determine the accuracy of MRI in the detection of infraspinatus tendon tears. The number of long TR/TE coronal images on which a tendon defect could be seen, the angle subtended by the tear on axial images, and the extent of tendon signal abnormality on sagittal images were correlated with the presence of additional infrasprinatus tendon tear (ITT).
Methods: The MR studies of patients who had supraspinatus tendon tears (STT) at surgery were retrospectively reviewed. Imaging was performed at 1.5 T in the axial, oblique coronal, and sagittal planes with proton-density and T2-weighted sequences at 4-mm intervals. The axial angle was measured by using the center of the humeral head as a reference point at the level of the maximum size of the tear. These data were analyzed for patients with and without ITTs at surgery by using the Mann-Whitney U test for the difference of two means.
Results: Eighteen of 41 patients (44%) had ITTs at surgery. Standard assessment of the MR images resulted in 10 of 18 (56%) tears being correctly diagnosed. The mean angle subtended by the signal abnormality was 75.6° in patients with ITTs versus 40° in those without, and this difference was significant ($P < .001$, $t = 3.06$). The mean number of coronal images in which tendon abnormality could be seen was 5.4 in the ITT group versus 2.9 in those with no tear, and this difference was also significant ($P < .001$, $t = 4.45$). The mean sagittal extent of tendon abnormality was 24.6 mm in the ITT group and 11.6 in those without ITT, but this difference was found not to be significant ($t = 1.1364$).
Conclusion: In symptomatic patients with MR evidence of STT, the diagnosis of associated ITT may be facilitated by (*a*) evaluation of the number of coronal images that demonstrate the signal abnormality, and (*b*) by measuring the angle subtended by the abnormal tendon signal intensity on the axial images. Accurate evaluation of the extent of rotator cuff

tear is important because limited tears can be dealt with arthroscopically, while larger tears require arthrotomy.

324 • 4:21 PM

Value of Contrast-enhanced MR Imaging Evaluation of Osteomyelitis of the Foot

AK Wang, R Chambers, L Chiu, D Braslau
Rancho Los Amigos Medical Center, Downey, CA

Purpose: The extent and severity of osteomyelitis in the foot are difficult to assess with routine MRI protocols, especially in the presence of fracture or neuropathic changes. The utility of gadolinium infusion in evaluation of these entities was investigated.
Methods: A group of 150 patients was studied prospectively with T1-weighted fat-saturation MRI after intravenous administration of gadopentetate dimeglumine. Comparison was made with routine unenhanced images (T1-weighted and STIR) obtained at the same sitting. Results were correlated with pathologic specimens obtained from subsequent amputation or biopsy.
Results: T1-weighted, fat-saturated, contrast-enhanced images were found to be as sensitive as STIR images with a 98% correlation. We noted cases in which chronic fibrosis in chronic infection failed to exhibit contrast enhancement despite displaying high signal intensity on STIR images. Dry gangrene displayed low signal intensity with all sequences, as expected. The resolution of T1-weighted, fat-saturated, contrast-enhanced images is superior to that of STIR images in most cases. In cases of acute Charcot joints or other fractures, we observed false-positive findings where pathologic specimens revealed only fibrosis.
Conclusion: Gadolinium enhancement increases diagnostic accuracy in detection and depiction of extent of osteomyelitis in the foot by allowing the differentiation of chronic fibrosis from acute inflammation. The advantages of this technique may be offset by the additional expense and the lack of availability of fat-saturation sequences at some centers.

325 • 4:33 PM

MR Imaging of Neuroarthropathy in the Diabetic Foot with IR, MTC, and Long TE Gradient-Echo Sequences

NJ Shah, H Koerperich, J Reinhardt, A Bergmann, G Notohamiprodjo
Heart and Diabetes Center, Bad Oeynhausen, Germany

Purpose: We present MR images of the diabetic foot obtained by using tailored sequences and make a comparison with regular T1- and T2-weighted spin-echo sequences. The early changes of diabetic neuroarthropathy of the foot might be depicted earlier with these new sequences.
Methods: MR images of the diabetic foot were obtained with the following protocols, with times given in milliseconds: (*a*) T1-weighted spin-echo, TE/TR = 16/460; (*b*) dual-echo proton-density and T2-weighted spin-echo, TE/TR = 20,80/2,500; (*c*) long TE gradient-echo with 3rd order motion compensation, TE/TR = 30/2,000, with a resolution of 440 × 512; (*d*) dual-echo inversion-recovery (IR) technique (TI = 124, TE/TR = 18,78/2,400) with gradient-echo and spin-echo readouts for the first and second echoes, respectively. MTC saturation pulses were also added to delineate better between fat, fluid, and muscle. All images were acquired with a 1.5-T Picker HPQ system, with use of a standard quadrature transmit/receive head coil.
Results: The dual-echo IR sequence showed fluid as areas of high signal intensity with both echoes, which delineates bone and soft-tissue edema much better than the regular spin-echo sequences. The long TE gradient-echo images display almost artifact-free vessels and high intensity in the midphalangeal bones; this, however, is almost the same as for normals. Also, the anatomy of the bones and joint spaces is better visualized. The relative contrast is greatly enhanced for this particular sequence by using MTC. In the not-so-rare case of soft-tissue inflammation and possible involvement of the bone with osteomyelitis, the extent of osteomyelitis can be shown clearly on T1- and T2-weighted images, especially on the contrast-enhanced T1 images.
Conclusions: Manipulation of contrast on MR images of the diabetic foot by using IR, MTC, and long TE high-resolution gradient-echo sequences shows considerable promise. We will examine and comment on the possibility of early detection, with use of the sequences alluded to, of joint destruction and microfractures, which are typically seen in the metatarsophalangeal and in the tarsometatarsal joints in the diabetic foot.
N.J. Shah is an employee of Picker International.

326 • 4:45 PM

MR Imaging of Tuberculous Arthritis: Clinical and Experimental Studies

JS Suh, JD Lee, MJ Kim, EJ Kim, DY Han, NH Cho
Department of Diagnostic Radiology, Yonsei University College of Medicine, Seoul, Korea

Purpose: Identification of the infectious organism is essential for the diagnosis of tuberculous arthritis but is not always successful. The authors' purpose was to characterize signal intensities in tuberculous arthritis at MR imaging.
Methods: MR images of five patients with tuberculous arthritis (two knees, one hip, one shoulder, one ankle) were retrospectively reviewed. Experimentally, tuberculous arthritis was induced by the injection of heat-killed *Mycobacterium tuberculosis* bacilli in the knees of 10 rabbits. At 24 hours and every week thereafter, T2- and T1-weighted images before and after intravenous administrations of Gd-DTPA were obtained in the sagittal plane with use of a 3-inch dual coil on a 1.5-T imager. We compared each MR image with histologic (macroscopic) slides.
Results: Synovial lesions showed inhomogeneous signal intensities on both T1- and T2-weighted images in five patients. On T2-weighted images, we found areas of intermediate signal intensity as well as areas of high-signal-intensity fluid in the joints. On the histologic specimens of rabbits, caseous necrosis was extensive and correlated with areas of intermediate signal intensity on T2-weighted image, and granulomas correlated with areas of inhomogeneous and relatively high signal intensity on T1- and T2-weighted images. Areas of caseous necrosis were not enhanced, whereas granulomas were enhanced after gadolinium injection.
Conclusion: Most areas of caseous necrosis showed intermediate rather than high signal intensity on T2-weighted images in both clinical and experimental cases. This may be helpful in the differential diagnosis for synovial diseases.

327 • 4:57 PM

Curvilinear Reconstructions from 3D Data Sets in the Assessment of Posttraumatic Elbow Stiffness

MV Fortier, S Pinney, W Regan, B Forster
Department of Radiology, University Hospital, Vancouver, British Columbia, Canada

Purpose: Posttraumatic elbow stiffness is a known complication following radial head fracture. Preoperative assessment includes plain radiography and tomography, which are difficult to perform in the coronal plane because of flexion contracture. Surgical intervention involves empiric anterior capsulotomy. We conducted a prospective study to determine the usefulness of MRI and, more specifically, curvilinear reconstruction from 3D data sets in the preoperative evaluation of these patients.
Methods: Preoperative MR images of 10 consecutive patients with posttraumatic elbow stiffness and varying degrees of flexion contracture were prospectively reviewed by two radiologists. T1-weighted and dual-echo sequences were obtained in transverse and sagittal planes with a 1.5-T unit. In addition, a sagittally acquired spoiled gradient-echo 3D data set of the flexed elbow was obtained and reformatted coronally by using a curved plane of reconstruction. The MR findings were compared with those of preoperative plain radiography and tomography and surgical results.
Results: Abnormalities could be classified as intrinsic and/or extrinsic to the elbow joint. In three patients, MRI allowed identification of loose bodies that were poorly visualized, or not seen, on plain radiographs. MRI also revealed

posttraumatic osteoarthritis in the coronal plane in five cases in which plain radiographs were suboptimal because of flexion contracture. Importantly, MRI permitted detection of extrinsic soft-tissue abnormalities including ligamentous and capsular thickening in five patients.
Conclusion: MRI is valuable in the preoperative assessment of posttraumatic elbow stiffness and can guide the surgeon to intrinsic and extrinsic causes that may not be alleviated with empirical anterior capsulotomy.

Tuesday Afternoon • Morrocco Room
Papers 331–338

ABDOMEN AND MALE PELVIS

MODERATORS: DG Mitchell, MD
A Yang, MD

331 • 3:45 PM

Pancreatic Signal Intensity on T1-weighted Fat-Saturation Images: Clinical Correlation

CB Winston, D Mitchell, E Outwater, S Ehrlich
Department of Radiology, Thomas Jefferson University Hospital, Philadelphia, PA

Purpose: To assess the ability of pancreatic signal intensity on T1-weighted fat-saturated (T1FS) images to allow distinction between the normal and abnormal pancreas.
Methods: TIFS (500/16) abdominal MR images of 57 patients were evaluated blindly by 3 independent readers who graded pancreatic signal intensity as less than, equal to, or greater than that of liver. No assessment of morphology, architectural distortion, or peripancreatic abnormality was performed. The signal intensity was correlated with the patient's medical records regarding the diagnosis of pancreatitis, pancreatic mass, diabetes, and laboratory values.
Results: Of the 57 patients, 30 had no pancreatic disease, 13 had pancreatitis (10 acute, 13 chronic), 8 had pancreatic cancer, 5 had diabetes mellitus, and 1 had hemochromatosis. Of the 30 clinically normal pancreases, the entire pancreas had signal intensity greater than that of the liver in 26 (87% sensitive for normal). Of the 27 clinically abnormal patients, 22 had focal or diffuse pancreatic signal intensity less than or equal to that of the liver (81% sensitive for abnormal). The positive predictive value for abnormal pancreatic signal intensity was 85%. False-negative findings included diabetes (n = 2), acute pancreatitis (n = 2), and small carcinoma (n = 1).
Conclusion: Pancreatic signal intensity on T1FS images may play an important role in distinguishing the normal from abnormal pancreas. Since hepatic pathology does not increase hepatic signal intensity on T1FS images, pancreatic signal intensity greater than that of liver has high correlation with a clinically normal organ. Focally or diffusely decreased pancreatic signal intensity has a high predictive value for pancreatic pathology.

332 • 3:57 PM

MR Urography Based on a Saturation Inversion Projection Technique

MV Knopp, L Schad, N Oesingmann, J Doersam, F Wenz, G Stähler, G van Kaick
Department of Radiology, German Cancer Research Center, Heidelberg, Germany

Purpose: To assess potential clinical applications and procedures for imaging of the genitourinary tract and evaluating renal function.
Methods: A saturation inversion projection (SIP) spin-echo (SE) technique enables suppression of all signals from regions with long T1, with selective visualization of regions with ultrashort T1. The selective T1 shortening is obtained as a result of the application of the paramagnetic contrast medium Gd-DTPA. Since Gd-DTPA is eliminated by glomerular filtration and its pharmacologic properties are well understood, this technique allows quantitative evaluation of renal function. With use of a sequential acquisition with an acquisition time of 18 seconds per image over a 15-minute period, functional renographic curves can be obtained with a region-of-interest (ROI) technique from each kidney selectively. Twenty patients with suspected renal cancer were imaged with this technique on a 1.5-T system (Magnetom SP, Siemens).
Results: The SIP technique allows direct visualization of the complete urogenital system in a coronal direction. ROI analysis results in renal curves that are comparable to scintigraphic findings. Global and selective functional information for each kidney can be obtained. With a cine display, the peristaltic transport of the contrast media can be observed from the renal pelvis to the bladder.
Conclusion: MR urography based on the SIP technique allows complete visualization of the urogenital system and a functional evaluation of renal performance. The clinical information obtained with this procedure combines the information of a conventional x-ray contrast-enhanced urogram and renal scintigraphy in one nonionizing procedure. This technique promises to have great clinical utility.

333 • 4:09 PM

Unfilled Bowel Mimicking Pathology in Abdominal MRI: Benefit of an Oral Gastrointestinal Contrast Agent

DL Rubin, MD Schnall, MD Rifkin, JC Peters, TS Mingo, ND LaFrance
Department of Radiology, Stanford University Medical Center, Stanford, CA

Purpose: To evaluate the potential of an oral gastrointestinal contrast agent for reducing confusion between unfilled bowel and pathologic masses in abdominal MRI.
Methods: WIN 39996 (iron oxide-coated polymer particles; 300cP formulation, 150 μg iron/mL, 500–1,000 mL) was administered to 64 normal human volunteers. Subjects were imaged at 1.5 T before, immediately after, and 1, 2, and 3 hours after ingestion of WIN 39996. T1-weighted SE, T2-weighted FSE, and breath-held SPGR sequences were performed. The images were evaluated independently by 3 radiologists for (*a*) the presence of findings simulating pathology and (*b*) confidence in a "normal" diagnosis.
Results: In 26 (41%) of the subjects, there were 45 images suggesting pathology before ingestion. Among these 45 images, the suspicious findings appeared resolved in 36 (80%) after ingestion. In the remaining 9 (20%), the appearance of pathology was not resolved after ingestion. Reader confidence that no pathology was present was significantly increased after ingestion.
Conclusion: WIN 39996 assisted in the exclusion of abnormality in this study and may be a useful gastrointestinal contrast agent in clinical abdominal imaging.
This research was supported by Sterling Winthrop, Inc. T.S. Mingo and N.D. LaFrance are employees of Sterling Winthrop, Inc.

334 • 4:21 PM

MR Imaging of the Pancreas after Stimulation with Secretin and Sincalide

RF Thoeni, P Rogalla, M Rigdon
Department of Radiology, University of California, San Francisco, CA

Purpose: To assess the synergistic effect of pancreas stimulation with secretin and sincalide on signal intensity of the pancreas on T1- and T2-weighted images, it is postulated that signal intensity changes are larger for normal pancreas than for tumor, thus increasing tumor conspicuity.
Methods: Seven healthy volunteers were examined with T1- and T2-weighted spin-echo (SE) sequences with and without fat suppression and T2-weighted FSE and fast multiplanar spoiled GRASS sequences before and after a bolus of secretin and, 30 minutes later, after sincalide. Signal intensities of pancreas and muscle were measured on all images, and the ratio of pancreas to muscle signal intensity (p/m) was calculated. Comparison was made between results from plain im-

aging of the pancreas and imaging after stimulation with secretin and sincalide.
Results: For T1-weighted dynamic sequences, stimulation with secretin/sincalide decreased the ratio p/m by a mean factor of 30%–35%, and for T2-weighted FSE, increased the signal intensity ratio by 25%.
Conclusion: Stimulation of the pancreas with secretin/sincalide resulted in a significant change in signal intensity of the normal pancreas on both T1- and T2-weighted images. Such change may be beneficial in improving the signal difference between tumor and normal pancreas for increased conspicuity of pancreatic lesions.

335 • 4:33 PM

Pancreatic MRI: Comparison of Five Pulse Sequences

CB Winston, D Mitchell, E Outwater, S Ehrlich
Department of Radiology, Thomas Jefferson University Hospital, Philadelphia, PA

Purpose: To compare the ability of 5 MRI pulse sequences to help define pancreatic borders and the pancreatic duct.
Methods: T1-weighted (500/12; 5 min) and T2-weighted (3,000/100; 14 min) SE, T1 fat-sat (500/16; 5 min), fast SE (3,500–7,000/102; 4–8 min), and spoiled GRE (102/2.3/90°; 16 sec) images of 60 patients were placed randomly in separate unlabeled jackets. Three independent readers graded each pulse sequence with regard to pancreatic border definition, cephalocaudal extent of pancreas, and the number of slices depicting the pancreatic duct (PD). The average scores for borders and PD and interobserver agreement for cephalocaudal extent were calculated for each sequence.
Results: The PD was visualized on the most sections with fast SE (2.3) and the least with T1 SE (1.2, $P < .05$) sequences. The pancreas was seen in more sections with T1 fat-sat (2.2) than with T1 SE (1.2) or GRE (1.6) sequences. Pancreatic borders were graded highest by each reader, in decreasing order, on T1 fat-sat, T1 SE, fast SE, GRE, and T2 SE images. Interobserver agreement for pancreatic extent was highest for the T1 fat-sat sequence.
Conclusion: T1 fat-sat images define best the pancreatic borders, while fast SE is best for visualizing the pancreatic duct. Fast SE images appear to depict the pancreas better than standard SE T2-weighted images. Spoiled GRE images with TE = 2.3 msec (fat-water opposed-phase) appear to have limited utility for the pancreas.

336 • 4:45 PM

Iron Oxide-coated Particles as a Gastrointestinal Contrast Agent for MRI: Phase I Clinical Trial

DL Rubin, MD Rifkin, JC Peters, TS Mingo, ND LaFrance
Department of Radiology, Stanford University Medical Center, Stanford, CA

Purpose: To evaluate the safety, tolerance, and efficacy of WIN 39996 as an oral MR gastrointestinal contrast agent and to determine the preferred dose regimen.
Methods: WIN 39996 (iron oxide-coated polymer particles; 300cP formulation, 150 μg iron/mL) was administered to a total of 64 normal human volunteers at two institutions. Subjects were divided into eight groups, differing in dose (500, 750, 1,000 mL) and ingestion time (30, 60, 120 minutes). All subjects were imaged at 1.5 T before, immediately after, and 1, 2, and 3 hours after ingestion of WIN 39996. T1-weighted SE, T2-weighted FSE, and breath-held SPGR sequences were performed. Contrast agent efficacy was evaluated independently by 3 radiologists.
Results: WIN 39996 was well tolerated, and there were no serious side effects. Bowel was effectively darkened with all pulse sequences, with no severe artifacts. Enhanced images showed improved delineation of abdominal organs and increased reader confidence that no pathology was present. The 1,000-mL dose with all ingestion times generally produced the greatest bowel enhancement and provided the widest time window for imaging.
Conclusion: The 1,000-mL dose effectively enhanced the gastrointestinal tract with all pulse sequences. WIN 39996 was safe and well tolerated and may be a useful contrast agent for bowel demarcation in abdominal MRI.
This research was supported by Sterling Winthrop, Inc. T.S. Mingo and N.D. LaFrance are employees of Sterling Winthrop, Inc.

337 • 4:57 PM

MRI Evaluation of Recurrent Prostate Cancer in Prostatectomy Patients with an Endorectal Probe Coil

JM Silverman, T Krebs
Department of Radiology, Cedars-Sinai Medical Center, Los Angeles, CA

Purpose: To evaluate the utility of MRI with an endorectal probe coil in patients who underwent prostatectomy but have a new nodule in the prostate bed and/or a rising PSA level.
Methods: Twenty patients who underwent prostatectomy and who had clinical suspicion of recurrent prostate cancer were enrolled in the study. All patients were examined with a GE 1.5-T Signa imager with an endorectal probe coil. Axial T1-weighted images with and without gadolinium enhancement, axial T2-weighted fast spin-echo images, and sagittal T2-weighted fast spin-echo images were acquired in all patients. Two radiologists experienced in the evaluation of prostate cancer with MRI independently reviewed all of the cases. Correlation with pathologic specimens was performed whenever possible.
Results: All patients demonstrated a soft-tissue mass within the prostate bed. These masses demonstrated short T2 signal as well as gadolinium enhancement. No cases of suspected or confirmed scar were seen.
Conclusions: MRI provides a useful imaging tool for evaluating patients who have undergone prostatectomy but are suspected of having recurrent cancer within the prostate bed. The addition of gadolinium enhancement provides increased confidence in the diagnosis.

HEAD AND NECK

MODERATORS: AN Hasso, MD
KL Nelson, MD

341 • 3:45 PM

Efficacy of T2-weighted Fast Spin-Echo Imaging with Fat Saturation in Identifying and Characterizing Lesions of the Head and Neck

MD Dubin, LM Teresi, JE Jordan, SK Goergen, JK Tam, WG Bradley, Jr
Memorial MR Center, Long Beach Memorial Medical Center, Long Beach, CA

Purpose: To compare the efficacy of T2W fast spin-echo sequences with fat saturation (FS-FSE) versus gadolinium-enhanced conventional T1W spin-echo sequences with fat saturation (FS-SE) in the detection and characterization of head and neck lesions.
Methods: MR images of 36 lesions in 21 patients with head and neck pathology were retrospectively analyzed. The conspicuity of head and neck lesions was assessed on the T2W FS-FSE (4,700/108) and on the Gd-enhanced T1W FS-SE (500/16) images by using a GE 1.5-T system. Lesion-to-background contrast was graded separately against muscle, fat, and mucosa: 0 = not seen, 1 = poorly seen, 2 = fairly well seen, 3 = well seen, and the best overall sequence was noted. Quantitative lesion-to-background ratios were obtained for each lesion.
Results: The average subjective lesion-to-background contrast ratings for the T2W FS-FSE sequences were lesion/muscle = 2.87, lesion/fat = 2.17, lesion/mucosa = 1.41; and for the Gd-enhanced T1W FS-SE sequences, lesion/muscle = 2.14, lesion/fat = 1.62, lesion/mucosa = 0.91. Overall, 79% of the lesions were better seen on the T2W FS-FSE images. Average quantitative lesion-to-background ratios for the T2W FS-FSE sequences were lesion/muscle = 7.79, lesion/fat = 1.17, lesion/mucosa = 1.06; and for the Gd-enhanced SE T1W FS sequences, lesion/muscle = 1.96, lesion/fat = 1.95, lesion/mucosa = 0.97.
Conclusions: T2W FS-FSE sequences offer better contrast between lesion, muscle, fat, and mucosa than do Gd-enhanced T1W FS-SE sequences. In addition, T2W FS-FSE sequences do not require intravenous contrast material and can be obtained more rapidly than T1W FS-SE sequences. Gd-enhanced T1W FS-SE sequences may offer complementary information in complex lesions with cystic components or septations.

342 • 3:57 PM

Contrast-enhanced MRI of Choroidal and Retinal Lesions

KL Gupta, JB Lindsey, JP Williams, III
Department of Radiology, Tulane University Medical Center, New Orleans, LA

Purpose: To compare contrast-enhanced MRI and ultrasound in evaluation of choroidal and retinal lesions.
Methods: The findings in 105 cases of choroidal and retinal and choroidal lesions (ie, melanoma, retinoblastoma, retinal hemorrhage, retinal detachment, choroid metastases) examined with contrast-enhanced MRI with a GE 1.5-T unit and with ultrasound were compared.
Results: Both modalities depicted the majority of lesions; however, MRI better depicted retrobulbar lesions and extension into the brain and optic nerve.
Conclusion: MRI and orbital ultrasound are excellent imaging modalities for evaluation of abnormalities of the pediatric orbit, although MRI has more utility in evaluation of deeper lesions.

343 • 4:09 PM

Evaluation of Choroidal Melanoma with Optimal-Pulse-Sequence MRI and Ultrasound

JB Lindsey, KL Gupta, JP Williams, III
Department of Radiology, Tulane University Medical Center, New Orleans, LA

Purpose: To compare MRI and ultrasound imaging of choroidal melanoma.
Methods: Ninety-three patients with choroidal melanoma were examined with MRI and ultrasound. Forty-seven underwent contrast-enhanced MRI. The findings from MRI with various pulse sequences and from ultrasound were compared.
Results: Tumor size with MRI and ultrasound correlated well. All tumors were detected with ultrasound; however, one small melanoma was not detected with MRI. T1-weighted images with and without contrast material proved to be superior in evaluation of choroidal lesions. However, T2-weighted images are needed for evaluation of retinal detachment and hemorrhages. Ultrasound provided sensitive but nonspecific imaging.
Conclusion: MRI and ultrasound are complementary in evaluation of choroidal melanoma.

344 • 4:21 PM

Comparison of High-Resolution MRI, Routine Enhanced MRI, and Ultrasound in Evaluation of Orbital Tumors

JB Lindsey, KL Gupta, JP Williams, III
Department of Radiology, Tulane University Medical Center, New Orleans, LA

Purpose: To compare high-resolution MRI, routine enhanced MRI, and ultrasound in evaluation of orbital tumors.
Methods: Two hundred seventy cases of orbital lesions were evaluated with both enhanced MRI with a 1.5-T GE imager and orbital ultrasound.
Results: MRI provided better soft-tissue contrast, which facilitated specific diagnoses of hemorrhage, melanoma, and retinoblastoma. This was enhanced by the use of contrast material and additional gradient-echo pulse sequences in some cases. High-resolution MRI may prove to add even greater soft-tissue contrast. Ultrasound was more sensitive for small lesions of 2 mm or less. However, deeper portions of the retrobulbar area and intracranial involvement were better evaluated with MRI.
Conclusion: MRI and ultrasound are complementary in the evaluation of orbital tumors in the majority of cases. High-resolution MRI may prove to be superior to routine enhanced MRI in evaluation of orbital tumors.

345 • 4:33 PM

SPIR MR Imaging of Orbital Lesions

CS Zee, HD Segall, PM Colletti, B Horvath
LAC/USC Imaging Science Center, Los Angeles, CA

Purpose: To evaluate the role of SPIR (a chemical shift fat-suppression technique) in the evaluation of orbital lesions, especially when used in conjunction with contrast enhancement.
Methods: Twenty patients with orbital pathology were studied with a T1-weighted SPIR technique before and after the injection of gadolinium, with a Philips ACS Gyroscan. Comparison was made with conventional T1- and T2-weighted images by using a four-point grading system. Five patients without orbital pathology were also studied to define normal anatomy.
Results: Because of volume averaging of high-signal-intensity fat and normal structures, and chemical shift artifact, it is difficult to define the normal anatomy on conventional MR images. SPIR images clearly show the optic nerve (which does not enhance) and rectus muscles and lacrimal glands (which enhance intensely). The SPIR technique was superior to conventional MR imaging in the evaluation of orbital lesions including optic nerve meningioma ($n = 2$), optic glioma ($n = 1$), optic canal meningioma ($n = 3$), Graves disease ($n = 5$), pseudotumor ($n = 2$), and one case each of lymphoma, metastasis, neurofibromatosis, schwannoma, sacroid, orbital

melanoma, benign mixed lacrimal tumor, and carotid-cavernous fistula.
Conclusions: (1) The SPIR technique in conjunction with gadolinium injection is superior to conventional MRI in defining normal anatomy of the orbit. (2) SPIR increases the conspicuity of the enhancing lesions and should be used routinely in evaluating orbital lesions. (3) Expansion of the dynamic gray scale is possible with fat suppression. (4) A major disadvantage is the presence of artifact due to signal loss at the air-bone interfaces.

346 • 4:45 PM

New MR Methods in the Diagnosis of Orbital Masses

KEW Eberhardt, HP Hollenbach, WJ Huk, B Beck
Department of Neuroradiology, Neurosurgical Clinic, University of Erlangen, Erlangen, Germany

Purpose: MRI techniques play an increasing role in the diagnosis of orbital masses. In the present study, new MRI techniques are discussed and compared with CT and sonography. The results were compared with intraoperative findings.
Methods: In a comparable case study, 30 patients with tumors and other masses of the orbital cavity were examined preoperatively with a 1.0-T whole-body MR system (Siemens Magnetom Impact). The results concerning histological grading, dignity, and delimitation to anatomic neighbor structures were evaluated. A T1-weighted spin-echo sequence (TR/TE, 370/15 msec), a T2-weighted spin-echo double-echo sequence (TR/TE, 2,000/20,80 msec), and an inversion recovery turbo-spin-echo sequence (TR/TE/TI, 4,900/60/150 msec) were applied in a transverse orientation with use of a circularly polarized head coil. The first two sequences used a frequency selective 1331 prepulse to obtain fat suppression. The T1-weighted spin-echo sequence was repeated after contrast medium (Gd-DTPA) was injected. The highest spatial resolution was 1.10 × 0.57 × 3.00 mm. To reduce artifacts due to eye motion, the patients had to wear pinhole blinders. The examination time was about 30 minutes.
Results: Our results demonstrate that MRI, particularly with the use of fat-suppressing sequences, is superior to sonography and CT concerning dignity and delimitation of orbital masses. The sensitivity for detecting masses in the retrobulbous fat tissue is higher for MRI with the fat-suppressing technique than for CT and sonography.
Conclusion: MRI has important advantages over sonography and CT for the diagnosis of orbital tumors and masses because of the use of fat-suppressing sequences.

347 • 4:57 PM

Intraindividual Comparison of High-Dose Gadodiamide Injection with the Standard Dose of Gd-DTPA

TJ Vogl, MG Mack, M Juergens, M Stark, G Grevers, A Western, R Felix
Department of Radiology, Free University of Berlin, Berlin, Germany

Purpose: The aim of the study was to compare the diagnostic values of high-dose gadodiamide injection (0.3 mmol/kg b.w.) with the standard dose of Gd-DTPA (0.1 mmol/kg b.w.) for MR imaging of tumors of the head and neck.
Methods: Forty-six patients underwent two MR examinations without intervening surgery, chemotherapy, or radiation therapy over 10 days: one examination used the high-dose gadodiamide injection, and the second used the standard dose of Gd-DTPA. T2- and T1-weighted SE images were obtained before injection, and a T1-weighted image was obtained after injection. All parameters were held constant for the two intraindividual contrast media applications. The evaluation criteria (delineation of the lesion, contrast between tumor and surrounding tissue, C/N between tumor and brain, percentage enhancement) were compared.
Results: The statistical analysis (Friedman test and Wilcoxon test) of the contrast-to noise ratios between tumor and white matter, the percentage enhancement, and the visual assessment rating revealed a statistically significant superiority of high-dose gadodiamide injection in comparison to the standard dose of Gd-DTPA ($P < .05$). For the major evaluation criterion (delineation of the lesion), high-dose gadodiamide injection was superior in 12 cases, equivalent in 33 cases, and negligible in 1 case.
Conclusion: The intraindividual comparison in 46 patients has shown that the use of high-dose gadodiamide injection results in a statistically significant improvement in the ability to diagnose lesions of the head and neck with MRI.

Tuesday Afternoon • Topaz Room
Papers 351–359

SPINE

MODERATORS: M Rothman, MD
BD Flannigan-Sprague, MD

351 • 3:45 PM

MR Imaging of Experimental Spinal Cord Radiation Injury

JD Hazle, NE Leeds, RE Price, KK Ang
M.D. Anderson Cancer Center, University of Texas, Houston, TX

Purpose: The spinal cord is a major dose-limiting normal tissue in radiation therapy. A simian model of cord damage has been developed for radiation therapy retreatment studies. Longitudinal MR images were obtained up to 2 years after different irradiation schemes. The goal of this work is to quantitate residual radiation injury and determine the mechanisms of injury.
Methods: Twelve retired breeder Rhesus monkeys (*Mucaca mulatta*) were included in the longitudinal study. Six animals each were included from groups initially receiving fractionated doses of 22 or 44 Gy, respectively. Total cumulative dose after reirradiation was 101.4 Gy. MRI studies were performed on a 1.5-T Signa whole-body imager. Either single 3-inch or dual 4-inch coil multicoil arrays were used. Imaging sequences included T1-weighted enhanced and unenhanced, proton-density, and T2-weighted imaging, diffusion-weighted imaging, and magnetization transfer imaging.
Results: The spinal cords of all 12 animals were consistent in their preirradiation MRI appearance. Gray/white matter signal pattern changes were noted in some animals after irradiation. Swelling and edema were prevalent in the animals that received the 44-Gy initial dose and after retreatment. Signal patterns consistent with previous findings in symptomatic animals were detected by using diffusion-weighted imaging before these patterns were observed with conventional techniques.
Conclusion: MRI can successfully demonstrate presymptomatic changes in the spinal cord of monkeys irradiated with doses of 44 Gy. Because of the phylogenic proximity of these animals to man, these results may be used to initiate clinical trials in humans.

352 • 3:57 PM

Spinal Bone Marrow MR Imaging: Comparison between T2-weighted Fast Spin-Echo Imaging with Fat Suppression and STIR

JK Tam, JE Jordan, LM Teresi, SK Goergen, MD Dubin, PJ Pema, WG Bradley, Jr
Memorial MR Center, Long Beach Memorial Medical Center, Long Beach, CA

Purpose: To compare the sensitivity of T2-weighted fast spin-echo imaging with fat suppression (FS-FSE) and short TI inversion recovery (STIR) in detecting bone marrow abnormalities, as an adjunct to T1-weighted imaging.
Methods: STIR and FS-FSE sequences were obtained in 15 patients with a variety of spinal lesions (trauma, neoplasm, degeneration, and other benign diseases) with a 1.5-T GE system. STIR parameters were TR 1400/TE 45/TI 140, 256 × 128, 28-cm FOV, 2 NEX; parameters for FS-FSE were TR 4,500/TE 102 Ef, 256 × 256, 28-cm FOV, 2 NEX with fat suppression. T1-weighted images (SE 500/20) were also ob-

tained. Conspicuity of lesions on FS-FSE and STIR images was subjectively rated. Quantitative lesion-to-background ratios were also measured.
Results: Fifty-seven lesions were identified on either T1-weighted, STIR, or FS-FSE images. Every lesion identified on STIR images was also seen on FS-FSE images. Forty-one (72%) lesions were more conspicuous with STIR, 9 (16%) lesions were better demonstrated with FS-FSE, and 7 (12.3%) lesions were equally conspicuous with FS-FSE and STIR. T1-weighted sequences depicted most lesions, but marrow heterogeneity in some patients led to decreased conspicuity of some lesions compared with that on STIR or FS-FSE images. Lesion-to-background ratios were also larger for STIR compared with FS-FSE (4.6 vs 2.8). The size of the lesions and the extent of marrow abnormality were not significantly different.
Conclusion: Although lesions are not as conspicuous with FS-FSE as with STIR sequences, FS-FSE is as sensitive as STIR for identifying and determining the extent of bone marrow abnormalities. FS-FSE with its shorter imaging time (2.5 minutes vs 7 minutes for STIR) can replace STIR in imaging of the spine to enhance bone marrow lesion detection as an adjunct to T1-weighted imaging.

353 • 4:09 PM
Comparison of FSE with MPGR in Diagnosing Metastases to the Spine
JF Norfray, PE Weinberg
Chicago Northside MRI Center, Chicago, IL
Purpose: To determine if fast spin-echo (FSE) T2 images can replace multiplanar gradient-recalled acquisition in the steady state (MPGR) T2 images in diagnosing metastases to the spine.
Methods: Thirty patients with proven cancer underwent spinal imaging to evaluate extent of disease, cord compression, and/or pathologic fractures before receiving radiation, chemotherapy, or surgical decompression. All patients were studied with SAG T1 = 500/11; SAG (FSE) T2 = 4,000/102, ETL = 16; SAG (MPGR ∝ 15) T2 = 450/11. Edema in marrow was accentuated by eliminating fat signal with opposed phase signal in MPGR and a presaturation frequency pulse in FSE. C/N was obtained in a single lesion in each patient to assess lesion detection. Thirty lesions were studied.
Results: Five lesions were not seen with FSE; all were seen with MPGR. One case of epidural spread of tumors was seen only with FSE; five epidural tumors were better seen with FSE. C/N was consistently better with MPGR than with FSE, except in five patients with previous radiation therapy to the spine.
Conclusions: MPGR should not be used in patients with previous radiation therapy to the spine because an increase in the yellow marrow effects chemical shift phase cancellation. FSE better depicted epidural spread of tumor because of edge enhancement. Five lesions were not seen with FSE because tumor in FSE has a progressive exponential loss of transverse magnetization and may become isointense with marrow. In MPGR, the tumor signal is maintained in the transverse plane by a steady state, which prevents an isointensity with marrow.

354 • 4:21 PM
Normal and Abnormal Enhancement of the Pediatric Spine after Administration of Single- and Triple-Dose Gadolinium
JK Tam, WG Bradley, Jr, SK Goergen, MD Dubin, PJ Pema, LM Teresi, JE Jordan
Memorial MR Center, Long Beach Memorial Medical Center, Long Beach, CA
Purpose: To assess the appearance of normal and abnormal nerve root and cord enhancement in the pediatric spine by using single- and triple-dose gadolinium.
Methods: The spinal cord of 5 normal and 7 abnormal children (including 5 with known medulloblastoma and suspected drop metastases) was evaluated prospectively. The patients ranged in age from 18 months to 18 years. All children were given 0.1 mmol/kg (single dose) gadolinium, imaged, given an additional dose of 0.2 mmol/kg Gd, and reimaged with a T1-weighted axial sequence. Two patients underwent 32-partition, 3D time-of-flight MR angiography (FISP 4/7/15°) with a 2.4-cm sagittal slab centered at the conus (to distinguish enhancing veins from drop metastases).
Results: Vascular enhancement related to the cord surface and emerging roots was observed in both normal and abnormal spines. This was more prominent in the lumbar than in the cervicothoracic region and was exaggerated by the administration of triple-dose contrast material. Nerve root enhancement, also more evident with triple-dose contrast material, was seen as a normal finding. Abnormal nerve root and pial enhancement was nodular in cases of drop metastasis and linear in patients who underwent radiation therapy, as well as in one case of Guillain-Barré syndrome.
Conclusion: Small veins on the surface of the spinal cord and nerve roots can normally enhance, particularly with triple-dose Gd. Degree of enhancement and nodularity must be assessed before diagnosis of pathology.

355 • 4:33 PM
MRI of Spinal Cysticercosis
AT Watanabe, CS Zee
Department of Neuroradiology, University of Southern California, Los Angeles, CA
Purpose: Neurocysticercosis involving the spinal canal and spinal cord is a relatively unusual manifestation of this disease. We present the clinical and magnetic resonance (MR) imaging findings in four patients with spinal cysticercosis.
Methods: Four patients with previously diagnosed intracranial cysticercosis underwent MR imaging of the entire spine. All of the patients had symptoms of back pain and/or myelopathy. All studies were performed with gadolinium and a 1.5-T magnet (Philips Gyroscan or General Electric Signa). The brain MR studies and clinical histories were also reviewed.
Results: Spinal cysts were identified in three cases. Some, but not all, cysts enhanced. Two patients had cord compression from the cysts with progressive quadraparesis. One of these patients eventually developed a syrinx. All of the patients had spinal meningeal enhancement. The results of biopsy of the enhancing tissue in one case revealed fibrous tissue with chronic inflammation and microcalcifications, consistent with cysticercosis. There was arachnoiditis, characterized by clumping of nerve roots, in two patients who had lumbar involvement. In all instances, there were intraventricular cysts in the basal cisterns. Surgical decompression prevented progression of symptoms in one patient. The other patient with cord compression refused surgical treatment and died a few days later from sepsis, presumably a disseminated systemic infection.
Conclusion: MR imaging of the spine appears to be the noninvasive modality of choice for diagnosing spinal cysticercosis. Spinal cysticercosis should be considered in patients with myelopathy, in the proper clinical setting. The intraventricular cysts most likely migrate into the spinal canal via the cerebrospinal fluid.

356 • 4:45 PM
Prediction of Outcome for Conservation Therapy of Lumbar Disk Extrusion with Gd-DTPA—enhanced MRI
JR Knorr, RL Ragland, DD Stark
Department of Radiology, University of Massachusetts Medical Center, Worcester, MA
Purpose: Laboratory studies of extrusion modeled by placing disk material in the epidural space of animals have shown a distinctive inflammatory response associated with phospholipase A_2 activity. Unlike simple herniation, extruded disk material has direct contact with epidural tissues. The potential relationship of laboratory phenomena to the clinical pain, neuropathy, and heterogeneous composition of epidural masses visualized with MRI or CT has not, to our knowledge, been previously investigated.
Methods: Imaging was performed at 0.3 and 1.5 T before and after infusion of Gd-DTPA (0.1 mmol/kg) within 1 week of

clinical signs or symptoms of extrusion and serially at 30-day intervals.
Results: Acute postextrusion images showed no difference between an epidural mass and the donor disk nuclear material. After infusion of Gd-DTPA, a central nonenhancing nidus of disk material was sharply delineated from the surrounding enhancing granulation tissue. Over intervals of 30–60 days after the acute event, the overall size of the complex epidural mass was observed to decrease. The central nidus of extruded disk decreased in size more rapidly than the surrounding inflammatory tissue. The end result of resorption of the disk material was a small focus of residual enhancing scar with significant diminution or complete resolution of disk fragment size.
Conclusion: Lumbar disk extrusion can be distinguished from disk herniation in the degree of inflammatory response provoked by the exposure of unencapsulated nuclear material to the immune system and circulating macrophages. Gd-DTPA–enhanced MRI aids in distinction of central avascularized disk material, which often comprises a minor fraction of the total epidural mass. A larger prospective series is being evaluated to further document the value of Gd-DTPA in defining lumbar disk extrusion as a medical, rather than surgical, disease.
1. Franson RC, et al. Spine 17(suppl 6), 1992, S129–32. 2. Fagerlund MKJ, et al. Acta Radiololgica 31 (1990) 555–58. 3. Ilkko E, et al. EJR 16 (1993) 186–189. 4. Bozzao A, et al. Radiology, 1992; 185:135–141.

357 • 4:57 PM

Metallic MRI Artifacts after Spinal Implants: In Vitro and in Vivo Quantification

P Vinée, G Weyrich, KH Hauenstein, G Sigmund, B Brunot, S Petkov, A Constantinesco
Laboratory of Biophysics and Nuclear Medicine, CHU Hautepierre, Strasbourg, France

Purpose: To evaluate the factors influencing the intensity of metallic artifacts in spinal implants.
Methods: Eighteen patients with vertebral fractures stabilized by internal spinal skeletal fixation systems were examined with MRI (at 0.23 and 2 T) after removal of the metallic spinal implants. Furthermore, in vitro studies were conducted to control the quantity of metal deposit.
Results: In every case, imaging artifacts in the paraspinal extensor muscles were evident on MR images. These were especially found in the region of the previous site of the metallic clip jaw bearing. In fewer cases, artifacts were also present within the vertebra or the vertebral arcus, but only if the vertebra had been surgically reconstructed by transpedicular spongiosa implantation. None or only minor artifacts of metallic rubbing were seen when the screws (modified from those of Schanz) had been intraoperatively stable. Evidence of augmented metallic rubbing on MR images therefore indicated a chronic straining of the implant site, which has been shown to be a risk factor for loosening of the implant. In vitro studies with pieces of metallic alloys showed that amounts of metal as small as 1 mg can be detected as artifacts with spin-echo sequences.
Conclusion: MR imaging is the method of choice for detection of amounts of metal as small as 1 mg. Artifacts due to augmented metallic rubbing indicate a chronic straining of the implant, a risk factor for loosening.

358 • 5:09 PM

MR Imaging during Treatment of Spinal Infection

WS Kubal, EO Thompson, RA Blinder
Department of Radiology, McGuire VA Medical Center and Medical College of Virginia, Richmond, VA

Purpose: MRI has become the study of choice in the diagnosis of spinal infection. We will demonstrate its utility during the treatment of spinal infection.
Methods: We present 16 MRI examinations obtained in 7 adult patients to follow treatment of documented spinal infection. MRI examinations, obtained with a 1.5-T Signa imager, consisted of T1-weighted, T2-weighted, and contrast-enhanced images in sagittal and/or axial planes.
Results: All infected intervertebral disk spaces showed abnormal signal intensity. These findings persisted after laboratory values had returned to normal and may reflect chronic inflammatory change. Vertebral body abnormalities included abnormal signal intensity and loss of definition of the end plates. As patients were successfully treated, definition of the end plates improved, but the signal intensity changes in the vertebral bodies tended to lag behind laboratory findings. Sequential examinations clearly delineated thecal sac compression due to epidural infection or bone deformity. The degree and level of compression correlated closely with neurologic dysfunction.
Conclusion: Our series catalogs changes in the MRI appearance of the spine and surrounding soft tissues during the treatment of spinal infection. Knowledge of these changes and their clinical correlates aids the radiologist in the assessment of treatment.
W.S. Kubal is a member of the Berlex Laboratories Speaker Panel.

359 • 5:21 PM

3D MR Myelography Compared with X-ray Myelography in Cases of Extreme Spinal Stenosis and Spondylolisthesis

KEW Eberhardt, HP Hollenbach, WJ Huk
Department of Neuroradiology, Neurosurgical Clinic, University of Erlangen, Erlangen, Germany

Purpose: In the present study, 3D MR myelography (3D-MRM) of the whole spine was compared with conventional x-ray myelography in cases of extreme canal stenosis and spondylolisthesis.
Methods: In 50 patients (15 patients with a complete contrast material blockage on conventional x-ray myelograms), we compared in a prospective case study the sensitivity of 3D-MRM with x-ray myelography of the whole spine. We compared the results of both methods with the intraoperative findings. The patients were examined with a 1.0-T whole-body MR system (Siemens Magnetom Impact). For the examination of the lumbar spine, a strongly $T2^*$-weighted 3D-FISP sequence (TR/TE/FA = 73 msec/21 msec/7°) with fat saturation was applied in the sagittal orientation with a circularly polarized oval spine coil. For the thoracic spine, the same coil and the same sequence (73/21/5°) with a magnetization transfer contrast prepulse were used. For the cervical spine, a Helmholtz neck coil and the same sequence as for the thoracic spine were applied. The spatial resolution was 1.56 × 1.17 × 1.40 mm. The 3D data sets were evaluated by using a maximum intensity projection program. The measurement time was 7 minutes 30 seconds.
Results: The diagnostic sensitivity for detecting nerve root compression syndromes in cases of extreme canal stenosis and spondylolisthesis was higher for 3D-MRM than for conventional x-ray myelography.
Conclusion: The MR technique has advantages in cases of canal stenosis and spondylolisthesis over conventional x-ray myelography and postmyelographic CT. The 3D-MRM could be the method of choice in cases of extreme canal stenosis with a contrast material blockage on the x-ray myelogram.

CARDIAC II: Coronary Imaging

MODERATORS: D Li, MS
JD Pearlman, MD, PhD

401 • 10:30 AM

Coronary Angiography with Magnetization-prepared T2 Contrast

JH Brittain, GA Wright, BS Hu, DG Nishimura
Information Systems Laboratory, Stanford University, Stanford, CA

Purpose: Coronary arteries reside on the surface of the myocardium and are often surrounded by fat. For these vessels to be visible, contrast must be developed between oxygenated blood, muscle, and fat. We propose a motion and flow insensitive magnetization-preparation sequence to provide muscle-suppressing T2 contrast. When combined with fat suppression, this T2 weighting allows visualization of the coronary arteries.
Methods: The preparation sequence consists of a nonselective 90°_x pulse followed by a train of equally spaced nonselective 180°_y pulses for increased immunity to B_0/B_1 inhomogeneity. At the echo of the final refocusing pulse, a nonselective 270°_x–360°_x pair robustly returns the T2-weighted magnetization to the longitudinal axis. Any residual transverse magnetization is then dephased by a large spoiling gradient. The T2-weighted M_z may be sampled with any excite/read combination. We utilize a spatial-spectral pulse, which suppresses fat while isolating the slice of interest, with a spiral readout. To avoid respiratory artifacts, the cardiac-gated sequence is completed within a breath-holding interval.
Results: Coronary images obtained with our preparation sequence demonstrate up to an eightfold increase in contrast-to-noise ratio for blood versus myocardium compared with images generated without magnetization preparation. Since the entire preparation sequence is nonselective, we observe no image degradation due to heart motion or flow.
Conclusion: A nonselective T2 magnetization-preparation sequence offers enhanced muscle/blood contrast with minimal flow or motion sensitivity. When augmented with fat suppression, this sequence provides effective visualization of the coronary arteries.

402 • 10:42 AM

Multislice Coronary Angiography within a Single Breath Hold

PA Wielopolski, JG Scharf, RR Edelman
Department of Radiology, MRI, Beth Israel Hospital, Boston, MA

Purpose: To improve the depiction of coronary vessels by using a multislice segmented technique within 1 breath hold.
Methods: Volunteer studies were performed with a 1.5-T Siemens Magnetom with an improved gradient system. By setting a maximum data acquisition window of 130 msec, several schemes were developed to collect 2–6 contiguous slices. For example, with an acquisition bandwidth of 195 Hz/pixel, 21 lines per heartbeat (which corresponded to 3 slices and 7 lines per segment) were acquired in an interleaved fashion (slice 1-line 1, slice 3-line 1, slice 2-line 1, slice 1-line 2, slice 3-line 2, slice 2-line 2, etc). The acquisition matrix was such that the data were always collected in 19 heartbeats. With higher acquisition bandwidths, more slices and/or higher acquisition matrices can be acquired. No flow compensation was used. Typical TEs ranged between 2 and 3 msec. Quadrature body and spine coils were used. Images were collected during diastole.
Results: With 3-mm-thick slices, the right coronary artery was visualized from its origin to the apex (typically 8 cm). Saturation effects for moving blood through the slices were not noticeable, and no signal loss from moving spins was seen even without motion compensation. Higher acquisition bandwidths provided a noisier image, although more slices could be acquired.
Conclusions: Multislice coverage with enhanced gradient systems makes it possible to image the whole coronary artery in a single breath hold. Nevertheless, higher acquisition bandwidths require better receiver coils to improve S/N.

403 • 10:54 AM

Hemodynamically Significant Coronary Artery Lesions Missed with MR Coronary Angiography

AJ Duerinckx, MK Urman
Radiology Service, MRI, Veterans Affairs Medical Center, West Los Angeles, Los Angeles, CA

Purpose: Noninvasive MR coronary angiographic techniques have recently become available, with a reported sensitivity and specificity for the detection of severe proximal coronary lesions (>50% angiographic stenosis) of 90% and 95%, respectively. We investigated whether hemodynamically significant lesions (>90% stenosis) can be missed with these techniques.
Methods: Fifteen patients who underwent elective coronary angiography were studied. Five of these patients had significant proximal right coronary artery (RCA) stenosis (>50%). We evaluated a noninvasive MR coronary angiographic technique that uses a fat-suppressed ECG-gated gradient-echo sequence with k-space segmentation on a 1.5-T imager (Magnetom SP, Siemens). Images were acquired during a single breath hold, with the patient lying prone on a surface coil. Slice thickness was 4 mm, field of view was 32 cm, and matrix size was 144 × 256. Images were acquired in middle to late diastole. Double oblique planes along the course of the right coronary artery and transaxial planes through the proximal left coronary system were used.
Results: The proximal and middle segments of the RCA were visualized in a caudal LAO-equivalent view. Branch vessels of the RCA were visualized in an LAO-equivalent view (by using a 2D plane tangential to the right atrioventricular groove). Many signal void artifacts were seen within normal RCAs. Five severe RCA lesions, including a 95% proximal RCA lesion, were not visualized on the MR coronary angiogram.
Conclusions: Noninvasive MR coronary angiography appears very promising but has important limitations. Improvements in technical factors will be needed before it can be generally used in patient screening.

404 • 11:06 AM

Breath-Hold Turbo Cine MRI for 4D Localization of Coronary Arteries

S Mukundan, Jr, JN Oshinski, RI Pettigrew
Department of Radiology, Emory University School of Medicine, Atlanta, GA

Purpose: Visualization of coronary arteries is complicated by respiratory and cardiac motion, vessel tortuosity, and flow pulsatility. Previous approaches to coronary MR imaging have not temporally optimized data acquisition. In this study, we used breath-hold turbo cine MRI to spatially and temporally (4D) localize coronary arteries for optimal diagnostic imaging.
Methods: Two or 3 transverse turbo gradient-echo images containing 8 cardiac phases were obtained at the aortic root. Images were acquired during a 12-second breath hold; 12 lines of k space were acquired for each cardiac phase per heartbeat. Images were acquired with a Philips Medical Systems 1.5-T imager with use of a body coil, a 128^2 matrix with 70% acquisition, and 250-mm FOV. High-resolution (256^2 matrix) oblique sagittal breath-hold turbo gradient-echo sequences were planned from the transverse cine images.
Results: The right and left coronary ostia were seen on the transverse cine images. A review of the images in cine mode allowed spatial localization of the coronaries at several points in the cardiac cycle. The cine method determined the time, on a patient-by-patient basis, when coronary flow is best visualized. The temporal information was used to determine the trigger delay and the data acquisition window for optimal visualization of the coronaries on the high-resolution images. Setup time for high-resolution images was also significantly reduced.
Conclusions: Breath-hold turbo cine imaging can provide

the patient-specific optimal trigger delay for coronary flow visualization and can aid in determining image geometry and in reducing setup time.

405 • 11:18 AM

Rapid Black-Blood Imaging of the Heart with Turbo Spin-Echo and Turbo Gradient Spin-Echo Techniques

OP Simonetti, B Kiefer, G Laub, H Flügel, JP Finn
MR Research and Development, Siemens Medical Systems, Iselin, NJ

Purpose: Cardiac-triggered spin-echo imaging of the thorax has become the standard MRI technique for visualization of cardiac and great vessel anatomy. However, multiple averages are required with this technique to reduce respiratory motion artifacts; this leads to excessive imaging time, particularly if multiphase, multislice information is required. The goal of this work is to develop turbo spin-echo (turboSE) and turbo gradient spin-echo (turboGSE) pulse sequences that maintain or increase black-blood contrast while achieving a significant reduction in imaging time.
Methods: Measurements were performed on a 1.0-T imaging system with 15 mT/m gradients. Several turboSE and turboGSE sequence design parameters were investigated, including echo train length, echo-echo spacing, effective TE, phase sensitivity to velocity, phase encode ordering, sampling bandwidth, and trigger delay time. TurboSE and turboGSE sequences with use of three to five readouts per 90° excitation pulse were developed with gradient waveforms designed to dephase blood flowing through the slice plane.
Results: In volunteer studies, fast black-blood images of the heart were obtained with contrast comparable to standard spin-echo acquisitions. Some blurring due to the acquisition of multiple data lines during each RR interval was observed; this effect was reduced by minimizing echo-echo spacing.
Conclusion: Rapid black-blood imaging of the heart can be performed by using turboSE and turboGSE techniques, which result in a three- to fivefold time savings over conventional spin-echo sequences.
O.P. Simonetti, B. Kiefer, G. Laub, and J.P. Finn are employees of Siemens Medical Systems.

406 • 11:30 AM

3D Coronary Artery Holograms Prepared with CUBE from Breath-Hold MRA

JD Pearlman, W Li, ML Chuang
Department of Radiology, Beth Israel Hospital, Boston, MA

Purpose: To achieve holographic 3D visualization of the human coronary artery tree noninvasively, on the basis of 3D image processing of breath-hold cardiac MRA.
Methods: Images were acquired with breath-hold segmented TurboFLASH sequence with variable tip angle on a 1.5-T Magnetom (Siemens). Different viewing angles were prescribed graphically for RCA, LCx, and LAD visualization, each covered as a stack of 6 overlapping 3-mm slices. Rather than identify coronary arteries, analysis focused on removal of blood pools that obstruct 3D visualization. This was achieved by using CUBE (UMS, Brookline, MA) software on a Sun Sparc2 workstation. The software is trained by one click of a mouse button to identify the blood pool throughout the 3D image stack. Another click previews the 3D result, and a third click exports the results for conversion by Voxel (Laguna Hills, CA) to a hologram.
Results: CUBE software successfully identified and removed obstructive blood pools (atria and ventricles) without hand tracing in all cases. The projective combination shows as much as 20 times more of the vascular tree than direct projection (MIP) without automated recognition and removal of overlay, and 2–8 times more than is captured on individual images in the absence of critical stenoses or severe narrowing. Individual images show areas of false stenosis due to nonplanar vessel position; these are corrected in the processed images and in the resultant hologram.
Conclusion: Removal of overlying atrioventricular blood-pool signal by automated analysis greatly improves visualization of the coronary artery tree obtained with noninvasive MRA. It also facilitates holographic viewing, which aids 3D visualization of the coronary tree and may play a useful role in training and in presenting data to patients.
J.D. Pearlman is the founder of UMS.

407 • 11:42 AM

Limitations of MR Coronary Angiography

AJ Duerinckx, MK Urman, DJ Atkinson, OP Simonetti, U Sinha, B Lewis
Radiology Service, MRI, Veterans Affairs Medical Center, West Los Angeles, Los Angeles, CA

Purpose: Noninvasive MR coronary angiographic techniques have recently become available. Difficulties in distinguishing artifacts from real lesions limit the clinical utility of these techniques. The limitations of one of the MR coronary angiographic techniques were evaluated.
Methods: Forty-four subjects, including 15 patients who underwent elective coronary angiography, were studied. We evaluated a noninvasive MR coronary angiographic technique that uses a fat-suppressed, ECG-gated, gradient-echo sequence with k-space segmentation on a 1.5-T imager (Magnetom SP, Siemens). Images were acquired during a single breath hold with the patient lying prone on a surface coil. Double oblique planes along the course of the right coronary artery and transaxial planes through the proximal left coronary system were used.
Results: We measured the length of each coronary vessel as seen in a subgroup of 15 subjects. The average lengths of coronary arteries that were clearly visualized were 78.4 mm for the right coronary artery, 13.9 mm for the left main, 54.9 mm for the left anterior descending, and 14.7 for the circumflex. Branch vessels were seldom visualized, except for the right coronary artery branches. The proximal circumflex coronary artery was very poorly visualized. Fat suppression was inadequate in 13% of patients. Many signal void artifacts were seen within normal coronary arteries. Oblique imaging through the left proximal coronary system made evaluation of those vessels difficult.
Conclusions: Noninvasive MR coronary angiography appears very promising but has certain limitations. Improvements in the selection of imaging planes and technical factors will be required before it can be generally used in patient screening.
D.J. Atkinson and O.P. Simonetti are employees of Siemens Medical Systems.

Wednesday Morning • Metropolitan Room
Papers 411–417

MR ANGIOGRAPHY I: Neuro

MODERATORS: C Dumoulin, PhD
KR Maravilla, MD

411 • 10:30 AM

Dynamic MR Angiography with STAR Sequences

RR Edelman, M Kennedy, M Nissenbaum, B Sievert, P Wielopolski
Department of Radiology, Beth Israel Hospital, Boston, MA

Purpose: We describe an MRA method for bright- or dark-blood imaging, called STAR (signal targeting with alternating radio frequency). The method consists of a preparation phase, during which the longitudinal magnetization of the target tissue is inverted at alternate acquisitions, followed by a readout phase with a cine segmented TurboFLASH sequence. Complex subtraction cancels background signals.
Methods: A cine segmented TurboFLASH sequence was used with TR/TE/flip angle = 13 msec/2.5 or 7 msec/20°, 7–10 lines per segment, section thickness = 25 or 5 mm for bright- or dark-blood MRA, respectively. For bright-blood MRA, a 90-mm preinversion of the inflowing blood was applied, and

the imaging volume was presaturated. The method was applied to the circle of Willis, carotid bifurcation, and renal arteries in volunteers and patients.
Results: Essentially perfect background suppression was obtained. A remarkable degree of vascular detail and coverage was obtained in a single section. For instance, the entire length of the renal artery including first order, and sometimes second order, intrarenal branches was routinely visualized on a single breath-hold image. The cine acquisition gave a dynamic display of flow patterns within the vessel. No vascular signal intensity was present on black-blood images.
Conclusions: The STAR method has ideal features for MRA: (*a*) extensive vascular coverage in a single section, (*b*) no partial volume averaging, and (*c*) dynamic flow patterns are shown. The method overcomes many of the current limitations of MRA and could be particularly useful for carotid and renal artery imaging.

412 • 10:42 AM
Time-of-Flight MR Angiography of the Head Improved with Optimized Magnetization Transfer Technique in Clinical Situations
J Mao, JJ Steinbach
Department of Radiology, University of Florida, Gainesville, FL

Purpose: To find an optimized MT technique for time-of-flight MR angiography of the head in clinical situations and to qualitatively comprehend this technique.
Methods: Optimized 180° frequency selective pulses were used at the front of a 3D FISP time-of-flight sequence to transfer magnetization more efficiently compared with a conventional Gaussian pulse in a commercial system. One single optimized pulse may not deliver enough power to transfer the possibly transferable magnetization under the limitation of the SAR: 8 W/kg. Two optimized pulses were used. The length of the Gaussian pulse is 8.192 msec. The length of each optimized pulse is 4.096 msec. Other parameters were the same. Two pulses have three frequency shift combinations: both pulses are one-side shifted (both are positively shifted and both are negatively shifted); and one is positively shifted while another is negatively shifted (hybrid shifted). Images were compared for these combinations in clinical situations.
Results: The signal intensity of head angiograms obtained by means of the optimized pulses is about 8% less than that obtained with the Gaussian pulse, while the signal intensity of stationary phantom water obtained with the optimized pulse is about 4% high than that obtained with the Gaussian pulse. The angiogram after MIP shows more details for small vessels by using the optimized pulses. The signal intensity obtained with the hybrid shifted pulses is about 5% less than that obtained with one-side shifted pulses.
Conclusion: Main magnetic field may not be well shimmed in clinical situations because of imaging time limitation, and thus the free water proton line width is inhomogeneously broadened. The magnetization transfer effect is stronger with hybrid shifted pulses, which can be explained by the broadened line-width and the exponential-like relation between the delivered power and the transfered magnetization. It is expected that hybrid shifted pulses perform better at higher field strength.

413 • 10:54 AM
Magnetization Transfer Angiography Compared with Postprocessing Background Suppression
M Kouwenhoven, L Holland, A van Muiswinkel
MR Clinical Science, Philips Medical Systems, Best, The Netherlands

Purpose: Magnetization transfer angiography has proved to be effective in suppressing static tissues such as white and gray matter, thus increasing the contrast for blood vessels in the head. Postprocessing of the original slices (before MIP) has also allowed effective suppression of the static tissues, which becomes apparent in the MIP. Both techniques are helpful in improving small vessel conspicuity.
Methods: Postprocessing background suppression involves several steps: (*a*) clipping of the signal of the original data above a certain level, (*b*) low-pass filtering of the remainder, and (*c*) adding the clipped data to the low-pass filtered data. The resultant image will still contain all blood vessels, but the signal intensity of the stationary tissue will be greatly reduced. Because there is local variation in the signal intensity of the background, this background suppression technique is effective in better visualizing small vessels in the MIP. Magnetization transfer angiography was performed in the head, with off-resonance RF pulses, with a duration of 15 msec and a flip angle of 600° (for 1.5 T) or 1,000° (for 0.5 T).
Results: Results show that both MTC and postprocessing background suppression are effective in enhancing small vessel conspicuity.
Conclusions: The techniques can be combined, but each is more effective if used alone. The advantage of using postprocessing background suppression without using MTC is that the imaging time is not increased by the longer TR needed for MTC. However, in most cases, MTC is superior in enhancing small vessel contrast.
M. Kouwenhoven is an employee of Philips Medical Systems.

414 • 11:06 AM
Reduction of the Venetian Blind Artifact in Sequential 3D TOF Carotid MR Angiography: Acquisition and Postprocessing
X Ding, JA Tkach, PM Ruggieri, TJ Masaryk
Cleveland Clinic Foundation, Cleveland, OH

Purpose: The MIP images from multiple overlapping 3D TOF MRA acquisitions exhibit the venetian blind artifact in regions of overlap, due to the nonuniform signal intensity caused by spin saturation and inadequate postprocessing. The purpose of this study was to incorporate spatially variable RF pulses (TONE) in the multislab acquisition and to develop a new postprocessing technique for reducing the artifact.
Methods: Ten normal volunteers underwent carotid MRA studies that were performed with a 1-T Siemens whole-body imager. Three transverse overlapping volumes were acquired by using a 3D RF spoiled gradient-echo sequence. Sinc and TONE pulses were tested at flip angles of 20°, 25°, and 30°. The images in the overlapping regions were combined either by a new method of taking the higher intensity of the pair on a pixel-by-pixel basis or manually. The MIP images were evaluated by visual inspection as well as by computing the standard deviation along a profile through the vessels.
Results: Compared with the sinc pulse acquisition, the TONE acquisition improved vessel contrast and signal uniformity and allowed a smaller percentage of overlap to be used. The improvement in MIP image quality with the new postprocessing technique was appreciably greater than that obtained through optimization of the acquisition parameters alone.
Conclusion: The venetian blind artifact in multislab 3D MRA acquisitions can be appreciably reduced by the use of TONE RF pulses in combination with a technique of optimally combining the data in regions of overlap.

415 • 11:18 AM
High-Resolution MR Angiographic Evaluation of Heterotopic Pancreatic Transplants
TL Krebs, BD Daly, CC Chow, S Pomerantz, ST Bartlett, EJ Schweitzer, DM Geehan
Department of Diagnostic Radiology, University of Maryland, Baltimore, MD

Purpose: Pancreatic transplantation is being performed more frequently in the treatment of type 1 diabetes mellitus. The rate of success of the procedure is increasing, but significant postprocedural complications remain. Common causes of dysfunction include rejection, ischemia, pancreatitis, and sepsis. Clinical assessment of the allograft remains difficult, hence, the utility of imaging. We designed a study to examine the usefulness of 2D time-of-flight imaging in the MR evaluation of the pancreatic transplant by using a phased-array surface coil.
Methods: With a 1.5-T GE Signa, 10 MR studies were per-

formed (2 days to 6 months after surgery) in 6 patients who underwent simultaneous kidney and pancreatic transplantation. All patients were studied with a phased-array surface coil by using the following sequences: T1 and T2 fast spin echo, fast multiplanar spoiled GRASS (FMPSPGR) Gd-DTPA–enhanced dynamic perfusion, and 2D time-of-flight imaging. Two-dimensional time-of-flight images were acquired in axial planes before contrast material injection. Correlation with results of serum and urinary amylase levels, percutaneous biopsy, and, in some cases, surgical exploration was made.
Results: Two of the 6 patients were found to have partial or total thrombosis of the pancreatic transplant graft vessels, which correlated well with surgical findings. The other 4 patients were found to have patent vessels.
Conclusion: High-resolution imaging of the transplanted pancreas greatly improved interpretive ability. The two cases of vascular thrombosis were diagnosed because of the enhanced capability of following the course of transplanted vessels. Time-of-flight imaging greatly aided in this interpretation.

416 • 11:30 AM
MR Angiographic Evaluation of Symptomatic Vertebrobasilar Stenosis
PM Ruggieri, JS Ross, MT Modic, N Obuchowski, R Zepp, JP Hanna, AJ Furlan, TJ Masaryk
MRI/Radiology Department, Cleveland Clinic Foundation, Cleveland, OH

Purpose: MRA is rapidly replacing transcranial ultrasound for the screening of posterior fossa vasoocclusive disease. Our purpose was to compare 3D TOF MRA with intraarterial digital subtraction angiography (IADSA) in the evaluation of the distal vertebral and basilar arteries in patients with symptoms of vertebrobasilar insufficiency.
Methods: We performed spin-echo imaging of the head and single-volume 3D TOF MRA (TR 40/TE 6.5/FA 20/0.9 mm/16-cm FOV/magnetization transfer saturation) of the posterior fossa in each of 22 patients. MR angiograms were reformatted with a conventional MIP algorithm. All patients also underwent high-resolution IADSA of the posterior circulation in the AP and lateral projections. Images were blindly evaluated by 3 neuroradiologists and were rated for technical quality, degree and length of stenosis, level of confidence, patency of vessels with spin-echo criteria, presence of distal infarcts, and final diagnoses.
Results: We were able to individually compare 53 vessels in the 22 patients. This group included 30 vessels with atherosclerotic disease, 8 dissections, 3 vessels with vasculitis, and 11 normal vessels. By using "possibly normal/abnormal" ratings as a cutoff, we found a sensitivity of approximately 90% and specificity of 75%. The stenoses were over- and undergraded in similar percentages. If a rating within one degree of severity is considered acceptable, the number of disagreements was reduced by approximately 65%. Errors were most frequent in the evaluation of the vertebral arteries. If the basilar trunk was solely evaluated and a difference in one degree is acceptable, no errors were found among any of the readers.
Conclusions: 3D TOF MRA is a highly sensitive means of evaluating large vessel occlusive disease in the posterior fossa and can likely replace transcranial Doppler ultrasound in the screening of patients with vertebrobasilar ischemic symptoms. The basilar trunk was more accurately evaluated with MRA, likely due to its larger size.

417 • 11:42 AM
Role of MRA in the Evaluation of Patients with Ischemic Cerebrovascular Disease
RG Bhatia, AR Gillams, AP Carter
BCH Center for MRI, Boston University Medical School, Boston, MA

Purpose: MRA provides the opportunity to study the vascular anatomy in patients who would be considered at too high risk for conventional angiography. With the advent of new treatment regimes for acute stroke, the ability to accurately delineate the vascular as well as the parenchymal lesion is of increasing importance.
Methods: All patients with cerebrovascular ischemia who underwent MRI and MRA of the carotid vessels and intracranial circulation (ICC) were included in the study. The MR images were evaluated for cortical stroke or lacunar infarction, and the age of the stroke was estimated from the clinical presentation, presence or absence of edema, or enhancement with gadolinium.
Results: There were 23 patients (15 men, 8 women; mean age, 56 years; age range, 32–92 years) with 31 ischemic lesions. All patients underwent 2D time-of-flight imaging of the neck vessels, 13 underwent phase-contrast MRA, and 10 underwent 3D time-of-flight imaging of the ICC. There were 9 cortical infarcts, 8 of which were acute, and causal MRA lesions were seen in all 8. There was 1 old cortical infarct with an intact ICC. In 3 of 9, there was proximal atherosclerotic disease. There were 22 lacunar infarcts; 6 of 22 had evidence of vascular disease in the major neck vessels that corresponded to the affected vascular territory. In 5 of 22, the MR angiogram showed unrelated atherosclerotic disease in the proximal circulation. In 11 patients with lacunar infarction, the MR angiogram was completely normal.
Conclusion: MRA demonstrated a causal lesion in all patients with acute cortical infarction, and in 6 of 8, this was an isolated lesion. Further in nearly 1 of 3 of patients with lacunar infarction, a causal proximal atherosclerotic lesion was identified.

Wednesday Morning • Miro Room
Papers 421–427

MUSCULOSKELETAL II
MODERATORS: JB Kneeland, MD
S Majumdar, PhD

421 • 10:30 AM
MRI Evaluation of Aggressive Fibromatosis before and after Radiation Therapy
PT Weatherall, GE Maale, DE Schwarz, HR Pascoe
Rogers MR Center, University of Texas Southwestern Medical Center, Dallas, TX

Purpose: To characterize the postirradiation MRI appearance of fibromatosis to determine whether the observed decrease in signal intensity corresponds with complete regression.
Methods: We used serial MRI to evaluate 15 patients, aged 2–56 years (median age, 26 years) with extraabdominal aggressive fibromatosis who were treated with 5,000 cGy of radiation. Examinations were performed with magnets from 0.3 to 1.5 T, by using T1, T2, and STIR (short TI inversion recovery) techniques in each case. Fourteen patients were followed up for at least 12 months with MRI (median follow-up, 22 months) and clinically (median follow-up, 31 months). This assessment is retrospective.
Results: Preirradiation characteristics included prominent heterogeneity (93%), ill-defined margins (67%), multicompartment involvement (93%), and predominantly increased or equal signal intensity relative to muscle on T1 and STIR images (84%). Sizable zones of decreased signal intensity were seen in 33% of these studies. The T2 images demonstrated marked heterogeneity. The dominant signal intensity was less than that of fat but greater than that of muscle in 43% and equal to or greater than that of fat in 50%. The postirradiation appearance was more well defined (86%), and 8 of 14 markedly decreased in size. Seven of these 8 had corresponding marked decrease in signal intensity of greater than 2 points on a 5-point (−2 to 2+) scale, whereas 3 of 4 that enlarged had persistent increased signal intensity. These 2 exceptions were in early follow-up periods. The most useful discriminator was STIR, with only 2 size/signal "discrepancies," both relating to extension of tumor beyond radiation port margins. There has been no progression in the other patients.

Conclusion: MRI of aggressive fibromatosis provided accurate localization of the tumor margin for subsequent irradiation and allowed monitoring of complete and incomplete response to therapy. Marked decrease in signal intensity within 6–9 months corresponds to a positive response.

422 • 10:42 AM

MR Features of Glomus Tumor of the Finger with a Dedicated 0.1-T Imager

P Vinee, S Ravier, P Germain, G Foucher, B Brunot, A Constantinesco
Laboratory of Biophysics and Nuclear Medicine, CHU Hautepierre, Strasbourg, France

Purpose: To report the low-field-strength MRI characteristics of glomus tumors in fingers and to discuss the interest of dedicated MR imagers for use in detecting small tumors of the hand.
Methods: Five patients with suspected glomus tumors of the fingers were examined with a custom-made MR system dedicated to hand and wrist imaging, with a vertical low field strength (0.1 T) provided by a water-cooled electromagnet with an air gap of 18 cm. Specific solenoidal coils for finger imaging with different diameters (20–40 mm) according to finger anatomy were used. All the examinations consisted of sagittal, axial, and frontal 3D-T1W (GE 90°/12/200, NEX = 2) and 3D-T2W (SHARE 100/2,000, NEX = 2) imaging sequences. Mean examination time was 30 minutes.
Results: All tumors exhibited low (3 patients) or absent (2 patients) signal intensity on T1W images (FOV ranged from 20 to 30 mm, allowing a pixel resolution as high as 300 × 300 μm). T2W images showed a homogeneous high signal intensity in all 5 patients. Histologic confirmation of glomus tumor was obtained in every case after surgery.
Conclusion: Accurate detection of small glomus tumors can be achieved at low field strength by using a dedicated MR imaging system that provides high-resolution images of the fingers with reasonable acquisition time and without any patient discomfort.

423 • 10:54 AM

Quantitative Bone Marrow MR Imaging in Healthy Individuals: Age- and Sex-related Variations in ^{1}H-CSI Data

K Jarosch, S Heiland, G Brix, W Semmler, MV Knopp, G van Kaick
Research Program "Radiological Diagnostics and Therapy," German Cancer Research Center, Heidelberg, Germany

Purpose: To establish and quantify the physiologic distribution and functional dependencies of the relative fat signal fraction (r_{Fat}) of normal bone marrow by using a proton chemical shift imaging (^{1}H-CSI) method.
Method: The bone marrow (L-2–L-5, pelvis, and head, neck, and shaft of the femur) was examined in standardized, user-defined regions of interest (ROIs) in 66 healthy individuals (34 women: age range, 19–69 years; 32 men: age range, 21–70 years) with a ^{1}H-CSI technique according to Dixon (SE 1,200/22), with modified postprocessing for evaluation of r_{Fat}. Subcutaneous fat served as a reference region. Examinations were performed on a Magnetom SP (Siemens, Erlangen, Germany) 1.5-T whole-body MR system.
Results: ^{1}H-CSI data revealed that in the regions examined, there was a more prominent age dependence of r_{Fat} in the female study group. In younger women, r_{Fat} was up to 14% lower, with respect to the corresponding age-matched ROIs in men. The most notable age-related r_{Fat} changes were observed in the lumbar vertebrae of women, with an increase of nearly 0.8% per year. The femoral head did not show any significant age or sex variations for r_{Fat}. In old subjects, r_{Fat} values—independent of bone marrow area and sex—were nearly identical to r_{Fat} of subcutaneous fat.
Conclusion: ^{1}H-CSI data reflect the physiologic age- and sex-dependent activation of cellular bone marrow and its conversion to fatty marrow with advancing age. The knowledge of these dependencies is a prerequisite for applying ^{1}H-CSI for diagnosis and therapy monitoring of infiltrative bone marrow diseases.

424 • 11:06 AM

MRI of the Injured and Persistently Painful Ankle

JD Reeder, S Gordon, L Goldstein
Whitesquare Imaging, Baltimore, MD

Purpose: This study was designed to investigate the nature and clinical significance of MRI findings in patients experiencing persistent pain after an ankle injury.
Methods: MR images of 67 patients, consecutively referred for persistent pain after ankle injury, were reviewed. The time interval between injury and imaging varied from approximately 2 weeks to 1 year. Patients with Achilles tendon injuries or radiographically apparent fractures were excluded from the study. The examinations were performed on 1- or 1.5-T systems. Routine imaging parameters included sagittal and coronal short TE/TR acquisitions and a dual-echo long TR axial sequence.
Results: Transchondral injuries were observed in 12 of the 67 patients (18%). Ten of these lesions involved the talus and 2 involved the distal tibia. Three of these patients required surgery. A bone bruise involving the talus was observed in 9 patients (13%). An ankle joint effusion was identified in 36 patients, and abnormal signal intensity was detected within the sinus tarsi in 11 patients (16%). Anterior talofibular ligament injuries were detected in 23 patients (34%), and calcaneofibular ligament injuries were detected in 10 patients (14%). Tibialis posterior tendon abnormalities were observed in 6 patients, and peroneous tendon injuries were observed in 4 patients (1 of these patients required surgery).
Conclusion: MRI provides a means to detect clinically significant pathology and to discriminate soft-tissue from osseous injury in patients experiencing persistent pain after ankle trauma. Identification of transchondral fractures and tendon tears affects patient selection for surgical management.

425 • 11:18 AM

MRI Appearance of Meniscal Cysts

LL Tyson, TC Daughters, RKU Ryu, JV Crues III
Department of Radiology, University of Utah Medical Center, Salt Lake City, Utah

Purpose: To establish precise criteria for the diagnosis of meniscal cysts with MRI, so that they may be distinguished from other lesions that mimic meniscal cysts, and appropriate treatment may be planned.
Methods: We performed a retrospective review of 62 knee MR images with a possible finding of meniscal cysts. The type of meniscal tear associated with the cyst was noted, and the appearance of the connection between the cyst and the meniscal tear was described. The location, size, morphology, and signal characteristics of the meniscal cysts were recorded. Other types of fluid collections that had been mistaken for meniscal cysts were described.
Results: Meniscal cysts were most commonly associated with tears of the anterior horn of the lateral meniscus (49%), followed by the posterior horn of the medial meniscus (29%). Horizontal cleavage tears were present in most cases (98%). Most of the meniscal cysts (91%) occurred immediately adjacent to the meniscal tear, with the tear leading directly into the cyst. In two cases, the cyst had dissected into the soft tissues distant from the meniscus, and a connecting stalk was visualized. Fluid collections in normal bursa and recesses that had been mistaken for meniscal cysts had no direct connection to a meniscal tear.
Conclusion: MRI can be used to distinguish meniscal cysts from other fluid collections that may mimic meniscal cysts. Pitfalls can be avoided through familiarity with the normal bursal and capsular anatomy and by the application of specific diagnostic criteria.

426 • 11:30 AM

MR Imaging of Knee Abnormalities with an MTC 3D GRASS Pulse Sequence: Comparison with an IR-FSE Pulse Sequence

FG Shellock, E Schneider, J Mink, A Deutsch, S Hinks
Tower Imaging, Los Angeles, CA

Purpose: IR-FSE images of the knee are useful for identifying joint fluid, cartilaginous lesions, bone contusions, and marrow changes. An MTC pulse sequence improves contrast in GRE imaging; however, it is presently unknown whether this sequence can aid in detection of various abnormalities that may be encountered during MRI of the knee. Therefore, MTC 3D GRASS images were compared with IR-FSE images for the ability to identify the aforementioned findings.
Methods: Knee MRI was performed in 38 knees by using MTC 3D GRASS (15° flip angle, 60/15 TR/TE, MT pulse length of 14 msec, 1.2 kHz off resonance, 1.5-mm slices) and IR-FSE (2,800/130/35, 4-mm slices) sequences to obtain axial plane images. MTC 3D GRASS images were compared with IR-FSE images obtained at the same section locations with respect to showing joint fluid, cartilaginous lesions, bone contusions, or marrow changes.
Results: MTC 3D GRASS images showed areas of joint fluid and cartilaginous lesions similar to those on IR-FSE images but did not show bone contusions or marrow changes.
Conclusions: MTC 3D GRASS images were not useful for showing bone contusions or marrow changes. However, the higher spatial resolution afforded by the thin-slice MTC images and good delineation between fluid and cartilage suggest that this sequence would be more advantageous for characterizing cartilaginous defects than would the IR-FSE images.
E. Schneider and S. Hinks are employees of GE Medical Systems.

427 • 11:42 AM

Evaluation of Internal Derangement of the Knee with a New 3D Gradient-Echo Sequence: Potential for a One-Sequence Knee Examination

MP Recht, D Piraino, J Schils, BJ Richmond, GH Belhobek, N Obuchowski
Cleveland Clinic Foundation, Cleveland, OH

Purpose: To determine if a newly developed 3D gradient-echo sequence (DESS) that acquires and combines both the FID and spin echo (SE) created from one RF pulse into a single image has the potential to replace SE sequences in the evaluation of internal derangement of the knee.
Methods: Twenty-five knees examined for internal derangement were imaged by using the DESS sequence. DESS images were reconstructed in both sagittal and coronal planes as 3-mm contiguous sections. T1-weighted coronal and T1- and T2-weighted sagittal SE images were also acquired. The images were read by 3 radiologists in a blinded fashion. Arthroscopy was performed in 14 knees.
Results: Acquisition time was 8:24 minutes for DESS and 15:44 minutes for the SE sequences. Diagnostic accuracy for meniscal, ligamentous, and chondral abnormalities were equal, as determined by ROC analysis for 2 readers. One reader was more accurate with DESS for chondral abnormalities and with SE for ligamentous abnormalities.
Conclusions: The diagnostic accuracy of DESS and SE sequences was equal for internal derangement of the knee. If confirmed in a larger clinical study now under way, the advantage of the multiplanar reconstructive capability of DESS, and thus increased time efficiency, should lead to its replacing SE sequences for the evaluation of internal derangement of the knee.

Wednesday Morning • Morrocco Room
Papers 431–437

IMAGING TECHNIQUES II

MODERATORS: K Butts, PhD
EM Haacke, PhD

431 • 10:30 AM

Simultaneous Temporal Resolution of Cardiac and Respiratory Motion

JO Fredrickson, H Wegmueller, RJ Herfkens, NJ Pelc
Radiologic Sciences Laboratory, Stanford University, Stanford, CA

Purpose: In time-resolved MR imaging of motion and flow throughout the cardiac cycle, the effects of respiration are masked, since respiratory motion is usually suspended, suppressed, or ignored. We have developed a method that permits simultaneous resolution of both the cardiac and respiratory cycles to study the effects of both under the more physiologic condition of normal breathing.
Methods: A cine phase contrast sequence that provides temporal resolution of the cardiac cycle was modified to simultaneously resolve the respiratory cycle by the addition of TRIADS (time-resolved imaging by automatic data segmentation). TRIADS automatically sorts the data into a (user-specified) number of temporal frames of the respiratory cycle and provides motion compensation within each frame. At the beginning of each cardiac cycle, TRIADS determines a phase-encoding amplitude to apply on the basis of the position within the respiratory cycle. Data acquired with this sequence were compared with regular cine acquisitions with identical imaging parameters and respiratory compensation, in normal volunteers.
Results: When the heart is imaged, motion due to cardiac dynamics can be separated from the respiration-induced excursion of the inferior wall of the heart (~ 1.5 cm). In the portal vein, changes in flow rate can be three times greater due to respiratory effects compared with cardiac pulsatility. Compared with the respiratory-compensated image, resolution is improved because of reduced motion blurring and artifacts.
Conclusions: Simultaneously resolving cardiac and respiratory cycles produces a more physiologic view of the effects of both in normal and pathologic states.

432 • 10:42 AM

Initial Clinical Experience with an Optimized Fast FLAIR Pulse Sequence

JN Rydberg, CA Hammond, RC Grimm, BJ Erickson, CR Jack, J Huston III, SJ Riederer
MR Laboratory, Mayo Clinic, Rochester, MN

Purpose: Fluid-attenuated inversion recovery (FLAIR) has been demonstrated at 1.0 T and recently for multiple sclerosis (MS) at 1.5 T. The purpose of this study was to optimize a FLAIR sequence and to evaluate additional pathologies at 1.5 T.
Methods: The fast FLAIR (fFLAIR) sequence was improved over original FLAIR in 3 ways. First, fFLAIR used a RARE readout (16 echoes per excitation pulse). Second, use of 2 interleaved inversion-readout groups per TR (9 sections per group) reduced time wasted for longitudinal magnetization recovery. Finally, fFLAIR's phase-encoding technique alternated echoes (1 and 16, 2 and 15, ..., 8 and 9) to minimize flow artifacts. Twenty-one patients (MS [n = 5], small vessel disease [n = 6], infarction [n = 9], and inflammation [n = 1]) were imaged by using fFLAIR (TI/effTE/TR = 2,600/145/1,1000 msec). Up to 36 slices (slice thickness/gap = 4/1 or 5/0) were acquired in 5:08 minutes and were compared with T2-weighted spin-echo (T2SE) images (TE/TR = 30,80/2,250–2,500 msec). Both sequences had 192 × 256 resolution, and one signal acquisition.
Results: Because of the removal of CSF signal intensity, fFLAIR increased lesion conspicuity in 20 of 21 cases and was equivalent to T2SE in the remaining case. In the patient with an inflammatory process, fFLAIR displayed 2 areas of high signal intensity not readily visible with T2SE. Even in

areas of high velocity flow, CSF pulsation did not compromise image interpretation.
Conclusion: With fFLAIR, an entire head can be imaged in approximately 5 minutes, with improved lesion conspicuity. We conclude that fFLAIR shows great promise and should be tested in additional pathologies.

433 • 10:54 AM

CSF-suppressed T2-weighted 3D MP-RAGE: A Sequence for the Detection of White Matter Disease

FH Epstein, JP Mugler, III, WS Cail, JR Brookeman
MRI Facility, Department of Radiology, University of Virginia, Charlottesville, VA

Purpose: To develop a three-dimensional (3D) CSF-suppressed T2-weighted pulse sequence capable of imaging the entire brain in under 10 minutes. This technique, which combines contrast similar to the FLAIR pulse sequence (1) with the coverage of a 3D gradient-echo pulse sequence, is intended for the detection of white matter disease.
Methods: CSF-suppressed T2-weighted 3D MP-RAGE was implemented on a 1.5-T whole-body imager (Magnetom 63SP, Siemens Medical Systems, Iselin, NJ) as follows: The magnetization preparation consisted of a 180° BIR-4 RF pulse and a 3,000 msec inversion time for CSF suppression, followed by a 90°-TE/2-180°-TE/2-90° BIR-4 driven equilibrium pulse set for T2 weighting. The gradient-echo acquisition utilized a spoiled gradient structure, a low flip angle ($< 10°$), and centric phase encoding. Finally, a 4,000 msec recovery time was inserted subsequent to the gradient-echo acquisition. These pulse sequence parameters were chosen by using a theoretical model.
Results: With use of a 128 × 256 matrix and 64 3D sections, coverage of the entire head was achieved in under 10 minutes. In healthy volunteers, the resulting images displayed excellent CSF suppression and moderate gray matter–white matter differentiation. Preliminary experience with MS patients has shown that this technique is very sensitive to white matter disease and appears particularly advantageous for the detection of periventricular lesions.
Conclusions: The proposed pulse sequence achieved the desired CSF-suppressed T2-weighted contrast combined with the excellent coverage of a 3D technique. Future work entails refinement of pulse sequence parameter values and further clinical evaluation.
1. De Coene B, Hajnal JV, Pennock JM, Bydder GM. MRI of the Brain Stem Using Fluid Attenuated Inversion Recovery Pulse Sequences. Neuroradiology 1993; 35:327–331.

434 • 11:06 AM

Modified TurboSTIR: Improved Conspicuity and Anatomic Detail

MP Recht, D Piraino, P Hardy, BJ Richmond, J Schils, GH Belhobek
Cleveland Clinic Foundation, Cleveland, OH

Purpose: Short inversion time inversion-recovery (STIR) imaging has been found to be sensitive in depicting abnormalities in the musculoskeletal system. However, its long imaging time and low signal to noise have limited its clinical acceptance. To reduce these problems while maintaining high sensitivity to pathology, a double-echo TurboSTIR sequence was modified by combining the images from the early and late echoes.
Methods: A TurboSTIR sequence that produced images with TE = 20 and 90 msec was performed in 10 patients with various musculoskeletal abnormalities. The resultant images were then combined in various ways to find an improved image by combining the anatomic detail of the first echo and the sensitivity to pathology of the second echo. Images were combined with levels of thresholding varying upward from zero. Contrast between fluid, muscle, fat, and bone marrow was quantitatively compared on all images. The images were also reviewed subjectively by two musculoskeletal radiologists for conspicuity of fluid and/or pathology.
Results: The combination of the short and long TE images improved the contrast of the short TE image by a factor of two, while maintaining its anatomic detail. The optimum contrast-to-noise ratios of fluid–bone marrow and fluid-muscle were produced by thresholding the second echo image to eliminate all signal except that of fluid.
Conclusion: The modified TurboSTIR sequence maintains the high sensitivity of STIR sequences while allowing better anatomic detail and shorter imaging time. A larger clinical study is warranted to assess the clinical utility of this sequence.

435 • 11:18 AM

Contrast Optimization in MR Imaging of Demyelinating Disease

JA Tkach, X Ding, PM Ruggieri, R Rudick, TJ Masaryk
Department of Radiology, Cleveland Clinic Foundation, Cleveland, OH

Purpose: To optimize and assess the efficacy of a heavily T2-weighted fluid-attenuated inversion-recovery (FLAIR) fast spin-echo sequence employing fat saturation and MTC in detecting MS lesions in the brain.
Methods: Studies were acquired with a 1-T Siemens whole-body MR imager in normal volunteers and 10 patients with known or suspected demyelinating disease. An inversion-recovery fast spin-echo sequence, T1 selected to null CSF signal, was modified to apply a frequency-selective fat-saturation and/or a pulsed off-resonance MTS pulse during the latter portion of the T1 interval. In an effort to maximize lesion sensitivity, the following parameters were varied: (*a*) echo train length, 7–15; (*b*) effective TE (90–160 msec) T1 (1.8–2.3 seconds). The acquisition parameters that remained constant in all studies were TR = 6 seconds, thickness = 5 mm, di = 1.0 (full gap), FOV = 230, 210 × 256, 2 acquisitions: imaging time: 10 slices per 6 minutes, 6 seconds, 2 acquisitions; 9 slices when both MTS and FS were applied. All studies were performed within FDA guidelines for SAR.
Results: Preliminary studies in MS patients and normal volunteers confirmed previous reports of improved sensitivity and high contrast for long T2 tissues, with negligible signal from CSF, by using FLAIR sequences. This finding was most dramatic at longer effective TEs. Residual high signal intensity was occasionally seen near the normal frontal horns, at the choroid plexus, and secondary to flow phenomena. The addition of MTS to these sequences improved lesion contrast slightly but at the expense of image slice number and image signal to noise. T2 contrast was not significantly affected by the addition of RF fat saturation. Tissue contrast was more stable when the sequences were implemented with a full gap and filled with a second acquisition.
Conclusion: Serial plaque quantification and monitoring plaque load with MRI has become important in the management of MS patients. To date, this has either been performed empirically or semiquantitatively by means of labor-intensive techniques. The implementation of FLAIR sequences with fat saturation and MTC may provide image contrast suitable for more automated tissue discrimination and plaque quantification.

436 • 11:30 AM

Image Acquisition in a Second with Half-Fourier-Acquisition Single-Shot Turbo Spin Echo

B Kiefer, J Grässner, R Hausmann
Medical Engineering Group, Siemens AG, Erlangen, Germany

Purpose: HASTE (half-Fourier-acquisition single-shot turbo spin echo) is a susceptibility insensitive single-shot sequence that allows the ultrafast acquisition of high-resolution images with normal T2 weighting. Potential applications and first clinical results are shown.
Methods: Experiments were conducted on a 1.0-T MR imager (Siemens Magnetom Impact) and a 1.5-T imager with enhanced gradient system. HASTE is based on turbo spin echo, where RF-refocused echoes in a multiple-echo pulse train are sequentially phase encoded. Only half of k space is measured and then reconstructed by means of a half-Fourier method. HASTE can be combined with preceding RF pulses for spin preparation. A spectral selective prepulse is used to

obtain images with fat saturation. A 180° inversion prepulse is used to suppress fat (STIR method) or fluid (dark-fluid method), dependent on the inversion time.
Results: HASTE worked most impressively in the head and spine, with a spatial resolution of less than 1 mm^2 and good signal-to-noise ratio in 1.2-second acquisition time. On axial spine images (FOV = 200 mm), moderate T2-weighted contrast between CSF, disks, and muscle was obtained; the nerve roots were clearly resolved. Because of the fast acquisition time, artifacts due to patient motion were eliminated. Prepulses for fluid and fat suppression made lesions more visible.
Conclusion: HASTE has the potential to be an ideal screening technique for neurologic applications. In suspicious regions, the clinical examinations can be extended by a fast HASTE examination to observe lesions otherwise obscured by bright fat or fluid.
B. Kiefer is an employee of Siemens Medical Systems.

437 • 11:42 AM
Single-Breath-Hold Imaging of the Entire Liver with Ultrafast Turbo Spin Echo
JJ van Vaals, GH van Yperen
Philips Medical Systems, Best, The Netherlands
Purpose: Preferably, the entire liver should be imaged in a single breath hold to eliminate possible mismatch of slices. This should improve the detection of very small lesions. So far, this was only possible with EPI, by using dedicated hardware, and with relatively low-resolution images. We present an ultrafast turbo spin echo (TSE) method that covers the entire liver within a single breath hold.
Methods: We adapted a TSE sequence to achieve an echo spacing of approximately 6 msec on a standard 1.5-T Philips ACS-II. With use of a rectangular FOV, typically around 70%, and partial matrix acquisition, a 128 × 256 slice could be measured in a single shot of less than 400 msec. Alternatively, a 3D protocol was developed with similar acquisition parameters.
Results: Both multislice and 3D measurements were evaluated. In the multislice protocol, each slice is measured in a single shot and therefore has an infinite TR. To have an effective long relaxation period between successive shots in the 3D protocol, multichunk acquisition was applied. Typically, 20–36 slices (128 × 256, TE = 70–100 msec) were measured in a single 10–20-second breath hold.
Conclusion: With a standard state-of-the-art MR system, single-breath-hold imaging of the entire liver is possible by using an ultrafast TSE sequence. This eliminates possible mismatch of different slices between successive breath holds. Both multislice and 3D protocols are feasible for a 128 × 256 matrix within a comfortable breath-hold time of 10–20 seconds.
J.J. van Vaals is an employee of Philips Medical Systems.

Wednesday Morning • Sapphire Room
Papers 441–448

IMAGE PROCESSING
MODERATORS: JR MacFall, PhD
S Napel, PhD

441 • 10:30 AM
3D Warping of Digital Anatomic Atlas onto a Patient's Data Set
R Kikinis, J Dengler, D Metcalf, H Hokama, ME Shenton, FA Jolesz
Department of Radiology, Brigham and Women's Hospital and Harvard Medical School, Boston, MA
Purpose: To use information obtained from an MRI-derived digital anatomic atlas for providing anatomic definitions within a patient's data set.
Methods: By using MRI volume data and manual postprocessing, we have developed a digital anatomic atlas of the brain. We used a fully automated 3D warping algorithm that permits warping of the white matter from the atlas onto the white matter of the patient's data set. To identify the white matter, a semiautomated segmentation of the MRI data was used.
Results: The 3D warping was applied to 3D-rendered MRI data sets from normal volunteers and patients with brain tumors. The warping allowed easy determination of the localization of some anatomic areas of interest, such as the gyral anatomy, even in the presence of mass-related distortions.
Conclusion: Three-dimensional warping of a digital anatomic atlas onto normal and tumor-deformed MRI volume data sets has the potential to improve the definition of anatomic regions. This can be utilized for surgical planning, simulation, and training. It can also be helpful in automating morphometric procedures.

442 • 10:42 AM
Pre- and Intraoperative Tumor Localization with 3D MRI
R Kikinis, WE Lorensen, HE Cline, L Gleason, FA Jolesz
Department of Radiology, Brigham and Women's Hospital and Harvard Medical School, Boston, MA
Purpose: We have developed a new technique for preoperative planning and subsequent intraoperative guiding of neurosurgical procedures by merging live video images with 3D computer reconstructions of a patient's extra- or intracranial structures derived from diagnostic MR images.
Methods: The rendering parameters of the 3D reconstruction are adjusted interactively by using a rendering of the skin surface for reference, until the two images are identical in terms of scale, position, and rotation. Once the video and 3D computer images of the patient's scalp surface have been aligned, the computer image of the skin is removed, which leaves the 3D image of the underlying cranial or spinal contents superimposed on the video image of the patient's skin.
Results: The technique was applied in 12 patients with brain tumors, one patient with a spinal tumor, and two patients undergoing craniofacial surgery. In all cases, there was excellent correlation between the preoperative prediction and the intraoperative findings. The setup for the video registration (consisting of cart-mounted equipment) was taken into the operating room, and the registration was performed before the patient was draped. Validation was achieved by simultaneously using stereotactic and video localization.
Conclusion: The use of this technique intraoperatively permits definition of tumor margins and localization of subcortical tumors. It not only facilitates surgical procedures but also provides good definition of tumor margins and the exposed anatomy during surgery, without interfering with the procedure.

443 • 10:54 AM
3D Segmentation with High-Resolution MRI: Improved Accuracy and Stability
S Vinitski, S Seshagiri, CF Gonzalez, FB Mohamed, HV Ortega, S Albert
Department of Radiology, Thomas Jefferson University Hospital, Philadelphia, PA
Purpose: In semiautomatic methods of segmentation, the weakest link is probably the interaction between the observer and the computer. Thus, our aim was to develop a stable and accurate 3D tissue segmentation method to measure the regional distribution of specific tissues.
Methods: We used a multispectral analysis approach. Three or more MRI data sets (voxel size as small as 0.3 mm^3) were used as an input to calculate a 3D feature map. The observer "seeds" the tissue samples. Each sample population was tested with the statistical filter. These data were used to create a stack of 2D color-coded segmented images. A k-nearest-neighbors segmentation algorithm was used. Tissue volume was measured by the integration and correction for the partial volume. Next, the operator defined Cartesian and polar coordinates of the regions of interest, and then the software defined their boundaries. The methodology was applied to create five separate lobes of the brain. Phantoms, experimen-

tal brain edema in cats, five normals, and seven patients with MS were studied. The SUN SparcStation2 computer and 1.5-T GE Signa imager were used.
Results: The subimage postprocessing produced low-noise segmentation images. The volumetric measurements obtained in the phantom study show accuracy between 6% and 11%. In the animal experiments, interobserver variability (SD/mean) ranged between 6.6% and 9.3%. Intraobserver variability was between 8.3% and 10.4%. In patients, interobserver variability ranged between 0.4% and 5.3%. Additionally, improved resolution of MRI resulted in detection of new lesions. The larger concentration of MS lesions was observed at the periventricular level in both parietooccipital regions, and, particularly in new lesions, correlated well with prior neuropsychologic examinations that indicated potential MR lesions in these areas.
Conclusion: The technique is promising for studying the regional distribution of lesions. It provides accurate, reliable, and stable results.

444 • 11:06 AM
Efficient Registration Method for 3D Brain Images
EE Fitchard, PA Narayana
Department of Radiology, University of Texas Medical School, Houston, TX

Purpose: The quality of image registration will have a significant effect on quantitative image analysis in longitudinal patient studies. We present here an efficient, automatic, and robust method for 3D MR image registration.
Method: A least squares fit algorithm was used to determine the midline fissure plane for rotated and unrotated MR brain images. The polar coordinates of the normal vectors to this plane yielded two rotation angles. The third angle was obtained by a cross correlation of the radial coordinates of the brain edges. The linear displacement was determined by computing the centroid for each data set. The algorithm was implemented in the C programming language on a Sparc 10 workstation. Multislice MR images of a phantom and human brain were acquired with a 1.5-T imager for evaluating the registration method.
Results: From data sets with known relative rotations and linear offsets, the angular errors were found to be less than 0.5° and the linear error less than 0.5 pixel. Subtraction of the registered from the original images indicated excellent registration. The computation time for image registration for approximately 100 slices was less than 5 minutes.
Conclusions: The proposed 3D registration method is automatic, efficient, and robust. The modular structure of this program makes it adaptable for other image registration applications.

445 • 11:18 AM
Registration of Gated Cardiac MR and PET Studies for Regional Myocardial Function Evaluation
S Sinha, U Sinha, J Czernin, H Schelbert
Department of Radiological Sciences, UCLA, Los Angeles, CA

Purpose: To combine the high-resolution anatomic information of gated cardiac MR images with the physiologic information of gated PET images by registering the PET images onto the MR images, thereby allowing improved interpretation of PET data.
Method: Different MR imaging sequences were developed and compared in terms of their efficacy in yielding 3D volume images of the heart in reasonable imaging times, with good S/N and contrast (both bright and dark blood). Two registration algorithms, an iterative surface fitting algorithm by Pelizzari et al, and a stochastic sign-change method were tested for accuracy and reliability.
Results: Three-dimensional images of the heart in 16 cardiac phases were obtained in 6 volunteers and 1 patient with left coronary artery (LCA) disease both with MRI and PET. The first method was more robust for registration. Accuracy of correlation of 5 different internal landmarks between MRI and PET yielded a slope of 1.007 (compared with 1.0 for perfect registration) and a coefficient of linear regression of 0.9985. Short-axis views could be obtained for estimation of cardiac wall thickness.
Conclusions: Feasibility of structure-function correlation in the heart was graphically demonstrated in the patient with an LCA defect, where wall thickness could be estimated from the registered MR image in the diseased myocardial region, and where PET showed very little tracer uptake. The resultant complex images allow detailed study of regional perfusion, metabolic activity, and contractile status of the myocardium and their alterations in different myocardial diseases.

446 • 11:30 AM
MR Image Selection for Segmentation of the Brain
KJ McClain, JD Hazle
Department of Radiology, M.D. Anderson Cancer Center, University of Texas, Houston, TX

Purpose: This work was performed to optimize the subset of MR images used to segment tumor, edema, necrosis, gray matter, and white matter.
Methods: Approximately 40 patients with brain tumors were imaged with 1.5-T GE Signa systems. Registered proton density (PD), T2, T1, and T1 postcontrast axial images were collected. Typical imaging parameters were 24-cm FOV; 256 × 192 acquisition matrix; and 2,000/20, 2,000/80, and 600/20 TR/TE. Multispectral statistical measures were used to identify the optimal type and number of MR images for segmentation. Training fields for each tissue type were selected manually. Feature selection criteria ranked the statistical separation of tissues by calculating the statistical distance between all class pairs with use of the Bhattacharyya distance measure. From this, the ranking of all image combinations was obtained to determine the best images for classification. Feature extraction using decision boundaries determined the number of images for a given classification accuracy and generated eigenimages for further classification.
Results: In general, three MR images were required to obtain high-accuracy tissue classification (defined as greater than 90% correct classification of training fields). The best three-image combination was PD, T1, and T1 postcontrast. Use of the three best MR images for segmentation as indicated by means of feature selection gave nearly identical results to using three eigenimages generated by means of feature extraction. However, when using only two images, the eigenimages generally provided better results.
Conclusion: We found that feature selection and extraction criteria were helpful in choosing among several possible combinations of MR images for tissue segmentation. Our results show that three or more MR images may be needed for accurate classification. Fortunately, most segmentation methods can be extended to three or more dimensions.

447 • 11:42 AM
Automated Volumetric and Morphologic Analysis of the Evolution of Focal Multiple Sclerosis Lesions
CRG Guttmann, R Kikinis, D Metcalf, FA Jolesz
Department of Radiology, Brigham and Women's Hospital and Harvard Medical School, Boston, MA

Purpose: The asynchronous appearance and evolution of disseminated focal lesions of white matter are leading features of multiple sclerosis (MS). We propose an automated method to follow the volumetric and tridimensional morphologic development of individual focal lesions at MRI.
Methods: MS patients underwent a minimum of 22 MRI sessions at varying intervals over 1 year. Long TR spin-echo images with 3-mm thick sections covering the whole brain without gaps were obtained and processed following these steps: (*a*) pixel assignment to a tissue category based on multivariant statistical analysis, (*b*) extraction of all pixels included in the intracranial cavity (ICC), (*c*) automatic repositioning of all 3D data sets of a patient by using the ICC at one time point as a template (3D image registration), and (*d*) automatic identification and temporal tracking of the shape, size, and anatomic context of individual focal abnormalities in white matter.

Results: Individual focal lesions were detected and their volumes measured at various times in their evolution. Shapes and anatomic context were analyzed with the aid of 3D renderings. Confluence or fragmentation of lesions was frequently observed.
Conclusions: Spatial dynamics of lesions can be routinely assessed in a quantitative fashion and in the proper anatomic context. These tools provide significant help in assessing disease course and single lesion activity. We believe that this approach may greatly benefit the efficacy assessments of therapeutic trials, as well as efforts to correlate anatomic damage with functional impairment.

448 • 11:54 AM
Correction of MRI Intensity Inhomogeneities by Using Tissue Properties
WM Wells III, WEL Grimson, R Kikinis, FA Jolesz
Department of Radiology, Brigham and Women's Hospital, Boston, MA

Purpose: MR images usually have some variation in the signal intensity that is not due to tissue properties. This is present on most MR images and is especially pronounced on images obtained with surface coils. We describe a correction method that segments the images and improves their appearance.
Methods: A Bayesian method was used that estimates the tissue type and the RF gain throughout the image, simultaneously. It uses a priori knowledge of the tissue type to help infer the RF gain. Because of this, it is able to provide better estimates of RF gain than methods that do not separate the effect of tissue and equipment characteristics on signal intensity.
Results: We have applied the method to images of the following types: T2-weighted axial, SPGR coronal, and 5-inch surface coil brain images, and spine images obtained with a posterior neck coil and a phased-array coil. The method produces good gray matter/white matter segmentation and, in the case of surface coil images, generates corrected images that are substantially easier to view, although the weak signal-to-noise characteristics at large distances from the coil are not improved. As currently implemented, the method requires an ROI to be supplied as input.
Conclusion: The method makes segmenting of MR images into tissue classes more practical, thus facilitating quantitative studies of anatomic structures. It also improves the appearance of images that have pronounced gain artifact.

Wednesday Afternoon • Monet Room
Papers 501–507

MAMMOGRAPHY II: Contrast
MODERATORS: SE Harms, MD
CL Partain, MD, PhD

501 • 2:45 PM
MR Mammography for Monitoring of Neoadjuvant Therapy: Assessment of Pharmacokinetic Changes
MV Knopp, T Hess, G Brix, H Junkermann, U Hoffmann, P Sinn, D von Fournier, G van Kaick
Department of Radiology, German Cancer Research Center, Heidelberg, Germany

Purpose: To evaluate the possible clinical application of dynamic MR mammography (MRM) for monitoring of induction chemotherapy. This therapeutic concept is of increasing importance because it has shown clinical benefits.
Methods: Twenty-four patients with subsequent histologically confirmed breast cancer were studied with MRM during the diagnostic workup and subsequently after each cycle of chemotherapy. The final study was performed before surgical enucleation of the tumor. The standard double breast coil was used on a 1.5-T Siemens Magnetom SP. Pre- and postcontrast 3D FLASH and a specially designed dynamic multislice TurboFLASH techniques (TR = 8 msec, TE = 2.7 msec, TI = 125 msec, $\alpha = 12°$) were used. Gd-DTPA (0.1 mmol/kg) was administered intravenously over 1 minute by using an infusion pump (PIM 717, Doltron AG, Switzerland). The pharmacokinetic analysis was performed on a pixel-by-pixel basis, which resulted in color-coded projection images. The detailed analysis of each lesion was done with a cine mode display and a region-of-interest technique to determine the individual signal-time curves. Objective and subjective parameters, such as signal changes of the static images and time to maximum slope of the signal-time curve for the dynamic sequence, were analyzed. After surgical enucleation of the tumor, a detailed histologic workup was performed.
Results: The pharmacokinetic characteristics of the contrast enhancement show a clear pattern in the 14 patients for whom evaluation has currently been completed. A decrease in the signal amplitude and increase in tissue distribution time correlates with a subsequent decrease in tumor volume, clinical response to therapy, and histopathologically altered tumor tissue characterized by extensive sclerotic changes. No substantial change in the pharmacodynamic properties of the contrast enhancement coincides with insufficient response to therapy despite initial tumor volume reduction.
Conclusion: MRM can be used for early monitoring of response to neoadjuvant therapy in breast cancer patients. With use of an automated pharmacokinetic analysis, a reliable, distinct characterization of response seems possible.

502 • 2:57 PM
Clinical Experience with a Model for Distinguishing Benign from Malignant Breast Lesions Detected with Dynamic Gd-enhanced MRI
F Kelcz, GE Santyr, SJ Mongin, EJ Fairbanks, FA Quintanna
Department of Radiology, University Hospital, University of Wisconsin, Madison, WI

Purpose: Dynamic Gd-enhanced breast MRI holds promise as an adjunctive method of mammography in the diagnosis and management of breast disease. However, methods for distinguishing benign from malignant lesions are still under investigation.
Methods: We used a dedicated breast coil to image 47 lesions in 45 women after bolus intravenous administration of Gd-DTPA (0.1 mmol/kg). A dynamic imaging sequence (SPGR or FSPGR) was used to achieve 15-second temporal resolution. We fit the temporal change in signal intensity (SI) of 30 enhancing lesions to a saturation model previously described. We had hypothesized that one parameter, M, which corresponded to the normalized slope at half the maximal SI increase, would correlate with malignancy.
Results: The lesions consisted of 10 malignancies, 12 fibroadenomas, and 25 other benign breast changes. Signal intensity versus time data for the 30 enhancing lesions was fit to the proposed model. The choice of M greater than 4.5 to signify malignancy resulted in a correct diagnosis in 7 of 10 malignancies and 19 of 20 benign enhancing lesions. Two of the 3 false-negative results were associated with ductal carcinoma in situ manifesting as clusters of microcalcifications less than 8 mm in diameter.
Conclusions: We conclude that the proposed mathematical approach may be useful for discriminating benign from malignant enhancing breast lesions. This model can distinguish subtle changes in Gd uptake that are not visually apparent. However, the sensitivity of the technique to cancers associated with subcentimeter clusters of microcalcifications may be limited.

503 • 3:09 PM
Dynamic Contrast-enhanced MRI of the Normal Breast during the Menstrual Cycle
RH Patt, S Ascher, J Goldberg, T Marchand, SS Rajan
MRI Center, Georgetown University Medical Center, Washington, DC

Purpose: To evaluate the effects of the menstrual cycle on the normal breast by using dynamic contrast-enhanced breast MR imaging.
Methods: Thirty women (age range, 20–50) were examined

each once weekly over their menstrual cycles by using a 3D gradient-echo (FISP; 12/4.8/40°) pulse sequence before and after the bolus administration of IV Gd-DTPA. Five postcontrast measurements were used to plot time-intensity curves of normal breast parenchyma. Additional measurements that were compared over the menstrual cycle in each subject included duct size, size and enhancement of circumscribed masses, skin thickness, nipple enhancement, and overall glandular volume. Subjects receiving hormonal therapy were excluded from the study. Comparison was made with conventional mammography where clinically warranted.
Results: Consistent changes in the intensity and rate of enhancement were noted throughout the menstrual cycle with peak enhancement in the week before menstruation. Overall glandular volume was estimated and noted to vary with changes in the cycle as well. Further results from detected focal lesions and physiological-anatomical changes will be presented.
Conclusion: Dynamic contrast-enhanced breast MRI has been proposed as a useful technique for detecting and quantifying breast lesions, especially in women who may have dense breast tissue at conventional mammography. Our study suggests that there is an optimal time period to image the premenopausal breast with this technique to minimize background enhancement and improve lesion detection, and to avoid mistaking normal structures for pathology.

504 • 3:21 PM

Dynamic Enhancement of Breast MRI at 30 Seconds Improves Discrimination of Sclerosing Adenosis from Invasive Breast Cancer

CB Stelling, VM Runge, DD Davey, PM Linville, JW Wells, DE Kenady, PC McGrath, DA Sloan, JE Kirsch
University of Kentucky School of Medicine, Lexington, KY

Purpose: To improve breast MRI specificity by evaluating dynamic enhancement at 30 seconds after infusion of contrast material.
Methods: Twenty-four women (age range, 36–74 years) with breast lesions that required biopsy were scanned before excision (1.5 T, double breast coil). 2D FLASH pulse sequences (TR 14/TE 6/FA 34) were performed before and 30 seconds after the end of gadoteridol infusion (1 mL per second) at doses of 0.1–0.3 mmol/kg. A slab of 7 interleaved slices was obtained every 30 seconds to 5 minutes. Percent enhancement of the lesion was calculated for the ROI.
Results: By 30 seconds, all 7 invasive ductal carcinomas enhanced 80% or more (range, 80%–390%). All 9 women with fibrocystic changes, including 5 with sclerosing adenosis, showed 40% or less enhancement by 30 seconds and 70% or less by 60 seconds. Three women with ductal carcinoma in situ showed no enhancement by 5 minutes. Five women with benign tumors had 70%–330% lesion enhancement by 30 seconds.
Conclusions: (*a*) Dynamic phase at 30 seconds minimizes enhancement of sclerosing adenosis. (*b*) Enhanced breast MRI shows invasive but not in situ ductal carcinoma. (*c*) Enhancement curves of benign tumors mimic invasive breast cancers. (*d*) A technique is needed to sample lesions detected with MRI that enhance more than 50% by 30 seconds, to differentiate circumscribed invasive cancers from fibroadenomas. (*e*) Contrast-enhanced breast MRI has potential for evaluation of the presence and extent of invasion.
This research was supported in part by Squibb Diagnostics, Inc.

505 • 3:33 PM

Dynamic Sequential Gadolinium-enhanced MRI of the Whole Breast

E Heiberg, WH Perman, VM Herrmann, CG Janney, DJ Grunz
Department of Radiology, St Louis University Health Sciences Center, St Louis, MO

Purpose: The reported specificity of Gd-DTPA–enhanced breast lesions ranges between 37% and 98%, with higher specificity for dynamic MRI studies. The limitations of dynamic contrast-enhanced 2D imaging of the breast are the low number of slices that can be acquired, and the need to know the location of the lesion a priori to correctly select the noncontiguous 2D slice locations. These problems are exacerbated when multifocal disease is present but not anticipated. We have developed a 3D method in which the entire breast can be imaged in 44 seconds and followed sequentially without an interscan delay, which eliminates the need for a priori knowledge concerning the location of the lesion(s).
Methods: A sagittal 3D spoiled GRASS acquisition is graphically prescribed to cover the entire breast and chest wall. The parameters are TR/TE = 10.6/2.2 msec, FOV = 180 mm, flip angle = 20°, thickness = 3–4 mm, 32 × 128 phase encodings, 256 readout points, NEX = 0.75, for an imaging time per 3D image of 44 seconds. We have modified the 3D FLASH pulse sequence so that 8 3D data sets are acquired at the same location without the typical 35–60-second interscan delay.
Results: We studied 26 patients with 36 lesions, with surgical confirmation in 31 lesions. With an enhancement of more than 90% within the first 2 minutes as a criterion for possible malignancy, all 7 malignancies and 18 of 23 benign lesions were correctly categorized. Dynamic Gd-DTPA profiles were obtained in 2 lesions that were not seen on T1- and T2-weighted spin-echo images. One was a papillomatous mass that was not detected with mammography, and the other was a 7 × 5 × 4-mm, nonpalpable, invasive lobular carcinoma.
Conclusion: We find that dynamic 3D imaging of lesion enhancement with Gd-DTPA achieves a specificity of 78% and allows quantitation of enhancing lesions that are not seen at conventional 2D spin-echo imaging.

506 • 3:45 PM

Breast Lesion Differentiation Based on the Pharmacokinetic Behavior of Gd-DTPA

J Smink, JA den Boer, G Dornseiffen, PWAA Koch, JH Mulder, CH Slump, EDP Volker, RAI de Vos
Philips Medical Systems, Best, The Netherlands

Purpose: High false-positive rates in MRI assessment of breast carcinoma are reported when the MR data are subjectively evaluated. We hypothesized that the clinical accuracy of MRI can be improved by using a pharmacokinetic analysis of accurate quantitative, dynamic 3D Gd-DTPA data.
Methods: The dynamic MR data obtained with our technique allowed calculation of the time course of Gd-DTPA and the native T1 in our patient studies. Curve fitting to match a pharmacokinetic three-compartment model was used to find the leakage rate k_{31}. This objective analysis of the MR data proceeds in two steps: (*a*) T1 and initial enhancement slope are used to select one positive and two negative vectors of an eigen image filter and reduce the original time series to a single 3D functional image set. (*b*) For each slice of this set, the bright areas, suspicious for malignancy, are segmented out and analyzed further.
Results: Fifteen patients (age range, 32–70 years) with histologically confirmed breast lesions were analyzed: Fat: native T1, 120–260 msec; k_{31}, 0–1 × 10^{-3} s^{-1}. Parenchyma: native T1, 200–900 msec; k_{31}, 0–2 × 10^{-3} s^{-1}. Carcinomas: native T1, 800–1800 msec; k_{31}, 8–40 × 10^{-3} s^{-1}.
Conclusion: The proposed analysis gives fully objective MR system–independent data. It is a prerequisite for specificity in MR-based breast tumor diagnosis. Blind testing of a series of patients with nonpalpable tumors suspicious for cancer after population screening is in progress. Results will be reported.
J.A. den Boer is an adviser for Philips Medical Systems.

507 • 3:57 PM

Quantitative 3D Temporal Tracking of Redistribution of Gd-DTPA in the Mamma

JA den Boer, G Dornseiffen, A Elevelt, PWAA Koch, HJ Mulder, J Smink, EDP Volker, RAI de Vos
Philips Medical Systems, Best, The Netherlands

Purpose: Optimization of dynamic MRI for quantitative observation of the postinjection time course of Gd-DTPA, to improve specificity of differential diagnosis of breast lesions.
Methods: The requirements include the following: (*a*) sufficient temporal resolution to detect time constants as low as

20 seconds (maximum leakage rate for malignant breast lesions, (*b*) isotropic spatial resolution sufficient to detect 6-mm lesions, and (*c*) quantitative Gd-DTPA assessment based on knowledge of native T1. The methods were dynamic 3D FFE with 3 × 2.3 × 1.2-mm resolution; TR/TE/flip = 19/6/45° at 30 seconds per frame. Bolus injection of 15 mL of Gd-DTPA (7.5 mmol) starting 10 seconds before the start of frame 2 and reaching the mamma before the effective image reckoning time of this frame, 15 seconds later. T1 calculation per voxel based on only one additional 3D FFE scan (19/6/5°) of 30-seconds duration, before injection. Flip angles are accurate by hardware provisions. Their values are optimized for T1 accuracy between 100 and 3,000 msec.
Results: We found native T1 values of mamma carcinoma ranging from 800 to 2,800 msec in 12 patients. On the basis of published T1 and T2* relaxivity, the proposed technique shows [Gd-DTPA] per voxel with an accuracy of 0.04 mmol/L.
Conclusions: An imaging technique is realized for accurate and quantitative dynamic tracking of [Gd-DTPA] on the basis of combined pre- and postinjection FFE images. The technique is a prerequisite for high specificity in MR-based breast lesion differentiation. It is presently under test in a clinical trial.
J.A. den Boer is an adviser for Philips Medical Systems.

Wednesday Afternoon • Metropolitan Room
Papers 511–516

BRAIN III: CSF Flow, Other

MODERATORS: WG Bradley, Jr, MD, PhD
VM Runge, MD

511 • 2:45 PM

Quantitative CSF Velocity Imaging in the Evaluation of Patients with Suspected NPH

WB Bradley, Jr, D Atkinson, WM Nitz, DY Cheng
Memorial MR Center, Long Beach Memorial Medical Center, Long Beach, CA

Purpose: To compare quantitative phase contrast CSF velocity imaging and the aqueductal CSF flow void with clinical response to a ventriculoperitoneal (VP) shunt in patients with normal pressure hydrocephalus (NPH).
Methods: Twenty elderly patients (age range, 54–84 years) with gait disturbance and dementia suggestive of NPH underwent routine MR imaging, quantitative CSF velocity imaging, and creation of a VP shunt. Aqueductal CSF stroke volumes (SV) (in microliters) (ie, the volume of CSF passing through the aqueduct with each beat of the heart) were calculated for all patients and verified with a pulsatile flow phantom. The CSF flow void was quantified on a 4-point scale by using the SE 3,000/22 image with first-order flow compensation. Response to surgery was rated "good" or "poor" based on evaluation of mental status and gait 1 month after surgery.
Results: Of 14 patients with "hyperdynamic" CSF flow (SV > 40 μL), 13 (93%) responded well to surgery. The one patient who did not respond had known chronic MS. Of six patients with CSF stroke volumes less than 40 μL, three (50%) had a "good" surgical response and three (50%) had a "poor" response. Only seven of 14 (50%) patients with SV greater than 40 μL had prominent (grade 3 or 4) aqueductal CSF flow voids on the SE 3,000/22 image, probably reflecting the use of flow compensation.
Conclusion: Quantitative CSF velocity imaging is more accurate than the aqueductal CSF flow void in predicting response to a VP shunt for NPH.
This research was supported in part by Siemens Medical Systems.

512 • 2:57 PM

Diagnostic Value of Cerebrospinal Fluid Motion Studies with Steady-State Free Precession Technique

BC Sander, JC Böck, N Hosten, J Hierholzer, TJ Vogl, R Felix
Department of Radiology, University Hospital Rudolf Virchow, Berlin, Germany

Purpose: To outline the diagnostic value of cerebrospinal fluid (CSF) motion studies in clinical MR imaging.
Methods: A retrospectively ECG-gated steady-state free precession sequence was used (1.5-T Siemens Magnetom; TR, 20 msec; TE, 10 msec; flip angle, 80°; FOV, 230 mm; matrix, 256 × 256; slice thickness, 5 mm; acquisition time, 4 minutes; amplitude of the readout gradient, 3.4 mT/m). We studied 37 patients with hydrocephalus, 12 with syringomyelia, 11 with arachnoidal cysts, 13 with cystic tumors, 3 with arachnopathy, and 23 patients without MR pathology.
Results: In all cases, communicating and noncommunicating hydrocephalus could be differentiated. The various types of communicating hydrocephalus could not be further delineated. In the patients with syringomyelia, one group (6/12) was found with strong CSF pulsations within the syrinx, and the other group (6/12) had low or absent CSF motion. In 7 of 11 archnoidal cysts, the cystic wall could be better delineated from surrounding subarachnoidal space. CSF motion could be shown in 10 of 11 arachnoidal cysts, whereas motion was absent within cystic tumors. In patients with arachnopathy, circumscribed disturbances of CSF motion were found within the subarachnoidal space.
Conclusion: Steady-state free precession CSF motion studies are of great diagnostic value in differentiating communicating and noncommunicating hydrocephalus, in delineation of archnoidal cyst, in differentiation between archnoidal cysts and tumor cysts, and in detection of archnopathy. The information about CSF motion within the syrinx might be of diagnostic value with respect to delineating septa within the syrinx or outlining communication.

513 • 3:09 PM

CSF Flow Disorders Due to Intracranial Septations Evaluated with an ECG-retrogated 2D FISP Sequence

A Goldmann, U Kunz, U Karras, JM Friedrich
Department of Diagnostic Radiology, University of Ulm, Ulm, Germany

Purpose: Measurement of pulse-related CSF flow velocities in patients with intracranial septations of the CSF pathway to visualize alterations of the normal CSF pulsation pattern.
Methods: Nine patients with intracranial cystic septations were examined with an ECG-retrogated 2D FISP sequence (1.5-T Magnetom 63 SP). The imaging plane was midline through the aqueduct and through the septation, with a slice thickness of 4 mm with a high-resolution sagittal technique. In 7 cases, cysternography was performed to allow an exact determination of the communication of the septations. For better interpretation of the results, the MRI findings of 2 patients with tumors of the 4th ventricle (1 solid and 1 cystic) that caused occlusive hydrocephalus were compared. Ten healthy volunteers were examined as a control group.
Results: ECG-retrogated phase MRI allowed good delineation of the intracranial cystic septations. A different flow direction and velocity of the to-and-fro pulsatile CSF motion between the CSF within the cyst and the surroundings was measured, which caused a phase shift of the pulse-related velocity curves. The phase differences of the velocity curves depended on the degree of communication.
Conclusion: MRI with retrospective cardiac gating, first introduced by Nitz and Bradley (Radiology 1992), enables continuous measurements throughout the cardiac cycle and is a robust technique for examining patients with CSF flow disorders. It is clinically useful not only in patients with communicating hydrocephalus but also in other forms of CSF flow disorders and allows a better understanding of CSF flow pathology.

514 • 3:21 PM

MRI and MR Angiography of Vertebral Artery Dissection

SR Felber, G Hamann, T Penz, GG Birbamer, H Henkes, FT Aichner, U Piepgras
Department of Magnetic Resonance Imaging, University of Innsbruck, Innsbruck, Austria

Purpose: Initial symptoms of vertebral artery dissection (VAD) may be unspecific but followed by severe neurologic deficit. We investigated the potential role of MRI and MR angiography (MRA) for diagnosis of VAD.
Methods: Sixteen patients were examined on 1- and 1.5-T imagers with use of a circular polarized head coil, spin-echo sequences, and time-of-flight 3D MRA (FISP, TR = 40 msec, TE = 7 msec). Clinical records, conventional angiograms, and CT scans were available in all patients.
Results: The initial CT scan was normal in all patients, while MRI revealed ischemic changes confined to the posterior circulation in 15 patients. MRA showed thrombus or missing flow in the vertebral artery in 9 of 11 patients who were examined in the acute stage and occlusion of the vertebral artery in 4 patients examined in the chronic stage.
Conclusions: MRI is superior for parenchymal ischemic sequelae of VAD. MRA in our series revealed occlusions and stenosis associated with VAD but failed to visualize specific findings (pseudoaneurysm and false lumen) in 2 patients. Thus, MRA is helpful and complementary to MRI but presently cannot replace conventional angiography.

515 • 3:33 PM

MR Imaging of Blood-Brain-Barrier Disruption with a New Gd Complex as a Contrast Agent: Experimental Study in Rats and Rabbits

GK Schneider, K Urbschat, KB Bruck, M Uder, B Kramann
Department of Radiodiagnostics, University of Saarland, Homburg, Germany

Purpose: In this experimental study, a new contrast agent for MRI was tested in four animal models. The new synthesized Gd complex was investigated for its contrast enhancement in healthy animals, as well as in animals with local and general disruption of the blood-brain barrier (BBB) and presence or absence of brain perfusion.
Methods: T1- and T2-weighted images were obtained with a 1.0-T magnet (Siemens, Magnetom). To investigate imaging qualities of the new contrast agent, 2 experimental models in rats without pathologic alterations (model A) and with general osmotic disruption of BBB (model B), and 2 models in rabbits with experimentally induced ischemic brain infarction (model C) and experimentally induced brain abscess (model D) were studied.
Results: In model A, signal intensity (SI) of the kidney significantly increased, whereas in healthy brain tissue, muscle, and liver, no significant change was observed. In model B with general disruption of BBB, SI of the brain increased about 15%–20%. In model C, contrast-enhanced T1-weighted images, 8 hours after ischemic infarction, showed an increase in SI of up to 23% in the edema surrounding the not perfused central core of the infarction. In model D, an increase in SI in the abscess area of about 24%, after administration of the new Gd complex, with clear delineation between brain abscess and healthy brain tissue, could be demonstrated.
Conclusion: The new Gd complex tested in these experimental studies shows good enhancement of SI in regions with disrupted BBB and so can be categorized as a potential new contrast agent for MRI.

516 • 3:45 PM

MR Imaging of an Experimental Model of Intracranial Metastatic Disease: A Study of Lesion Detectability

VM Runge, JW Wells, JN Dunworth, CE Woolfolk, JE Kirsch
University of Kentucky, Lexington, KY

Purpose: The detectability of brain metastases was evaluated in a rabbit model, with attention to dose of MR contrast agent and timing of image acquisition after injection.
Methods: Five New Zealand white rabbits were studied at 1.5 T at both 6–7 days and 11–12 days after surgical implantation of an adenocarcinoma tumor nidus. T1- and T2-weighted SE images (0.9 × 0.9 × 2 mm voxel size) were obtained before injection. T1 images were repeated at 5, 15, and 30 minutes after IV injection of 0.1 mmol/kg gadoteridol. At 40 minutes, a supplemental dose of 0.2 mmol/kg (0.3 mmol/kg cumulative) was administered, with T1 images repeated at 5, 15, and 30 minutes after this second injection.
Results: At 6–7 days, lesion enhancement (percent change, normalization to baseline, and equilibrium values) was 42% ± 9 at 5 minutes, 48% ± 9 at 15 minutes, and 42% ± 10 at 30 minutes after a dose of 0.1 mmol/kg. After a dose of 0.3 mmol/kg, lesion enhancement was 110% ± 13 at 5 minutes, 116% ± 8 at 15 minutes, and 100% at 30 minutes. On film review, 3 of 5 lesions were not detectable at 6–7 days after implantation with a dose of 0.1 mmol/kg. The 0.3 mmol/kg dose provided identification in each instance. At 11–12 days, all lesions were detectable with a dose of 0.1 mmol/kg; however, enhancement did increase from 39% ± 16 to 104% ± 10 with the 0.3 mmol/kg dose.
Conclusion: Improved metastatic lesion detectability is shown, with pathologic correlation, at a dose of 0.3 mmol/kg compared with 0.1 mmol/kg, the latter dose failing to show small lesions.

Wednesday Afternoon • Miro Room
Papers 521–527

MR ANGIOGRAPHY II

MODERATORS: JE Siebert, MD
S Wann, MD

521 • 2:45 PM

2D Phase-Contrast Cine MRA Flow Dynamics in the Head and Neck: Normal and Pathologic Cases

JR Pernicone, TG Cooper, JE Siebert, RA Meyer, EJ Potchen
Department of Radiology, Michigan State University, East Lansing, MI

Purpose: This clinical series demonstrates that quantified flow and flow patterns in vessels during the cardiac cycle furnish useful information for more definitive diagnoses.
Methods: Acquisition parameters were as follows: cine 2D phase-contrast (retrospective cardiac-gating method; 1.5-T GE Signa), 27/10.1/30° (TR/TE/FA), 1 NEX, 20-cm FOV, 128 × 256 acquisition matrix, 4-mm slice thickness, fingertip peripheral gating, 80 cm/sec velocity encoding, 1 slice location per acquisition, with 4–6 axial locations acquired in the neck and about the circle of Willis. Sixteen cardiac phases were reconstructed. Velocity-phase (no magnitude weighting) and magnitude images served as inputs to graphical software (XVESSEL, Michigan State University). A region-of-interest (ROI) mask was then determined automatically by thresholded region growing. Flow versus time and ROI plots were inspected. A flow impedance index, ZI = average flow/diastolic flow, avoids the systolic measurement error. Twenty normals and 15 patients with pathology were studied with this method.
Results: ZI is normally ~ 1.5. In patients with stenotic lesions, the ZI was elevated proximally. Distal to the stenoses, peak systole tended to be delayed and widened, and ZI had a reduced value. For the artery leading to an AVM, ZI was reduced, while elevated contralaterally, and the reflection was absent. In small vessel disease, ZI was increased (lupus). Right-left comparisons of ZI eliminated factors extrinsic to that vessel. Flow quantitation altered the impression significantly from morphologic MRA alone in 2 cases.
Conclusion: Two-dimensional phase contrast cine analysis of flow during the cardiac cycle complements information obtained from standard MRA techniques. Flow quantitation should be applied in the routine practice of clinical MRA.

522 • 2:57 PM

MRA Technique and Vessel Diameter

AR Gillams, MS Benjamin, AP Carter
BCH Center for MRI, Boston University Hospital, Boston, MA

Purpose: Visualized vessel diameters vary with the MRA technique used. A comparison of 5 different MRA techniques with reference to vessel diameter was undertaken in the carotid artery. We evaluated 3D phase-contrast (PCA), nonsegmented 2D (2DTOF), segmented 2D (2DTFE), nonsegmented 3D (3DTOF), and segmented 3D (3DTFE) techniques.
Methods: Seven healthy volunteers (3 men, 4 women; median age, 31 years; age range, 23–55 years) underwent all 5 sequences. Sequence parameters were TR/TE/flip angle = 20/8/20° for PCA, 26/8/60° for 2DTOF, 16/8/60° for 2DTFE, 31/7/25° for 3DTOF, and 21/7/25° for 3DTFE. Slice thickness was 0.6 mm for the 3D sequences with a 512 reconstruction matrix in the 3DTOF and 3DTFE sequences. Slice thickness was 3 mm with 1-mm overlap for 2DTOF and 2DTFE sequences. The segmented sequences had a 180° inversion prepulse for maximum fat suppression. Acquisition times were 8:34 for PCA, 5:22 for 2DTOF, 6:54 for 2DTFE, 6:38 for 3DTOF, and 5:37 for 3DTFE. Maximum intensity projections were performed and the vessel diameters measured.
Results: Mean diameter of the carotid bifurcation was 6.9 ± 1.6 for PCA (velocity encoding, 60 cm/sec), 11.5 ± 2.2 for 2DTOF, 11.4 ± 1.5 for 2DTFE, 10 ± 1.1 for 3DTOF, and 11.3 ± 1.4 for 3DTFE. The only significant difference was between the PCA and the other sequences; there were no significant differences between the 4 TOF sequences.
Conclusion: The 4 TOF techniques were interchangeable in terms of vessel diameter. PCA diameters depended on the selected velocity encoding but were consistently less than those measured with the TOF technique.

523 • 3:09 PM

Optimization and Improvements in Head and Neck MRA at 0.5 T

SN Sarkar, A Merello, K Tran, T Lee, C Kirby, M Calderon
Houston Imaging Center, Houston, TX

Purpose: Long neck coils, computer workstations, and high field strengths have traditionally been assumed to be prerequisites for high-quality head and neck MRA. We are proposing a technique for producing high-quality MR angiograms at 0.5 T with a standard computer and a standard head coil.
Methods: Ten volunteers and 30 patients were the subjects of investigation. Varying degrees of head tilting were necessary to image the circle of Willis. By grouping normal volunteers into different age groups, several sets of TR/flip angle/slab volume/slice width values were experimentally optimized. A quadrature head coil was positioned off center. B_1 inhomogeneity was compensated at coil edges by superior B_0 homogeneity available at the center of the magnet. Angioreconstruction was limited to three orthogonal planes.
Results: Head tilting of 20°–30° was found optimal for best visualization of cerebral arteries. A TR of 22 msec and a 15°–25° flip angle at 1.3 mm or less slice thickness proved best for imaging the circle of Willis. A larger flip angle was noted to be better for imaging basilar and presiphon arteries. Venous presaturation was necessary only for neck carotid arteries. Carotid bifurcations and vertebral arteries were better visualized by off-centering the standard head coil by 5–10 cm, depending on the patient's neck size. The angiograms obtained were of high diagnostic utility and will be compared with images from other modalities.
Conclusion: Optimized orientation of patient or imaging slab can open up the intracranial circle without use of a workstation. Optimum imaging parameters have a strong dependence on age. Repositioning of the standard head coil is a viable alternative to dedicated long neck coils.

524 • 3:21 PM

MRA in the Upper Thorax With Segmented, Breath-Hold 2D TOF Sequences

AJ Duerinckx, U Sinha, DJ Atkinson, OP Simonetti
Radiology Service, Veterans Affairs Medical Center, West Los Angeles, Los Angeles, CA

Purpose: Respiratory motion, cardiac motion, and the pulsatility of blood flow in the thoracic aorta create significant artifacts on MR angiograms of vessels in the upper thorax. Visualization of the aortic arch and surrounding vessels by using an ECG-gated breath-hold segmented 2D TOF MRA technique was evaluated.
Methods: Normal volunteers and patients with acquired thoracic aortic disease or congenital heart disease were imaged. Images were acquired on a 1.5-T imager (Magnetom SP, Siemens) by using an ECG-gated flow-compensated gradient-echo (2D TurboFLASH) sequence with breath-hold and k-space segmentation. Images were acquired in both the transaxial and oblique coronal planes. Maximum intensity projections (MIPs) and 3D reconstructions of the different MR angiograms were compared with the angiographic views (in patients).
Results: The segmented breath-hold 2D TOF MRAs were of superior quality compared with nongated 2D TOF MR angiograms. In all cases, the MR angiogram clearly showed the pathology. Pulsatility artifacts were significantly reduced. A cine loop version of this MRA technique demonstrated the dynamics of flow in the true and false channels of aortic dissections.
Conclusions: ECG-gated segmented breath-hold 2D TOF MRA in the upper thorax provides significantly improved images of the vasculature when compared with nongated MRA techniques.
D.J. Atkinson and O.P. Simonetti are employees of Siemens Medical Systems.

525 • 3:33 PM

MR Angiography of the Aortic Arch

ML Switzer, RJ Witte, RW Jones, TC Goertzen, TG Lynch, BT Baxter
University of Nebraska Medical Center, Omaha, NE

Purpose: Although great advances have been made in MR angiography of the carotids and intracranial circulation, investigation of the aortic arch has been limited. This has been partly due to the geometry of the great vessels, as well as problems encountered with venous return and the pulsatile motion of aortic flow. It has also been due to the lack of specific, highly sensitive surface coils created for imaging this geometrically difficult region of the body. Our purpose was to image the aortic arch and origins of the great vessels by using TOF techniques.
Methods: We used a GE 1.5-T Signa imager with a standard 2D TOF technique and a specialized quadrature surface coil that required no special software or hardware interface. The coil capitalized on the depth-focused magnetic sensitivity profiles of solenoidal coil geometries. Both normal volunteers and patients suspected to have atherosclerotic vascular disease were used in the study. Correlation with conventional angiography was performed when possible.
Results: The use of the cardiac surface coil resulted in an improved signal-to-noise ratio throughout the entire imaging range, which led to improved visualization of the great vessel origins. Good correlation with conventional angiography was seen.
Conclusion: This 2D TOF technique can be used to obtain clinically useful images from the aortic arch and great vessel origins to the carotid bifurcation. It is especially useful in patients who are at increased risk with conventional angiography or when a screening examination is desired to determine the need for further intervention.
R.W. Jones is president of ScanMed.

526 • 3:45 PM

Visualizing Flow Patterns in the Ascending Aorta by Using Streamlines

MH Buonocore
Department of Radiology, University of California Davis Medical Center, Sacramento, CA

Purpose: To display streamlines of flow in the ascending aorta and show the convergence of streamlines into the left and right coronary arteries.

Methods: Velocity-encoded phase-contrast cine was used to acquire 2D coronal images at different anterior/posterior (A/P) levels that show the heart, aortic valve, ascending aorta, aortic arch, and vessel branches. Streamlines were calculated from this time-resolved data by using first-order forward or backward integration of the velocity field. A movie loop of amplitude images at a single A/P level is displayed on the screen. Streamlines are superimposed on these images. Streamline segments within the slice during the displayed time frame are shown in red. Streamline segments move forward as subsequent frames are displayed. The movement appears smooth. Optionally, streamline segments in the contiguous anterior slice are shown in a different color, and segments in the contiguous posterior slice are shown in a third color. Starting spots are positioned by clicking on the amplitude image and typing in a spot radius.

Results: Rapid systolic flow through the ascending aorta into the brachiocephalic and left common carotid artery is easily visualized. Diastolic recirculating flows in the ascending aorta, left ventricle, and above the aortic valves are usually visualized. By backward integrating from a small spot in the left coronary artery, streamlines flowing into the artery are found.

Conclusion: Streamlines facilitate the interpretation of time-resolved 3D velocity data.

527 • 3:57 PM

Velocity-Sensitive Surface-rendered Display in Cerebral MR Angiography

L Shapiro, DR Tien, JG Felsberg, MS Totterman, JS Golding
Department of Radiology, Duke University, Durham, NC

Purpose: We have used MR angiography in conjunction with a velocity-sensitive surface-rendering display method to examine various cerebral vascular pathologies. Our goal was to determine the types of pathologies best demonstrated with this technique.

Methods: Thirty-two patients underwent MRA with a GE 1.5-T MR imaging system. Postprocessing was conducted on a SUN workstation by using the Sunvision reconstruction algorithm and specific software that we developed. In our reconstruction technique, the original images were segmented into five flow velocities that were assigned varying opacities in the surface-rendered display. The images were evaluated by two neuroradiologists and compared with MIP MRA, angiography, CT, and surgery findings, when available.

Results: Surface-rendered MRA demonstrated vascular anatomy far more clearly than did MIP MRA. Surface rendering delineated overlapping vessels, but with our special velocity segmentation technique, information about flow at the surface of the vessel, as well as in the lumen, was appreciated. In all aneurysm cases, this technique showed the shape and structure of aneurysms better than any other modality, including visualizing two aneurysms that were missed with MIP MRA. In AVMs, this technique defined specific aberrant feeder vessels not seen with other modalities. This technique showed the exact location of a C-C fistula that could not be seen with any other modality because of complex vascular anatomy and flow dynamics.

Conclusion: Surface-rendered MRA is useful in visualizing the shape of aneurysms and in determining spatial relations between pathology and normal structures. We believe that this technique not only helps neuroradiologists in interpretation but also helps neurosurgeons in planning.

Wednesday Afternoon • Morrocco Room
Papers 531–537

SPECTROSCOPY III

MODERATORS: DN Levin, MD
MD Osbakken, PhD

531 • 2:45 PM

Heterogeneity of Citrate Content within Normal Prostate Determined with Proton MRS

M Lowry, LW Turnbull, DJ Manton, SJ Blackband, A Horsman
Center for MRI, Hull Royal Infirmary, Hull, England

Purpose: Citrate content may provide an indicator of the malignancy of prostatic lesions (1). In this study, we set out to quantify the amount and distribution of citrate within normal prostate as an adjunct to studies of patients with prostatic disease.

Methods: Five volunteers were studied by using a GE 1.5-T Signa imager and a pelvic phased-array multicoil for signal reception with body coil transmission. Voxels (3–5 mL) localized from an axial FSE image (TR/TE, 3,200/160 msec) were placed within the central (CZ) or peripheral (PZ) zone of the gland. Spectroscopic localization was performed by using STEAM with a TR/TE of 1,000/50 msec and 512 averages. Water reference spectra were also acquired. Concentrations were calculated by the method of Barker et al (2) assuming values for citrate T1 and T2 and tissue water content of 1.5 seconds, 0.25 seconds, and 44 mmol/g fresh weight, respectively.

Results: The coil combination used in this study allowed homogeneous excitation of the prostate along with sensitive signal reception. The spectra had excellent SNR and spectral resolution, showing a major peak from citrate and several smaller peaks, including choline. Citrate content of CZ was 60 ± 35 μmol/g (mean ± SD). In each case, PZ citrate content was greater than CZ with a mean of 117 ± 66 μmol/g ($P < .05$; paired t test), although individual values varied according to the anteroposterior location of the voxel.

Conclusions: This demonstration of differences in citrate content of CZ and PZ was only possible by adopting a quantitative method. The large heterogeneity emphasizes the necessity for careful consideration of voxel location during future studies of prostatic disease.

1. Thomas, M.A. et al. (1990). J. Magn. Res. 87 610–619. 2. Barker, P.B. et al (1993). NMR Biomed. 6 89–94.

532 • 2:57 PM

^{31}P MRS of Psoriasis and Skin Tumors: Correlation with Chromatographic Data

A Zemtsov, L Dixon, G Cameron
Texas Tech University School of Medicine, Lubbock, TX

Purpose: Psoriasis is a severe skin disease that affects 1% of the U.S. population. Skin cancers are the most common human malignancy, responsible for approximately 10,000 deaths annually in the United States. Both conditions are characterized by cellular hyperproliferation. At present, no single objective technique (serologic, radiologic, etc) exists to monitor disease activity in psoriasis or to assess the efficacy of systemic or topical chemotherapy in skin cancers.

Methods: Ten patients with psoriasis, 10 patients with skin cancers, and 5 volunteers were enrolled in this study. ^{31}P MRS analysis of psoriatic skin and skin tumors was performed with a 1.5-T unit by using the protocol described by a number of research groups (1). ^{31}P MRS data were correlated with analytic chromatographic data as was previously described (2). In a number of patients with psoriasis and melanomas, ^{31}P MRS examination was repeated after topical and systemic chemotherapy.

Results: Relative amounts of PME and the PME/PDE ratio appear to be sensitive markers of disease activity in psoriasis. Phosphocreatine is highly elevated in psoriatic tissue on the basis of both ^{31}P MRS and HPLC data. Intracellular pH is normal in psoriasis. The tumor type and its differentiation profoundly affected ^{31}P MRS and HPLC data.

Conclusion: ^{31}P MRS appears to be a promising clinical tool for assessing and comparing efficacy of new therapeutic modalities to treat psoriasis. Further work on ^{31}P MRS of skin tumors is warranted.

1. Zemtsov A, et al. Editorial. Arch Dermatol 1993; 129:215–218. 2. Zemtsov A, et al. Am J Med Sci 1993; 305:8–11.

533 • 3:33 PM

Ischemic Injury in Diseased Cardiac Myocytes

MD Osbakken, D Zhang, T Ivanics
Bristol-Myers Squibb, Princeton, NJ

Purpose: Cardiac myocytes from organisms with systemic diseases, such as hypertension (SH) and/or diabetes mellitus (DM), may be more susceptible to ischemic damage than myocytes from nondiseased organisms. It is known that sodium transport abnormalities are associated with both disease processes, and it is possible that the increased risk for ischemic heart disease and/or acute ischemic injury is related to abnormalities in Na transport. This study was designed to further investigate these phenomena.
Methods: To further evaluate the relationship of ischemic damage to Na transport abnormalities as related to changes in bioenergetics, combined ^{23}Na and ^{31}P nuclear magnetic resonance (MR) spectroscopy were used to monitor changes in intracellular sodium (Na_i) and high-energy phosphates, respectively, during and after acute episodes of ischemia in isolated superfused cardiac myocytes from rat models of SH and DM.
Results: In DM (n = 5), exposure to 60 minutes of ischemia was associated with a significantly larger increase in Na_i (percent change from baseline) than occurred in controls (CON) (n = 5) or in SH (n = 7): CON = 50 ± 21%; SH = 79 ± 44%; DM = 209 ± 10%; $P < 0.05$. Reperfusion Na_i returned to baseline in CON but not in DM or SH: CON = 13 ± 14%; SH = 56 ± 26%; DM = 74 ± 40%. Baseline PCr/ATP was similar for all groups: CON = 1.45 ± 0.18; SH = 1.34 ± 0.15; DM = 1.4 ± 0.26. PCr/ATP recovered to 80% of baseline in CON but to only 50% of baseline in SH or DM.
Conclusion: These data suggest that DM myocytes are more susceptible to ischemic injury, whereas both DM and SH myocytes are equally susceptible to reperfusion injury, both phenomena documented as abnormalities in Na transport with ^{23}Na MR spectroscopy. ^{31}P MR data (PCr/ATP) document bioenergetic relationships to the abnormalities in Na transport. While the reperfusion injury might be related to similar global bioenergetic compromise with resultant ion transport abnormalities, the larger ischemia-induced change in Na_i in DM myocytes cannot be explained by bioenergetic phenomena alone, and may be related to membrane damage secondary to chronic exposure of myocytes to ketones and other FFA associated with the hyperglycemic condition.

534 • 3:21 PM

Myocardial Ischemia and Reperfusion Damage: A New Model for In Vivo Study

AJ Farrall, G Wisenberg, DJ Drost, C Rajgopal, RT Thompson
Department of Nuclear Medicine, University of Western Ontario, London, Ontario, Canada

Purpose: Long-term assessment of ischemic and reperfusion damage to the myocardium is important to assess the necessity of surgical or drug intervention. We have developed an animal model to measure, over 4 weeks, changes in ^{31}P-containing myocardial metabolite levels noninvasively and in vivo by using 2D ^{31}P chemical shift resolved spectroscopic imaging (2D-CSI).
Methods: Four sham-operated dogs served as controls; 6 dogs were subjected to left anterior coronary artery occlusion for 2 hours with subsequent occlusion release. ^{31}P 2D-CSI spectra were acquired with an external half-saddle coil on a 2-T Siemens Helicon system, before, during the occlusion, during the first hour of reperfusion, and at 1, 2, and 3 weeks after infarction. Relative tissue concentrations of phosphocreatine (PCr) and inorganic phosphate (Pi) from 2 × 2 × 3 cm myocardial tissue volumes were determined with Siemens software; regional gadolinium-enhanced ^{1}H MRI enabled identification of the zone at risk. Radioactive ^{85}Sr and ^{46}Sc microspheres helped verify occluded or reperfused zones.
Results: Preocclusion PCr:Pi ratios were set to 100%; myocardial pH was 7.03 ± 0.03 (mean ± SEM). Significant ($P < .05$) changes were subsequently observed in the zone at risk. PCr:Pi was reduced to 46 ± 8% (pH = 6.75 ± 0.09) during the first hour of occlusion, to 32 ± 11% (pH = 6.86 ± 0.04) during the second hour of occlusion, and to 50 ± 14% (pH = 6.88 ± 0.05) during the first hour of reperfusion. At 1, 2, and 3 weeks after occlusion release, PCr:Pi ratios ranged from a low of 13% of preocclusion levels, to 100%; pH ranged from 6.7 to 7.1.
Conclusions: For the first time, an in vivo, noninvasive MR model has been developed that can help assess metabolic derangement from myocardial ischemia and reperfusion, over a period of weeks. This model has future potential in the study of mitigating drug action at the metabolic level during myocardial ischemia and reperfusion.

535 • 3:33 PM

Low Extracellular Magnesium Level Induces Ischemia, Intracellular Acidosis, Depletion of Phosphometabolites and Cardiac Failure in Intact Hearts: A ^{31}P MR Study

BM Altura, RL Barbour, TL Dowd, F Wu, BT Altura, RK Gupta
Department of Physiology, SUNY Health Science Center, Brooklyn, NY

Purpose: Deficits in myocardial Mg have been postulated to result in coronary heart disease (CHD) and sudden death ischemic heart disease (SDIHD). There are no controlled studies using either intact laboratory animals or the isolated intact myocardium that have determined whether low extracellular Mg ($[Mg^{2+}]_o$) can result in biochemical signs of myocardial ischemia and whether such effects are reversible.
Methods: Hemodynamic and ^{31}P MR spectroscopic studies were performed on intact, perfused working rat hearts exposed to low (0.3 mM) extracellular Mg($[Mg^{2+}]_o$).
Results: Low $[Mg^{2+}]_o$ perfusion resulted in rapid and significant falls in cardiac output, coronary flow, stroke volume, developed pressure, and the rate-pressure product. Concomitant with this, O_2 consumption decreased and lactate production increased. Hearts perfused with 0.3 mM, instead of 1.2 mM, $[Mg^{2+}]_o$ exhibited significant reductions in ATP, PCr, intracellular free Mg ($[Mg^{2+}]_i$), and pHi; a marked rise in intracellular Pi corresponding to a precipitous fall in the cytosolic phosphorylation potential was seen. Reintroduction of 1.2 mM $[Mg^{2+}]_o$ failed to reestablish either normal hemodynamics or high-energy phosphates and intracellular Pi, which suggests irreversible myocyte injury.
Conclusions: These observations are consistent with the tenet that low $[Mg^{2+}]_o$ can result in marked reduction in oxygen and substrate delivery to the cardiac myocytes, probably as a result of coronary vasoconstriction, which could lead to CHD and SDIHD.

536 • 3:45 PM

Magnesium Pretreatment Protects against Alcohol-induced Hemorrhagic Stroke in Brain: An in Vivo ^{31}P MR Study

BM Altura, BT Altura, A Gebrewold, RK Gupta
Department of Physiology, SUNY Health Science Center, Brooklyn, NY

Purpose: Acute "binge drinking" of alcohol is associated with an ever-growing number of hemorrhagic strokes (HS) and sudden death (SD). It is, however, not clear how alcohol does this, nor is their an acceptable in vivo brain animal model for its study. Since alcohol has long been known to cause depletion of magnesium from the body, we hypothesized that a rapid alcohol-induced loss of brain Mg might precipitate HS and SD, and that Mg pretreatment might prevent the latter.
Methods: Intact rats and ^{31}P MR spectroscopy were used.
Results: All anesthetized rats that received 6.6 g/kg of ethanol i.p. died within 10–35 minutes of alcohol injection. At autopsy of the brain, all demonstrated profound subarachnoid

and intracranial bleeding, clear signs of hemorrhagic stroke. Pretreatment of rats with 4 μmol/min $MgCl_2$, via IV administration for 30–45 minutes, prevented HS in all animals treated with alcohol. Alcohol resulted in rapid (within 3–5 minutes) deficits in whole brain intracellular free Mg ($[Mg^{2+}]_i$) as observed by in vivo ^{31}P MR spectroscopy. Intracellular pH (pHi) and the phosphocreatine (PCr/ATP) ratio also fell. Brains of rats that exhibited HS demonstrated continued and marked intracellular acidosis with progressive fall in the PCR/ATP ratio and elevation in P_i and $[Mg^{2+}]_i$. Rats pretreated with $MgCl_2$ exhibited relatively stable brain $[Mg^{2+}]_i$ and essentially unchanged pHi, PCr, ATP, or P_i after alcohol, although such animals exhibited 3-fold alterations in plasma Mg^{2+}, as measured by ion-selective electrodes.
Conclusions: These observations suggest that heavy alcohol ingestion can result in severe vasospasm, ischemia, and rupture of blood vessels (HS) probably as a consequence of depletion of brain $[Mg^{2+}]_i$. Pretreatment with Mg^{2+} can effectively prevent HS in this model.

537 • 3:57 PM
MR Imaging and MR Spectroscopy of Propionic Acidemia
AP Chemelli, SR Felber, W Sperl, S Bösch, G Birbamer, W Endres, FT Aichner
Department of Magnetic Resonance Imaging, University of Innsbruck, Innsbruck, Austria
Purpose: We investigated changes in MRI and MRS results in children with treated propionic acidemia (PA).
Methods: All children had their disease biochemically diagnosed before and were investigated during adequate therapy. One mother, who presented with neurologic symptoms, was also examined. The studies were performed with a whole-body 1.5-T Magnetom (Siemens) with a circular polarized head coil for imaging and for localized proton spectroscopy. The imaging protocol consisted of sagittal T1-weighted and proton-density/T2-weighted double-echo sequences in 2 orientations. The volumes of interest (27 mL) for MRS were targeted to the white matter by using a stimulated-echo sequence (TR = 1,500 msec, TE = 270 msec).
Results: With MRS, all 3 children showed a doublet resonance at 1.3 ppm. MRI yielded signal alterations within the white matter (2 children) and within the basal ganglia (1 child). The father of 2 children was normal at MRI and MRS, but the mother had signal alterations in the white matter and proton spectra revealed a peak at 1.3 ppm. Follow-up MRS results after the neurologic symptoms had resolved were normal.
Conclusion: The doublet at 1.3 ppm on the spectra most likely reflected lactate and indicated metabolic impairment despite adequate treatment. In combination with MRI, MRS may become a useful tool for investigating this rare inborn error of metabolism.

Wednesday Afternoon • Sapphire Room
Papers 541–547

DIFFUSION
MODERATORS: JA Helpern, PhD
RR Price, PhD

541 • 2:45 PM
High-Speed MRI Protocol for the Evaluation of a Putative Cerebroprotective Agent: Recombinant Human Basic Fibroblast Growth Factor
TP Roberts, ZS Vexler, N Derugin, ME Moseley, J Kucharczyk, C Emmett
Department of Radiology, University of California, San Francisco, CA
Purpose: This study evaluated the cerebroprotective effects of recombinant human basic fibroblast growth factor (rh-bFGF) (Syntex/Synergen Neuroscience Joint Venture) in acute cerebral ischemia. Diffusion- and perfusion-sensitive echo-planar imaging were used in a cat model of stroke.
Method: Twenty-two cats underwent 2-hour unilateral occlusion of the middle cerebral artery (MCA), with 10 hours of reperfusion, during which the animals received continual intravenous rhbFGF infusion. The extent and severity of cytotoxic edema was assessed with diffusion-sensitive imaging, and perfusion deficits were evaluated with Dy-DTPA-BMA–enhanced (0.25 mmol/kg Sprodiamide, Sanofi-Winthrop) echo-planar imaging. After 10 hours, histologic examination was performed.
Results: Histologically measured damage in control animals comprised 30.7 ± 15% of the right hemisphere. In rhbFGF-treated groups, injury volumes were 18.7 ± 3.8% (14 μg/kg/hr), 24.1 ± 6% (42 μg/kg/hr), and 15.9 ± 9.6% (125 μg/kg/hr). These were not significantly different from control ($P > .05$). Ten hours after reperfusion in control animals, cerebral blood volume (CBV) in the ischemic hemisphere was 58 ± 17% of the contralateral hemisphere. In drug-treated groups, CBV ratios were not different ($P > .05$): 54 ± 16% (14 μg/kg/hr), 40 ± 19% (42 μg/kg/hr), 75 ± 8% (125 μg/kg/hr). During occlusion, the apparent diffusion coefficient (ADC) was reduced in the ischemic MCA territory (0.64 ± 0.02 × 10^{-5} cm^2/sec) compared with that of the contralateral hemisphere (0.76 ± 0.01 × 10^{-5} cm^2/sec). After reperfusion, there was no significant difference in ADC between hemispheres.
Conclusion: High-speed MRI enabled a serial assessment of the action of rhbFGF in acute regional ischemia. At the doses studied, rhbFGF did not improve cerebral perfusion or confer significant cerebroprotective benefit.
C. Emmett is an employee of Syntex Corporation.

542 • 2:57 PM
Diffusion-weighted MR Imaging and Perfusion Echo-Planar Imaging in a Rat Stroke Model
W Reith, B Elger, M Forsting, S Heiland, J Seega, J Weber, K Sartor
Department of Neuroradiology, University of Heidelberg, Heidelberg, Germany
Purpose: Diffusion-weighted imaging (DWI) can quantitatively display ischemic lesions within minutes after the onset of ischemia. Perfusion imaging is usually performed by injecting a bolus of a contrast agent and then obtaining a rapid series of MR images by using an ultrafast technique. We performed this study to determine the effects of 1-hour temporary ischemia with use of DWI and perfusion echo-planar imaging (EPI).
Methods: Focal ischemia was induced in eight Wistar rats by using a suture occlusion of the middle cerebral artery (MCA). Reperfusion was achieved by withdrawing the suture thread. Thirty minutes after MCA occlusion, coronal multislice DWI spin echo and single-slice DWI-EPI studies at the optic chisma were performed. Forty-eight coronal single-slice perfusion EPI studies at the optic chiasm were acquired within 48 seconds after administration of a bolus of superparamagnetic iron particles. The same MRI protocol was used 15 and 60 minutes after reperfusion. Twenty-four hours later, DWI and T2-weighted spin-echo imaging were performed, and the infarcted area was confirmed with TTC staining.
Results: DWI clearly demonstrated the ischemic area 30 minutes after MCA occlusion and showed a reduction of this area after reperfusion. Pre-reperfusion EPI perfusion images showed a perfusion deficit in the territory of the occluded MCA, which corresponded well to the region of DWI changes. After reperfusion, a delay in signal reduction occurred indicating that reperfusion was not complete.
Conclusion: Our results suggest that DWI and perfusion EPI are both useful in the early detection of ischemia. Early DWI can display not only irreversible but also reversible ischemic brain damage. The combination of DWI and perfusion images may be helpful in the prediction of ischemic lesions that can be rescued either by reperfusion or by therapeutic intervention.

543 • 3:09 PM

Bandwidth Comparison of EPI Diffusion Sequences for Stroke Imaging

F Schmitt, S Waraoh, P Wielopolski, RR Edelman
Siemens Medical Systems, Erlangen, Germany; Beth Israel Hospital, Boston, Mass

Purpose: Low- and high-bandwidth (BW) EPI spin-echo diffusion-weighted sequences were compared to evaluate susceptibility effects, signal to noise (SNR), and spatial resolution for stroke imaging.
Method: EPI comparison studies were performed on a 1.5-T whole-body imager equipped with a three-axis echo-planar gradient system (Siemens Medical System, Erlangen, Germany). The fastest EPI sequence uses a 1-kHz readout gradient with 0.5-msec measurement time per projection. The low-BW sequence uses a measurement time of 0.7 msec per projection. In both sequences, 200 data points per projection were measured to avoid aliasing. The 200 acquired samples were interpolated to 128 data points and afterward were Fourier transformed to the final image. Both sequences were fixed to a given minimal field of view (FOV) of 25 cm in the single-shot mode. Also, the matrix size (128^2) and slice thickness, as well as the number of slices in the multislice mode, were kept constant. The TE was fixed at 100 msec.
Results: The SE-EPI diffusion-weighted sequence was used for brain imaging in stroke patients and in volunteers. In stroke patients, the stroke lesion was clearly visible with both sequences without any differences. Both sequences used diffusion b values of 0/34/137/307/546/856 sec/mm^2. Susceptibility artifacts visible in the sinus region were slightly more pronounced on the low-BW images due to the longer readout time and the lower phase-encoding gradient. SNR was proportional to $1/\sqrt{BW}$. Low-BW images had therefore a higher SNR as expected by theory. Image sharpness was the same in both sequences because motion in the brain, such as CSF pulsation effects, is frozen with both BW sequences.
Conclusions: Low- and high-BW EPI show similar results for diffusion-weighted imaging in stroke patients. SNR is better in the low-BW sequence. However, susceptibility effects are more pronounced with the low-BW sequence.
F. Schmitt is an employee of Siemens Medical Systems.

544 • 3:21 PM

Diffusion-weighted Echo-Planar Imaging of Brain Tumors

RL De La Paz, A Knott, M Rohan, M Matuzek
Department of Radiology, Memorial Sloan-Kettering Cancer Center, New York, NY

Purpose: Evaluation of water proton diffusion in brain tumors and surrounding abnormal tissue by using diffusion-weighted echo-planar imaging (DW-EPI).
Methods: Diffusion-weighted images were obtained with a Stejskal-Tanner spin-echo EPI technique by using a 1.5-T GE Signa MR upgrade (Instascan, Advanced NMR) with TR = 4000 msec and TE = 135 and 50 msec diffusion gradient pulses. Multiplanar images (5 mm thick, 2.5 mm gap, 256 × 128 matrix, 1.5 × 1.5-mm pixels, 2 NEX) were obtained without motion artifact from unrestrained patients in 37–64 seconds by using 4–6 gradient steps (0 to 10 mT/m, b values from 0 to 730 sec/mm^2). Apparent diffusion coefficients (ADCs) (mm^2/sec) were calculated as the slope of the semilog plot of signal intensity versus b. Twenty-two patients (age range, 7–81 years) with diagnoses of astrocytoma (n = 8), primary CNS lymphoma ([PCNSL] n = 5), and metastases (n = 9) were studied.
Results: ADC values (10^{-3} mm^2/sec) ranged from 0.55 to 3.99. The highest mean ADC values were seen in ventricular CSF (3.82) and cyst fluid (3.32). Areas of postsurgical encephalomalacia (2.66) and white matter vasogenic edema (2.14) showed higher mean values than radiation necrosis (1.93) or tumor necrosis (1.85), which were substantially higher than normal GM (1.06) or WM (0.87). Mean ADC values varied by tumor type and were highest in metastases (1.72) and astrocytoma (1.49) and substantially lower in PCNSL (0.77). No consistent differences were seen between enhancing and nonenhancing tumor tissue or between grades of astrocytoma.
Conclusion: DW-EPI images provide unique information, not available on T1W or T2W images, which can help discriminate between cyctic and solid lesions and may help identify specific tumor types, such as PCNSL.

545 • 3:33 PM

Multiexponential Diffusion Signal Decays in Human Brain at Large b Values

KK Kwong, YC Chen, TL Davis, BR Rosen
NMR Center, Massachusetts General Hospital, Charlestown, MA

Purpose: To study the nonlinear characteristics of MR diffusion decay in human brain tissues as a function of MR diffusion sensitivity (b value) and to study the contribution of different mechanisms to such nonlinearity.
Methods: We acquired human brain diffusion data with a spin-echo diffusion-weighted sequence with a 1.5-T GE imager equipped with echo-planar Instascan. Diffusion gradients stepped from zero to the maximum of 1 G/cm for the x, y and z axes, giving a maximum of 1.73 G/cm. The diffusion gradient duration was fixed at 70 msec, diffusion time at 73 msec, and TE at 185 msec.
Results: As b values increase from 0 to 6,000 sec/mm^2, we measured multiple diffusion coefficients in brain white matter, cortical gray matter, and deep gray matter such as the putamen and caudate nucleus. The MR signal was characterized by a multiexponential decay.
Discussion: Multiexponential behavior reflects the presence of different tissue populations. The partial volume effect of CSF is small here because CSF signal decays away at a large b value. White matter anisotropy contributes to the multiexponential decay. However, factors other than anisotropy are also at work as evidenced by the presence of multiexponential decay in cortical gray and deep gray matter. In addition, diffusion tensor measurement shows that multiexponential decay in white matter exists even in the largest diffusional direction. Our in vivo results agree with cell culture results (1), which suggest that the multiexponentials also reflect extracellular versus intracellular water.
1. Niendorf et al (1993) Proceedings SMRM, 2, 600.

546 • 3:45 PM

In Vivo Echo-Planar Diffusion Mapping of the Kidney

MF Mueller, PV Prasad, B Siewert, RR Edelman
Department of Radiology, MRI, Harvard Medical School and Beth Israel Hospital, Boston, MA

Purpose: To measure the effect of acute dehydration and hydration, renal artery occlusion, and unilateral ureteral occlusion on diffusion measurements, and to evaluate the intravoxel incoherent motion (IVIM) model in the kidney.
Methods: A stimulated-echo acquisition method (STEAM), echo-planar imaging (EPI), and a spin-echo (SE) EPI sequence were used to perform the diffusion measurements with a 1.5-T Siemens whole-body MR imager. Eighteen normal volunteers were examined dehydrated (12 hours of fasting) and rehydrated (1 hour after drinking 20 mL of water per kg of body weight). Additionally, an SE EPI sequence was used to evaluate the IVIM model in 6 normal volunteers. In a pig model, the effect of acute renal artery occlusion and ureteral occlusion was studied.
Results: The paired t test showed a significant ($P < .0001$) increase in the ADC from the dehydrated (mean: 2.9×10^{-3} mm^2/sec ± 0.57) to the hydrated (mean: 3.6×10^{-3} mm^2/sec ± 0.37) state. Dehydration and hydration were confirmed by examining urine osmolality. A significant decrease in the ADC after occlusion of the renal artery and/or ureter could be observed.
Conclusion: In vivo diffusion measurements in the kidneys are now possible by using a STEAM EPI or SE EPI sequence. A significant difference was observed between acute dehydration and rehydration, before and after obstruction of the renal artery and/or the ureter. We did not observe any evidence for the IVIM model in the kidney.

547 • 3:57 PM

3D Evolution of Ischemia in a Rat Stroke Model Studied with Diffusion Mapping

LL Latour, Y Hasegawa, W Reith, BJ Dardzinski, M Fisher, CH Sotak

Department of Biomedical Engineering, Worcester Polytechnic Institute, Worcester, MA

Purpose: Previous studies of the evolution of ischemia provide 2D information at the optic chiasm but give no information for the other parts of the brain involved in the ischemic region. With use of the apparent diffusion coefficient (ADC), a reliable predictor of ischemic regions, the aim of this study was to show the 3D evolution of ischemia over time.
Method: In 8 Sprague-Dawley rats, ischemic infarction was induced by means of intravascular suture occlusion of the middle cerebral artery (MCA). Eight contiguous coronal slices (1.5 mm thick) were acquired with echo-planar imaging (EPI) by using 8 different gradient strengths (G = 2–16 gauss/cm, δ = 10 msec, Δ = 25 msec) for calculation of the ADC. Thirteen time points were collected from 3 to 180 minutes after the occlusion. We defined *ischemic* tissue as having ADC values below 0.6 cm^2 sec^{-1} and monitored the 3D spread of ischemia.
Results: Within 5 minutes after the onset of ischemia, the 2 slices adjacent to the optic chiasm showed an ischemic area in the territory of the MCA. The area in these slices evolved over 60 minutes to its maximum size, which corresponded to postmortem TTC staining, while the absolute value of the ADC still continued to decrease over time. In the frontal and occipital part of the brain, the ADC decreased later, which indicated a delayed spread of the ischemic lesion.
Conclusion: Within 1 hour, the ischemic regions in optic chiasm slices reached their maximum size, while later, spreading to the frontal and occipital part of the brain could be observed. The 3D monitoring of ischemia over time gives new insights into the pattern of evolution of acute ischemic stroke in this experimental stroke model.

Wednesday Afternoon • Topaz Room
Papers 551–558

OTHER: Instrumentation, Safety, Relaxometry

MODERATORS: E Kanal, MD
SR Thomas, PhD

551 • 2:45 PM

Wireless Operation of Receive Surface Coils

GJ Misic

Medrad, Inc, Indianola, PA

Purpose: The connecting cable between a surface coil and the host MRI system often presents a logistical inconvenience during patient imaging, and may create a potential safety hazard due to effects on the transmit RF B_1 and electric fields. Our goal was to create a means of eliminating the surface coil cable without creating any degradation in imaging performance of the host system. A secondary benefit was sought in the elimination of signal losses due to the attenuation inherent in the cable and connectors.
Methods: To achieve our goal, two devices were developed to transmit the surface coil signal to the receiver input of the host MRI system via a high-frequency RF telemetry link. The contrivance added to the surface coil included a preamplifier, an RF transmitter operating in the UHF band, and a modulator to apply the surface coil signal to the transmitter output. Battery power was used to operate the device. Located adjacent to the system receiver port was a compatible telemetry receiver including a demodulator intended to recover the surface coil signal without loss of dynamic range or signal phase information.
Results: The system was built and optimized. Comparisons were then made between a surface coil utilizing the described hardware and a similar surface coil employing a conventional coaxial output cable. Image quality was then compared between the two devices, with favorable results for the wireless coil design.
Conclusions: Our hardware system provides the stated advantages without a performance penalty.

552 • 2:57 PM

Quadrature Transmit/Receive Coil for Neurovascular Imaging

GJ Misic, WJ Monski

Medrad, Inc, Indianola, PA

Purpose: Quadrature coil technology has been shown to provide substantial benefit in image signal-to-noise ratio (SNR). Creation of a coil capable of imaging from the aortic arch to the top of the brain while maintaining quadrature field uniformity over the entire volume is complicated by the presence of the shoulders. Distorted bird-cage geometries do not provide sufficient uniformity over this volume. We developed a geometry that possessed sufficient uniformity over the target anatomy to enable operation as a transmit/receive coil while allowing patient access.
Methods: A coil geometry was developed that maintained satisfactory uniformity from both quadrature modes over the entire imaging volume, while simultaneously providing excellent patient access. Two versions were constructed, one capable of acquiring the imaging data from the entire region in a single acquisition, and a second coil having reduced coverage in the superior-to-inferior direction but providing substantially greater image signal-to-noise performance. A unique geometry that operates the conductors in two simultaneous modes was employed.
Results: The fields created by the coils were mapped and found to possess sufficient uniformity for use with the anticipated imaging techniques. Each of the coils was then compared for image SNR with the system head coil as a baseline. The longer single-acquisition coil was found to produce 85% of the reference SNR; the dual acquisition coil measured 115% of the reference.
Conclusions: Our devices enable quality neurovascular studies to be accomplished by using the benefits of both quadrature and transmit/receive technology.
G.J. Misic and W.J. Monski are employed on the Medrad, Inc, engineering staff.

553 • 3:09 PM

Flexible Quadrature Surface Coils with Automatic Isolation Optimization

GJ Misic

Medrad, Inc, Indianola, PA

Purpose: Quadrature coil technology has been shown to provide substantial benefit in image signal-to-noise ratio; however, the isolation of one coil mode from the other must be maintained at a high level to realize this advantage. Flexible surface coils impart advantages in filling factor and patient comfort; however, the variability of the coil geometry generally precludes the use of quadrature technique due to the loss of defined geometry. Our goal was to develop a means of optimizing both the coil tuning and quadrature isolation on a per-patient basis in an automatic manner.
Methods: To achieve our goal, a device was developed that was capable of both tuning each of the two quadrature modes of the flexible coil and then optimizing the isolation between the modes via an electronic isolation adjustment with scalar network analysis techniques. An S11 measurement was used to correct the tuning of each coil mode; an S21 criterion optimized the isolation. Included within the device architecture was a means of performing several iterations due to the interactive nature of the adjustments. A flexible surface coil of quadrature design was built and interfaced to the tuning device.
Results: Without use of the tuning device, quadrature isolation was found to drop from a nominal −30 dB to a value inferior to −10 dB. Use of the automatic isolation device returned the quadrature isolation to a value better than −23 dB. Image signal-to-noise ratio comparisons disclosed an improvement of 30% with the optimized coil.

Conclusions: Our device enhances quadrature flexible surface coil performance while maintaining the quadrature benefit.

554 • 3:21 PM

Global Optimization Design of Elliptical Z-Gradient Coils

Y Du, DL Parker
Radiology Department, University of Utah Health Sciences Center, Salt Lake City, UT

Purpose: Conventional MRI gradient coils have a circular cross section. Local optimization algorithms are commonly used for the design of these z-gradient coils. In this presentation, we report on (*a*) a numerical study of the inductance dependency on different ellipticities of z-gradient coils and (*b*) a global optimization algorithm that provides a z-gradient coil design with the best achievable coil performance.
Methods: The magnetic field, and thereby the gradient strength Gz, induced by the current in an elliptical loop was calculated by using Biot-Savart law. For a specified geometry of a loop, Gz at a test point P(x, y, z) is a function of x and y and the longitudinal distance between the loop and the test point. The mutual inductance M of two loops is a function of the distance between the two loops. Two look-up tables for Gz and M can be built for all the test points and possible loop positions. The global optimization algorithm searches all the possible loop combinations for the best coil performance by using these two look-up tables.
Results: The global optimization of a 16-loop z-gradient coil design results in a considerable reduction in both coil inductance and root-mean-square error of gradient linearity compared with a published circular coil with the same coil configuration. The computation time of the global optimization process was within one-half hour on a Sun Sparc10.
Conclusion: The use of elliptical gradient coils considerably reduces coil inductance while maintaining patient accommodation. By applying the "look-up table" approach, the global optimization achieves the best performance with a reasonable computation time.

555 • 3:33 PM

Effects of MR Gradient Noise on Vital Signs of Term Newborns With and Without Cerebral Anomaly

MK Philbin, LA Hayman
School of Nursing, University of Texas, Houston, TX

Purpose: Newborn infants can respond to sensory stimulation with changes in vital signs (1), and their systemic blood pressure has been shown to directly influence cerebral blood flow (2). While mild stimulation can elicit autonomic instability in the preterm, intense stimulation is usually required to elicit such instability in the term infant. This study examines the effects magnetic resonance (MR) gradient noise on vital signs of term newborns with and without cerebral anomaly during high-field scans.
Methods: Four term newborns were monitored (Invivo Research, Inc) for heart rate (HR), blood pressure (BP), and oxygen (O_2) saturation during brain imaging with a GE 1.5-T Signa imager. Infants were sedated with chloral hydrate, swaddled, and stabilized with foam padding around the head and ears. HRs were averaged over 3 to 7 samples per minute.
Results: A normal newborn had HRs that rose and fell in 2 to 4-min cycles between 126 beats per min (bpm) and 240 bpm for 10 of the first 20 min of scanning. Another normal newborn had BPs that rose throughout the scan from a normal level of 84/64/44 mm Hg to levels meeting systolic and diastolic criteria for hypertension at 96/83/78 mm Hg. An infant with Chiari syndrome had an HR that rose during the first 6 min of scanning from 100 to 178 bpm, a level above the 97th percentile of resting rates in the 1st week after birth. It remained outside the normal range, between 150–170 bpm, for 40 additional min until the scan was complete. A newborn with Dandy Walker variant had an initial high-normal BP at 85/72/57 mm Hg, which dropped to normal at 54/44/41 mm Hg by the end of scanning. O_2 saturation fell steadily from 96% to 93%.
Conclusions: Sedated term infants with and without brain anomaly showed unexpected variability in HR, BP, and O_2 saturation during MRI. This autonomic instability in sedated newborns may be related to auditory stimulation of the brain stem produced by MR gradient noise. Greater effects of auditory stimulation could logically be expected in the preterm infant. Clinicians may wish to investigate these phenomena in their own settings and to establish guidelines for monitoring the newborn during MRI and for terminating the procedure.
1. Als H. (1986) A synactive model of neonatal behavioral organization. In: J.K. Sweeny (ed). The high-risk neonate: developmental therapy perspectives. *Physical Occupational Therapy in Pediatrics.* 6 (3/4):3–53. 2. Lou HC, Lassen NA, Friis-Hansen B. (1979) Impaired autoregulation of cerebral blood flow in the distressed newborn. J Pediatr 94, 1:118–121.

556 • 3:45 PM

Measurement of Acoustic Noise During MR Imaging: Evaluation of Six Different Worst-Case Pulse Sequences

FG Shellock, M Ziarati
Tower Imaging, Los Angeles, CA

Purpose: To determine the acoustic noise associated with MR imaging by using various worst-case pulse sequences.
Methods: Acoustic noise levels were measured during MR imaging with a 1.5-T GE MR system (4X software). Acoustic measurements were made at the entrance and at the center of the magnet with a modified device that is unperturbed by electromagnetic radiation. Ambient noise (ie, during operation of the fan and cryogen reclamation system) and 6 worst case (ie, small FOV, small slice thickness, short TE/TR) pulse sequences were evaluated: 4 gradient echo, 1 spin echo, and 1 reduced-flip-angle, fast spin echo.
Results: Ambient noise levels were 73 dB at the entrance of the magnet and 84 dB at the center of the magnet (A-weighted scale). The highest noise levels during MR imaging occurred with the gradient-echo pulse sequences and were 102 dB at the entrance of the magnet and 103 dB at the center of the magnet (A-weighted scale).
Conclusions: MR imaging performed with worst-case pulse sequences did not produce noise levels that exceeded OSHA guidelines. However, the acoustic sounds were at levels that can impair oral communication and annoy patients undergoing MR procedures. Therefore, techniques to attenuate acoustic noise and improve patient communication should be used during MR imaging, especially during the use of gradient-echo pulse sequences.

557 • 3:57 PM

Modeling of Collagen Molecular Motion with the Magic Angle Effect

P Vinée, B Meurer, A Constantinesco
CHU Hautepierre, Strasbourg, France

Purpose: The fiber-to-field angular dependence of the transverse relaxation times in tendons has been demonstrated by using a biexponential model (Fullerton et al) or a quadriexponential decay (Peto et al). Our purposes are to complement the description of the anisotropy of transverse relaxation characteristics and to model the molecular motion of collagen in tendon by using solid-state MR techniques (1) to identify the signal of the collagen molecule ($T2 \approx 18$ μsec).
Methods: ^1H MR in vitro measurements were made at 90 MHz. We measured the second moment M_2 of the line shape and the T2 of collagen as well as magnetization amplitudes (global and of collagen) in patellar tendon obtained from fresh human cadavers. The samples were placed in a special gyroscopic device that allowed monitoring of the angle γ between the orientation axis of the tendinous fibers and the direction of H_0. The measurements were repeated stepwise every 5° in the range from −30° to 210°. The experimental results were compared with the expected theoretical angular dependence obtained from computer calculations by using a molecular collagen model and a molecular motion model (1).
Results: All the measured parameters had an angular dependence. This dependence is well fitted by a polynom of second

and fourth order Legendre polynoms of γ, as predicted by theory (2). Confrontation of experimental measurements and theoretical calculations allows precise modeling of collagen macromolecular motion.
Conclusions: We present a model for collagen macromolecular motion. Furthermore, our results complement the description of the angular dependence of transverse relaxation parameters in tendon, a highly oriented tissue. The obtained experimental values are consistent with the results of computer simulation of the fiber-to-field dependence of the second moment of the line shape M_2 according to general theory of MR in macromolecules.
1. Vinée Ph et al. Magn Reson Med 1993; 29:292–295. 2. Olf HG, Peterlin A. Journal of Polymer Science: Part A-2, Vol. 8:753–770, 1970.

558 • 4:09 PM

Simulation of Peripheral Muscle Response to Externally Applied Temperature Stress in Volunteers

IR Young, JW Hand
NMR Unit, Royal Postgraduate Medical School, Hammersmith Hospital, London, England

Purpose: To attempt to model the changes in MR tissue parameters reported previously (1) so as to assess the contributions from perfusion on the one hand and diffusion or T1 on the other as the temperature of tissue is varied.
Method: A theoretical model was developed on the basis of there being two sources of the MR signals seen in vivo (blood and muscle parenchyma), to describe both the diffusion-weighted (2) and T1-dependent (3) systems, which have been the basis of the vast majority of in vivo experimental work thus far. The choice of parameters for the modeling was the work reported previously (1).
Results: The model showed how the earlier T1-dependent experiments could achieve the apparently good results they did (2), while at the same time failing to detect that the time-temperature coefficient of T1 was far from that observed. Models for both diffusion and T1 dependency emphasized how important it is that all the observations used in the calculation of a parameter be obtained at the same temperature.
Conclusion: The approach to temperature observation that uses diffusion weighting is more robust than that which uses T1. However, anisotropy considerations were not included in the model studied, and this means that the normal approach represents a significant reduction in the complexities of the model.
1. I.R. Young et al, Proc SMRM, New York, 1993, p 1279. 2. D. LeBihan et al, Radiology, 171, 853–857 (1989). 3. R.B. Dickinson et al, J Comput Assist Tomogr, 10, 468–479 (1986).
I.R. Young receives partial funding from Picker International.

Notes

Notes

Scientific Posters

The Scientific Poster Exhibits offer SMR attendees an opportunity to examine and discuss scientific material in a more intimate atmosphere.

Discussion periods, moderated by individual Scientific Poster presenters, are scheduled daily throughout the Meeting. A schedule of the discussion times follow:

Section:	**Diffusion/Perfusion/Functional/ Contrast Agents/Spectroscopy**
Poster #:	**P001-P019**
Day, Date:	**Sunday, March 6**
Time:	**12:00 PM - 1:30 PM**
Section:	**Clinical MRI: Head, Spine and Body**
Poster #:	**P101-P145**
Day, Date:	**Monday, March 7**
Time:	**12:30 PM - 1:30 PM**
Section:	**Artifacts/Instrumentation/ Safety/Pulse Sequences**
Poster #:	**P201-P220**
Day, Date:	**Tuesday, March 8**
Time:	**12:15 PM - 1:30 PM**
Section:	**Vascular Imaging & Flow Quantification/Cardiac**
Poster #:	**P301-P318**
Day, Date:	**Wednesday, March 9**
Time:	**12:15 PM - 1:00 PM**

SCIENTIFIC POSTER EXHIBIT AREA

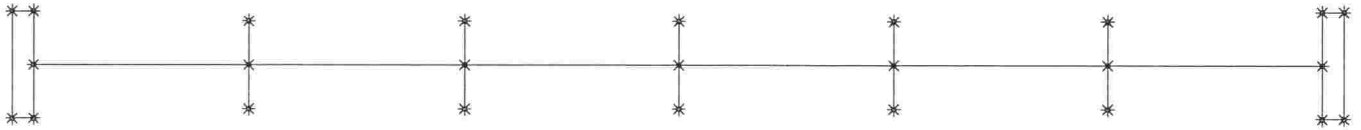

AISLE 000 –Diffusion/Perfusion/Functional/Contrast Agents/Spectroscopy

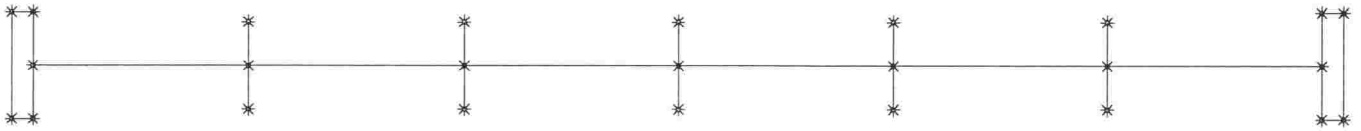

AISLE 100 – Clinical MRI: Head, Spine, and Body

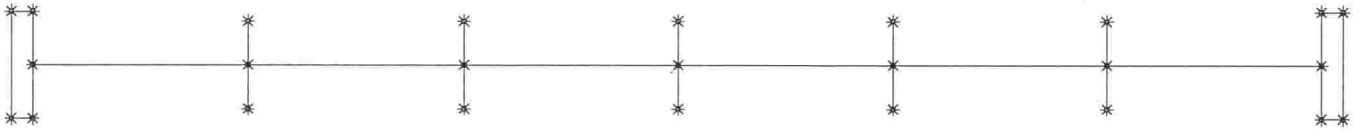

AISLE 200 – Artifacts/Instrumentation/Safety/Pulse Sequences

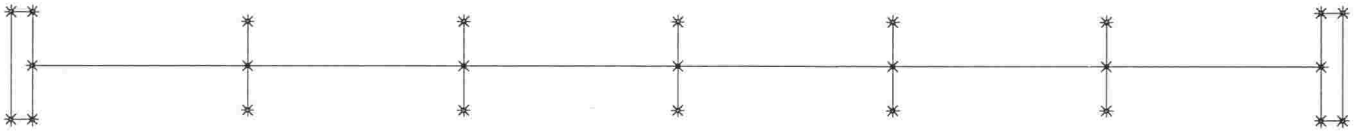

AISLE 300 – Vascular Imaging & Flow Quantification/Cardiac

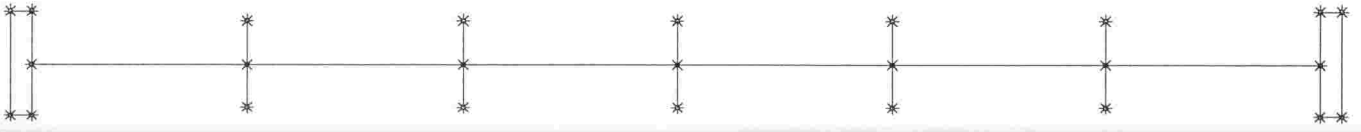

SMR '94 First Meeting of the SMR
Poster Abstracts

Sunday, March 6, 12:00 PM–1:30 PM
Diffusion/Perfusion/Functional/Contrast Agents/Spectroscopy

Posters P001–P019

P001

Determination of Anisotropic Diffusion and Convection Parameters in 3D with a Combination of an MRI Contrast Agent Concentration Profile and Diffusion-weighted Imaging

VD Calhoun, S Kalyanasundaram, A Su, S Eller, KW Leong
The Johns Hopkins University, Baltimore, MD

Purpose: In this study, methods of drug delivery that bypass the blood brain barrier by directly placing the drug at the site of interest were investigated by using MRI data in a novel way. Diffusion-weighted imaging combined with T1-weighted imaging is shown to allow determination of various parameters: the proper dose level, release rate, and drug distribution due to both diffusional and bulk flow terms in the brain tissue.

Methods: We delivered paramagnetic contrast agents of varying molecular weights into rabbit brain parenchyma using both a liquid solution of the drug and implantation of an implantable controlled release device. Diffusion-weighted imaging was utilized to determine the diffusion coefficient tensor of water and then combined with T1-weighted spoiled-GRASS imaging to create a relaxation rate-distance map and determine the spatial tortuosity of the rabbit brain. Then, the convection-diffusion equation was solved for the bulk flow term. Both edematous and aedematous conditions were explored.

Results: We calculate diffusion coefficients of various "drugs" in agar, the apparent diffusion coefficient of our drug in the brain tissue, the tortuosity of the brain tissue, and the velocity. We show that the bulk flow vectors are quite irregular, but their magnitudes are similar to that previously published. Flow along the white matter tracts was observed in edematous conditions.

Conclusion: This method of parametric determination is shown to be highly versatile, and has a large advantage over conventional methods due to its noninvasive nature.

P002

Multislice, Fast, Inflow-Sensitized Turbo Spin-Echo Functional Brain Imaging

PR Luyten, GH van Yperen, RW de Boer
Philips Medical Systems, Best, The Netherlands

Purpose: Image contrast during brain activation as studied with functional MRI has been hypothesized to originate from a number of different physiological changes in the neuronal system. Hemodynamic alterations and concomitant oxygen consumption response may result in MR-detectable changes in susceptibility and flow patterns. Since susceptibility changes may have a strong contrast effect at field strengths higher than 2 T, we have optimized a pulse sequence that generates contrast by flow changes that may dominate the functional image contrast mechanism at 1.5 T.

Methods: The sequence comprises a fast, single-shot turbo spin-echo (TSE) (RARE, FSE) sequence that is flow sensitized by a slice-selective inversion pulse. The inversion delay may be tuned to optimize for extreme slow flow patterns in the smaller vessels around the activation focus. Also, outflow effects during the acquisition may be corrected for by varying the slice width of the refocusing pulses.

Results: The single-shot measurements generate images in a 300-msec acquisition time. Resolution is 103 × 128, with a 5-mm slice width. Interleaved multislice applications show increased signal in the left and right precentral gyrus during motor activation. The (transverse) multislice results were reformatted to coronal and sagittal views by maximum intensity projection algorithms.

Conclusion: Inflow-sensitized TSE is an adequate sequence to generate functional image contrast. The sequence can be tuned to slow flow processes, to "zoom" in for parenchymal changes related to brain activation.

P.R. Luyten is an employee of Philips Medical Systems.

P003

Functional MRI of the Supplementary Motor Area and Anterior Cingulate Cortex at 1.5 T

JM Tyszka, W Chew, ST Grafton, PM Colletti
LAC/USC Imaging Science Center, Los Angeles, CA

Purpose: To determine whether oxygenation contrast functional MRI (fMRI) at 1.5 T can isolate the supplementary motor area (SMA) and anterior cingulate cortex (ACC) during real and imagined motor tasks. The SMA is often considered to be the executor of motor activation for the primary motor cortex and the ACC the "gateway" from limbic frontal areas to the motor system.

Methods: We have studied the activation of the SMA and ACC in six normal, right-handed volunteers (ages, 23–46) using both real and imagined finger tapping of the dominant hand. All images were generated with an unmodified 1.5-T GE MR unit and an RF spoiled gradient-echo technique. A single 10-mm-thick coronal slice through the left SMA and ACC was imaged in five sets of five active/five resting tasks. All functional images were reregistered to the first in the set (1) and F-maps calculated by using a single factor ANOVA test between resting and active images on a pixel by pixel basis.

Results: All F-maps showed highly significant ($P < .01$) areas of signal change in the SMA and ACC regions during actual motor tasks. During ideation, highly significant signal changes were typically seen in the ACC, with the SMA responses being greatly reduced or absent.

Conclusion: The locations of movement-associated responses are consistent with PET observations (2) at these locations and suggest that the ACC is involved in ideation of motor behavior.

1. Woods RP, Mazziotta JC, Cherry SR. *JCAT* 1993; 17:536–546. 2. Paus T, Petrides M, Evans AC, et al. *J Neurophysiol* (in press).

P004

Dynamic, Contrast-enhanced MRI at High Spatial Resolution of Implanted MCF7 Breast Cancer during Hormonal Manipulation

H Degani, E Furman, R Margalit, P Bendel
Department of Chemical Physics, Weizmann Institute of Science, Rehovot, Israel

Purpose: Recently we proposed a new hypothesis for the antiestrogenic mechanism of tamoxifen based on inhibition of

angiogenesis and impairment of tumor perfusion (Furman et al, *Cancer Commun* 1991; 3:287–297). Here we present the development of dynamic, contrast enhanced MRI at high spatial resolution aimed at verifying this hypothesis.

Methods: MCF7 cells were implanted in CDI-NU female athymic mice. Hormonal control was maintained with slow-releasing pellets of 17β-estradiol or of tamoxifen. H-1 images were recorded at 4.7 T with T1- and T2*-weighted fast gradient-echo sequences. The resolution ranged between 1 × 0.14 × 0.14 mm and 1.5 × 0.14 × 0.39 mm.

Results: The distribution of intensities in the tumor varied in space and with time following a bolus injection of Gd-DTPA $(NMG)_2$. Decreased intensity on T2*-weighted images revealed the presence of intact microvessels while increased intensity on T1-weighted images revealed large intact vessels and leaky microvessels. Leakage of the contrast agent and slow accumulation in necrotic regions were also followed over time. Tamoxifen treatment (1–2 weeks) led to central necrosis surrounded by regions showing fast contrast enhancement due to rapid leakage from microvessels. This was verified on computed maps of initial enhancement rates and by statistical analysis of the overall enhancement (a twofold increase in maximum percentage of enhancement within 7 days of treatment, n = 7).

Conclusion: Tamoxifen induced leakage from tumor microvessels, thus diminishing their capacity to further deliver nutrients and oxygen into inner parts. Furthermore, changes revealed by contrast enhanced MRI may be used to rapidly evaluate response to tamoxifen therapy.

P005

Complete Elimination of Gd-EOB-DTPA in Hepatic or Renal Dysfunction

A Mühler, I Heinzelmann, HJ Weinmann
Schering AG, Berlin, Germany

Purpose: Gd-EOB-DTPA is a hepatobiliary MR contrast agent with dual elimination by the kidneys and by the liver. The study was designed to investigate (1) whether the dysfunction of either one of the elimination pathways can be fully compensated for by the remaining pathway and (2) whether the elimination of Gd-EOB-DTPA is complete in hepatic or renal dysfunction.

Methods: The study was performed in two groups of rats: group A with ligation of the common bile duct (n = 11) and group B with ligation of renal blood vessels (n = 8). A dose of 0.1 mmol/kg Gd-EOB-DTPA or Gd-DTPA (control) was injected via a tail vein. Bile or urine was collected in fractions of 0–1, 1–2, 2–4, and 4–8 hours following administration of either contrast agent. At the end of the experiments, retention of the contrast agents in the carcasses was determined by measurement of gadolinium concentrations (by means of ICP-AES at a wavelength of 342.247 nm).

Results: Most of the Gd-EOB-DTPA was rapidly cleared from the body, 89.4 ± 7.5% of the injected dose within 4 hours following bile duct ligation (group A) and 87.0 ± 6.0% within 1 hour following ligation of renal vessels (group B). At 8 hours following injection of Gd-EOB-DTPA, 3.0 ± 2.4% of the administered dose of this contrast agent was found in the carcasses of group A, and 1.3 ± 0.6% in those of group B. By comparison, at this time point 1.9 ± 3.2% of the injected Gd-DTPA was found in group A (no statistically significant difference compared with Gd-EOB-DTPA), and 96.3 ± 3.3% in group B.

Conclusion: Based on the rat model, it is expected that the MRI contrast agent Gd-EOB-DTPA is rapidly and effectively eliminated in patients with severely impaired liver or kidney excretory function by virtue of its dual elimination pathway. The dysfunction of liver or kidney may be fully compensated by the remaining elimination pathway.

A. Mühler, I. Heinzelmann, and H.J. Weinmann are employees of Schering AG.

P006

Gd-DTPA Cross-linked with Dextran as a Polymeric Intravascular MR Contrast Agent

NR Puttagunta, WA Gibby, VL Puttagunta
Magnetic Research, Inc, Provo, UT

Purpose: We have developed a polymeric conjugate for use as an intravascular MR contrast agent. Such agents may aid in the assessment of tissue perfusion, capillary integrity, and blood volume.

Methods: A cross-linked Gd-DTPA-dextran polymer was prepared by reacting dextran (77.8 kd) and DTPA-bisanhydride in a 1:10 ratio of DTPA to glucose followed by chelation. MR imaging was performed in Rex rabbits (0.1 mM Gd(III)/kg IV) with a clinical scanner at 1.5 T with spin-echo pulse sequences. Relaxivities were determined at 1.5 T.

Results: The Gd-DTPA-dextran polymer shows higher contrast enhancement in liver (43% vs 15%), and better relaxation rates compared with Gd-DTPA (R_1 = 6.6 s^{-1} mM^{-1}, R_2 = 8.7 s^{-1} mM^{-1} vs R_1 = 4.7 s^{-1} mM^{-1}, R_2 = 5.9 s^{-1} · mM^{-1}). Biodistribution studies showed that blood concentration of the polymer was 140 times greater than that of Gd-DTPA at 30 minutes; only 0.02% of the injected dose was in the blood at 24 hours.

Conclusion: The Gd-DTPA-dextran polymer has a prolonged vascular half-life compared with Gd-DTPA but is easily metabolized and eliminated by 24 hours. A high density of paramagnetic centers results in a low osmotic load per Gd(III) ion compared with other macromolecular agents.

N.R. Puttagunta is an employee of Magnetic Research, Inc.

P007

ASG Receptor–directed Contrast-enhanced Liver MR

VM Runge, JN Dunworth, JW Wells, JE Kirsch, CE Woolfolk
University of Kentucky, Lexington, KY

Purpose: An asialoglycoprotein receptor–directed superparamagnetic iron oxide, designed as an IV contrast agent for liver MR, was evaluated and compared with ultrasmall superparamagnetic iron oxide (USPIO) in an abscess model.

Methods: Fourteen rabbits with a liver abscess were imaged at 1.5 T prior to and 10 and 60 minutes following BMS 180550 injection (Squibb Diagnostics). Five animals were studied at 0.8 mg Fe/kg. A dose range study was also performed in nine animals, evaluating doses of 0.03–1.7 mg Fe/kg. Both SE (TR/TE = 2,500/45, 90; 5.4-minute acquisition time) and breath-hold fast SE (2,500/90; 20-second acquisition time) T2-weighted techniques were employed. Results were compared with USPIO studies in 14 rabbits.

Results: Normal liver decreased in signal intensity by 79 ± 12% at 10 and 78 ± 11% at 60 minutes after 0.8 mg Fe/kg, with no change noted in signal intensity of the lesion. A comparable improvement in lesion detectability was seen on fast SE images, with additional reduction of respiratory artifacts. Doses of 0.3–1.7 mg Fe/kg were equally effective, with a dose response seen only below 0.3 mg Fe/kg. These results did not differ statistically from those seen with USPIO.

Conclusion: Asialoglycoprotein receptor–directed superparamagnetic iron oxide can be employed at 1.5 T to improve liver lesion delineation, in addition to providing receptor-specific information.

P008

Intravenous MR Lymphography in Rats with Gd-DTPA-BSA and Iron Oxide Particles: Influence of Dextran on Interlymphonodal Distribution of Contrast Agents

D Pfefferer, S Wagner, W Ebert, M Kresse, M Taupitz, W Semmler
Institut Für Diagnostik Forschung, Berlin, Germany

Purpose: Evaluation of the rat-specific sensitivity to dextran with respect to the alteration in interlymphonodal distribution of intravenously administered colloidal MR contrast agents.

Methods: MRI was performed at 1.5 T by using SE 2,000/15 and GRE 135/15/15° sequences. The interlymphonodal distributions of superparamagnetic iron oxide particles (SIP, 200 μmol Fe/kg) or Gd-DTPA-BSA (200 μmol Gd/kg) were examined after 24 hours with ex vivo MRI of different lymph nodes embedded in agarose gel. The contrast medium administrations were preceded (1–2 minutes) by IV injection of saline or dextran T70 (25 mg/kg, Pharmacia).

Results: After saline injection, both SIP and Gd-DTPA-BSA are inhomogenously distributed over the different lymph nodes. Both contrast media show highest accumulation in mesenteric lymph nodes. Dextran administration changed the distribution pattern of both contrast media. The accumulation of SIP in mesenteric lymph nodes is dramatically decreased compared with Gd-DTPA-BSA, but the distributions are strongly increased in the peripheral lymph nodes for both (31% higher enhancement [SE] in popliteal lymph nodes for Gd-DTPA-BSA compared with saline injection).

Conclusion: Our earlier observations, that the interlymphonodal distribution pattern of SIP in rats is influenced by the immunosensitivity of this species to dextran, were verified by demonstrating altered distribution behavior of two different contrast media after intravenous dextran administration. Future investigations will concentrate on the evaluation of SIP distribution in different species.

P009

Pharmacokinetic Properties of Gadodiamide Injection in Patients with Impaired Renal Function

MG Svaland, KJ Berg, V Reinton
Nycomed Imaging AS, Oslo, Norway

Purpose: The pharmacokinetic properties of the low-osmolarity, nonionic paramagnetic MR contrast medium gadodiamide injection (Nycomed Imaging AS, Oslo, Norway; and Sanofi Winthrop, New York, NY) were investigated in 10 patients with kidney transplants showing signs of impaired renal function (serum creatinine, 194–362 μmol/L).

Methods: Gadodiamide injection was given intravenously at a dose of 0.1 mmol/kg body weight. Urine and feces were collected at 24-hour intervals for 3 days (four patients) or 5 days (six patients) after injection. I-125 iothalamate (2 MBq) was given concomitantly with gadodiamide injection to study renal excretion. Measurements of gadodiamide were performed by ICP-AES (serum and feces) or HPLC (urine).

Results: The mean elimination half-life for gadodiamide injection was 5.8 hours, about five times that in healthy volunteers. The apparent volume of distribution was 0.21 L/kg body weight, indicating distribution to extracellular fluid only. Three days after injection, a mean of 92% (range, 80%–100%) of the dose was recovered in urine; this figure was unchanged 5 days after injection. The fecal excretion was approximately 0.5% of the dose administered. Total body clearance and renal clearance of gadodiamide injection and iothalamate are almost identical, and this strongly indicates that gadodiamide injection is mainly excreted by means of glomerular filtration. The pharmacokinetics of gadodiamide injection are comparable with those reported for similar agents.

Conclusion: Gadodiamide injection given at a dose of 0.1 mmol/kg to patients with impaired renal function is distributed only to extracellular fluid, and the main route of excretion is glomerular filtration.

M.G. Svaland, K.J. Berg, and V. Reinton are employees of Nycomed Imaging.

P010

Safety of Gadoteridol Injection in the U.S. Clinical Trial Experience

AY Olukotun, JR Parker, CH Rhoda, MA Lucas, DN DeSimone, KM Brooks, TR Lucas, and the Multicenter ProHance Investigators
Squibb Diagnostics, Princeton, NJ

Purpose: This report summarizes the safety experience of gadoteridol injection (ProHance, Squibb Diagnostics) as assessed in 16 U.S. clinical trials.

Methods: Gadoteridol injection was administered intravenously to 1,596 adult and 113 pediatric (< 18 years) patients at rates from slow infusion (< 1 mL/sec) to bolus (≥ 1 mL/sec) and at doses ranging from 0.05 to 0.3 mmol/kg. Patient safety monitoring included physical examinations, vital signs, clinical laboratory results, and adverse events.

Results: No clinically significant changes in physical examination or electrocardiographic findings attributable to gadoteridol injection were noted. Three clinically significant changes in vital signs were observed (one case of hypertension and two cases of hypotension). A total of 81 laboratory changes possibly or probably related to gadoteridol injection were noted in 55 patients (3.2%). Of these, the most common were changes in serum iron (1.6%), TIBC (0.5%), and transferrin (0.3%). No consistent trend in serum iron or serum bilirubin levels was noted. Of 180 adverse events observed in 119 patients (7%), 105 events in 79 patients (4.6%) were considered definitely, probably, or possibly related to gadoteridol injection. The most common drug-related adverse events were nausea (1.5%), taste disturbance (1.3%), and headache (0.9%). No serious adverse events were observed in these trials.

Conclusion: In 16 U.S. clinical trials, gadoteridol injection was shown to be safe for use at injection rates from slow infusion to bolus and at doses from 0.05 to 0.3 mmol/kg.

A.Y. Olukotun is an employee of Squibb Diagnostics.

P011

Eddy Current Correction in Volume Localized MR Spectroscopy

C Lin, AD LeBlanc, HJ Evans, RE Wendt III, RM Rowe
Department of Medicine, Baylor College of Medicine, Houston, TX

Purpose: To obtain accurate MR spectra from a gradient localized volume, the distortion caused by eddy currents must be corrected. Eddy current correction is currently done during postprocessing by using a single-frequency reference FID acquired with the same sequence. Collecting this reference FID internally is not always possible and using an external phantom results in other errors. We investigated a new method based on gradient inversion that does not require a reference FID.

Methods: This technique employs two FIDs from the same selected volume and uses two sequences with opposite gradient waveforms. By multiplying these two FIDs, the phase distortions due to the eddy currents are canceled. The square root of this product is then Fourier transformed to produce the final spectrum. We tested this method in a phantom of corn oil and water mixture simulating fatty bone marrow. Normal and gradient inverted STEAM sequences with 12 ms TE and 4 mT/m gradients were used to collect FIDs on a clinical imager.

Results: The effect of eddy currents is completely removed in the final spectrum. All peaks are correctly registered, including the one from —CH=CH— protons, which otherwise is undetectable. Their relative intensities match those measured with a high-resolution spectrometer.

Conclusion: Eddy current correction with gradient inversion offers many advantages over the current methods using a reference FID. The principles of eddy current correction with gradient inversion may be applied to correct eddy current artifacts in other types of MR imaging.

P012

Automated Processing Software for Proton Spectroscopic Image Data

TJ Doyle, PA Narayana, R Pathuk
Department of Radiology, University of Texas Medical School, Houston, TX

Purpose: Development of an algorithm for automatic processing of multivoxel proton magnetic spectroscopic data and generation of metabolic images.

Methods: Software has been developed as two independent algorithms, automated spectral processing and image dis-

play, and implemented on a SPARCstation 10. Spectroscopic processing is provided through a main window where various functions (baseline correction, apodization, filtration, zero filling, automatic zero-order phase correction with unsuppressed spectral data, postacquisition water suppression, and FFT) are selected. Default functions can be easily hard-coded for processing serial studies or with user-defined values. The spectroscopic data are automatically registered to high-resolution images. The phased spectral peaks are automatically fitted and the areas are normalized to the unsuppressed water (from the spectroscopy volume of interest) to quantify changes in serial studies. Metabolic maps can be viewed in either color or black and white, with shades independently controlled by using sliders. Image processing includes interpolation and superimposition of metabolic images on high-resolution images. The operator can view spectra from any desired location on metabolic or high-resolution images.

Results: The algorithm has been tested in phantoms as well as human volunteers, both normal and with MS. It is found to be robust, efficient, and most importantly, operator independent. It takes about 40 minutes to completely process 32 × 32 CSI data, including generation of metabolic maps.

Conclusion: We have developed a completely automated multivoxel spectral processing algorithm for generating metabolic images that is robust, efficient, and user friendly.

P013

Fast Single-Spectrum Extraction from CSI Data

TR Brown, R Stoyanova, T Javaid, H Jiang
NMR Department, Fox Chase Cancer Center, Philadelphia, PA

Purpose: Chemical shift imaging (CSI) is becoming the method of choice for spectral localization in a wide variety of circumstances. In the case of volume studies, when a 3D data set is acquired, a large number of voxels contain information and their evaluation requires off-line processing and considerable time. Alternatively, in the surface coil studies of tumors, either with ^{31}P to measure phosphomonoesters or ^{19}F to follow 5-Fu uptake in metastases, often only the spectra from a few voxels within the region of interest (ROI) have significant information. This makes the experimental parameters such as shimming, coil position, and so on, over the ROI important for the quality of the data. A rapid feedback from the CSI experiment can provide the investigator with information on what parameters of the experiment need adjustment while the patient is still present.

Methods: After the ROI is identified on the MR image, the investigator inputs the voxel coordinates in millimeters. The program then calculates and applies the appropriate phase factors to voxel shift the desired region to the center of the reconstruction. The FIDs are summed over all k space, and the single resultant FID is displayed on the instrument console. Further processing is then done through the normal processing steps of the instrument. This procedure was developed and installed on a Siemens SP Magnetom.

Results and Conclusion: The procedure is fast and easy to use and allows insight into the quality of data from an examination in a very rapid turnaround time. Operationally, this is an asset because any error, misadjustment, or other experimental problems can be rapidly fixed while the patient is still in the magnet. The addition of this technique should make the CSI acquisition techniques more available to the clinical user, since rapid feedback enhances their utility considerably.

P014

Quantitation of Muscle and Tumor Metabolites from CSI Spectra with a Surface Coil

J Murphy-Boesch, H Jiang, R Stoyanova, F Kappler, WG Negendank, TR Brown
NMR Department, Fox Chase Cancer Center, Philadelphia, PA

Purpose: To develop an automated approach to quantitation of ^{31}P chemical shift imaging (CSI) spectra from human muscle and tumors, taking into account RF magnetic (B_1) field inhomogeneity and the CSI point spread function by using spatial information derived from MR images.

Methods: We have developed an integral expression that incorporates the local B_1 field of surface coils, variable tip angles, and T1 saturation with the point spread function associated with Fourier transformation of CSI data. By using the assumption that a metabolite is uniformly distributed within a well-defined region, which is identifiable on an H-1 image, this expression may be numerically integrated to yield a single normalization constant for the signal from a specified voxel. A standard fixed to the coil is used for overall calibration. We have tested the procedure by using a 100-mL sphere of doped Pi placed in several locations near a 12-cm surface coil. Additionally, we have acquired 27-cm^3 data sets from thigh muscle of normal volunteers.

Results: For five CSI acquisitions from three locations of the 100-mL sphere and nominal tip angles of 45°, 60°, 90°, and 120°, the concentrations of Pi were found to be 97 ± 4% of the correct value. Phosphocreatine (PCr) measured in the thigh muscle of two volunteers was found to be 25.1 ± 0.9 and 21.6 ± 1.6 μmol/mL averaged over four and nine voxels, respectively. In two lymphomas, the concentrations of phosphoethanolomine were 10 and 4 μmol/mL, while those of phosphocholine were 3 and 1.4 μmol/mL (T1 = 1.4 sec, NOE = 1.2).

Conclusion: For homogeneous objects identifiable from MR images, accurate estimates of metabolite concentrations can be made by using a new procedure that corrects for B_1 field, tip angle, point spread effects, and, with knowledge of T1, for partial saturation. Measured PCr concentrations in muscle compare favorably with tissue biopsy results. Automation of these procedures will permit clinical tracking of tumor metabolite levels.

P015

CSI Autoshim: A Fast, Reliable, Automatic Shimming Procedure

TR Brown, J Hu, T Javaid, F Arias-Mendoza
NMR Department, Fox Chase Cancer Center, Philadelphia, PA

Purpose: How well the magnetic field is shimmed determines the spectroscopic resolution, the quality of gradient echo and fat suppression imaging sequences, and water suppression in proton spectroscopy in vivo. We report here a fully automatic shimming procedure (CSI Autoshim) that uses all available shim coils, can deal with combined lipid/water signals, and takes only a few minutes on a standard clinical instrument.

Methods: Chemical shift imaging (CSI) is used to measure the field distributions of the shim coils (once, initially) and of the region of interest (ROI) under study each time the currents are to be adjusted. The procedure minimizes the mean squared error integrated over the ROI between a constant field and the sum of all the shim coil fields plus the measured field. This produces a set of linear equations for the shim currents that can be solved by standard matrix methods. If the resultant shim is not satisfactory, the procedure can be repeated. A single iteration takes ~2 minutes, depending on the computer being used for processing. If the starting shim set is poor, several iterations may be needed.

Results: We have used this procedure in over 100 brain studies with starting line widths of the water peak of an entire head ranging from 20 to 150 Hz. Only one iteration was needed in 50% of cases, two in 40%, and three or more in the remainder. The best line width obtained from an entire head was 7 Hz. The mean and standard deviation of the final line width were 11 ± 3 Hz. Measuring the field distributions of the shim coils over a large region enables the entire pelvis to be shimmed to a 10-Hz water line width. CSI Autoshim has also been used in calf and forearm muscle studies with coils placed 10–15 cm from the magnet center.

Conclusion: CSI Autoshim can be implemented for both MRI and MRS studies with very little time penalty and has been transferred successfully to several sites. It is fully automatic, fast, reliable, and versatile.

P016

Ischemic Injury in Diseased Cardiomyocytes

MD Osbakken, D Zhang, T Ivanics
Bristol-Myers Squibb, Princeton, NJ

Purpose: Cardiac myocytes from organisms with systemic disease (such as hypertension [SH] and/or diabetes mellitus [DM]) may be more susceptible to ischemic damage than myocytes from nondiseased organisms. It is known that sodium transport abnormalities are associated with both disease processes, and it is possible that the increased risk for ischemic heart disease and/or acute ischemic injury is related to abnormalities in sodium transport. This study was designed to further investigate these phenomena.

Methods: To further evaluate the relationship of ischemic damage to Na transport abnormalities as related to changes in bioenergetics, combined ^{23}Na and ^{31}P nuclear magnetic resonance (NMR) spectroscopy were used to monitor changes in intracellular sodium (Na_i) and high-energy phosphates, respectively, during and after acute episodes of ischemia in isolated superfused cardiomyocytes from rat models of SH and DM.

Results: In DM ($n = 5$), exposure to 60 min of ischemia was associated with a significantly larger increase in Na_i (% change from baseline) than occurred in controls (CON) ($n = 5$) or in SH ($n = 7$): CON = 50 ± 21%; SH = 79 ± 44%; DM = 209 ± 10%; $P < .05$. Reperfusion Na_i returned to baseline in CON but not in DM or SH: CON = 13 ± 14%; SH = 56 ± 26%; DM = 74 ± 40%. Baseline PCr/ATP was similar for all groups: CON = 1.45 ± 0.18; SH = 1.34 ± 0.15; DM = 1.4 ± 0.26. PCr/ATP recovered to 80% of baseline in CON but to only 50% of baseline in SH or DM.

Conclusion: These data suggest that DM myocytes are more susceptible to ischemic injury, whereas both DM and SH are equally susceptible to reperfusion injury, both phenomena documented as abnormalities in Na transport by ^{23}Na NMR. ^{31}P NMR data (PCr/ATP) document bioenergetic relationships to the abnormalities in Na transport. While the reperfusion injury might be related to similar global bioenergetic compromise with resultant ion transport abnormalities, the larger ischemia-induced change in Na_i in DM myocytes cannot be explained by bioenergetic phenomena alone and may be related to membrane damage secondary to chronic exposure of myocytes to ketones and other FFA associated with the hyperglycemic condition.

P017

MR Proton Spectroscopy of Patients with Temporal Lobe Epilepsy by Using Different TEs

M Schneider, U Jahnke, H Stefan, P Schüler, H Kolem, K Wicklow, R Sauter
Siemens AG, Erlangen, Germany

Purpose: Previous studies with sequences using an echo time of 135 ms have shown that proton MR spectroscopy of temporal lobe epilepsy can detect focal changes in the ratio NAA/(Cr + Cho) (1,2). For temporal lobe epilepsy changes in glutamate are also of interest. Sequences using shorter echo times give access to these resonances. The purpose of this study was to evaluate the use of different echo times.

Methods: In a pilot study with seven patients, single-volume sequences with different echo times (SE TE = 135 ms, STEAM TE = 20 ms, TR = 1.5 sec, TA = 6–12 min, VOI = 2–7 mL) and a Hybrid CSI sequence (preselection of a large volume by a STEAM TE = 20 ms sequence, further spatial resolution by 2D phase encoding with a matrix size of 16 × 16, TR = 1.5 sec, TA = 12 min, resulting voxel size = 2–3 mL) were applied. The volumes were positioned in the temporal lobe, including mesial structures. The measurements were performed with a Siemens Magnetom operating at 1.5 T.

Results: Spectra obtained with the SE TE = 135 ms single-volume sequence show a decrease of the ratio NAA/(Cr + Cho) in the epileptogenic focus compared with normal controls. For some patients, a bilateral decrease was found. The additional information obtained with the short echo time sequences showed no significant results. An increase in the glutamate region of the spectra could be found in only two patients.

Conclusion: For the determination of the epileptogenic focus in temporal lobe epilepsy with MR proton spectroscopy, the sequences with a long echo time seem to be appropriate.

1. A. Connelly et al., SMRM Book of Abstracts, 234, 1992. 2. Y.G. Comair et al., SMRM Book of Abstracts, 1945, 1992.

M. Schneider is an employee of Siemens Medical Systems.

P018

Combined H-1 MR Spectroscopy and Imaging of Normal Human Breast and Breast Tumors

IS Gribbestad, G Nilsen, HE Fjøsne, OA Haugen, S Kvinnsland, PA Rinck
MR-Center, Sintef Unimed, and University Hospital of Trondheim, Trondheim, Norway

Purpose: The aim of this study was to obtain diagnostically valuable MR images and spectroscopic information in breast tumors during the same examination.

Methods: The studies were performed with a 1.5-T whole-body system (Gyroscan S15, Philips) using a dedicated double breast coil (constructed at our site). The MRI examination protocol consisted of non-contrast-enhanced SE sequences (TR 450–550/TE 20) in transverse and sagittal planes, followed by volume localized H-1 MR spectroscopy using the PRIME pulse sequence (TR 2,000/TE 136, 256 scans) with water suppression. Studies were performed in patients ($n = 10$) aged 47–88 years with palpable breast tumors > 3 cm and in control subjects ($n = 15$) aged 25–60 years.

Results: Combined MRI and MRS of the breast was performed within a total examination time of 60 min maximum. All the tumors proved to be ductal carcinomas at histopathology. The MR images demonstrated the tumor outline and the exact size in all three spatial directions. Only water and lipid signals were detected in the H-1 spectra from control subjects. An additional signal at 3.2 ppm, caused by choline compounds, was detected in the tumor spectra.

Conclusion: Combined MR imaging and H-1 MR spectroscopy of large breast tumors can be performed within a reasonable examination time. The MR images are of clinical value for planning radiation treatment and surgery. The detection and level of choline compounds in the tumors might be of value for monitoring treatment response.

P019

Spectral Characterization of Red to Yellow Marrow Conversion in the Knee with Inner Volume Spectroscopic CPMG Sequences

RV Mulkern, K Oshio, J Meng, CRG Guttmann, D Jaramillo
Department of Radiology, Children's Hospital, Boston, MA

Purpose: To characterize age-dependent H-1 spectral changes in knee marrow at high spatial resolution. Spectral characterization of the red to yellow marrow conversion process in children is a prelude to using such methods to study pathologies affecting marrow cellularity.

Methods: An inner-volume spectroscopic CPMG sequence, yielding spectra at eight separate echo times (48–384 ms) at 128 positions along a column (20 cm long, 5 × 5 mm cross-section) was used for data collection. A 2-s TR and 128 phase encode steps resulted in scan times of 4 minutes 18 seconds. Automated postprocessing routines provided spectral T2 values and relative spectral peak areas extrapolated to zero echo time within the 5 × 5 × 1.6 mm voxels. Eight adults and 10 children from 2 to 16 years of age were studied with the technique.

Results: In fully developed adult yellow marrow, four peaks were identified and quantified: vinyl protons (≈ 12%), water protons (≈ 8%), $(-CH_2-)_n$ protons (≈ 72%), and $O{=}C\text{-}CH_2\text{-}(CH_2)_n$ protons (≈ 8%). Spectra from marrow voxels were largely independent of column position in the adults. In red marrow of children under 2 years of age, the vinyl proton peak was completely obscured by the neighboring water peak. In older children, the vinyl proton peak emerged as a

distinct spectral feature, sooner in epiphyseal marrow than in metaphyseal marrow.

Conclusions: The appearance of spectra characteristic of adults within the epiphyses prior to the metaphyses is in agreement with the well-known temporal/spatial conversion of red to yellow marrow within the knee. Our methods provide a convenient tool for spectroscopically differentiating hematopoietic from fatty marrow and characterizing the marrow transformation.

Monday, March 7, 12:30 PM–1:30 PM
CLINICAL MRI: Head, Spine, Body

Posters P101–P144

P101

FSPGR Sequence with Multiphase for Studying Hypophyseal Microadenomas following Gd-DTPA Bolus

VM Sanjuan, SR Penderia, AB Ferrandis, JJ Garcia Nieto, JC Marin, EM Gil, LA Ibanez, E Bueso
MRI Center, Hospital General Universitario, Valencia, Spain

Purpose: To describe and comment on our clinical experience in patients with hypophyseal microadenoma, using a Gd-DTPA bolus and obtaining images with the 2D FSPGR technique with multiphase.

Methods: Our study protocol includes (*a*) prior to Gd-DTPA injection, sagittal SE T1W, coronal SE T1W, and axial FSE PD and T2W imaging (all brain); and (*b*) following Gd-DTPA injection, sagittal FSPGR with multiphase, sagittal SE T1W, and coronal SE T1W imaging. The FSPGR sequence has the following parameters: flip angle 30°, TR 12 msec, TE 4.2 msec, 16KH2, FOV 20 cm, 7-mm sections, 256 × 192, 1 NEX, 15 images, scan time 36 sec. The procedure followed involves Gd-DTPA injection, with section acquisition after 5–8 sec. The sections are posteriorly viewed one by one and passed in PAGING mode.

Results: With the SE T1W sequences, microadenomas are seen as small, hypointense nodules smaller than the rest of the gland. After injection of Gd-DTPA, with this sequence, the paramagnetic contrast agent is seen to distribute within the hypophyseal gland but not in the microadenoma.

Conclusion: We believe this sequence to be very useful, particularly in relation to images that are equivocal, for homogenization of the gland tends to occur after a few minutes, and not initially after the contrast agent bolus.

P102

MRI Features of Capillary Venous Malformation of a Whole Hemicerebellum

P Vinee, OM Tanyu, M Schumacher, B Brunot, A Constantinesco
Laboratoire de Biophysique, CHU Hautepierre, Strasbourg, France

Purpose: To report the MRI appearance of an infratentorial capillary venous malformation involving the whole left hemicerebellum of a 7-year-old boy with a history of progressive vomiting and chronic constipation.

Methods: MRI (axial and coronal proton density and T2-weighted SE and coronal pre- and post-Gd-DTPA T1-weighted at 2.0 T) as well as selective angiography and CT were performed.

Results and Conclusion: This case has some extraordinary findings: infratentorial location and involvement of the whole left cerebellum and the clinical history of progressive vomiting and chronic constipation. MRI findings were consistent with the diagnosis of vascular malformation that was reached by means of angiography, showing the enlarged cortical, interhemispheric, and midline crossing veins partly reaching the prepontine region. MRI shows the hemorrhagic foci in angiographically occult malformations. MRI proved to be valuable for follow-up studies of this venous angioma. Gd-DTPA enabled the detection of angiomas that were not seen on the conventional MR scans.

P103

MR Imaging of Venous Angiomas of the Brain

BJ Wagner, KJ Richardson, DA Carrier, PM Chappell, AM Moran
Wilford Hall Medical Center, San Antonio, TX

Purpose: To present a pictorial review of the imaging appearance of venous angiomas of the brain.

Methods: Retrospective review of MR studies of more than 50 such lesions encountered over a 24-month period was performed.

Results: Imaging features allowed a confident radiologic diagnosis in almost all cases; three cases were complicated by hemorrhage and were therefore confirmed with conventional angiography prior to surgery. In addition, two cases were evaluated with MR angiography.

Conclusion: This exhibit illustrates the varied MR appearance of venous angiomas, the most common vascular malformation of the brain. Additionally, correlative images from among CT and conventional angiograms are shown, along with a review of the clinical and pathophysiologic characteristics of these lesions.

P104

Cranial MR Imaging in Ataxia-Telangiectasia

RC Parodi, F Sardanelli, C Ottonello
Institute of Radiology, University of Genoa, Genoa, Italy

Purpose: To define MR imaging (MRI) findings in patients affected by ataxia-telangiectasia (AT), a recessive autosomal disease (incidence, 1/20,000–100,000) with defective DNA repair and high frequency of sinopulmonary infections and cancer (lymphoma and leukemia) mortality.

Methods: Five male patients with AT confirmed by laboratory research, aged 9–28 years, underwent cranial MRI several times (nine examinations: five at 0.15 T, three at 0.5 T, one at 1.5 T). Intermediate, T1-, T2-, and T2*-weighted spin-echo and gradient-echo sequences were performed. The absence of female patients can be considered a matter of chance.

Results: Five patients showed vermis atrophy and an enlarged fourth ventricle and cisterna magna, four showed hemispheric cerebellar atrophy, two showed enlarged infracerebellar subarachnoid spaces, and four showed sinusitis (auxiliary sign). No other morphologic brain abnormality or focal brain signal abnormality was observed. The oldest patient had diffuse high signal intensity in the central cerebral white matter, a relatively minor degenerative change of the multisystem progeric syndrome.

Conclusion: AT is considered the most important human model of inherited cancer susceptibility and multisystemic aging; as in xeroderma pigmentosum and other "breakage syndromes," ionizing radiation should be avoided. For these reasons, MRI should be preferred to computed tomography in patients with AT or suspected AT and those with undefined pediatric ataxias of nontraumatic origin. If hemispheric cerebellar atrophy, especially of the vermis, is noted, laboratory studies should be performed to confirm AT diagnosis.

1. Boder E (1985). Ataxia-telangiectasia: an overview. In: Gatti RA, Swift M (eds). Ataxia-telangiectasia: genetics, neuropathology, and immunology of a degenerative disease of childhood. Alan R Liss, New York, pp 1–63. 2. Assencio-Ferreira VJ, Bancovsky I, Diament AJ, Gherpelli JLD, Moreira FA (1981). Computed tomography in ataxia-telangiectasia. J Comput Assist Tomogr 5:660–661. 3. Waldmann TA, Misiti J, Nelson DL (1983). Ataxia-telangiectasia: a multisystemic hereditary disease with immunodeficiency, impaired maturation, x-ray hypersensitivity, and a high incidence of neoplasia. Ann Intern Med 99:367–379.

P105

Correlation of MRI and MRA in the Evaluation of Sickle Cell Patients with Prior Stroke

SS Goldwag, KL Gupta, MS Kogutt, K Kaneko, JR Humbert
Department of Radiology, Tulane University Medical Center, New Orleans, LA

Purpose: To compare MRI and MRA findings in patients with sickle cell disease and a history of prior stroke and to determine the sensitivity and reliability of MRA as a screening tool in these patients.

Methods: Fourteen pediatric patients with sickle cell disease and a history of prior stroke were prospectively evaluated with MRI and MRA. Standard MRI sequences included sagittal T1W and axial VEMP at TR 3,000/TE 17 and 85, and 3D time-of-flight MRA was performed.

Results: Parenchymal abnormalities were noted at MRI in 13 of 14 patients with a clinical history of stroke. Nine of 10 patients with evidence of large-vessel parenchymal infarct at MRI had an MRA stenosis or occlusion that correlated with the distribution of the infarct. Each side of the intracranial circulation was then evaluated independently, and both small- and large-vessel MRI abnormalities were considered positive results. When comparing MRA with MRI as the standard study, there was 68% sensitivity, 66% specificity, 88% positive predictive value, and 36% negative predictive value.

Conclusion: MRA is an effective screening study in children with sickle cell disease, a history of stroke, and intracerebral large-vessel disease. A combination of MRI and MRA offers an effective noninvasive evaluation of the brain parenchyma and vasculature in these patients.

P106

Evaluation of the Parasellar Region with a 3D T1-weighted Fast Spin-Echo Technique

E Weinberger, C Yuan, DWW Shaw, KS White, KR Maravilla, J Murakami
Department of Radiology, Children's Hospital and Medical Center, Seattle, WA

Purpose: To evaluate the clinical application in the sellar region of a T1-weighted 3D fast spin-echo (FSE) technique, which reduces 3D acquisition to clinically feasible times without the susceptibility artifacts of gradient-echo techniques.

Methods: A T1-weighted 3D FSE pulse sequence (TR 500–600 ms, $TE_{effective}$ 21 ms, echo spacing 21 ms, echo train length 8, 32-mm slab with 32 partitions, imaging time 8–10 min) was evaluated in two normal volunteers and four patients with sellar/parasellar masses. Images were compared with conventional 2D spin-echo (SE) images in all cases and with 3D gradient-echo (SPGR) images in the volunteers.

Results: The 3D FSE sequence resulted in high-quality in-plane images without the susceptibility artifacts of the SPGR sequence. Contrast characteristics of the T1-weighted 2D SE and 3D FSE T1-weighted sequences were similar. Summing of three 1-mm slices from the 3D acquisition resulted in images comparable to and in some cases better than the 3-mm 2D SE images. The quality of multiplanar reformatted images was good, although affected by some edge blurring due to T2 filtering during multiecho data collection.

Conclusion: The T1-weighted 3D FSE pulse sequence provides high-resolution 3D image data without SPGR susceptibility artifacts in an 8–10-minute acquisition. Multiplanar reformatting can be easily performed.

P107

Systematic MRI Studies of the Brain in Patients with Liver Cirrhosis

C Ehrenheim, K Weissenborn, A Hori, S Kubicka, M Manns, H Hundeshagen
Abteilung Nuklearmedizin, Medizinische Hochschule, Hannover, Germany

Purpose: Recent MRI studies of the brain in patients with cirrhosis and hepatic encephalopathy (HE) revealed basal ganglia lesions in some cases. It was the aim of our study to analyze whether the signal changes correlate with the grade of encephalopathy, the portion of portosystemic shunts, the duration of liver disease, actual liver function, and plasma ammonia levels.

Methods: We performed MRI studies in 50 patients with nonalcoholic cirrhosis and HE grade 0–II and related the results to the data mentioned before. Conventional T1- and T2-weighted sequences were used for MR imaging with a 1-T machine. In 11 patients, follow-up examinations were performed, and in seven, examinations were performed before and 3–6 months after liver transplantation.

Results: Hyperintense signal changes to a different extent were seen on the T1-weighted images in 46 of 50 patients examined. The globus pallidus of both hemispheres was commonly involved, and hyperintensities were found bilaterally in the brain peduncles and the substantia nigra in most patients. No other patients have shown comparable signal changes in our series. The image characteristics suggest that the changes may be related to astrocytic glycogen deposition. No correlation was observed between the degree of the signal changes on MR images and the grade of HE, duration of the disease, plasma ammonia levels, and so forth. The follow-up studies, however, showed an increasing signal of the lesions with more pronounced HE in each case, as well as a decline or complete remission in the changes after liver transplantation.

Conclusion: MRI revealed characteristic signal changes in the basal ganglia in patients with liver cirrhosis. We could demonstrate the reversibility of these findings, especially after liver transplantation. Histopathologic correlation supports the theory of astrocytic glycogen deposition being the pathogenetic mechanism.

P108

MR Enhancement and White Matter Hyperintensity Associated with Low-Activity Brachytherapy of Pediatric Brain Tumors

DWW Shaw, JR Geyer, TA Buchholz, MS Berger, E Weinberger
Department of Radiology, University of Washington School of Medicine Seattle, WA

Purpose: Low-activity I-125 implants have been recently employed in treatment of grossly resected recurrent tumors that have an otherwise high probability of failure with conventional treatment. We reviewed the MR changes associated with these implants.

Methods: Four patients (aged 3–13 years) received permanent low-activity I-125 implants following gross total resection of recurrent tumors (two PNETs, one malignant ependymoma, one astrocytoma). MR scans obtained approximately every 3 months during follow-up ranging from 6 months to 2 years were retrospectively reviewed and correlated with clinical data.

Results: A thin rim of enhancement was seen about the seed-implanted cavities and evolved over several months to a thickness of up to 1 cm. Additionally, hyperintensity developed in the white matter as much as several centimeters about the implants. Two of the cases have had recurrences remote from the implants. No recurrences have been demonstrated within the approximately 1-cm effective radiation dose range of the implant seeds.

Conclusion: A variable rim of enhancement was seen about the low-activity implants that could potentially mimic or obscure tumor. Enhancement beyond approximately 1 cm from the nearest implant ultimately proved to be recurrence. Despite a lower radiation dose to normal brain, white matter hyperintensity, extensive in two cases, developed in a pattern suggesting vasogenic edema. Factors that may have influenced these changes include previous radiation and chemotherapy, volume of brain implanted, and age of the patient.

P109

Added-Gradient-Echo Pulse Sequence Technique: Application to Fluid Imaging of the Temporomandibular Joint

KA Bell, JP Jones, KD Miller
Ochsner Medical Institutions, New Orleans, LA

Purpose: We assessed the value of an added gradient-echo in the same pulse sequence with a T1-weighted spin echo in order to determine the presence of an abnormal fluid collection in the temporomandibular joint (TMJ), with no additional imaging time.

Methods: To the standard T1-weighted sequence used in cine TMJ imaging, a readout gradient reversal was added, and the resulting gradient echo was collected. This image was compared with standard T1- and T2-weighted sequences, a STIR sequence, and a small-flip-angle FLASH gradient-echo sequence.

Results: The T1-weighted spin echo preceding the added gradient echo is not affected by the gradient reversal, but the additional gradient echo adds T2* contrast information that displays fluid as bright and compares favorably with other fluid detection sequences.

Conclusion: The added-gradient-echo technique adds sensitivity for the detection of an abnormal increase in fluid in the TMJ without adding to the overall imaging time of a routine T1-weighted sequence.

P110

MRI Findings in Biopsy-proved Lymphoid Hyperplasia of the Adult Nasopharynx

WS Kubal, S Mucci, RA Blinder
Department of Radiology, McGuire Veterans Administration Medical Center and Medical College of Virginia, Richmond, VA

Purpose: A mass in the adult nasopharynx raises diagnostic considerations that include lymphoid hyperplasia and squamous carcinoma. We present MR imaging (MRI) findings in 15 adult patients with biopsy-proved lymphoid hyperplasia and attempt to identify those MRI features most characteristic of benignancy.

Methods: Axial T1-weighted, T2-weighted, and Gd-DTPA–enhanced T1-weighted images were obtained with a 1.5-T Signa magnet. Biopsies were performed within 8 weeks of imaging.

Results: On T2-weighted images, the lymphoid hyperplasia was homogeneously hyperintense compared with muscle. On T1-weighted sequences, lymphoid hyperplasia was isointense compared with muscle; following contrast administration, it showed a striated pattern that was more intense than muscle. In all cases the lymphoid hyperplasia was clearly marginated, showing no evidence of muscle invasion or infiltration. These findings were best seen on T2-weighted and contrast-enhanced T1-weighted images. The thickness of the hyperplasia varied from 3 to 10 mm but was quite uniform in 13 of 15 cases.

Conclusion: T2-weighted and contrast-enhanced T1-weighted images are most useful in delineating and diagnosing lymphoid hyperplasia. Consistent MRI features in our series are homogeneous hyperintensity in muscle on T2-weighted images, striated enhancement pattern, and well-defined margins without evidence of muscle invasion.

W.S. Kubal is a member of the Berlex Laboratories Speaker Panel.

P111

MR Imaging of the Brachial Plexus and Thoracic Outlet Vasculature

SN Noujaim, RR Jason, KG Bis, AN Shetty, AA Cacciarelli
Department of Diagnostic Radiology, William Beaumont Hospital, Royal Oak, MI

Purpose: The purpose of this presentation is to review and display a state-of-the-art technique for MR imaging of the brachial plexus and of the thoracic outlet vascular structures. In addition, the anatomy will be reviewed in detail, along with a demonstration of the various pathologic processes involving the neurovascular bundle.

Methods: MRI is performed at 1.5 T with a combination of body, neck, and surface coils. A variety of pulse sequences are used, including conventional (T1, T2) and fast (turbo) (T2) spin-echo imaging as well as contrast-enhanced T1-weighted imaging. Contrast-enhanced fat-saturation and STIR sequences are also employed. MR angiography is performed with contrast-enhanced fat-saturation breath-hold 3D gradient-echo or 2D time-of-flight gradient-echo sequences with selective arterial or venous spatial presaturation to yield venograms or arteriograms, respectively.

Results: The anatomy of the various components of the brachial plexus is displayed by means of T1-weighted spin-echo images in the transverse, sagittal, and coronal planes. Arterial and venous anatomy is also reviewed. The utility of MR imaging is shown by demonstrating multiple examples of the following: primary (pulmonary, neurogenic, osseous, lymphoma, lymphangioma) metastatic (breast, pancreatic, renal, adrenal and thyroid) neoplasms, and traumatic (pre- and postganglionic nerve avulsions), inflammatory (neuritis), and iatrogenic processes (postoperative fibrosis and irradiation). Abnormalities affecting the arterial and venous structures, such as thrombosis and extrinsic compression by masses, are displayed with the use of MR imaging in thoracic outlet syndrome.

Conclusion: MRI is the modality of choice for evaluation of the brachial plexus and thoracic outlet vasculature due to its multiplanar capabilities and enhanced soft-tissue contrast and spatial resolution.

P112

3D Surface Rendering of the Inner Ear

WCE Kwok, J Chang, B Kraft, L Shapiro, S Totterman
University of Rochester Medical Center, Rochester, NY

Purpose: To improve the visualization of the inner ear on MR images with 3D surface rendering technique.

Methods: The study was performed with a 1.5-T GE Signa scanner. Volunteers were imaged with a 4-inch circular surface coil and a 3D GRASS sequence (TR/TE = 30/10, flip angle 90°, 12-cm FOV, 0.7-mm sections, 256 × 256 matrix, 28 sections, 4 NEX, 16:24 minute scanning time). Surface rendering was performed on a SUN Sparc 10 workstation with SunVision of Sun Microsystems. Additional computer programs were developed by L.S. for data format conversion and final reconstruction. Spatial clipping and intensity thresholding were used to remove unwanted regions and background noise. Surface rendering was then performed to give 128 angular projections, 360° about two orthogonal axes, each with 64 projections. Surface-rendered (SR) and maximum-intensity-pixel (MIP) reconstructions were compared on a GE Independent Console.

Results: SR was found to be superior to MIP. It gave a 3D perspective to the anatomic structures and their orientation. It improved the visualization of the three semicircular canals, cochlea, vestibular duct, and structures in the inner auditory canal.

Conclusion: MRI is superior to CT in the imaging of the inner ear because it depicts the labyrinth instead of the bony structures. With SR display, one can see the 3D structural orientation of the inner ear and the abnormalities of its components, such as labyrinthine cause of hearing loss, vestibular duct dilatation in Meniere disease, and acoustic neuroma.

P113

Role of MR Imaging versus Ultrasound in the Evaluation of Pediatric Orbital Pathology

JP Williams, JB Lindsey, KL Gupta
Department of Radiology, Tulane University Medical Center, New Orleans, LA

Purpose: To determine the sensitivity and specificity of MR imaging and orbital ultrasonography (US) in the evaluation of pediatric orbital pathology.

Methods: Sixty-seven pediatric patients with orbital lesions

(retinoblastoma, coloboma, microphthalmus, Coat disease, optic nerve glioma, perioptic nerve meningioma, hemangioma, lymphangioma, cellulitis, nasopharyngeal cancer, osteosarcoma, and hematoma) were evaluated with a 1.5-T GE MR scanner and with orbital US.

Results: Both modalities showed the majority of lesions; however, MRI was better for showing retrobulbar lesions and extension into the brain and optic nerve.

Conclusion: MRI and orbital US have been extensively used for evaluation of pediatric orbit abnormalities. Though both have been shown to be excellent modalities, MRI proves superior for deeper lesions.

P114

Evaluation of Choroidal Melanoma with Optimal-Pulse-Sequence MRI and Ultrasound

JB Lindsey, KL Gupta, JP Williams
Department of Radiology, Tulane University Medical Center, New Orleans, LA

Purpose: To compare MR and ultrasound (US) imaging of choroidal melanoma.

Methods: Ninety-three patients with choroidal melanoma were examined with MR imaging. Forty-seven underwent contrast-enhanced MR imaging. MR imaging with various pulse sequences was compared with US.

Results: Tumor size with MR imaging and ultrasound correlated well. All tumors were detected with US; however, one small melanoma was not detected with MR imaging. T1-weighted images with and without contrast enhancement proved superior in evaluation of choroidal lesions. However, T2-weighted images are needed for evaluation of retinal detachments and hemorrhages. US was sensitive but nonspecific.

Conclusion: MR imaging and US are complementary in the evaluation of uveal melanoma.

P115

Comparison of High-Resolution MRI, Routine Enhanced MRI and Ultrasound in Evaluation of Orbital Tumors

JB Lindsey, KL Gupta, JP Williams
Department of Radiology, Tulane University Medical Center, New Orleans, LA

Purpose: To compare high-resolution MRI, routine enhanced MRI, and ultrasound (US) in the evaluation of orbital tumors.

Methods: Two hundred seventy cases of orbital lesions were evaluated with both enhanced MR imaging (1.5-T GE unit) and orbital US.

Results: MRI proved to have better soft-tissue contrast, which facilitated specific diagnoses of hemorrhage, melanoma, and retinoblastoma. This was enhanced by the use of contrast material and additional gradient-echo pulse sequences in some cases. High-resolution MRI may add even greater soft-tissue contrast. US was more sensitive for small lesions (<2 mm). However, deeper portions of the retrobulbar area and intracranial involvement were better evaluated with MRI.

Conclusion: MR imaging and US are complementary in the evaluation of orbital tumors in the majority of cases. High-resolution MRI may prove to be superior to routine enhanced MRI.

P116

Contrast-enhanced MR Imaging of Choroidal and Retinal Lesions

KL Gupta, JB Lindsey, JP Williams
Department of Radiology, Tulane University Medical Center, New Orleans, LA

Purpose: To compare contrast-enhanced MRI and ultrasound (US) in evaluation of choroidal and retinal lesions.

Methods: One hundred five cases of choroidal and retinal and choroidal lesions (melanoma, retinoblastoma, retinal hemorrhage, retinal detachment, choroid metastases) examined with contrast-enhanced MRI (GE 1.5-T unit) and US were compared.

Results: Both modalities showed the majority of lesions; however, MRI was better for showing retrobulbar lesions and extension into the brain and optic nerve.

Conclusion: MRI and orbital US are excellent imaging modalities for evaluation of abnormalities of the pediatric orbit, although MRI has increased utility in evaluating deeper lesions.

P117

Clinical Usefulness of the New Developmental Head and Neck Surface Coil for MR Imaging

M Shimada, S Hayashi, A Senoo, H Moriya, T Kogure, K Ito, T Nanba, S Tsuchida
First Department of Radiology, Toho University, Tokyo, Japan

Purpose: When images of the head and neck regions are obtained with a head coil, the signal intensity and SNR of regions below the oropharynx are lower. When such images are obtained with an anterior neck coil, the signal intensity and SNR of the upper regions, from the epipharynx, are lower. We developed a new head and neck coil and studied its clinical usefulness.

Methods: Forty-eight consecutive patients referred with clinical suspicion of head and neck disease were studied. All studies were performed on a 1.5-T system with the new head and neck coil. Axial precontrast and postcontrast T1-weighted and coronal postcontrast images were reviewed retrospectively. The results were compared with images obtained with a head coil and with an anterior neck coil.

Results: In 47 cases (97.9%), we obtained good images from regions below the oropharynx to the epipharyngeal upper regions with this new coil and also saved imaging time. The safety of this new head and neck coil was confirmed.

Conclusion: MR imaging with this new head and neck coil is valuable in the evaluation and treatment of head and neck disease.

P118

MRI of the Recently Operated Cervical Spine: Differentiation of Infection from Normal Postsurgical Change

WS Kubal, B Greenwald, EO Thompson
Department of Radiology, McGuire Veterans Administration Medical Center and Medical College of Virginia, Richmond, VA

Purpose: MR diagnosis of infection in the recently operated spine can be difficult. This study was conducted to describe the postoperative patterns of MR contrast enhancement following anterior cervical fusion (ACF) and to differentiate these patterns from spinal infection.

Methods: Ten clinically normal patients were imaged at 1–2 days and 45–65 days following ACF. Pre- and postcontrast (Gd-DTPA) fat-suppressed sagittal short TR, short TE images were obtained on a General Electric 1.5-T imager with a volume neck coil.

Results: The immediate postoperative images showed retropharyngeal enhancement, no fusion plug or vertebral body enhancement, and minimal enhancement at the plug–vertebral body interface. The delayed images showed partial resolution of retropharyngeal enhancement, inhomogeneous enhancement of the fusion plug and vertebral body, and marked enhancement of the plug-vertebra interface.

Conclusion: We demonstrated the evolution of the normal enhancement pattern in the first 65 days following ACF. Comparing the postoperative enhancement with that seen in spinal infection revealed several points of differentiation. Osseous enhancement in infection was more nearly uniform. The infectious paraspinal enhancement was more prominent and

often showed central hypointensity. Postoperative spines showed no enhancing epidural mass.

W.S. Kubal is a member of the Berlex Laboratories Speaker Panel.

P119

Optimization and Initial Experience with High-Resolution 3D Fast Spin-Echo Imaging of the Cervical Spine

GA Holland, J Mitchell, J Listerud, BB Kneeland, S Atlas, MD Schnall

Department of Radiology, Hospital of the University of Pennsylvania, Philadelphia, PA

Purpose: The purpose of this study was to optimize a 3D FSE technique for the cervical spine.

Methods: A 2DFT FSE sequence was modified to perform multislab 3DFT FSE (written by J.M.). All imaging was performed at 1.5 T with a cervical multicoil array, a 24-cm field of view, and a 256 × 256 matrix (5.3 Signa, GEMS, Milwaukee, WI). The sequence was performed in the sagittal plane with conventional RF pulses and pulses optimized with the Shinnar/LeRoux algorithm. The following parameters were systematically varied: ETL 16–36, RBW ±16–32 kHz, TE 80–130 msec, slice thickness 1.0–1.5 mm, 10–14 partitions, and 4–6 slices/partition. Imaging was performed both with and without the following: fat saturation, flow compensation, and random phase reordering. These images were obtained in five asymptomatic volunteers and six patients. The sagittal and axially reformatted images were scored by three radiologists. These images were compared with 2D FSE images with identical parameters other than slice thickness.

Results: The following was considered the optimal sequence: TE 100 msec, BW 21.4, ETL 24, slice thickness 1.2 mm, FC with optimized RF pulses, and 12 partitions. Fat saturation improved visualization of the disk. The optimized RF pulses provided better reformatted images than the conventional RF pulses. The near isotropic 3D FSE images were completed in 6–7 minutes. This sagittal acquisition could be reformatted into multiple planes and provided superior anatomic detail compared with the 2D FSE and 3D gradient-echo images images, as evidenced by the routine visualization of the ventral and dorsal nerve roots.

Conclusion: Three-dimensional FSE provides high-resolution T2-weighted images of the cervical spine that can be reformatted retrospectively into multiple planes. These preliminary results suggest that this sequence may potentially replace 2D FSE and 3D gradient-echo imaging of the cervical spine, pending further comparisons.

P120

Pediatric Spinal Blastomycosis

M Hardjasudarma, R Edwards, C Black-Payne, PC Meyers, J Wolfson, M Wood, L Nall, J Milner

Department of Radiology, Louisiana State University Medical Center, Shreveport, LA

Purpose: Blastomycosis is an uncommon fungal infection in children, and it rarely affects the spine. In adults, multiple contiguous vertebrae and intervening disk spaces may be involved. We proposed to study the imaging characteristics of pediatric spinal blastomycosis in a recent case at our institution.

Methods: The plain radiographs and CT, MRI, nuclear medicine, and ultrasound studies of a 5-year-old boy were studied.

Results: The patient presented with flank pain, limping, weight loss, fever, and cachexia. Plain radiographs of the lumbosacral spine showed destructive changes in L-5 and S-1 and a prevertebral soft-tissue mass. CT revealed destruction of the vertebral bodies, pre- and paravertebral soft-tissue swelling, and bilateral psoas abscesses extending into the retroperitoneum. This was also documented with MRI, which in addition showed a large epidural inflammatory mass and lack of involvement of the disk spaces between the affected vertebrae. Needle aspiration of the retroperitoneal fluid collections under ultrasound guidance yielded purulent material, from which *Blastomyces dermatitidis* was isolated. Additional studies, including a bone scan, failed to reveal abnormalities elsewhere.

Conclusion: The spinal changes were best demonstrated with MRI. CT provided additional information on the retroperitoneal abnormalities. Sparing of the disk spaces on MR images suggests that the spread of infection is by way of paravertebral structures, such as the longitudinal spinal ligaments, and the potential spaces around these structures.

P121

Magnetization Transfer Contrast For MR Imaging of the Breast

GE Santyr, F Kelcz, EJ Fairbanks, E Schneider

University of Wisconsin, Madison, WI

Purpose: Conventional MR images of the breast are often confusing due to ambiguous contrast arising from the overlap in relaxation times between lesions and normal breast tissues. Magnetization transfer contrast (MTC) may help improve detection of breast lesions by suppressing signal from fibroglandular tissue. The purpose of this work was to investigate the application of MTC to MR imaging of the breast.

Methods: Imaging was performed with a GE Signa MR imaging system (Milwaukee, WI). MTC was generated by using a magnetization preparation consisting of either an off-resonance adiabatic spin-locking RF pulse or a train of off-resonance sinc RF pulses. The spin-locking pulse had a length of 190 ms, an amplitude of approximately 100 Hz, and a resonance offset (Δ) of 100–200 Hz. The off-resonance sinc pulses each had a length of 19 ms, a flip angle of 2,000°, and Δ = 1–2 kHz.

Results: Both the spin-locking and off-resonance RF preparations resulted in significant reduction in fibroglandular signal (50–90%). The spin-locking pulse resulted in better suppression largely due to the smaller value of Δ, which increased direct saturation of signal in addition to the indirect saturation due to magnetization transfer. Although the off-resonance sinc pulse train provided less suppression, this was due almost entirely to magnetization transfer. Both MTC methods were found to be helpful for distinguishing lesions from adjacent normal breast tissues.

Conclusion: MTC with off-resonance RF preparation pulses reduces signal from normal fibroglandular breast tissue. This may be useful for improving detection of breast lesions with MR imaging.

E. Schneider is an employee of GE Medical Systems.

P122

Comparison of Fast Spin-Echo and Conventional Spin-Echo MR Imaging in the Evaluation of Orbital Pathology

DF Frei, SS Goldwag, KL Gupta

Department of Radiology, Tulane University Medical Center, New Orleans, LA

Purpose: To compare fast spin-echo with conventional spin-echo MRI in the evaluation of patients with pathologic conditions of the orbit.

Methods: We prospectively evaluated 15 patients with known orbital pathology with both conventional and fast spin-echo, axial, T2-weighted imaging. Two blinded observers evaluated each set of images for motion artifact, image quality, lesion definition, optic nerve definition, extraocular muscle definition, vitreous homogeneity, and fat plane integrity.

Results: In the majority of patients, there was less motion artifact, improved image quality, and better lesion definition. Better definition of the optic nerve, extraocular muscles, and vitreous homogeneity was a less frequent finding with fast spin-echo imaging. There was no appreciable loss of image quality or lesion definition on any fast spin-echo images when compared with conventional spin-echo images.

Conclusion: Fast spin-echo MR imaging of the orbit is superior to conventional spin-echo imaging.

P123

MRI and Ultrasound in the Detection and Evaluation of Intraocular Hemorrhage Associated with Retinoblastoma

JP Williams, KL Gupta, CM Arcement
Department of Radiology, Tulane University Medical Center, New Orleans, LA

Purpose: To determine the sensitivity and specificity of MRI evaluation of intraocular hemorrhage and retinoblastoma in pediatric patients compared with funduscopic and ultrasound (US) evaluation.

Methods: Thirty-two pediatric patients with retinoblastoma were evaluated with funduscopy, 10-MHz orbital US, and MRI with gadolinium enhancement (1.5-T GE unit).

Results: Eight cases of choroidal hemorrhage were detected. All cases detected with US and clinical examination were detected with enhanced MRI.

Conclusion: Both MRI and US were found to be equally sensitive in detecting intraocular hemorrhage and retinoblastoma. MRI signal characteristics are sufficiently different to differentiate hemorrhage and tumor. Contrast MRI increases the sensitivity and specificity for hemorrhage and tumor. US and MR imaging are complementary in their evaluation of intraocular lesions and correlated well with the funduscopic and clinical examinations.

P124

Procto-Defecography with MRI

VM Sanjuan, RML Llorens, V Garrigues, AM Flores, E Esteban, E Llopis, SR Penderia, AB Ferrandis
MRI Center, Hospital General Universitario, Valencia, Spain

Purpose: Description of a new MR imaging technique as an alternative to defecography with conventional x rays.

Methods: Lesser pelvis sagittal images are obtained, with sections passing through the rectum and sphincter areas, both before and after contrast administration. The MRI sequence is 2D FSPGR with flip angle 90°, TE 4.2 msec, TR 12 msec, multiphase; 20 planes were obtained, with minimum delay between acquisitions. This sequence is obtained at rest with the Valsalva maneuver and with elevation. Contrast material is then introduced rectally (mixture of barium sulfate 350 g, dried mashed potato 15 g, and warm water 450 mL) with a syringe through a Vaseline-lubricated sonde (no local anesthesia); 220–250 mL is introduced. The same MRI sequences are again performed, and the study is completed by obtaining images during defecation. The following measurements are made: anorectal angle, pelvic floor descent, aperture of anal canal during defecation, presence of puborectal muscle imprint, and evaluation of rectal residue.

Results: The iconography obained in studying patients with defectation disorders is presented. A comparative study with defecography using static and dynamic x rays is performed.

Conclusion: We consider procto-defecography with MRI to constitute an alternative to conventional x-ray techniques, in spite of the greater costs involved, for it offers the advantage of not directly irradiating either testicles or ovaries in generally young or middle-aged patients.

P125

Detection of Perivesicular Infiltration of Bladder Carcinoma with MRI

A Dessl, W Judmaier, J Eberle, K Wicke, R Knapp, J Feichtinger, S Peer, G Bartsch
Department of Magnetic Resonance Imaging, University of Innsbruck, Innsbruck, Austria

Purpose: We assessed the accuracy of MRI in differentiating bladder carcinoma up to stage pT3a versus pT3b and beyond.

Methods: Fifty patients scheduled for total bladder resection were examined with contrast-enhanced MRI in a 1.5-T scanner. The patients were selected by means of preoperative clinical staging, including deep bladder wall biopsy. The MRI staging results were compared with the pathology reports on the whole-bladder resection specimens.

Results: The overall accuracy of MRI in differentiating the two groups was 76%. In 22 patients the tumor was confined to the bladder wall (pT3a or less), and in 28, perivesicular spread was proved histologically. MRI correctly demonstrated 26 of the latter cases and missed perivesicular infiltration in two. In carcinomas confined to the wall, MRI showed a tendency to overstage tumor progression in 12 of 22 patients.

Conclusion: MRI shows a high accuracy in excluding perivesicular spread of bladder carcinoma. The high frequency of false-positive results in the MRI diagnosis of stage pT3b carcinoma and beyond may be due to postbiopsy changes and limits the value of bladder carcinoma staging with MRI.

P126

Changes in MR Images of Muscle Depend on Exercise Intensity and Duration

G Jenner, JM Foley, TG Cooper, EJ Potchen, RA Meyer
Clinical Center, Michigan State University, East Lansing, MI

Purpose: Numerous recent investigations demonstrate that exercise increases the MR signal intensity of recruited skeletal muscle on T2-weighted images. Several of these studies exploit changes in the apparent T2 (or signal intensity) to visualize specific muscle recruitment patterns during various exercise regimens. This study uses echo-planar MR imaging to quantify the effect of exercise rate and duration on the anterior tibialis MR signal intensity in normal human subjects.

Methods: Each of six adult subjects lay supine in the magnet with their right lower leg in a custom-made boot designed for measuring the force of dorsiflexion. We acquired axial spin-echo echo-planar images (TR/TE 6,000/45 msec, 128 × 64, 1.0-cm slice thickness) at the rate of 10 per minute for 16 minutes. After the first 10 images, subjects began submaximal isotonic ankle dorsiflexion at a rate of 10, 20, or 30 contractions per minute. For each subject, we determined the signal intensity time course by extracting the mean signal intensity in the anterior tibialis muscle from all images. We then normalized this time course to the mean intensity of the first 10 images. Finally, we used a nonlinear least-squares fitting algorithm to fit the time course to an exponential function.

Results: During exercise (within the same individual), the anterior tibialis MR signal intensity exponentially approaches a steady-state value that is dependent on the rate of dorsiflexion.

Conclusion: Echo-planar MR imaging techniques provide a valuable tool for monitoring the recruitment of specific muscle groups during exercise.

P127

Optimum Flip Angle for Dynamic Gd-DTPA–enhanced FLASH MR Imaging of Musculoskeletal Tumors

SA Gronemeyer
St Jude Children's Research Hospital, Memphis, TN

Purpose: Dynamic Gd-DTPA–enhanced FLASH MRI (DEMRI) shows promise in evaluating musculoskeletal tumor chemotherapy response. However, controversy exists regarding the optimum FLASH flip angle (1,2).

Methods: Serial dilution phantoms containing 0.05–12.8 mM Gd-DTPA (Magnevist) in physiologic saline were imaged with FLASH at 1.0 T (TR/TE = 30/10) and 1.5 T (TR/TE = 23/10) with flip angles of 10°–90°. Eight (four at 1.0 T and four at 1.5 T) musculoskeletal tumor patients were imaged before and after contrast administration with FLASH and flip angles of 40°–90°.

Results: The Gd-DTPA phantom signal intensity ratio (SIR) to physiologic saline solute increased with flip angle for concentrations of over 0.4 mM at 1.0 and 1.5 T. For flip angles of 30°–90° and a given concentration of 0.4 mM or less, the SIR varied little with flip angle at both 1.0 and 1.5 T. Subtraction

of pre- from postcontrast 40°–90° FLASH images suggest that 40° is comparable or superior to 90° at both 1.0 and 1.5 T.

Conclusion: Postcontrast musculoskeletal tumor SI was relatively independent of flip angle at 1.0 and 1.5 T. Therefore, 40° and 90° FLASH should give similar tumor uptake slope values. The flip angle insensitivity suggests that the Gd-DTPA concentration delivered to tumor is of the order of one-tenth or less that injected into the blood pool (2.0 mM).

1. Fletcher BD, Hanna SL. Radiology 1992; 177:287–288.
2. Fletcher BD, Hanna SL, Fairclough DL, Gronemeyer SA. Radiology 1993; 186:904–905.

P128

MRI Evaluation of Chronic Shoulder Pain with Clinical and Radiographic Correlation

JP Williams, EH De Mouy, K Kaneko
Department of Radiology, Tulane University Medical Center, New Orleans, LA

Purpose: Correlation of MRI, clinical, and radiographic findings in the evaluation of chronic shoulder pain.

Methods: The cases of 204 patients who presented to our institution with a complaint of chronic shoulder pain were reviewed. Each patient was evaluated with plain radiography, including at least two views, and MR imaging (1.5-T GE Signa scanner). In addition, some patients were also evaluated with gadolinium enhancement and MR saline arthrography.

Results: Multiple different causes of chronic shoulder pain were diagnosed, including rotator cuff disease and neoplastic and inflammatory processes. In many cases, review of "normal" or "near-normal" radiographs following MRI revealed overlooked findings that correlated well with the MRI diagnoses.

Conclusion: MR imaging proved to be more sensitive and specific, although in a large amount of cases, the plain film and MRI findings were highly correlated. Although plain radiography continues to be the primary imaging modality, MRI has proved to be superior in the evaluation of chronic shoulder pain.

P129

MR Imaging for More Accurate Diagnosis and Staging of Osteochondral Lesions of the Talar Dome

T Nakamura, S Nakashima, S Nomura, T Hara, E Nakamura, M Matsumoto, S Masumi, Y Ueda
Department of Orthopedic Surgery, Kyusyu Rosai Hospital, Kitakyushu City, Japan

Purpose: The objective of this study was to investigate the use of MRI for more accurate diagnosis and staging of osteochondral lesion of the talar dome.

Methods: Clinical cases and cadaveric feet were used as the subjects of this study. The subjects were staged according to the Berndt-Harty classification by means of plain radiography. The clinical cases consisted of eight feet of four controls (two male, two female; aged 19–30 years, with a mean age of 25 years) and 13 feet of 11 patients (six male, five female; aged 15–53 years, with a mean age of 37 years) with radiographically diagnosed osteochondral lesions of the talar dome. Four feet were stage III and nine were stage IV. Five cadaveric feet were also used as subjects of the study; one control foot was used, and three stage I feet and one stage II foot were injured for the purpose of the investigation. T1-weighted (T1WI) and T2-weighted images (T2WI) were produced in the sagittal plane with a 1.5- or 0.5-T MRI unit.

Results: In stage I subjects, a region of low-intensity signal was present in the articular cartilage tissue on T1WI, but a region of high-intensity signal was not present on T2WI. In stage II–IV subjects, a region of low-intensity signal was present in the subchondral bone tissue on T1WI and a region of high-intensity signal on T2WI.

Conclusion: The presence of a region of high-intensity signal in the subchondral bone tissue on T2-weighted images is a characteristic finding of damaged articular cartilage.

P130

MR Arthrography of the Knee: Is There Any Advantage over Conventional MR Imaging?

V Prakash, A Wolf
Loma Linda University, Loma Linda, CA

Purpose: This study was undertaken to evaluate the usefulness of MR arthrography of the knee over conventional MR imaging.

Methods: Seventy-five patients, referred for evaluation of knee pain, underwent MR imaging of the knee (46 male, 29 female). The mean age was 48 (range, 12–75 years). In 64 patients, the knee joint was injected with 10 mL of Renografin 60, 8 mL of Marcaine 0.5%, and 2 mL of dexamethasone suspension, prior to MR imaging. In the remaining 11 patients, MR imaging was performed without injection. T1-weighted coronal, T2-weighted sagittal, and axial images were obtained with a General Electric Max 0.5-T magnet and a surface coil.

Results: Of the 64 patients who underwent MR arthrography, degenerative changes were seen in 24 patients, osteochondritis dessicans in two, and bone contusion in one. Meniscal tears were seen in 30 patients, cruciate ligament tears in 23, patellar chondromalacia in 30 patients, and popliteal cyst in 13. In 11 patients with MR imaging without contrast injection, small joint effusion was present in eight patients and moderate effusion in three. Meniscal tears were seen in four patients, cruciate ligament tears in three, degenerative changes in three, chondromalacia of patella in five, and popliteal cyst in two.

Conclusion: In our series, all patients without the injection had small to moderate effusion with optimal visualization of intraarticular structures. Therefore, in our experience, MR arthrography of the knee has no significant advantage over conventional MR imaging.

P131

Quantitative MR Evaluation of Intraarterial Lymphocyte Injection Therapy for Lymphedema

M Harada, K Matsuzaki, Y Hayashi, H Nishitani, M Yoshizumi, I Katoh
Department of Radiology, University of Tokushima, Tokushima, Japan

Purpose: To determine the characteristic MR findings of lymphedema and reactions after intraarterial lymphocyte injection therapy and to quantitatively evaluate the effect of such injection.

Methods: Five patients were treated with several intraarterial lymphocyte injections. We measured the T2 value of edematous tissue using a triple echo sequence and short TI IR (STIR) images to assess the extent of lymphedema. Measurements were made before and after each intraarterial lymphocyte injection. The mean T2 and standard deviation (SD) of T2 distribution were obtained from T2-calculated images.

Results: Characteristic findings of lymphedema were the thickening of subcutaneous tissue, meshed pattern of fluid, thickening of skin, and fluid on the fascia. After therapy, the thickness of subcutaneous tissue and the meshed pattern had greatly decreased, but the thickening of skin and fluid on the fascia still remained. The mean T2 and SD in edematous tissue were much higher than in normal tissue. Both decreased greatly after therapy in improved cases but did not change in cases where treatment was less effective.

Conclusion: STIR differentiated water from adipose tissue and clearly indicated the distribution of water. The mean T2 and SD of T2 distribution are useful indexes for quantitative evaluation of lymphedema and assessment of therapy.

P132

Gradient-Echo Perfusion of Musculoskeletal Abnormalities with Contrast-enhanced 2D Fat-Saturation FLASH Imaging

M Gurgun, KG Bis, AN Shetty, A Shirkhoda, MC Farah, JL Roberts, R Irwin
Department of Diagnostic Radiology, William Beaumont Hospital, Royal Oak, MI

Purpose: The purpose of this presentation is to display in a dynamic fashion the utility of MR perfusion imaging of various musculoskeletal abnormalities with a contrast-enhanced 2D fat-saturation FLASH sequence.

Methods: Imaging was performed at 1.5 T with a Siemens SP 4000 Magnetom (Iselin, NJ). A standard FLASH sequence was coupled to a fat-selective RF pulse to yield a fat-suppressed gradient-echo sequence with the following parameters: TR/TE 35/5 msec, 256 × 144 matrix, one acquisition, 5–8-mm slice thickness). Fat suppression was performed with a Gaussian pulse of bandwidth 220 Hz and offset at 240 Hz. The pulse sequence scheme is similar to CHESS. Auto shimming was performed prior to examination. Off-line imaging was performed and the sequence was begun, after which a bolus of contrast (gadopentatate dimeglumine, 01. mmol/kg) was administered intravenously over 5 seconds, followed by a saline flush. One section was obtained every 7 seconds over a period of 5 minutes. Signal intensity time curves were obtained, with calculation of the percentage of signal enhancement and the time to reach peak enhancement.

Results: Benign and malignant neoplasms as well as inflammatory processes of the bones and soft tissues are demonstrated. This sequence can also be used in accessing perfusion to osseous structures in cases of avascular necrosis.

Conclusion: Fat-saturation gradient-echo MR imaging provides high soft-tissue contrast and spatial and temporal resolution for assessing perfusion of musculoskeletal pathology.

P133

Interventional MRI: Initial Experience with a Dedicated Open Interventional Magnet

Y Anzai, A DeSalles, R Hamilton, S Sinha, K Farahani, K Black, R Lufkin
UCLA Medical Center, Los Angeles, CA

Purpose: Over the past several years, a number of techniques have been developed for MR-guided interventional procedures. While interventional MRI is clearly in an early stage, the development of MR-compatible instruments and associated technology allows interventional MRI to be a therapeutic procedure in selected situations. We will present initial clinical experience with MRI-guided biopsy and stereotaxic radio-frequency ablation for functional brain disorders, refractory pain syndrome, and some tumors.

Methods: At the time of submission of this abstract, we are installing the first of the new generation of open MR scanners designed specifically for interventional procedures. It is located in an operating room environment.

Results: MRI is a most powerful imaging technique which allows early and sensitive detection of tissue changes induced by interventional procedures. We present technical and clinical aspects of recent experience with interventional MRI.

Conclusion: The development of new MRI instruments and associated devices specifically designed for interventional use marks the beginning of a new era in which advanced procedures not possible with conventional MR equipment may be performed.

P134

Low Back Pain Treatment with Interventional MRI Guidance

DHW Grönemeyer, RMM Seibel, G Schmid, M Deli, M Friebe, M Busch
Institute of Diagnostic and Interventional Radiology, University of Witten/Herdecke, Mühlheim, Germany

Purpose: CT-guided pain therapy is a routine technique in our department. Interventional MR imaging is helpful in the therapy of facet and iliosacral joints.

Methods: For interventional procedures, a 0.064-T open-designed MR scanner, a helical CT scanner, and, for treatment, self-developed nitinol, titanium, or stainless steel (18 G) instruments were used. Local anesthesia and cortisone were used, and 1.0 mL of 50% ethanol was injected for the treatment of chronic facet joint pain.

Results: Twenty interventional MRI/CT-guided facet joint therapies and 20 iliosacral joint infiltrations were compared. MRI avoids ionization and allows 3D localization. An open access allows nearly real-time guidance of instruments. In CT the tip of the instruments is easy to define, especially if the guidance direction is oblique, but the patient has to be moved in and out of the gantry several times. In open MRI the treatment was done inside the gantry and tissue contrast changes with ethanol treatment were visible without contrast medium injection.

Conclusion: MRI-guided techniques are helpful for interventions in the field of low back pain therapy, when there are no important human structures such as motor nerves to damage. The infiltration of ethanol can be documented without contrast media. An open access allows nearly real-time guidance of instruments.

P135

Interventional MRI Guidance, Competition for CT in the Field of Microtherapy?

DHW Grönemeyer, RMM Seibel, M Deli, M Busch, MH Friebe, L Kaufman, M Stehling, D Boyd
Institute of Diagnostic and Interventional Radiology, University of Witten/Herdecke, Mülheim, Germany

Purpose: Interventional CT/fluoroscopy-guided microsurgery for biopsies, sympathectomies, cancer therapy, diskectomies, and pain therapy are increasingly used for minimally invasive therapy. Interventional MR imaging is a new monitoring tool in this environment.

Methods: For interventional MRI, two systems were used: an 0.064-T open scanner and a 1.0-T scanner. For monitoring of interventional procedures, fast MRI fluoroscopy and keyhole sequences were used. Self-developed biopsy instruments made of nitinol, titanium, or stainless steel (18 G) and microendoscopes (0.3–1.2 mm) were used for comparison with CT-guided interventions in a helical CT scanner (one slice per second) and an ultrafast CT scanner (up to 17 slices per second).

Results: Thirty interventional MRI- and CT-guided soft-tissue biopsies and endoscopies of animals and humans were compared. The average inaccuracy in determining the true location of the tip of the instruments with MRI was 0.6 to 2.5 mm. The combination of acquisition and reconstruction time was faster with MRI than with CT. The best feedback times between repositioning of the patient couch and patient access were found with the open low-field MR scanner.

Conclusion: MRI-guided techniques are helpful for biopsies and interventions in soft-tissue regions more than 1.0 cm in diameter, as in intratumoral therapies, and if the treatment is time consuming. CT/fluoroscopic guidance still is the gold standard for percutaneous diskectomies, sympathectomies, or biopsies in high-risk areas.

P136

Effect of Thermal Denaturation on the MR Parameters of Selected Tissues: Implications for MR-guided Surgery

SB Rao, JF Schenck, F Jolesz
General Electric Research and Development Center, Schenectady, NY

Purpose: A major limitation on the therapeutic use of precisely localized thermal tissue destruction by means such as focused ultrasound has been the inability to visualize the targeted tissue during treatment. Intraoperative MR imaging is therefore of immense potential. Relatively little work has been done on the MR characterization of thermally denatured tis-

sues. The work described here is an initial attempt at improving the quantitative understanding of the effect of coagulation necrosis on the MR appearance of various tissues.

Methods: Conventional spin-echo images were obtained with a commercial MR scanner (1.5 T). Meat, liver, and egg samples were cooked by traditional means. The gradient in extent of cooking was studied in a large skeletal muscle. For this sample, the relaxation times and proton densities were determined from axial images as functions of distance from the surface for the raw and cooked cases. Standard water samples were used to calibrate the mobile proton densities.

Results: To obtain a measure of the spin density independent of the machine parameters, we extrapolated the signal S to its maximum value MES, defined by $S = MES \cdot \exp(-TE/T2) \cdot [1 - \exp(-TR/T1)]$. A quantity f, which gives the measure of the concentrations of mobile protons, is defined by the equation $f = [MES_{Sample}/MES_{Water}] \cdot 100$. The f values were in approximate agreement with the literature values for the percentage concentration of water in the respective tissues. The quantity f decreases considerably with denaturation in the case of heavily cooked skeletal muscle, fat, and liver (for skeletal muscle, f raw = 87; f cooked = 68). The mobile proton density remains fairly constant during the cooking of egg white and yolk. The relaxation times tend to decrease in the cooked specimen (for liver, T1 raw = 545 ms, T1 cooked = 233 ms). Two things are noteworthy: (*a*) the relatively small T1 changes seen in the cooked egg white and egg yolk (for egg white, T1 raw = 1,586 ms, T1 cooked = 1,581 ms) and (*b*) the increase in the T2 of adipose tissue (T2 raw = 29 ms, T2 cooked = 36 ms).

Conclusion: Although, there is a significant change in the MR parameters when tissues are heated to the point of coagulation necrosis, there is a significant difference in the degree and the characteristic responses of different tissues. Studies such as the one reported here will be necessary to achieve the full possible benefits from the use of intraoperative MRI to enhance the effectiveness of thermal surgery techniques.

J.F. Schenck is an employee stockholder of GE Medical Systems.

P137

Evaluation of Breast Cancer Therapy with Contrast-enhanced MRI at High Spatial Resolution

H Degani, S Fields, R Catane, JM Gomori, T Peretz, A Libove
Department of Chemical Physics, Weizmann Institute of Science, Rehovot, Israel

Purpose: In any stage of breast cancer, it is of utmost importance to be able to assess as quickly as possible the effectiveness of therapy. We have initiated a program aimed at evaluating the potential use of MRI to rapidly verify the response to treatment of breast cancer patients. Here we describe the application of contrast-enhanced MRI at high spatial resolution to assess the effectiveness of chemotherapy in the treatment of advanced breast cancer prior to surgical resection.

Methods: Images were recorded prior to and after administration of Gd-DTPA $(NMG)_2$ (0.08 mmol/kg) at 2 T with a breast coil, and a 3D gradient-echo sequence (TE/TR = 8.5/20 msec, flip angle 25°) that allowed 32 slices to be obtained within 2 minutes at a resolution of 1.2 × 0.8 × 0.8 mm.

Results: Contrast-enhanced MRI of five patients with advanced disease was correlated with their corresponding histologic findings. Three patients were monitored before and after each course of therapy with cyclophosphamide, adriamicin, and 5-fluorouracil. In two patients a marked positive response was observed after the first course of chemotherapy. In one patient the response to chemotherapy was slow, but after one additional course of radiation therapy a significant response was detected. Chemotherapeutic effectiveness was seen as a decrease in the size of the tumor, a decrease in the degree of enhancement and the initial rate of enhancement, and an increase in enhancement inhomogeneity.

Conclusion: Contrast-enhanced MRI of breast carcinoma at high spatial resolution may be a useful clinical tool in the evaluation of response to treatment.

P138

Evaluation of Thermometry Sequences for Ultra-Low-Field MRI Systems

MH Friebe, M Busch, M Koch, M Schaldach, DHW Grönemeyer, RMM Seibel
University of Witten/Herdecke, Bochum, Germany

Purpose: Ultra-low-field MRI (ULFMRI) has distinct advantages over higher-field-strength systems in interventional applications. These include reduced metal artifacts, open access to the patient (Toshiba Access 0.064 T), and a small magnetic fringe field (allows close placement of life-monitoring equipment). ULFMRI can therefore be considered the best MR system for laser hyperthermia applications. It is necessary in these applications to monitor the tissue temperature closely and in almost real time. Many different approaches have been suggested, but their application in UFMRI is highly questionable, since they require high signal-to-noise ratios or special imaging equipment (EPI) or simply take too long. The purpose of our research was to evaluate current and new imaging techniques for ULFMRI with the goal of meeting the minimum temperature resolution necessary for in vivo hyperthermia applications (±1°C).

Methods: We compared new thermometry sequences based on the keyhole imaging technique in combination with diffusion imaging with standard diffusion-based (stimulated echo, Stesjkal/Tanner, navigator echo) and other temperature-sensitive sequences (Curie law). All sequences were implemented on our 0.064-T system and on a 1.5-T Siemens SP63.

Results: ULFMRI is able to produce repeatable temperature accuracy of ±2°C in a 1 × 1 × 5 mm voxel.

Conclusion: The results show that the new imaging technique offers sufficient speed (15 seconds per scan) for application in hyperthermia but still lacks the necessary temperature resolution. Continuous research in this field could further increase the accuracy and make thermometry feasible with ULFMRI.

P139

Composite 3D Spin-Echo, Gradient-Echo Data Set for Stereotaxic Surgical Planning

JA Bertolina, JW Snell, JC Goble, TA Spraggins, NF Kassell
Department of Neurosurgery, University of Virginia, Charlottesville, VA

Purpose: When acquiring images to be used for stereotaxic surgical planning, three goals should be kept in mind. First, the in-plane image matrix must be large enough to include the fiducial markers; second, the images should accurately depict (volumetrically as well as spatially) the lesion(s) of interest; third, the image matrix should include the whole head to show the relationship of the lesion(s) to other key anatomic structures. Gradient-echo (GRE) sequences are more time efficient than spin-echo (SE) sequences and are therefore better suited for acquiring image data sets of the whole head and fiducials. Unfortunately, their ability to accurately depict the size and shape of lesion(s) is suspect. They have been shown to suffer from intravoxel dephasing that leads to lesion misrepresentation (1–3). SE sequences are less susceptible to signal loss from spin dephasing and are therefore more reliable for accurate lesion depiction. They, however, are relatively time inefficient.

Methods and Results: To reduce the acquisition time, we have developed a 3D SE sequence that is volume selective (4). We acquire one data set (of the head and fiducials) with a 3D GRE sequence and a second data set (lesion and surrounding tissue) with the 3D volume-selective SE sequence. The SE data are pasted into the GRE data set with trilinear interpolation.

Conclusion: We have developed a method for creating and displaying a GRE/SE hybrid data set. It exploits the positive attributes of SE (accurate lesion representation) and GRE (time efficiency) sequences. The hybrid data set is used for stereotaxic surgical planning and analysis.

1. Jara H, Wehrli FW, Chung H, Ford JC. *MRM* 29:528 (1993). 2. Hackney DB, Lenkinski RE, Grossman RI, Zim-

merman RA, et al. *JCAT* 12(1):171 (1988). 3. Tsuruda JS, Remley K. *AJNR* 12:237 (1991). 4. Bertolina JA, Spraggins TA, Cail WS, Kassell NF, Goble JC. *Proceedings of the SMRM 12th Annual Meeting* Pg 902.

P140

MR Imaging and Elimination following Administration of Gd-EOB-DTPA in Transport-deficient Mutant Rats: Experimental Study Resembling the Human Dubin-Johnson Syndrome

A Mühler, RPJ Oude Elferink, HJ Weinmann
Schering AG, Berlin, Germany

Purpose: Gd-EOB-DTPA is a hepatobiliary MR contrast agent with dual elimination by the kidneys and liver. Mutant Wistar rats (TR-minus rats) are known for their deficiency of the canalicular transport system of the liver, which is used by Gd-EOB-DTPA for biliary excretion. This study was designed to investigate whether Gd-EOB-DTPA can be completely eliminated in TR-minus rats despite absence of the biliary elimination route and to show the MR imaging characteristics of Gd-EOB-DTPA in these mutant rats.

Methods: Biliary excretion rates of 0.05 mmol/kg Gd-EOB-DTPA were determined in TR-minus rats (n = 3) and in control rats (n = 3). The whole-body retention of the contrast agent was investigated 1 and 7 days following the dose of 0.25 mmol/kg. Gadolinium concentrations in bile, liver, kidneys, and carcass were measured by means of ICP-AES (λ = 342.247 nm). MR imaging was performed at 2 T and with a T1-weighted SE sequence (250/15/4, 256 × 256). Images were acquired prior to and following injection of Gd-EOB-DTPA (0.025 mmol/kg).

Results: In TR-minus rats, only insignificant biliary excretion was shown to occur (2.4 ± 0.4%). However, body gadolinium retention was less than 2% at 1 day and less than 0.7% at 7 days following intravenous injection. By comparison, in control rats the majority of the Gd-EOB-DTPA was eliminated via the biliary route (80.3 ± 3.9%), and body retention of the contrast agent was comparable to that in TR-minus rats. During MR imaging, strong initial liver enhancement was observed in both rat strains following injection of Gd-EOB-DTPA. Liver signal intensities returned to preinjection values in 6 hours (control rats) or within 24 hours (TR-minus rats).

Conclusions: The hepatobiliary MR contrast agent Gd-EOB-DTPA is completely removed from the body even in the case of severely impaired biliary secretion. The remaining urinary elimination pathway can fully compensate for the hepatic dysfunction. The uptake of Gd-EOB-DTPA into the liver cells of TR-minus rats was shown to be unaffected despite congenital hyperbilirubinemia.

A. Mühler and H.J. Weinmann are employees of Schering AG.

P141

Diagnosis and Differential Diagnosis of Pancreatic Tumors: Comparison of Contrast-enhanced CT and Gd-DTPA–enhanced MRI with Fat-suppressing Spin-Echo and FLASH Sequences

K Engelhard, HP Hollenbach
Radiological Department, Martha-Maria Hospital, Nürnberg, Germany

Purpose: To compare the diagnostic value of CT and MRI in the depiction and characterization of pancreatic masses.

Methods: Fifteen patients with clinical suspicion of pancreatic tumors underwent dynamic contrast-enhanced CT and MR examinations. The MR studies were performed with a 1.0-T whole-body MR system (Siemens Magnetom Impact). A T1-weighted FLASH sequence (TR/TE/FA 500/8/90°, before and after Gd-DTPA) and a T2-weighted spin-echo double-echo sequence (1,600/20/80/60°) were applied in a transverse orientation with use of the body resonator. The highest spatial resolution was 1.82 × 1.37 × 5.00 mm. Both sequences used a frequency selective 1331 fat-saturation prepulse. The whole measurement time was about 25 min. The final diagnosis of a malignant (n = 10) or inflammatory (n = 5) tumor was done on the basis of findings from surgery and follow-up (6–14 months).

Results: Correct diagnosis was made with CT in 10 of 15 cases and with MRI in all cases. Adenocarcinomas and one endocrine malignant tumor had low signal intensity with the fat-suppressing T1-weighted FLASH sequence in comparison with noninvolved pancreatic tissue. Solid tumor regions were isointense with the fat-suppressing T2-weighted SE pulse sequence in comparison with pancreatic tissue. One metastasis was high in signal intensity on T2-weighted SE images and isointense on T1-weighted FLASH images. In five cases, localized inflammatory tissue was isointense on the T2-weighted SE images. Gd-DTPA–enhanced FLASH sequences were superior to contrast-enhanced CT in demonstrating tissue necrosis and signs of infiltration in peripancreatic structures.

Conclusion: MRI with fat-suppressing FLASH and SE sequences is more accurate than CT in the diagnosis of pancreatic masses.

P142

MR Cholangiography: Comparison with 3D CT Cholangiography with Helical Scanning

K Ohgi, T Nakayama, H Yoshimura, T Furukawa, K Kurita, T Hayano, A Morimoto, H Nishio
Department of Radiology, Japanese Red Cross Medical Center, Tokyo, Japan

Purpose: To compare the usefulness of MR cholangiography with that of 3D CT cholangiography in the evaluation of biliary diseases.

Methods: MR cholangiography examinations were performed with 1.5-T superconductive units (MRT 200FX-III super; Toshiba, and Signa Advantage; GE Medical Systems) and with a fast spin-echo technique (TR = 4,000–7,300 msec, effective TE = 100–280 msec, echo train = 7–32). 3D CT cholangiography studies with helical scanning were performed with a TCT-900S/super Helix (Toshiba) scanner, after intravenous injection of iodine contrast medium (Biliscopin DIC 50; Schering). Twelve patients with biliary diseases (including biliary stones, cholangiocarcinoma, pancreas head carcinoma, gallbladder carcinoma, and adenomyomatosis of the gallbladder) were evaluated.

Results: CT cholangiography provided better spatial resolution and less artifact due to fluid-filled intestinal loops. On the other hand, nonvisualization of the gallbladder in cases of gallstones and poorly visualized biliary tract in cases of obstructive jaundice were the significant problems in CT cholangiography. MR cholangiography more consistently depicted dilated biliary tracts and had the advantages of no contrast medium and no radiation exposure.

Conclusion: MR cholangiography and CT cholangiography should be indicated in consideration of their advantages and disadvantages.

1. K Ohgi, et al. Acute Cholecystitis: MR Evaluation of Thickened Gallbladder Wall. 77th Scientific Assembly and Annual Meeting of Radiological Society of North America, 1991, Chicago. 2. K Ohgi, et al. MR imaging of Thickened Gallbladder Wall: Pathologic Correlation. 11th Annual Meeting of SMRI, 1993, San Francisco.

P143

Refined Protocol for Clinical MR Mammography Examinations

IS Gribbestad, G Nilsen, S Lundgren, HE Fjøsne, OA Haugen, PA Rinck
Sintef Unimed and University Hospital of Trondheim, Trondheim, Norway

Purpose: Dynamic contrast-enhanced MR mammography has proved to be of considerable benefit for characterization of breast lesions. Tumor necrosis might yield false-negative cases, due to slow contrast enhancement (1). In order to clearly identify necrotic area of tumors, we now suggest a refined examination protocol, including a turbo SE sequence for clinical MR mammographic examinations.

Methods: Patients with clinically palpable breast lesions were

examined with a 0.5-T whole-body system (Gyroscan T5, Philips). An SE sequence (TR 550/TE 18) was used in transverse and sagittal planes, followed by a dynamic gradient-echo sequence (TR 100/TE 15/flip angle 80° with IV bolus contrast injection of gadopentetate dimeglumine (0.1 mmol/kg body weight), and, finally, a turbo SE sequence (TR 4,000/TE 130) to demonstrate necrosis within the tumor.

Results: Malignant tumors showed large variations in signal enhancement inside each tumor. Less enhancing areas of the tumors in the dynamic series showed high signal intensity on T2-weighted turbo SE images, compatible with necrosis. This was confirmed at histopathology.

Conclusion: By including a T2-weighted sequence in the MR mammography examination protocol, necrotic fractions of malignant tumors can be identified and avoided when measuring contrast enhancement with dynamic sequences. This might reduce the possibility of false-negative cases. The examination time is still feasible for clinical use (30 min).

1. Gribbestad IS, Nilsen G, Fjøsne HE, Kvinnsland S, Haugen OA, Rinck PA. *Signal Intensity Measurement in Dynamic MR Mammography Studies,* 12th Annual Meeting of the Society of Magnetic Resonance in Medicine, New York, 1993; 854.

P144

Visualization on Gadolinium-enhanced MR Images of Breast Tumors with Intensity-Time Gradient Maps

S Sinha, U Sinha, D Gorczyka, D Farria, L Bassett
Department of Radiology, UCLA School of Medicine, Los Angeles, CA

Purpose: Dynamic contrast-enhanced studies of breast tumors have been shown to have the potential to distinguish between malignant and benign lesions. Visual inspection of the dynamic images does not always indicate the rate of enhancement of the tumors. We have applied a temporal gradient filter to the original images, and the processed images show the time and rate of maximum enhancement, the parameters of greatest importance in distinguishing between malignant and benign lesions.

Methods: Dynamic contrast-enhanced images of breast tumors in 19 patients were acquired at 1.5 T (GE Signa). Images were transferred to a SunSparc2 workstation for analysis. The temporal gradient at any pixel of each frame was estimated as the difference in intensity values at the same pixel location acquired at two adjacent time points. All the images were scaled by using the maximum and minimum pixel values of the entire set of images and then displayed in a cine loop.

Results: The gradient images showed the effects of enhancement more dramatically than the original images and enabled the radiologist to pick out the time frame of maximum enhancement. Visual inspection was sufficient to distinguish between malignant and benign lesions, and the diagnosis agreed well with quantitative analysis of regions of interest.

Conclusion: This is a simple postprocessing scheme with which the effects of contrast enhancement can be visualized.

Tuesday, March 8, 12:15 PM–1:30 PM
Vascular Imaging and Flow/ Quantification/Cardiac

Posters P201–P220

P201

Optimization of Imaging Parameters in 3D Intracranial MR Angiography

Y Du, DL Parker, WL Davis, DD Blatter
Department of Radiology, University of Utah Health Sciences Center, Salt Lake City, UT

Purpose: In magnetic resonance angiography (MRA), the contrast-to-noise ratio (CNR) of vessels is strongly related to imaging parameters such as flip angle, field of view, echo time, and repetition time. The optimization of MRA imaging parameters improves the clinical utility of MRA techniques. An experimental study of the CNR dependencies on these imaging parameters provides a quantitative basis for such optimization.

Methods: Software was developed to measure CNR at all points along a vessel for 3D image data. The mean CNR and root mean square of CNR can also be calculated to estimate the visibility and signal uniformity of vessels. CNR measurements were performed on four sets of images. The images in each of these four sets had different values of one imaging parameter, while other imaging conditions were kept the same. Before the CNR measurements, band-limited interpolation was applied to all the image data sets to reduce partial volume artifacts.

Results: CNR dependencies on flip angle, field of view, echo time, and repetition time were experimentally studied in human intracranial MRA in a region around the circle of Willis, with use of the multiple-overlapping thin-slab acquisition (MOTSA) pulse sequence.

Conclusion: This study experimentally demonstrates the CNR dependencies on imaging parameters in human intracranial MRA with MOTSA. Such CNR measurements allow the optimization of MRA techniques.

P202

Cardiac-gated Phase-Contrast Angiography

M Kouwenhoven, M Wasser, RG de Graaf, JP Groen
MR Clinical Science, Philips Medical Systems, Best, The Netherlands

Purpose: Phase-contrast angiography has been applied successfully in several anatomic areas, but when the flow is very pulsatile, ghosting and flow voids will occur and will affect the clinical usefulness of the images. This can be overcome by limiting the acquisition to a part of the heart cycle where the flow in the vessels of interest is more or less steady.

Methods: Cardiac-gated phase-contrast angiography allows the user to limit the acquisition to a user-defined gate width, the offset from the ECG R-top being determined by the gate delay. The gate can be positioned both in systole and in diastole. Even though the acquisition is limited to this gate, the RF pulses and gradients are continued during the whole heart cycle in order to maintain a steady state. In order to determine the gate delay and gate width, a cardiac triggered quantitative flow measurement was performed.

Results: Measurements in healthy volunteers have proved that the determination of the gate delay and width is extremely critical, especially when the gate is in systole. For imaging of the renal arteries, cardiac-gated phase-contrast angiography significantly reduces pulsatility artifacts in the renal ostia and in the infrarenal aorta.

Conclusion: Cardiac-gated phase-contrast angiography is successful in imaging strongly pulsatile flow by reducing ghosting and flow voids, at the cost of scan time. The gate delay and the gate width are critical and should be determined beforehand by quantitatively measuring the flow in the vessels of interest.

M. Kouwenhoven is an employee of Philips Medical Systems.

P203

General Improvements to Selective Inversion-Recovery Angiography

AB Kerr, DG Nishimura
Information Systems Laboratory, Stanford University, Stanford, CA

Purpose: To design improvements to selective inversion-recovery (SIR) angiography in the four areas of (*a*) RF pulses, (*b*) elimination of the "venetian blind" artifact, (*c*) static signal suppression, and (*d*) 3D enhancements.

Methods: SIR is a cardiac-gated time-of-flight projection angiography method in which upstream blood is differentially tagged in two images so that only signal from blood is left in a

difference image. Quasi-adiabatic inversion excitation pulses designed by using the Shinnar-Le Roux algorithm have sharper transition bands, allowing closer abutment of the tagged and imaged regions to give greater flow sensitivity. The segmented k-space imaging nature of SIR also requires excitation pulses with a stable signal profile (1) to reduce ghosting artifacts and to minimize the venetian-blind artifact in multislab SIR. To further reduce this artifact, consecutive slabs in multislab SIR are partially overlapped so that voxels in the transition regions can be discarded. Static signal suppression of fat and long T1 species in the component images is obtained by using a double inversion-recovery sequence. Finally, coarse phase encoding in the projection direction is added to give a 3D data set.

Results: High-resolution, high-SNR images of the carotid arteries of several healthy volunteers were obtained with multislab SIR and demonstrated a significant reduction in the venetian-blind artifact and improved static suppression.

Conclusion: Improved RF pulses and sequence design make SIR angiography a robust and rapid method for acquiring MR angiograms.

1. A. Kerr *et al.*, 12th SMRM 1993, p. 1189

P204

Black Blood Angiography with A Multidimensional Saturation Pulse

S Singh, R Deslauriers
Institute for Biodiagnostics, National Research Council of Canada, Winnipeg, Manitoba, Canada

Purpose: To avoid possible interference from untargeted blood vessels during minimum-intensity projection in black blood angiography, we introduced a multidimensional saturation pulse that requires very low RF power to create a suitable flow marker for imaging black blood in the vessel of interest, even in the presence of disturbed and pulsatile flow.

Methods: Three-dimensional projection presaturation gradients were used to create a resultant gradient vector rotating stepwise in two or three dimensions (SMRM 1992, p. 3928). A single sinc saturation pulse with small tip angle was applied at each step of the rotating gradient to saturate a thin band of spins at that step. The intersection of these bands, a cylinder (which can be tilted along any orientation in space) and a sphere in two and three dimensions, respectively, was the desired flow marker for imaging black blood. This marker was selectively created in one of the flexible tubes of a flow phantom that allowed pulsatile flow of doped water and was surrounded by a water bath with higher doping. A nonselective inversion pulse was applied prior to creating the marker to enhance its degree of saturation. The marker was followed, and FLASH images were taken with acquisition window(s) selected about the null point.

Results: Coronal as well as axial multislice black blood FLASH images of the phantom with a 4.7-T/40-cm magnet showed good contrast throughout and clear delineation between the tube of interest and the remainder.

Conclusion: Creation of flow markers with a multidimensional saturation pulse is fast and requires only low RF power. The shape and size of the marker can be controlled independently of the size of the exterior volume. The method may have potential applications in imaging coronary, carotid, and other great vessels.

P205

Further Improvements in 3D FSE Black Blood Imaging with a Multislab Interleaved Acquisition

J Listerud, SW Atlas, J Mitchell
Department of Radiology, Hospital of the University of Pennsylvania, Philadelphia, PA

Purpose: Preliminary results with 3D FSE (1), a volume implementation of the RARE sequence (2), have demonstrated potential for high-resolution black blood MRA with spin-echo contrast (3,4). Here we describe ongoing optimization of this application.

Methods: A 3D FSE sequence running on a 5.x Signa MR scanner was modified to support (*a*) increased higher-order gradient moments in order to induce the anti-CPMG phase condition in the suppression of signal from flowing spins and (*b*) inversion recovery out of slab in order to null flowing spins. This new 3D FSE sequence supports interleaved multislab 3D acquisition. The 180° pulses employed the Shinnar-LeRoux algorithm.

Results: Preliminary results in normal volunteers indicate that elimination of signal from the zone of flow reversal and stasis within the carotid bulb can be obtained by the application of increased gradient moments. Multislab capability significantly improved the ability to obtain T1-weighted spin-echo contrast in stationary tissue in convenient imaging times (< 4 min).

Conclusion: Previous workers have shown that T1-weighted spin-echo contrast is superior to gradient echo in the context of 2D spin-echo black blood imaging (5). We have previously shown that 3D FSE is capable of good quality black blood imaging but that long imaging times limit the clinical utility of single-slab implementations. The multislab capability is an important step in making 3D FSE black blood imaging clinically useful.

1. K. Oshio, P.S. Melki, F.A. Jolesz SMRM Abstracts 842 (1991). 2. J. Hennig, A. Nauerth, H. Friedburg SMRM 3, 823 (1986). 3. J. Listerud, S.W. Atlas RSNA 149 (1991). 4. J. Listerud, S.W. Atlas, S. Hinks RSNA 347 (1993). 5. R.R. Edelman, H.P. Mattle, B. Wallner, et. al. Radiology 177:45–50 (1990).

P206

Three-dimensional MR Angiography of the Renal Arteries with a Selective Inversion-Recovery Rapid Gradient-Echo Sequence

D Li, M Hutton, EM Haacke
Washington University, Mallinckrodt Institute of Radiology, Clayton, MO

Purpose: To develop a 3D time-of-flight (TOF) MRA sequence to visualize the renal arteries and to evaluate the technique in normal volunteers.

Methods: A selective inversion-recovery (SIR) pulse is first applied to the imaging slab, followed by 32 partition-encoding steps. The inversion-recovery time is chosen so that stationary tissue is nulled and blood is refreshed, resulting in significantly increased vascular contrast compared with conventional 3D TOF MRA sequences. Fat signal is saturated by applying a spectrally selective pulse centered at the fat-resonant frequency before data acquisition. The sequence is ECG triggered so that blood inflow occurs during systole and data acquisition during diastole.

Results: By using 3D SIR-RAGE with fat saturation, the background signal was suppressed by over 50% while the blood signal remained the same or was further enhanced compared with conventional 3D TOF MRA techniques with the same imaging time. Thus, motion artifacts were dramatically reduced and the conspicuity of the arteries significantly improved. The ghosting artifacts from the pulsatile aortic blood flow were essentially eliminated by using ECG triggering. The first 4–5 cm of the proximal portion of the renal arteries was well visualized in all normal volunteers.

Conclusion: By using 3D SIR-RAGE with fat saturation and ECG triggering, the proximal renal arteries, especially their origination from the aorta, were well visualized, with excellent vascular contrast and dramatically reduced motion and flow artifacts. This technique could be very useful in delineating main renal artery stenoses.

P207

Dural Sinus Thrombosis in Pediatrics: Value of Venous MRA

AM Wang, AN Shetty, DP Wesolowski, MG Goetting, FY Tsai, WTC Yuh
Department of Diagnostic Radiology, William Beaumont Hospital, Royal Oak, MI

Purpose: The clinical diagnosis of dural sinus thrombosis in

pediatric patients is difficult, and early diagnosis is critical for the patient's clinical management. To determine if venous MRA can noninvasively provide an early conclusive diagnosis and play an important role in effective patient clinical management, we compared the clinical outcome of patients with dural sinus thrombosis studied with and without venous MRA.

Methods: Ten patients ranging from 4 days to 17 years old were included in this study. Eight underwent intracranial venous MRA studies. A sequential 2D TOF technique was used with flow compensation along the read and slice directions. The slices were placed parasagittally on an axial scout and axially on a sagittal scout image to maximize through-plane flow, and a SAT band was placed inferiorly to saturate arterial flow. The study was performed on a Siemens SP 63 Magnetom with A2.5 software.

Results: In the two patients who did not undergo venous MRA, dural sinus thrombosis was missed at CT and conventional MRI, and both patients died. In the eight patients who did undergo venous MRA, the early diagnosis was correctly made. All of these patients received endovascular thrombolytic treatment; seven recovered completely, and one had a posterior fossa stroke from the coexisting basilar artery occlusion.

Conclusion: The diagnostic confidence level of dural sinus thrombosis can be increased by adding venous MRA. Therefore, an early conclusive diagnosis can be made for successful clinical pediatric patient management.

P208

MR Venography of the Lower Extremities

DG Spigos, P Schmalbrock, AB Fontaine, AE Stockum
Department of Radiology, Ohio State University, Columbus, OH

Purpose: The purpose of this study was to evaluate whether time-of-flight MR venography can be a viable alternative to x-ray venography.

Methods: MR venograms were obtained with a 1.5-T system (GE, Signa) with use of the body RF coil and the 2D TOF method with TR/TE/FA of 46/35/30°, flow compensation, arterial presaturation, single excitation, 32–40-cm FOV, and 256 × 128 matrix size. For an overview of the venous structures from the IVC to below the intrapopliteal veins, 180 slices of 5-mm thickness were acquired in under 18 minutes. Additional sections with 1.5–3.0-mm thickness and smaller FOVs were acquired with an extremity coil for a more detailed evaluation.

Results: The technique was evaluated in healthy volunteers and in patients with venous pathology. The major venous branches were visualized from the IVC to the veins of the leg with the low-resolution protocol. The veins below the popliteal were better seen with the high-resolution protocol. Venous pathology was seen as areas of reduced flow (ie, reduced signal), and collateral pathways were also readily demonstrated.

Conclusion: Our initial experience shows that MR venography may be a valuable tool for diagnostic evaluation of patients with venous thrombosis.

P209

Which Combination of Techniques for MRA of the Carotid Arteries Is Optimal in Clinical Practice?

MS Benjamin, AR Gillams, AP Carter
Center for MRI, Boston University Medical School, Boston, MA

Purpose: As MRA is increasingly accepted into clinical practice, increasing expectations need to met with more sophisticated clinical protocols. Although there are comparisons of one technique versus another, it is now clear that a combination of techniques is required to fully assess the carotid artery clinically. We evaluated 3D phase-contrast (PCA), nonsegmented 2D (2D TOF), segmented 2D (2D TFE), nonsegmented 3D (3D TOF), and segmented 3D time-of-flight (3D TOF) to define which combination would be clinically optimal and practicable.

Methods: Seven volunteers (3 male, 4 female), median age 31 years (23–55) underwent all five sequences. Sequence parameters: TR/TE/flip angle 20/8/20° for PCA, 26/8/60° for 2D TOF, 16/8/60° for 2D TFE, 31/7/25° for 3D TOF, and 21/7/25° for 3D TFE. Slice thickness was 0.6 mm for the 3D sequences with a 512 reconstruction matrix in 3D TOF and 3D TFE. Slice thickness was 3 mm with 1-mm overlap for 2D TOF and 2D TFE. The segmented sequences had a 180° inversion prepulse for maximum fat suppression. Acquisition times were 8:34 for PCA, 5:22 for 2D TOF, 6:54 for 2D TFE, 6:38 for 3D TOF, and 5:37 for 3D TFE. Maximum-intensity projections were performed. Analysis was both qualitative and quantitative, with ROI intensity measurements of each of the major vessels; SNR and CNR were calculated.

Results: Mean CNR in the internal carotid artery was PCA 31 ± 17.5, 2D TOF 110 ± 41, 2D TFE 73 ± 38, 3D TOF 63 ± 22.5, and 3D TFE 69 ± 25. Mean SNR was PCA 44 ± 24, 2D TOF 124 ± 42, 2D TFE 83 ± 35, 3D TOF 99 ± 33, and 3D TFE 90 ± 25. Statistical analysis showed a significant improvement in SNR and CNR for 2D TOF versus 2D TFE. 3D TOF had significantly better SNR than 3D TFE. The 3D TFE had better CNR, but this did not reach significance. Both 2D TOF and 3D TOF were superior to PCA. PCA had optimal coverage of the vessels; 3D TFE had optimal resolution and CNR.

Conclusion: PCA should be the initial screening MR technique, followed by 3D TFE/3D TOF with a 512 matrix for any lesion and the bifurcation.

P210

MR Bolus Tracking of Intra- and Extracranial Arteries

KW Neff, M Daffertshofer, J Roether, J Kuehnen, A Schwartz
Department of Neurology, Klinikum Mannheim, University of Heidelberg, Heidelberg, Germany

Purpose: In the past few years, magnetic resonance angiography has become a powerful tool in the diagnosis of pathologic findings in intra- and extracranial arteries. Additionally, it is a technique for noninvasive measurement of blood flow velocity and blood flow volume. Studies were performed to assess the quality of such measurements.

Methods: Cardiac-triggered MR bolus-tracking sequences, based on different angiography sequences (TR/TE/flip/FOV/matrix/NSA: 40 ms/10 ms/30°/200 mm/192*256/1, 95 ms/20 ms/30°/230 mm/160*256/1; section thickness, 5–10 mm; partly with multiecho technique) were chosen for flow velocity and flow volume measurements in different intra- and extracranial arteries in the common carotid artery and the middle cerebral artery to study the quality of MR bolus-tracking measurements compared with continuous- and pulsed-wave Doppler signal analysis and duplex-system examinations in volunteers and patients. MR measurements were performed with a 1.5-T superconductive MR unit (Magnetom 63 SP, Siemens Medical Systems, Germany).

Results: Correlations between MR bolus-tracking measurements, Doppler signal analysis, and duplex examinations were excellent. Results from 20 examinations correlating MR bolus-tracking and sonography measurements showed a ratio of 1.04 ± 0.08 for systolic mean maximal velocities and 1.06 ± 0.10 for diastolic mean maximal velocities in the middle cerebral artery. An equally good correlation was obtained for measurements in the common carotid artery.

Conclusion: The results demonstrate the high quality of MR bolus-tracking measurements and the feasibility of measuring flow velocities and flow volumes in intra- and extracranial arteries with MR angiography. Systematic measurements of other intra- and extracranial arteries are currently being undertaken.

P211

Flow Model Studies of MR Bolus Tracking

KW Neff, P Grebe, M Just, H Schild, M Thelen
Department of Radiology, University of Mainz, Mainz, Germany

Purpose: The high-resolution flow sensitivity of magnetic

resonance leads to techniques for noninvasive measurement of blood flow velocity and blood flow volume. Flow model studies of MR bolus-tracking were carried out to assess the quality of such measurements.

Methods: Cardiac-triggered MR bolus-tracking measurements of flow velocity and flow volume were performed with flow-sensitive FFE sequences (TR/flip/FOV/matrix/NSA: 67–800 ms/30°/220 mm/256*256/2) at different echo times (TE = 7, 17, 37, 47 ms), with section thicknesses of 4–20 mm, partly with a multiecho technique and in a simple geometry flow model. Various diameters (25, 20, 12, and 7 mm) for straight and curved vessels were chosen to measure flow velocity and flow volume in comparison with mechanical flow meter measurements. MR flow velocity and flow volume were extracted by fitting the parabolic velocity flow profile and calculating velocity and volume. Flow velocities between 0 and 130 cm/sec for the different vessel diameters and echo times were investigated. Magnetic resonance measurements were performed with a 1.5-T superconductive MR unit (Gyroscan ACS, Philips Medical Systems, Best, The Netherlands).

Results: Correlations between MR bolus-tracking measurements and flow meter measurements were excellent. Results showed values for regression between $r = .990$ and .999 for the different examinations. Equally good results were obtained for inflow measurements into a user-defined rectangular presaturation volume as a modification of dynamic bolus tracking.

Conclusion: The results demonstrate the feasibility of measuring flow velocities and flow volumes with MR bolus tracking. The extraction of parabolic velocity profiles is also possible.

P212

Experimental Investigation of Complex Flow at an Arterial Bifurcation with AFP-MRA

AT Vu, HK Lee, PR Moran, JF Emerson, O Nalcioglu
Division of Physics and Engineering, Department of Radiological Sciences, University of California, Irvine, CA

Purpose: Complex arterial flow fields, such as those present in the region of the carotid bifurcation, have been implicated in atherogenesis (1). The purpose of this study was to investigate the characteristics of the complex arterial flow field near the carotid sinus with multizone adiabatic fast passage magnetic resonance angiography (AFP-MRA).

Methods: All studies were performed with a GE Signa 1.5-T imager. The pulse sequence used in the present work has been described elsewhere (2). With use of the multizone technique, adiabatic passage labeling at several locations can be achieved, yielding flow profile information at various spatial positions in one experiment. To minimize the flow-related dephasing effects of velocity and acceleration, the enhanced quasi-half-echo technique was also used.

Results: An in vivo flow profile at the carotid bifurcation of a healthy human volunteer was obtained by using the multizone AFP imaging pulse sequence. Qualitative characteristics of the flow profile were obtained, along with quantitative measurements of average blood flow velocities. The time-averaged velocity (over the whole cardiac cycle) in the common carotid artery was 25.9 ± 1.0 cm/s. The velocities in the internal and external carotid arteries distal to the bifurcation were 28.1 ± 1.0 and 18.8 ± 1.0 cm/s, respectively. These velocities fall within the range expected for a healthy subject.

Conclusion: Multizone AFP-MRA appears to be well-suited for studying the complex fluid mechanical phenomena at arterial bifurcations. It provides both qualitative and quantitative information that can be used to further our understanding of the development and localization of atherosclerotic lesions.

1. CG Caro, et al, Proc R Soc Lond B, 109, 1971. 2. AT Vu, et al MRI, 11, 1993.

P213

Measuring Correlation Time of Turbulence with an MR Technique

JH Gao, DK Kuethe
Research Imaging Center, University of Texas Health Science Center, San Antonio, TX

Purpose: It has been difficult to measure the Lagrangian velocity self-correlation time called for in statistical models of turbulence. We introduce an MR technique that can determine the correlation time from the decay of MR signal in imposed magnetic field gradients.

Methods: MR experiments were performed on the 1.4-T MR imaging system in the Francis Bitter National Magnet Laboratory at MIT. A spin-echo pulse sequence combined with a pair of turbulence-weighted bipolar gradients were used in our measurements. The MR data were collected for stationary spins (Re = 0), laminar flow (Re = 800), and turbulent flow (both Re = 6,505 and Re = 9,359). Assuming the phase of the transverse magnetization obeys Gaussian distribution, and applying the model that utilizes the statistical turbulent diffusion treatment, the measured MR signal decay of a tagged parcel of fluid can be used to determine the correlation time and turbulent intensity simultaneously.

Results: The correlation time T_0 measured with our MR method is $T_0 = 0.66 + 0.01$ s for Re = 6,505, and $T_0 = 0.32 + 0.03$ s for Re = 9,359. The ratio of rms values of the turbulent intensity and mean velocity approximates 5% for both Re values, and agrees well with the previous measurement.

Conclusion: The correlation time of turbulence has been successfully measured with the MR method. The MR technique has great advantages compared with other flow measurement methods. It is noninvasive and practical, since measurement takes only several hours.

P214

Quantitative, Linear Form of the Complex Difference Method of Phase-Contrast MR Angiography

CA Hamilton, PR Moran
Department of Radiology/MRI, Bowman Gray School of Medicine, Winston-Salem, NC

Purpose: The complex difference method provides useful angiographic images, but they are nonquantitative; that is, the voxel values are an estimate of average speed weighted by the total magnetization in the voxel. The complex difference method is also nonlinear if the phase shift in the voxel is greater than about 30°, due to the approximation of $\sin(x)$ as x that is inherent to this method. We present a new form that overcomes these limitations, providing quantitative estimates of average speed and allowing the velocity-induced phase shift its full range of 90°.

Methods: Careful analysis results in a new algorithm performed by dividing the complex difference by the average magnitude of the two encodings, which "unweights" the speed estimate, then linearizing the result by taking an arcsin. Computer simulations of flow in a single voxel are performed, and the resulting flow-encoded data are reconstructed with the standard complex difference method and the new method. Flow tube scanner experiments are also performed with the same parameters used in the simulations and then reconstructed with both methods.

Results: The computer simulations and scanner experiments illustrate the nonquantitativeness and nonlinearity of the current complex difference method and their accurate correction by the new method.

Conclusion: The new method does indeed provide a linear, quantitative form of the complex difference method.

P215

Effects of Intravoxel Velocity Distributions in Phase-Contrast MR Angiography

CA Hamilton, PR Moran
Department of Radiology, Bowman Gray School of Medicine, Winston-Salem, NC

Purpose: Intravoxel velocity distributions have been identi-

fied as sources of error in phase-contrast MRA, but quantitative error analysis has been lacking. We present analysis of these effects for both the phase difference method and the complex difference method.

Methods: Mathematical analysis of intravoxel velocity distributions provides expressions for the error in velocity estimates in both the phase difference and complex difference methods. Computer simulations and scanner experiments are performed that confirm the results of the analysis.

Results: The error in the phase difference method is dependent on the asymmetry of the velocity distribution. The complex difference method is dependent on the asymmetry and also the variance of the velocity distribution. The error is shown to be small for worst-case unidirectional flow—that is, all the flow in the voxel is in the same direction. For a voxel containing bidirectional flow, such as may occur in regions distal to a stenosis, the error can become quite large.

Conclusion: For arbitrarily distributed unidirectional flow, phase-contrast MRA provides good estimates of average velocity; intravoxel velocity distributions do not significantly affect average velocity accuracy, except for decreasing the signal-to-noise ratio. However, for bidirectional flow, very large errors in average velocity can result, even with no large decrease in signal-to-noise ratio.

P216

Investigation of Sensitivity of Slice-Selective Excitation to Flow

DP Lewis, BMW Tsui, PR Moran
Biomedical Engineering Department, University of North Carolina, Chapel Hill, NC

Purpose: We tested the hypothesis that RF pulses optimized for slice-selective excitation of stationary material may perform poorly for exciting flowing material and studied how the slice profile depends on the RF pulse, the gradient amplitude, and the velocity.

Methods: Several linear-phase, saturation, and inversion RF pulses were designed and simulation methods were used to calculate the corresponding slice profiles for plug and laminar flow at different velocities. Some of these RF pulses were implemented on our Philips Gyroscan system. Transverse slices of doped water flowing through a long straight tube in the z direction were excited and imaged in projection. Experimental profiles were compared with simulated profiles.

Results: For plug flow the slice profile can be significantly degraded by velocity when the RF pulse duration is long or when the RF pulse has several large lobes. Profiles from linear-phase RF pulses were relatively robust to flow. For saturation RF pulses, the leading slice edge remained sharp but the trailing edge did not, and there was ringing inside the slice. Inversion pulses failed to completely invert in-slice material when the bandwidth was low, but the performance improved with increasing bandwidth. Simulated slice profiles from the laminar flow model, derived from a spatial composite of plug flow with different velocities, agreed well with experimental profiles.

Conclusion: Velocity can adversely affect the slice profile, which may result in image artifacts and poor flow quantitation. The results of our study provide guidelines for designing slice-selective RF pulses for MR flow imaging.

P217

Optimization of Phase-Encode-Grouped Breath-Hold Cine MR Imaging of Myocardial Tag Lines

MS NessAiver
Picker International, Highland Heights, OH

Purpose: Five factors that can effect the quality of breath-hold cine MR imaging of myocardial tag lines are examined: (*a*) eddy currents, (*b*) RF sequence for producing the tag lines, (*c*) reduction in the acquisition matrix, (*d*) rotation of the tag lines, and (*e*) blurring due to motion between excitations within a phase-encode group (PEG).

Methods: Four different methods of moving through k space are examined. Eddy currents associated with each are measured by using a search coil. A spread sheet is used to model a spatial modulation of magnetization (SPAMM) RF sequence, and a nonlinear optimization routine is used to determine coefficients that improve tag line definition. The k-space representation of a 2D grid of tag lines is examined for the effects that reducing the acquisition matrix and rotation of the grid have on tag definition. The optimum matrix and rotation angles determined are then verified experimentally with a phantom.

Results: A symmetric, centrally ordered phase encode (SCOPEG) ordering was found to provide the best eddy current behavior. The SCOPEG ordering was also shown to reduce blurring due to motion between excitations. A 1:1.34:1.58:1.34:1 RF pulse sequence provides 28% sharper lines than a 1:4:6:4:1 binomial sequence. The optimum acquisition matrix is shown to be a function of the tag spacing and the degree of rotation.

Conclusion: Through careful modeling and examination of five factors, the quality of breath-hold cine imaging of myocardial tag lines can be significantly improved.

P218

Automatic Contours Recognition for Planimetric Quantification of Mitral and Tricuspid Regurgitations at Cine MRI

J Baruthio, S Zheng, JP Armspach, O Yu, F Wolff, P Germain, H Ohlenbusch, J Chambron
Faculté de Médécine, Institut de Physique Biologique, Strasbourg, France

Purpose: Gradient-echo cine MRI directly visualizes rapid and turbulent flows such as regurgitations. A precise quantification is achieved by planimetry of the signal loss jets in mitral (MR) and tricuspid (TR) regurgitations. Our first study concerns manual contour acquisition and shows that the most accurate quantification parameter is the mean surface area, which leads to a correlation of .84 with the reference explorations. Yet, manual contour acquisition is time consuming, since three to 10 contours must be acquired for each cine acquisition. In a second study, we developed a new and fast method for the automatic calculation of the severity grade; which automatically defines signal loss contours.

Methods: Our method consists of two main parts: dual segmentation and determination of guidance root. It is based on a six-step algorithm, as follows: (*a*) coarse segmentation; (*b*) extraction of the region of interest with a rough boundary; (*c*) research of a guidance root; (*d*) dual segmentation, which produces a binary region image by using the tissue-growing scheme that takes the above guidance root as a starting point; (*e*) connectivity labeling of the binary image, which displays an accurate boundary; the signal loss contours are found, and then the areas of the detected MR/TR regions are calculated; and (*f*) calculation of a new root for the next image, guided by the previous frame, and repetition of steps *d*–*f* for all the images.

Results: The quality of our algorithm has been tested through the correlation between manual and automatic acquisition ($r > .90$) and through the correlation between planimetry and the reference scores of severity ($.85 < r < .92$).

Conclusion: Our results show important improvements in comparison with manual outlining. A very high correlation is obtained between manual and automatic acquisition, and there is a better correlation between automatic planimetry and the reference methods than with manual processing. This important result proves the quality of our algorithm, and many clinical experiments have shown that this technique is fast and accurate and will be widely applied to other cardiac diseases.

P219

Coronary Artery Bypass Graft Imaging with MR Angiography

AJ Duerinckx, MK Urman, B Lewis
Radiology Service, Veterans Affairs Medical Center, West Los Angeles, Los Angeles, CA

Purpose: Noninvasive MR coronary angiography techniques

have recently become available. We evaluated the use of these techniques in the visualization of the native internal mammary arteries (IMAs) and coronary artery bypass grafts (CABGs).

Methods: Twelve patients with CABG surgery who underwent elective coronary angiography and had patent CABGs were studied. We also studied five normal volunteers. We evaluated a noninvasive MR coronary angiography technique that uses a fat-suppressed ECG-gated gradient-echo sequence with k-space segmentation on a 1.5-T imager (Magnetom SP, Siemens). Images were acquired during a single breath hold with the patient lying prone on a surface coil. Double oblique planes along the course of the bypass grafts and native IMAs were used.

Results: We were able to visualize the native IMAs in all volunteers. The origin on the native IMAs was not always clearly shown. We were able to follow long portions of the bypass grafts, excluding areas with surgical clips.

Conclusion: Noninvasive MR coronary angiography can help in the evaluation of CABG patency.

P220

Optimal Imaging Planes for Coronary MR Angiography

AJ Duerinckx, MK Urman, DJ Atkinson, OP Simonetti, U Sinha

Radiology Service, Veterans Affairs Medical Center, West Los Angeles, Los Angeles, CA

Purpose: Noninvasive 2D coronary MR angiography techniques have recently become available. We evaluated several approaches to 2D image plane selection for these techniques.

Methods: Ten normal volunteers were studied with a noninvasive coronary MR angiography technique that uses a fat-suppressed ECG-gated gradient-echo sequence with k-space segmentation on a 1.5-T imager (Magnetom SP, Siemens). The right coronary artery (RCA) system was imaged by using an iterative approach (using one image to find the location of the RCA for the next image) and an anatomic approach (using the atrioventricular groove on a two-chamber view to locate the RCA). The proximal left coronary artery system was visualized by using transaxial imaging planes (the traditional approach) and double oblique imaging planes tangential to the cardiac chamber along the interventricular groove.

Results: The anatomic approach to the localization of the RCA offered faster visualization of the first 7 cm of the RCA. Transaxial images of the left coronary system showed many signal void artifacts with blurred vessel boundaries due to the oblique section through the vessels. The double oblique tangential images were of superior quality and allowed (although at a cost of increased scanning time) us to visualize much longer portions of the left anterior descending coronary artery.

Conclusion: Noninvasive MR coronary angiography appears very promising but has certain limitations. Improvements in the selection of imaging planes will significantly improve the speed and quality of image acquisition.

D.J. Atkinson and O.P. Simonetti are employees of Siemens Medical Systems.

Wednesday, March 9, 12:15 PM–1:00 PM
Artifacts/Instrumentation/Safety/Pulse Sequences

Posters P301–P318

P301

Quantum and Digitizing Noise Sources in MR Imaging

JH Xiong, RF Williams, JL Lancaster, JH Gao, PT Fox

Research Imaging Center, University of Texas Health Sciences Center, San Antonio, TX

Purpose: Thermal noise, arising from the black body emission of the object and from random electron motion in the MR probe, is commonly considered as the predominant noise source in MR imaging. Our studies suggest there are two other important noise sources: quantum and digitizing noise. Quantum noise arises from fluctuation in the number of quanta emitted per unit time. Digitizing noise is due to analog-to-digital converter (ADC) changes with signal frequency, and depends on the "effective bits" of ADC.

Methods: Experiments were performed with a Bruker/General Electric CSI-II 2.0-T 45-cm-bore MR instrument with a uniform phantom consisting of a 25 × 60-mm vial filled with Cu_2SO_4 solution. The effect of digitizing noise was evaluated by changing the system gain setting and keeping all other parameters constant, and quantum noise was evaluated by changing the echo time and slice thickness independently.

Results: A typical experimental setup used a slice thickness of 10 mm and a receiver gain of 10 with a 12-bit ADC. Digitizing noise decreased the SNR by 3.7 times when the gain was changed from 20 to 5, and quantum noise decreased the SNR by 37%. The relative contribution of these noise sources to the total noise was estimated by a fit of the experimental data. The ratio of thermal noise to quantum noise to digitizing noise is 1:1.15:1.22.

Conclusion: Our results indicate that both quantum and digitizing noise can be significant noise sources, especially for imaging with a strong signal. The SNR for quantum noise alone is shown to be proportional to the one-fourth power of the number of received quanta.

P302

Removal of Noise from MR Images

SJ Garnier, GL Bilbro, WE Snyder, JW Gault

Department of Radiology, Bowman Gray School of Medicine, Winston-Salem, NC

Purpose: This purpose of this project is to develop a method for removing noise from MRI images, while preserving resolution and sharpness of edges.

Methods: We introduce a novel technique for MRI restoration, using a mathematical model of the image generation process. We determine a set of three basis images (proton density and nuclear relaxation times) from the MRI data with a nonlinear optimization method and use those images to obtain excellent restoration of the original image. The optimization method not only inverts the physical model but takes into account local smoothness in such a way that noise is removed, with edges preserved. MR images depend nonlinearly on proton density (PD), T1 and T2, and TE and TR. We model images as Markov random fields and introduce a maximum a posteriori restoration method, based on nonlinear optimization, which reduces noise while preserving resolution.

Results: We acquired several sets of three images each with a GE Signa 5.2 scanner with a 1.5-T magnet. Using the spin-echo mode, we acquired one T1-weighted study and one PD/T2-weighted multiecho study for a total of three images per set. A variety of different TE and TR values were used for various brain images, with varying slice thickness and interslice spacing. As expected, the thin-slice images possess more noise, and that noise is removed from the image very effectively. As a side effect of the algorithm, the actual values of T1, T2, and PD are derived and may be used to simulate other TE and TR parameter settings.

Conclusion: Although demonstrated with readily available spin-echo images, the method is readily adaptable to other MRI imaging modes by simply changing the form of the physical relation equation. When used in the spin-echo application the method suffers from the requirement that the patient must remain motionless between the two studies that use dissimilar TR values. It may be argued that on conventional spin-echo images, noiselike artifacts arise primarily from metabolic motion and are not (for the most part) from true random noise. However, on EPI images, acquisition times are so short that motion artifacts are significantly reduced and to some extent replaced by random noise (with which this algorithm performs best). In EPI imaging with an MTC prepara-

tory pulse, the formation equation has a form similar to that of the spin equation, and this method should be applicable to removing noise from such images. Investigations are under way.

P303

Increasing Stereotaxic Accuracy with High-Readout-Gradient Sequences

JA Bertolina, D Prasad, JC Goble, WS Cail, TA Spraggins, NF Kassell, L Steiner
Department of Neurosurgery, University of Virginia, Charlottesville, VA

Purpose: MRI is commonly used for stereotaxic surgical planning. Its superb soft-tissue differentiation makes it well suited for this task. However, MRI suffers from geometric distortion. This is of special concern for radiation-dose planning, where spatial accuracy is essential. Methods have been discussed to minimize distortions from field inhomogeneities (1–3). These require prewarping of the main field or multiple acquisitions followed by postprocessing. Since these are clinically inconvenient, we decided to investigate if the errors can be sufficiently reduced by simply increasing the readout gradient (4).

Methods: We use a readout gradient reversal method described previously (4) to determine the inhomogeneity-induced error. We acquire images of the fiducial box alone and the fiducial box and patient. We vary the readout gradient by keeping the FOV and bandwidth constant while changing the image matrix in the readout direction. All imaging is done with a standard Siemens 1.5-T imager with a 10 mT/m gradient limit.

Results: We show that for a readout gradient of 1.5 mT/m the fiducial markers as well as many regions of the brain are substantially distorted (by as much as 6 mm). We then show experimental verification of the inverse relationship between geometric error and readout gradient strength. At 7 mT/m, the 6-mm distortions have been reduced to approximately 1 mm.

Conclusion: Geometric distortions from field inhomogeneities can be minimized or effectively eliminated by increasing the readout gradient strength. This requires no pre- or post-processing. Acquisition time may need to be increased to compensate for SNR loss.

1. Schneider E, Glover G. MRM 18:335–347 (1991). 2. Mackenzie IS, Robinson EM, Wells AN, et al. MRM 5:262–268 (1987). 3. Fitzpatrick JM, Chang H, Willcott MR, Price RR. In Book of Abstracts: Ninth Annual Meeting of the Society of Magnetic Resonance in Medicine. Page 426 (1990). 4. Bakker CJG, Moerland MA, Bhagwandien R, Beersma R. MRI 10:597–608 (1992).

P304

Inner-Volume High-Resolution MR Imaging: A Simple Solution for Wraparound Problems

R Chandra, V Venkataraman
New York University Medical Center, New York, NY

Purpose: In MRI, whenever the field of view (FOV) is smaller than the length of an object in the phase-encode direction, the part of the object outside the field of view wraps around in the image. If one obtains a high-resolution image of a small volume inside a large object by decreasing the FOV, wraparound artifacts overlap the area of interest. One solution is to keep the FOV the same but increase the number of phase-encode steps. This, however, increases the time of study. Another method requires both hardware and software modifications.

Methods: The present method can produce high-resolution images of inner volumes without the wraparound effect and without the disadvantages of other methods. It depends on the use of small magnetic dipoles placed on the surface of an object to obliterate the signal from the outer volumes. The extent of loss of signal is controlled by the strength of the dipoles and their distance from the volume in which signal is to be destroyed. Images of a cylindric phantom and brain of a volunteer in a head coil were obtained at 1.5 T with and without the dipoles at FOVs of 200 and 120 mm.

Results: The small-FOV (high-resolution) images of the phantom as well as of the brain obtained with dipoles clearly showed areas without the presence of wraparound effect, compared with images taken without the dipoles.

Conclusion: We conclude that the present method works and that its clinical potential should be investigated.

P305

Finite Element Analysis and Field Measurements with Bird-Cage Coils

CC Guclu, G Kashmar, A Hacinliyan, O Nalcioglu
Division of Physics and Engineering, Department of Radiological Sciences, University of California, Irvine, CA

Purpose: Hayes et al have developed a high-quality RF coil referred to as a bird-cage coil. This type of coil is highly regarded for its high field homogeneity and SNR. To investigate detailed characteristics of these coils, we built one and mapped out its field. A model of the coil was designed and studied by means of finite element analysis.

Methods: A 10-cm-diameter eight-segment low-pass bird-cage coil with a 25-cm diameter shield was tested with a 13-mm magnetic field probe. Later, simulations were performed with a MacNeal-Schwendler EMAS electromagnetic finite element analysis software package. In the simulation studies, magnitude and direction of the field were displayed with arrows. This was done for both an empty coil and a coil containing a cylinder whose electromagnetic properties were that of human tissue. Because of our interest in coils for both 64-MHz (1.5-T) and 210-MHz (5-T) scanners, simulations were done at both frequencies and compared.

Results: Measurements and simulations with empty coils indicate that the magnetic field is very homogeneous in the center of the coil and inhomogeneity increases near the wires of the coil. In the simulation, it was further observed that when a human tissue cylinder was introduced into the coil, the homogeneity deteriorated and inhomogeneity was greater at the higher frequency.

Conclusion: It is concluded that the homogeneity measured with empty coils may not be representative of actual imaging conditions. Furthermore, the frequency dependence of the inhomogeneity seems reminiscent of far field reflection, and as the wavelength decreases at high frequency, the homogeneity becomes worse. As a next step, the effect of eddy currents in the sample will be investigated.

P306

MR Imaging of the Temporal Lobes with Phased-Array Temporal Lobe Coils at 1.5 T

RJ Peters, C Hayes, JS Tsuruda, C Yuan, M Mathis, V Terry
University of Washington Medical Center, Kirkwood, WA

Purpose: To illustrate new techniques used with MRI for optimizing high-resolution imaging of the hippocampus in temporal lobe epilepsy. MRI is rapidly becoming the imaging modality of choice for verification of a structural abnormality within the hippocampus prior to temporal lobe surgery.

Methods: All studies were performed with a GE 1.5-T Signa scanner. Special phased-array coils optimized for visualization of the medial temporal lobes were designed and built at our institution. The bilateral phased-array coils were positioned slightly anterior to each ear. A vacuum-assisted holder and Velcro fasteners were used to rigidly immobilize the head. Sagittal T1-weighted imaging (600 TR/10 TE) was used as a localizer for verification of hippocampal orientation. Oblique coronal T2-weighted fast spin-echo images were obtained perpendicular to the hippocampus/temporal horn (4,000 TR/102 TE/2 NEX/8 ETL/90° flip, 512 × 512 matrix, 16 FOV, 4-mm slice thickness with no gap, and approximately 15 slices). Other options included peripheral gating, fast scanning, graphic prescription, and no spatial presaturation. A coronal volume SPGR sequence was performed through the entire brain (23 TR/9 TE/1 NEX/45° flip angle, 256 × 256 matrix, 18 FOV, 1.2-mm slice thickness, and 124 slices). Graphic prescription, extended dynamic range, spatial presaturation in the inferior direction, and the frequency located in the S/I direction were selected.

Results: Compared with the quadrature drive head coil, phased-array MRI yields detailed depiction of both normal and abnormal anatomy of the hippocampus due to the improved SNR. With use of a coronal oblique angle, the intricate structures within the hippocampal and parahippocampal structures are visible. To date, 60 patients with suspected regional temporal sclerosis were studied with the dual phased-array coils. Twenty-one patients underwent hippocampalectomy with good correlation between pathologic and imaging results.

Conclusion: MR imaging with temporal phased-array coils can improve SNR within the hippocampal region, thus allowing increased resolution and detection of mesial temporal sclerosis. Proper technique, such as the orientation of the coronal sections, coil positioning, patient immobilization, and sufficient contrast weighting, is required for successful imaging.

P307

Numerical Simulation of Eddy Current Fields

J Ling, H Liu
Picker International, Highland Heights, OH

Purpose: To investigate by means of numerical simulation the characteristics of eddy current fields induced by magnetic gradients in a typical MR imaging system.

Methods: A general superconducting MRI system was modeled as a set of finite-length good-conductor cylinders and three finite-length gradient coil cylinders for the purpose of this study. The gradient pulse used in the simulation was a step waveform for transient study and sinusoidal for harmonic analysis (frequency response). The resulting spatially and temporally resolved eddy current field data and the frequency response were obtained with a commercial FEA software package, ANSYS. All numerical simulations were performed on an HP Apollo 700 workstation. The eddy current field data were in turn decomposed into their various spherical harmonic components.

Results: The numerical model was validated by an analytical solution for simple geometry. The eddy current fields were obtained for more realistic x, y, and z gradient pulses, respectively. The spherical harmonical decomposition and exponential decay expansion of the numerical results reveal the spatial and temporal characteristics of an eddy current field. The influence of positions of good conductors on the eddy current field was investigated, as well as their conductivity and the shapes of the input gradient pulses.

Conclusion: The induced eddy current field always has a dominant component similar in shape to the driving field but opposite in polarity in the vicinity of magnet isocenter. The information about eddy current field obtained in this study can be used as a priori information for various eddy current correction techniques.

P308

Single or Simultaneous Multiple-Slice FLASH MRI with Hard Pulse Excitations: New Developments

S Singh, R Deslauriers
Institute for Biodiagnostics, National Research Council of Canada, Winnipeg, Manitoba

Purpose: To develop a single-slice or simultaneous multiple-slice imaging method that uses hard pulse excitations with the shortest possible echo time for applications in imaging short T2/T2* species, cardiac and flow imaging, and MR angiography.

Methods: Single and multiple spatial-spectral slices of interest (SOIs) were defined in the presence of T1 variation and chemical shift with use of a spatial-spectral pulse (SMRM 1993, p 1245). Projection presaturation (PP) was applied during the null time to presaturate the volume outside an ROI of desired shape in the SOI(s) in order to suppress any flow and motion artifacts propagating into the ROI. A hard pulse excites the SOI magnetization. FLASH imaging gradients were used to acquire the 2DFT k-space data. For imaging multiple SOIs, an additional read gradient (ARG) was applied along the slice-select direction to prevent slice overlap in the image space.

Results: The method was implemented on 3-T, 1-m-bore and 4.7-T, 40-cm-bore magnets. Single-slice imaging of a kiwi fruit was performed. The image quality compared well with that obtained with the slice-selective excitation; in fact, the SNR was better because of the shorter TE. Multislice imaging using two as well as three slices was performed in a phantom and a kiwi fruit. For a wide interslice gap and relatively weak ARG, the image quality was good. With PP, the gap was reduced while the ROIs (round and oval shapes) were still separated in the individual slices. Use of a stronger ARG to further reduce the gap degraded the slice-image quality.

Conclusion: Single-slice as well as simultaneous multiple-slice imaging with hard pulse excitations was successful. Pre- and post-processing of data may be required to improve image quality when a strong ARG is used. This is currently under investigation.

P309

Temperature Effects on F-19 Relaxation Rates in Perflubron

Q Guo, RF Mattrey
Department of Radiology, University of California, San Diego, CA

Purpose: We have explored the possibility of using the F-19 1/T2 of CF_3 in $C_8F_{17}Br$ to determine Po_2 (1). The purpose of this study was to determine the effect of temperature on the T1 and T2 of CF_3 and CF_2Br in perflubron.

Methods: The TTISS scan sequence (1) was used interleaved to measure the T1 and T2 of F-19. Neat perflubron was saturated with pure nitrogen, room air, or pure oxygen and sealed in glass tubes. A thermos chamber was designed to control the cool-down from 45°C to 30°C within 3 hours, during which the TTISS sequence was performed four times. T1 and T2 were measured twice at each temperature, and the latter was measured three times (at 0, 1.5, and 3 hours). A nonlinear least-squares fit was used to calculate T1, T2, and temperature. All of the experiments in this study were performed on a GE 1.5-T Signa system.

Results and Conclusion: The relationship between 1/T1, 1/T2, and Po_2 from 40°C to 30°C had the following linear correlations: for CF_2Br, $1/T1 = 0.183 - 0.00164*T + 0.00332*P - 0.0000185*T*P$; for CF_3, $1/T1 = 0.181 - 0.00163*T + 0.00346*P - 0.0000193*T*P$; for CF_2Br, $1/T2 = 2.83 - 0.0242*T + 0.0126*P - 0.0000420*T*P$; and for CF_3, $1/T2 = 1.61 - 0.0125*T + 0.00994*P - 0.0000268*T*P$, where T is temperature (°C) and P is pressure (torr). Note that 1/T2 is more sensitive than 1/T1 for both T and P. From the preliminary data, the effects of a temperature change of 1°C at 37°C and 40 torr cause a Po_2 measurement error of 2% when T1 is used and 4% and 6% when the T2s of CF_3 and CF_2Br are used, respectively.

1. Guo Q., Mattrey R.F., Guclu C., Buxton R.B., Nalcioglu, O., 12th SMRM Meeting. 739, 1993.

Supported by Alliance Pharmaceutical Corporation.

P310

Development and Evaluation of an Automatic Linear Shim Technique in Combination with Spectral Presaturation at 0.5 T

AJ Elevelt, P van der Meulem, AJ dem Boef
Philips Medical Systems, Best, The Netherlands

Purpose: The purpose of this study is to develop a fast and volume-selective linear shimming routine, to be able to successfully use spectral presaturation as a fat-suppression technique at 0.5 T.

Methods: Our shim algorithm comprises a gradient-echo sequence. The echo is refocused by two 180° pulses, which are slice selective in the two other orthogonal directions, resulting in a three-dimensionally spatially resolved signal. The position of the top of the echo signal is a linear function of the inhomogeneity in the direction of the applied readout gradient. This sequence is repeated in three directions, after which

the optimal linear shim values can be determined. The total shimming procedure takes only 5 seconds to perform. Owing to improved homogeneity, a spectral presaturation pulse (sinc-gauss, three side lobes, bandwidth = 200 Hz, 30-Hz separation between complete and no saturation) with a total length of 30 ms resulted in excellent fat suppression at 0.5 T.

Results: The application of this shim algorithm in phantom studies resulted in typical line widths of the water spectrum of 20 Hz over a field of view of 350 mm. In patients, typical line widths of 30 Hz are found. Therefore, good fat suppression can be performed in different parts of the body, such as the abdomen, head, breasts, and extremities.

Conclusion: The clinical use of spectral presaturation is effectively improved by the development of a new shimming technique. This study illustrates a balanced compromise between relatively short prepulses and slightly increased TR values, which results in higher sensitivity to otherwise inconspicuous lesions.

A.J. Elevelt is an employee of Philips Medical Systems.

P311

Liver Metastases: Appearance with Delayed Gadolinium Enhancement

TH Pels Rijcken, A Davidoff, DA Davidson, J Colby, J Mukai, SA Alonso, DD Stark

Department of Radiology, University of Massachusetts Medical Center, Worcester, MA

Purpose: We studied 26 patients with known metastases to the liver to determine the morphologic pattern of gadolinium distribution on delayed images at 1.5 T.

Methods: Characterization of the lesions was performed with use of all available sequences (T1, T2, T2 FSE, dynamic gadolinium, and delayed T1 postgadolinium) and with standard ROI measurements (SNR, CNR). Delayed spin-echo T1-weighted images were obtained 15 minutes after gadolinium administration. These images were compared with the noncontrast T1-weighted images for exact parameters and locations.

Results: Eighteen of 26 patients (69%) showed delayed enhancement, with a variety of morphologic patterns. A minority of these lesions showed diffuse, almost homogeneous enhancement, simulating the pattern of hemangiomas. The morphologic patterns of delayed enhancement, their possible pathogenesis, and their distinction from hemangiomas will be elucidated.

P312

New Adventures in Spin Space: Exploring the Benefits of Phase Modulation

JB Murdoch

Picker International, Highland Heights, OH

Purpose: Beginning with the hyperbolic secant inversion pulse, phase-modulated (PM) RF waveforms have been investigated primarily as highly B_1-insensitive *adiabatic* pulses. However, with standard imaging transmit coils, only a modest degree of stability with respect to B_1 inhomogeneity is required. In this less stringent regimen, we have compared PM pulses with their purely amplitude-modulated (AM) brethren in terms of various pulse performance criteria: peak RF amplitude, integrated power, response profile quality, and so forth. PM pulses possess an extra degree of freedom: in general, magnetization response profiles M_x, M_y, and M_z are not symmetric or antisymmetric with respect to offset frequency unless we force them to be. Hence, PM pulses are often better suited for those applications—notably fat or water suppression—for which response profiles need only be constrained at positive (or negative) offset frequencies. With one-sided constraint, the transition zone between "in slice" and "out of slice" can be reduced.

Methods: A conjugate gradient minimization algorithm (or variants thereof) was used to iteratively generate a veritable cornucopia of optimized PM pulse shapes.

Results: PM pulses have been created for a variety of imaging and spectroscopic uses: fat suppression, water suppression (CHESS), out-of-slice saturation, self-refocused and "prefocused" excitation, and rapid selective excitation, as well as "matched sets" for spin-echo excitation and refocusing.

Conclusion: Phase modulation—it's not just for B_1 insensitivity anymore. Additional advantages include reduced peak amplitude and sharper selectivity, particularly when only one transition zone must be controlled.

J.B. Murdoch is an employee of Picker International.

P313

Study of Resolution Limits in MR Microscopy

WC Chu

Institute of Biomedical Engineering, National Yang Ming Medical College, Taipei, Taiwan

Purpose: To study the joint effects of resolution-limiting factors, diffusion, coil vibration, and field gradient strength, as well as to determine the ultimate achievable resolution in MR micrsocopy.

Methods: Diffusion motion–related resolution degradation is evaluated by using Monte Carlo simulation based on the random-walk model. Coil vibrational motion-induced resolution degradation is evaluated by using the finite element method (FEM). The degree of image blurring and the ultimate achievable resolution is determined from the concept of point spread functions (PSF).

Results: Monte Carlo simulation shows that when the sample diffusion coefficient is 2.0×10^{-5} cm^2/s, 2-μm image resolution cannot be attained if the gradient strength is below 230 G/cm. When a larger sample diffusion coefficient or higher image resolution is considered, a larger gradient is also needed. This large gradient produces large coil frame deformation and vibrational motion. The FEM study shows that with an acrylic coil frame, a gradient that generates a 2-μm-resolution image may result in a 1–5-pixel PSF degradation, depending on the thickness and the material.

Conclusion: Diffusion-related phase distortion can be reduced by fast A/D sampling and by employing larger field gradients (a result of fast sampling to preserve the Nyquist relationship). However, a large gradient produces large coil vibrational motion, which in turn causes image blurring. To obtain a higher-resolution microscopic MR image, it is important to suppress image degradation effects to their minimum.

P314

Alternative Efficient Phased-Array Image Combination Technique

H Liu

Picker International, Highland Heights, OH

Purpose: To investigate an alternative, more efficient MR phased-array image combination technique for achieving an optimal signal-to-noise ratio.

Methods: CTL phased-array images from multiple receiver channels obtained with a Picker Edge MRI system (1.5 T) are combined in a new fashion. This new image combination technique first generates two complex images for each receiver channel; one is a regular 2D Fourier transformation of the acquired raw data, and the other is a smoothed version of the previous one. Then the composite pixel intensity is determined with the following expression:

$$\sqrt{\left|\sum_{i=1}^{C} I_i S_i^*\right|}.$$

In the above equation, I_i is the pixel intensity value of a complex image from the ith receiver channel, C is the number of channels, S_i is the intensity of its smoothed version, and * is a complex conjugate operation. The required image smoothing was performed in the raw data domain with a low-pass filter. The resulting composite image is compared with its standard sum-of-squares counterpart.

Results: The resulting composite image shows an improved S/N over simple sum-of-squares images, especially in some high-noise-level regions. Noise signal is

combined less favorably in this technique, as expected. The S/N improvement was found to be as high as 30% at various locations on an image. Phantom as well as in vivo images are shown and compared with sum-of-squares images.

Conclusion: This image combination technique yields enhanced S/N and has roughly the same computational intensity as the simple sum-of-squares method. No coil reception field map is required in the processing.

1. Roemer, et. al. Magn. Reson. Med. 16, 192–225 (1990). 2. D. Molyneaux and H. Liu, SMRM 93 annual meeting, New York, 307.

P315

Segmentation and Volume Measurements with Thresholds in an Optimal Feature-Space Projection

EH Baker, JA Sorenson
University of Wisconsin, Madison, WI

Purpose: Volume calculations by vector decomposition suffer when there is poor separation of the prototype vectors in feature space and when tissues not represented by prototype vectors are present in the image. Our method maximizes the separation of prototype vectors by projecting a three-dimensional feature space into an optimal two-dimensional feature space and excludes voxels of contaminating tissues based on calculated fractional volumes.

Methods: Registered FSE brain scans were acquired in eight normal volunteers: a two-echo sequence for density- and T2-weighted images, and a single-echo sequence for T1-weighted images. A binary mask describing the contents of the cranium was found by gray-level tracking, and a 3D feature space was generated from its contents. The centroid vector and covariance matrix of the distribution derived from a hand-drawn pure-tissue mask were used to describe each tissue prototype. The centroids of three tissues of interest (eg, white matter, gray matter, and CSF) define a projection plane for 3D feature space. This optimizes the separation between tissues in the resulting 2D feature space. Vector decomposition can assign voxels nonphysical fractional volumes (ie, $f < 0$ or $f > 1$). Noise causes moderately nonphysical values, but unwanted tissues that remain after the masking operation (eg, meninges and blood vessels) give extreme values. Therefore, in calculating the total volume occupied by a tissue of interest, we set upper and lower bounds on the included fractional volumes that kept noise but excluded contaminants.

Results: Projection greatly improves the stability of volume calculations. Comparing 2D projections to density-T2 feature spaces, gray and white matter volumes were affected by the amount of CSF included within the binary mask much more in the latter case than in the former. For $n = 8$, the average range was 50 cm^3 when a projected feature space was used and 214 cm^3 when a density-T2 feature space was used. Exclusion of voxels having grossly nonphysical fractional volumes also improved the calculations.

Conclusion: Volumes of brain tissues calculated from MR images can be improved by using an optimal feature space projection and by placing bounds on the fractional volumes included in the calculation. In principle, this method can be extended to feature spaces of higher dimensions.

P316

Signal-to-Noise Ratio Improvement in High-Resolution Images Of the Inner Ear Obtained with Random-Pattern Complex Singular Value Decomposition

S Kurucay, B Clymer, P Schmalbrock
Department of Radiology, Ohio State University, Columbus, OH

Purpose: Poor signal-to-noise ratio (SNR) is the major limitation in high-resolution imaging. Random-pattern complex singular value decomposition (RPCSVD) was previously proposed as a noise filtration method (Nekolla, SMRM 1992, 480). The purpose of this study was to evaluate whether RPCSVD can yield improved SNR while preserving small anatomic details in high-resolution inner-ear images.

Methods: The raw data of 2D gradient-echo images of the inner ear were transferred to a workstation (HP9000/715) equipped with MATLAB software. Modifications of the previously proposed RPCSVD technique were necessary to prevent image artifacts; the origin of k space was not covered with the random matrices to eliminate rectangular structured artifacts, and the matrices were selected symmetric with respect to the center of k space to preserve the Hermitian symmetry of the raw data. Since the SNR is low, the recently introduced unbiased method (McGibney, Med Phys 20, 1993, 1077) rather than a more standard method was used to determine SNRs in the original and processed images.

Results: Improvements in SNR by a factor of up to 2.4 were obtained, while small anatomic details were maintained, such as the vestibulocochlear nerve complex within the internal auditory canal. The computation time was 2.7 hours for a 256×256 image matrix.

Conclusion: RPCSVD is a promising method for noise reduction in high-resolution MRI. The method is suitable for parallel processing, which could reduce the computation times to minutes. Further studies are needed to assess how RPCSVD can be used for fractional echoes or excitations and for 3D imaging.

P317

Visualizing Flow Patterns in the Ascending Aorta with Streamlines

MH Buonocore
Department of Radiology, University of California, Davis, Medical Center, Sacramento, CA

Purpose: To display streamlines of flow in the ascending aorta and show the convergence of streamlines into the left and right coronary arteries.

Methods: Velocity-encoded phase contrast cine imaging is used to acquire 2D coronal images at different A/P levels showing the heart, aortic valve, ascending aorta, aortic arch, and vessel branches. Streamlines are calculated from these time-resolved data by using first-order forward or backward integration of the velocity field. A movie loop of amplitude images at a single A/P level is displayed on the screen. Streamlines are superimposed on these images. Streamline segments within the slice during the displayed time frame are shown in red. Streamline segments move forward as subsequent frames are displayed. The movement appears smooth. Optionally, streamline segments in the contiguous anterior slice are shown in a different color, and segments in the contiguous posterior slice shown in a third color. Starting spots are positioned by clicking on the amplitude image and typing in a spot radius.

Results: Rapid systolic flow through the ascending aorta into the brachiocephalic and left common carotid artery is easily visualized. Diastolic recirculating flows in the ascending aorta, left ventricle, and above the aortic valves are usually visualized. By backward integrating from a small spot in the left coronary artery, streamlines flowing into the artery are found.

Conclusion: Streamlines facilitate the interpretation of time-resolved 3D velocity data.

P318

Registration of Functional MR Images with Use of the Principle-Axis Transformation

BJ Mock, DP Russell, JA Sorenson
University of Wisconsin, Madison, WI

Purpose: Subject motion during functional MR imaging (FMRI) studies of the human brain can seriously limit the usefulness of the data collected and lead to incorrect results (1). We have implemented and evaluated a two-dimensional registration algorithm based on the principle-axis transformation to reorient functional brain images (2).

Methods: Derived from classical rigid-body mechanics, the principle-axis transformation uniquely identifies an object's

location and orientation on the basis of its centroid position and rotation about its centroid. Translational registration of two images is achieved by calculating the separation of the image centroids. Rotational registration is accomplished by diagonalizing the second-moment (inertia) matrices to determine the rotation angle between the two images. The algorithm was implemented on a Sun Workstation and subsequently tested on computer-generated phantom images, MR axial human brain images with simulated motion, and motion-plagued FMRI gradient-echo axial brain image sets (GE Signa 1.5-T system). Performance of the algorithm was evaluated by comparing subtraction images and by calculating the cross-correlation coefficient before and after registration.

Results: Registration of motion-corrupted images (as reflected in an increase in the cross-correlation coefficient) demonstrated the ability to recover FMRI signal in the activated motor cortex, where subject motion obscured the signal in the unregistered data.

Conclusion: The principle-axis transformation represents a simple, computationally efficient, and analytic method of image registration for FMRI scans plagued by gross in-plane subject motion.

1. Hajnal VJ, et al, SMRM Abstracts, p 166, 12th Annual Meeting, New York, 1993. 2. Alpert NM, Bradshaw JF, Kennedy D, Correia JA. J Nucl Med 1990;31:1717–1722.

Notes

Notes

Indices and Information

- **Technical Exhibits Floorplan**
- **Technical and Interactive Education Exhibits Roster**
- **1994 Corporate Contributions and Acknowledgments**
- **Author Index**
- **SMR Membership Application**
- **SMRT Membership Application**

PLAN YOUR INDIVIDUAL ITINERARY

To help you plan your week at SMR, the Printed Program index lists all scientific plenary sessions, proffered papers and poster presentations. All papers are categorized by author with the abstract number of each symposium, paper, or exhibit found following the author name. The first eight co-authors per paper are listed individually.

The type of work is indicated by one of three abbreviations preceding the abstract number. An abbreviation key appears opposite the Author Index. All numbers listed in the index reference the paper number and not the page number on which the abstract may be found.

Please note that other pertinent information regarding the Technical Exhibits Program, SMR and SMRT membership information and Society Corporate Acknowledgments may also be found in this section.

EXHIBIT FLOOR PLAN

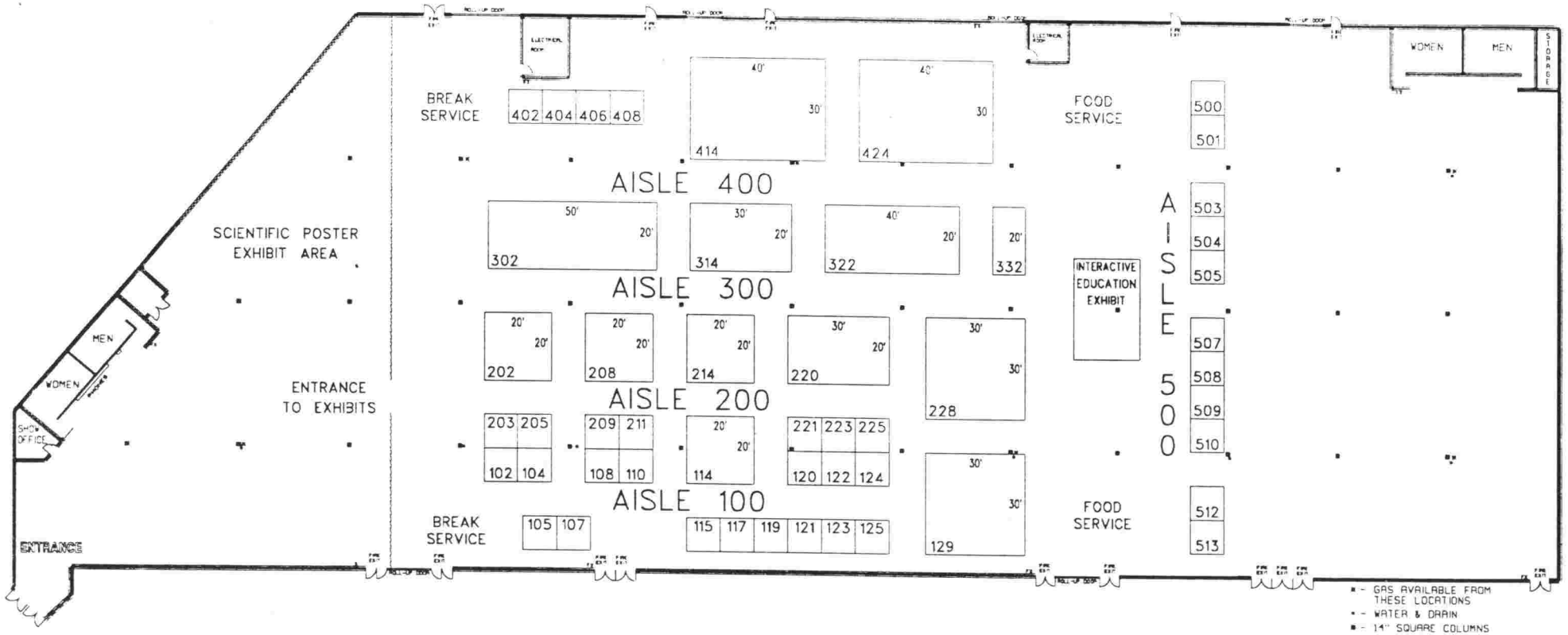

FIRST MEETING OF THE SMR
MARCH 5-9,1994
LOEWS ANATOLE-DALLAS
TRINITY EXHIBIT HALL

SMR 1994 Technical and Interactive Education Exhibitors

Alliance Pharmaceutical Corporation
3040 Science Park Road
San Diego, CA 92121
619/ 558-4300

American College of Radiology (ACR)
1891 Preston White Drive
Reston, VA 22091
703/ 648-8900

American Roentgen Ray Society (ARRS)
1891 Preston White Drive
Reston, VA 22091
703/ 648-8992

Analogic Corporation (Medical Division)
8 Centennial Drive
Peabody, MA 01960
508/ 977-3000

Applied Radiology
80 Shore Road
Port Washington, NY 11050
516/ 883-0164

Aries Systems Corporation
200 Sutton Street
North Andover, MA 01845
508/ 975-7570

Avotec
PO Box 1777
Jensen Beach, FL 34958
407/ 692-4405

Berlex Imaging
300 Fairfield Road
Wayne, NJ 07470
201/ 305-5082

Data Distributing Inc.
417-A Ingalls
Santa Cruz, CA 95060
408/ 457-3537

Diagnostic Imaging Magazine
600 Harrison Street
San Francisco, CA 94107
415/ 905-2200

Doty Scientific, Inc.
700 Clemson Road
Columbia, SC 29223
803/ 788-6497

Elscint, Inc.
505 Main Street
Hackensack, NJ 07601
201/ 342-2020

Elsevier Science Inc.
655 Avenue of the Americas
New York, NY 10010
212/ 989-5800

GE Medical Systems
P.O. Box 414 (W-439)
Milwaukee, WI 53201
414/ 548-2223

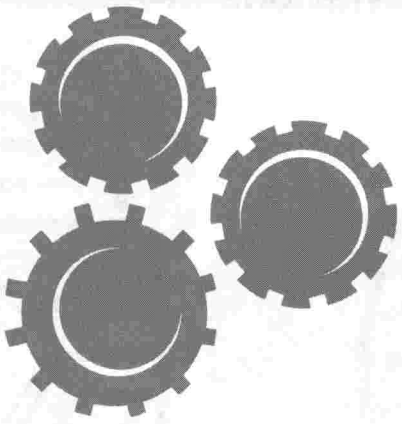

GMW Associates
629 Bair Island Road, #113
Redwood City, CA 94063
415/ 368-4884

Hitachi Medical Systems America, Inc.
1963 Case Parkway
Twinsburg, OH 44087
216/ 425-1313

Images-on-Call
10024 Monroe Drive
Dallas, TX 75229
214/ 902-8337

Journal of Magnetic Resonance Imaging (JMRI)
213 West Institute Place, Suite 501
Chicago, IL 60610
312/751-2590

Lunar Corporation
313 West Beltline Highway
Madison, WI 53713
608/ 274-2663

Magnetic Resonance in Medicine (MRM)
1918 University Avenue, Suite 3C
Berkeley, CA 94704
510/ 841-1899

Medical Advances, Inc.
10437 Innovation Drive
Milwaukee, WI 53226
317/ 258-3808

Medical Support Systems, Inc.
Two Central Square
Cambridge, MA 02139
617/ 868-7767

Medrad, Inc.
271 Kappa Drive
Pittsburgh, PA 15238
412/ 963-9700

Mosby-Churchill-Waverly
2408 Clublake Trail
McKinney, TX 75070
214/ 548-0016

Otsuka Electronics (USA) Inc.
2555 Midpoint Drive
Fort Collins, CO 80524
303/ 484-0428

Philips Medical Systems North America
710 Brideport Avenue
Shelton, CT 06484
203/ 926-7647

Picker International
595 Miner Road
Cleveland, OH 44143
216/ 473-3544

R Squared Scan Systems, Inc.
1611 Pomona Road
Corona, CA 91720
909/ 736-3700

Radiological Society of North America (RSNA)
2021 Spring Road, Suite 600
Oak Brook, IL 60521
708/ 571-2670

Raven Press
1185 Avenue of the Americas
New York, NY 10036
212/ 930-9500

Sanofi Winthrop Pharmaceuticals
90 Park Avenue
New York, NY 10016
212/ 907-3221

Scan Med of Medic, Inc.
P O Box 708
925 West 6th Street
Fremont, NE 68025
402/ 721-5800

Shimadzu Medical Systems
101 West Walnut Street
Gardena, CA 90248
800/ 228-1429

Siemens Medical Systems, Inc.
186 Wood Avenue South
Iselin, NJ 08830
908/ 321-4654

Society of Magnetic Resonance (SMR)/ Section for MR Technologists (SMRT)

Berkeley Office
1918 University Avenue, Suite 3C
Berkeley, CA 94704
510/ 841-1899

Chicago Office
213 West Institute Place, Suite 501
Chicago, IL 60610
312/ 751-2590

Squibb Diagnostics, Inc.
P.O. Box 4500
Princeton, NJ 08543-4500
609/ 897-3748

Toshiba America Medical Systems, Inc.
2441 Michelle Drive
Tustin, CA 92680
714/ 669-4118

Published based on information available December 17, 1993.

Key to Abbreviations in Author Index

A–award presentations

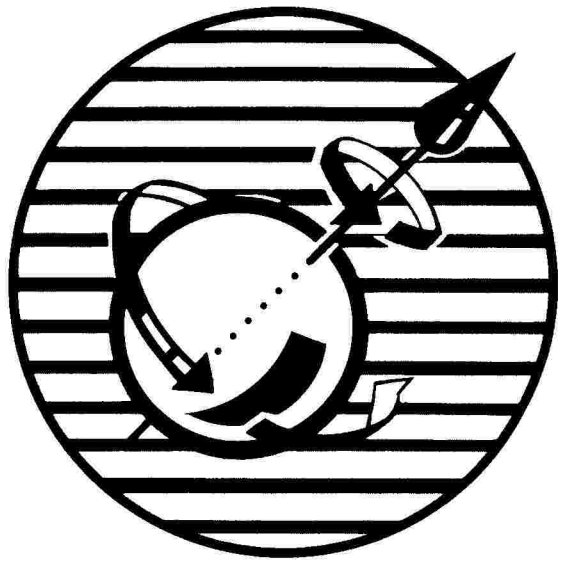

#–proffered papers

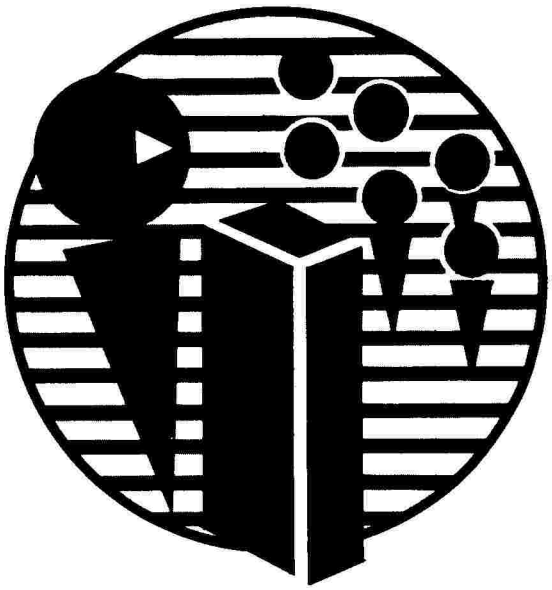

PS–plenary symposia

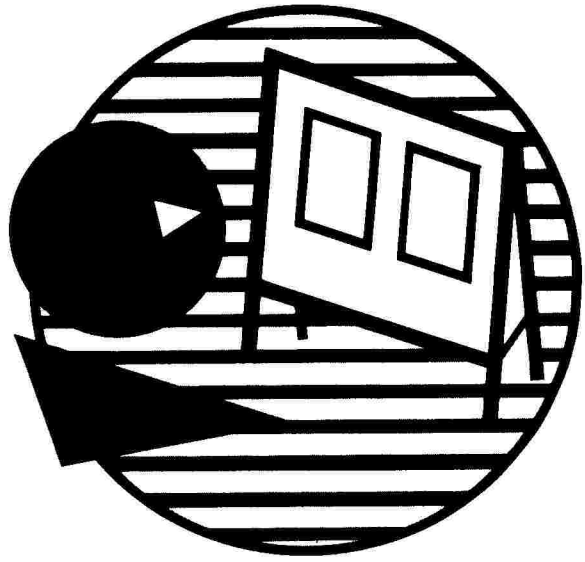

P–scientific poster presentations

Key to abbreviations:
A–award presentations
PS–plenary symposia
#–proffered papers
P–scientific poster presentations

E

F

G

M

N

O

P

Q

R

S

T

U

V

W

X

Y

Z

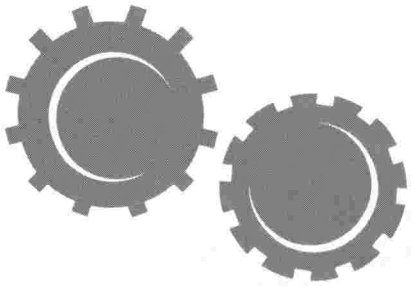

Program Objectives

Scientific Program

At the conclusion of this Program, participants should be able to:

- **identify** appropriate applications of MRI in a quality and cost sensitive environment;
- **evaluate** strategies for assessing MRI technology;
- **recognize** the potential impact of future MR system architectures on clinical practice;
- **comprehend** issues related to magnetic field strength in MRI;
- **recognize** current trends in the application of MRI for neurological, functional, musculoskeletal, cardiovascular, and breast imaging;

Scientific Program: Morning Tutorial

At the conclusion of this program, participants should be able to:

- **improve** their accuracy in clinical MRI interpretation;
- **develop** greater understanding of the basic physics and clinical interpretation of MRI.

Educational Program

At the conclusion of this program, participants should be able to:

- **understand** clinical MRI techniques and applications in multiple body parts, including brain, spine, abdomen/pelvis, musculoskeletal and breast imaging;
- **formulate** scanning strategies, for multiple anatomic locations, at multiple field strengths;
- **improve** their basic understanding of the technical basis of MRI, and how basic sequence parameters impact on image signal-to-noise, resolution and contrast;
- **appreciate** the uses of currently available contrast body agents in body and neurologic applications of MRI;
- **incorporate** new information on areas of most rapid development within MRI.

Educational Program: Economic Symposium

At the conclusion of this program, participants should be able to:

- evaluate and apply new developments in the acquisition, siting and operation of MRI and other imaging technologies.

FIRST MEETING OF THE SMR
C O M M E N T S

The meeting programming committees would appreciate receiving your comments regarding the First Meeting of the SMR in Dallas. Those comments will be collated and forwarded to the Annual Meeting and Education Coordination Council for possible incorporation in upcoming educational programming. While your comments may also be provided on the Evaluation/CME Accreditation Form distributed at each session, please let us know your thoughts regarding the following:

1. **Which Program did you attend?**_____

2. **Did it meet its stated objectives? Yes___No____Why?**_____

   _____

3. **What should have been included in the Program that was not?**

   _____

   _____

4. **What should have been excluded from the Program?**

   _____

   _____

5. **What Program revisions would you like to see implemented next year?**

   _____

   _____

6. **General Comments:**

   _____

   _____

Please return this form to the SMR Registration Area, Chantilly Foyer, Lobby Level of the Loews Anatole Hotel by Wednesday, March 9, or mail it to the SMR Central Office (Chicago location) at the following address:

Society of Magnetic Resonance, Chicago Office
213 West Institute Place, Suite 501
Chicago, Illinois 60610 USA

SOCIETY OF
SMR
MAGNETIC RESONANCE

Membership Information For Full or Student Members

The Society of Magnetic Resonance is a non-profit professional association formed in 1993 as a result of the merger between the Society of Magnetic Resonance in Medicine and the Society for Magnetic Resonance Imaging and is devoted to furthering the development and application of Magnetic Resonance techniques in medicine and biology. The Society holds annual scientific meetings and sponsors other major educational and scientific workshops.

MEMBERSHIP BENEFITS

- Choice of either of the official Society journals, *Magnetic Resonance in Medicine (MRM)* or *Journal of Magnetic Resonance Imaging (JMRI)* is included in the full membership dues. Full membership applicants may opt to select both journals, with dues adjusted to reflect the decision. Student membership applicants may opt to select neither, either or both Journals, with dues adjusted to reflect the decision. Subscriptions begin with the January issue of the year membership is effective.
- The Society newsletter, published three times annually.
- Advance notice and substantially reduced registration fees for the Annual Meeting and all Educational and Scientific Workshops organized by SMR.
- The Society Membership Directory, published annually.

MEMBERSHIP CALENDAR

Membership applications submitted and approved by September 30 are effective the calendar year of approval. Applications approved October 1 through December 31 are effective the next calendar year.

FUTURE SOCIETY MEETINGS

1994	March 5-9	(Dallas)
	August 6-12	(San Francisco)
1995	August 19-25	(Nice)
1996	Spring	(New York)
1997	April 10-19	(Vancouver)

DUES SCHEDULE

Dues remittance must accompany the membership application submission.

❒ Full Member (with one journal)	$125.00 USD
❒ Student Member (without journal)	$ 25.00
❒ Student Member (with one journal)	$ 40.00
❒ Second Journal	$ 55.00

Individuals may join both the SMR and the Section for Magnetic Resonance Technologists (SMRT). If you are interested in joining both Societies, please contact the Membership Coordinator at 510/841-1899 for information regarding dual membership benefits and application process.

DUES PAYMENT METHODS

❒ Checks: Accepted, must be payable "to" (not through) a U.S. Bank in U.S. Dollars and must be imprinted with the computer encoding and routing information authorized by the American Banking Association. Non-U.S. checks made payable in U.S. dollars to a U.S. bank, as above, are the only acceptable overseas checks.

❒ Travelers Checks: Accepted, if received in the exact amount and properly countersigned.

❒ International Money Order: Accepted, if in U.S. Dollars and imprinted with the computer encoding and routing information authorized by the American Banking Association.

❒ Credit Cards: Visa, MasterCard and Eurocard are accepted. To remit dues via credit card, please complete below:

❒ Visa ❒ MasterCard ❒ Eurocard

Card #: _____ Exp. Date: ____/____

Signature: _____ Amount: $ _____

Wire transfers are not accepted.

SOCIETY OF
SMR
MAGNETIC RESONANCE

Membership Application For Full or Student Members

For Office Use Only
ID#

❒ FULL MEMBER

An individual who is involved in Magnetic Resonance in medicine, biology or other related topics, research, education, manufacture or practice. Full members have the right to vote and hold office. The applicant must submit two copies of his/her curriculum vitae with, where possible, a list of peer-reviewed publications in the field of MR. Do not include abstracts or book chapters.

Sponsorship Requirements: Endorsement by one Full Member of the Society.

❒ STUDENT MEMBER

An individual enrolled full-time in an academic program that actively engages in the application of Magnetic Resonance in medicine and biology. The applicant must submit two copies of his/her abbreviated curriculum vitae and a brief statement on letterhead signed by a department head/advisor which describes the training program, type of degree, field of study and expected date of completion of the applicant. Eligibility for student membership must be confirmed annually.

Sponsorship Requirement: Endorsement by one Full Member of the Society.

Questions? Please contact SMR at:
Telephone: 510/841-1899
Facsimile: 510/841-2340

1 **Name,** please type or print legibly. All applications must be submitted in English.

(First, Middle, Last, Degree)

Title

Affiliation

2 **Address,** please provide preferred journal mailing address. Indicate if this is your
❒ home
❒ office
address.

Address

Address

City, State/Province Country Zip/Postal Code

Telephone Fax

Electronic Mail Address

3 **All Applicants,** please indicate professional affiliations (check as many as apply):

❒ AAN ❒ AAPM ❒ ACR ❒ ARRS
❒ ASNR ❒ ASRT ❒ ESMRMB ❒ JMRM
❒ RSNA ❒ SNM ❒ Other (_____)

4 **All Applicants,** please indicate professional classification:

❒ Basic Scientist ❒ Clinical Scientist
❒ Educator ❒ Industrial Management
❒ Professional Services Provider ❒ Radiology Support Personnel

5 **All Applicants,** please indicate your primary field of endeavor:

Basic Science
❒ Biochemistry ❒ Biophysics ❒ Chemistry
❒ Engineering ❒ Mathematics ❒ Physics
❒ Physiology ❒ Other _____

Clinical Science
❒ Cardiology ❒ Int. Medicine ❒ Neurology
❒ Psychology ❒ Radiology ❒ Surgery
❒ Other _____

6 **Applicants for Full Membership,** please indicate the year started and extent of your involvement with MR:

7 **All Applicants**, please select a journal: (See reverse side for details).

❒ JMRI
❒ MRM
❒ Both
❒ Neither (Student Only)

8 Please **confirm** completion of the required steps:

All Applicants:
❒ Completed application
❒ Signed Endorsement Form
❒ Membership dues
❒ Journal selection

Full Member Applicants:
❒ 2 copies of current cv
❒ List of MR-related publications

Student Applicants:
❒ 2 copies of abbreviated cv
❒ Letter of student certification

9 Please **forward** all necessary documents to:

Society of Magnetic Resonance, Inc.
Membership Coordinator
1918 University Avenue
Suite 3C
Berkeley, CA 94704 USA

10 **Applicant Signature:**

Signature

Date

SOCIETY OF

SMR

MAGNETIC RESONANCE

Endorsement Form

I endorse _____ for membership in the Society of Magnetic Resonance (SMR).

Sponsor Signature: _____

Sponsor Name: _____

Affiliation: _____

Date: _____

Comments: _____

_____

_____

Please return this completed form via facsimile or mail to the Society's membership office, listed below.

Thank you.

1918 University Avenue
Suite 3C
Berkeley, CA 94704, USA
Phone: 510/841-1899
Facsimile: 510/841-2340

COMBINED SECTION FOR MAGNETIC RESONANCE TECHNOLOGISTS
SMRT

Membership Application

The Society of Magnetic Resonance in Medicine, Inc., and the Society for Magnetic Resonance Imaging, Inc., non-profit professional associations, combined efforts in 1991 and formed the Section for Magnetic Resonance Technologists. SMRT is devoted to advancing the education, training and quality of Magnetic Resonance Technologists, to promoting world-wide communication of information in the field of Magnetic Resonance, and to establishing a forum for dissemination of this information.

Annual Meetings of SMRT

San Francisco (1991)
New York (1992)
New York (1993)

Membership Benefits

Technologist Membership in the Society of Magnetic Resonance in Medicine and the Society for Magnetic Resonance Imaging.

The journals, Magnetic Resonance in Medicine (published monthly) and/or Journal of Magnetic Resonance Imaging (published bimonthly) at a special SMRT member's rate. Subscriptions begin with the January issue for applications **completed** January 1 through September 30 and with the January issue of the following year for applications **completed** October 1 through December 31. Subscription to the journal(s) is optional.

SMRT Newsletter, *Signals*, (published biannually) will bring you the latest technical and educational news breakthroughs, as well as information on upcoming SMRT events.

SMRT Membership Directory, published annually.

Advance notice and substantially reduced registration fees for the Annual Meeting and SMRT workshops, as well as SMRM and SMRI meetings and workshops.

Membership Categories and Qualifications (please check one category).

Prior to final acceptance by the SMRT Policy Board, each application is reviewed by the Membership Committee for verification of eligibility.

[ ] Technologist (Voting) Member

In order to qualify as a voting member, you **must** be one of the following:

A. Certified by the American Registry of Radiologic Technologists
B. A Registered Diagnostic Medical Sonographer
C. A Certified Nuclear Medicine Technologist
D. Certified by an equivalent professional certifying organization;

and you **must** have practiced as a technologist in the field of magnetic resonance for a minimum of one year. The applicant **must** submit a completed SMRT application form and verification of the above. Sponsorship: Endorsement of two or more voting members of the SMRT, of the SMRM or of the SMRI;

OR

you **must** be able to demonstrate appropriate equivalent professional competence in radiologic practice or in work in support of biochemical, biophysical or biological programs, and you must have practiced as a magnetic resonance technologist for a minimum of two years. The applicant **must** submit a completed SMRT application form, and obtain the signature of their department head or administrator below. Sponsorship: Endorsement of two or more voting members of the SMRT, of the SMRM or of the SMRI.

I verify the above named applicant has at least two years' practice in an NMR modality.

_____
Department Head/Administrator Signature

[ ] Technologist (Non-Voting) Member:

An individual who shares the stated purposes of the SMRT, but does not meet the qualifications for voting membership. The applicant **must** submit a completed SMRT application form. Sponsorship: Endorsement of one or more voting members of the SMRT, of the SMRM or of the SMRI.

_____
Sponsor #1 Name (please print)

_____
Sponsor #1 Signature

_____
Sponsor #1 Society Affiliation

_____
Sponsor #2 Name (please print)

_____
Sponsor #2 Signature

_____
Sponsor #2 Society Affiliation

Rev. 6/93

I.D. # FOR OFFICE USE ONLY

Please mail the completed application **and** membership dues to:

SMRT
Combined Section for Magnetic Resonance Technologists

Membership Coordinator
1918 University Avenue
Suite 3C
Berkeley, CA 94704 U.S.A.

Telephone (510) 841-1899
Facsimile (510) 841-2340

In order to be considered for membership, all sections **MUST** be completed.

1. (Please Print Legibly) Date_____

Name_____

Degree_____ Title_____

Addresses **(Please provide both and check preferred journal mailing address)**

[ ] Office _____

_____

Country _____ Telephone _____

Fax _____

[ ] Home _____

_____

Country _____ Telephone _____

Fax _____

2. Primary Workplace: [ ] University Hospital/Medical School [ ] Industry [ ] Private Hospital/Clinic [ ] Government Lab [ ] Other _____

3. Are you currently working in the field of MRI? [ ] Yes [ ] No Date registered: ____/____ Registry #: _____

4. Please list your MRI experience, including education, employment, types of scanners used or attach a current resume. **MUST** include dates.

_____

_____

_____

_____

_____

_____

_____

5. Professional Affiliations: [ ] AAN [ ] ACR [ ] ARRS [ ] ASNR [ ] ASRT [ ] RSNA [ ] SNM [ ] Other _____

6. Dues Payment. Please make checks payable to **SMRT**.

$70.00 per year for Technologist [ ] Voting [ ] Non-Voting

$125.00 per year for Technologist [ ] Voting [ ] Non-Voting With Journal, **Magnetic Resonance in Medicine**

$120.00 per year for Technologist [ ] Voting [ ] Non-Voting With Journal, **Journal of Magnetic Resonance Imaging**

$175.00 per year for Technologist [ ] Voting [ ] Non-Voting With Both Journals

Payment Methods:

Check, Travelers Check, International Money Order: Must be payable "to" (not "through") a U.S. Bank in U.S. dollars and must be imprinted with the computer encoding and routing information authorized by the American Banking Association.

Credit Cards: To pay by credit card, please check: Visa [ ] MasterCard [ ] EuroCard [ ]

Card #: _____ Exp. Date: ___/___ Signature: _____

DO NOT PAY BY WIRE.

Future Meeting Dates

1995: August 19-25, Nice, France
1996: Spring, New York, NY
1997: April 10-19, Vancouver, BC

Society of Magnetic Resonance
Chicago Office
213 West Institute Place
Suite 501
Chicago, IL 60610

Phone: (312) 751-2590 Fax: (312) 951-6474

CALL FOR PAPERS

SECOND MEETING OF THE SOCIETY OF MAGNETIC RESONANCE

San Francisco, California, USA
August 6-12, 1994.

DEADLINE FOR SUBMISSION:
APRIL 12, 1994

For information and abstract forms, contact

Society of Magnetic Resonance
Berkeley Office
1918 University Avenue, Suite 3C
Berkeley, CA 94704 USA
Tel: (510) 841-1899
Fax: (510) 841-2340

1994 Corporate Acknowledgments

The Society gratefully acknowledges the generous grants received in support of Society goals and specific educational/scientific programs at the First Meeting of the SMR from the following corporate sponsors:

Society Corporate Contributions

Three-Year Gold Corporate Members

Siemens Medical Systems, Inc.
Squibb Diagnostics

Three-Year Silver Corporate Members

Picker International, Inc.
Sanofi Pharmaceuticals and Eastman Kodak Company, Health Sciences Division

Three-Year Bronze Corporate Members

Bruker Instruments, Inc.
Hitachi Medical Systems America, Inc.
Mallinckrodt Medical, Inc.

Educational Grants

Bracco s.p.a.
General Electric Medical Systems, Inc.
Sanofi Winthrop Pharmaceuticals
Siemens Medical Systems, Inc.
Squibb Diagnostics, Inc.
Toshiba America Medical Systems, Inc.

Meeting Totes

Squibb Diagnostics, Inc.

Meeting Luncheons

Berlex Laboratories, Division of Berlex Laboratories, Inc.

Published based on information available December 17, 1993.

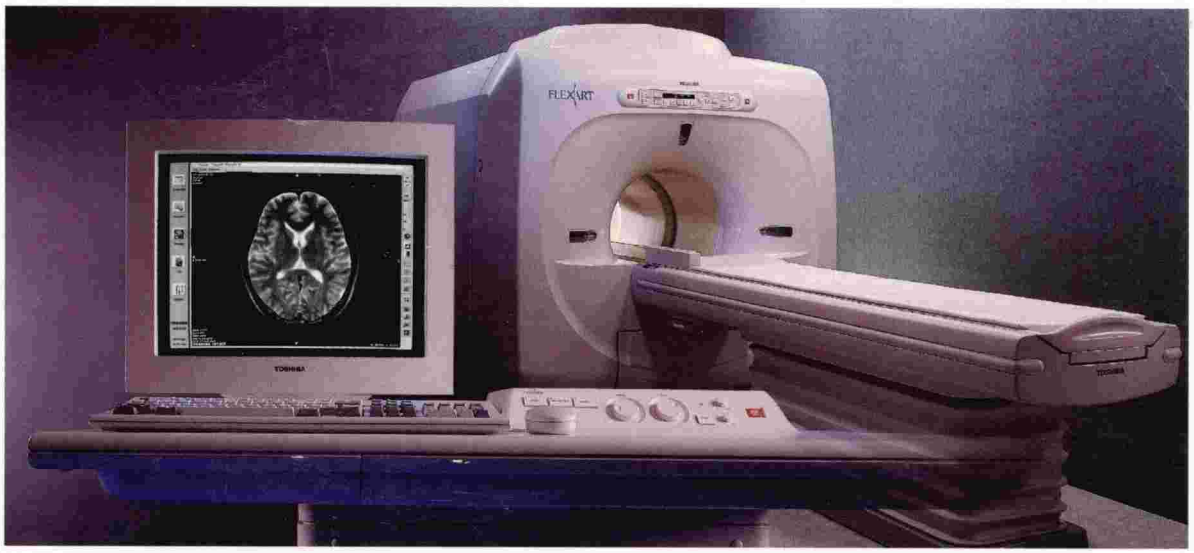

Just what the doctor ordered. And just what the administrator hoped for.

INTRODUCING FLEXART.™ Radiologists certainly have their priorities when it comes to MRI systems. And given the circumstances of healthcare today, everyone's agenda must concentrate on productivity and value.

Toshiba's remarkable new MRI system, FLEXART, embodies the most advanced technologies in medical imaging to provide a comprehensive answer to the demands of MRI today. With advanced digital architecture and innovative sequencing techniques, FLEXART delivers images of uncompromised quality.

FLEXART's unique feature set allows you to achieve a higher level of productivity. One of these features is the MRI industry's first truly icon-based interface. Technologists can simply point-and-click their way through the powerful menu choices with the speed of true multi-tasking.

It's time someone responded to the new requirements of MRI. Toshiba has. Call Toshiba ASSIST™ at 800-521-1968 if you'd like more information about the solution to the challenges you now face.

In Touch with Tomorrow

TOSHIBA

GLOBAL IMAGING ▪ MEDICAL SYSTEMS

Works in progress.

JMRI • SMR 1994 PRINTED PROGRAM ▪ Volume 4 (P)

PAGES 1–146